Identification of Signaling Pathways Involved in Ebola Virus Entry into Host Cells

Corina Stewart

This thesis is submitted to the Faculty of Medicine in partial fulfillment of the requirements for the degree of Doctor of Philosophy with specialization in Microbiology & Immunology

Department of Biochemistry, Microbiology, and Immunology
Faculty of Medicine, University of Ottawa

Abstract

Ebola virus (EBOV) is an enveloped virus of the family *Filoviridae* that causes outbreaks of hemorrhagic fever and for which there are no FDA-approved antiviral therapies. EBOV entry involves internalization and trafficking within host cells to facilitate delivery of the virus to its intracellular receptor, Niemann-Pick C1 (NPC1), which is localized in late endosomes/lysosomes. Given the requirements for internalization and endolysosomal trafficking, we hypothesized that EBOV activates signaling pathways to induce its uptake and regulate its trafficking to NPC1+ cellular compartments. To determine if signaling events induced by the virus play a role in infection, we screened a library of kinase inhibitors for their effect on infection by MLV pseudotypes bearing EBOV or vesicular stomatitis virus (VSV) glycoproteins. We subsequently identified and sought to characterize inhibitors of receptor tyrosine kinases (RTKs), sphingosine kinases (SKs), and diacylglycerol kinases (DGKs). Mechanistic studies revealed that EBOV activates RTK signaling to promote its trafficking to entry-conducive intracellular compartments. In addition, we also found that SKs are important for proper endocytic trafficking of EBOV to NPC1, while DGKs are required for EBOV internalization. Lastly, many of the kinase inhibitors we identified also inhibit entry of other late-penetrating viruses and may serve as potential starting points for the development of broad-spectrum host-directed antiviral therapeutics.

Acknowledgements

"It is time for you to spread your wings" - this was the advice I received from my undergraduate research supervisor, Dr. Erika Plettner, before beginning graduate school at the University of Ottawa. And what a journey it has been. Erika, thank you for encouraging me to go out of my comfort zone, move across the country, and study something I am passionate about.

I still remember the day Dr. Marceline Côté accepted me as her first graduate student – I was so excited to study emerging viruses (and in the middle of the ongoing Ebola epidemic!). Marceline, your encouragement, mentorship, and shared passion truly shaped me into the scientist I am today, and I am very grateful. When I began graduate school, I was young, inexperienced, and uncertain of myself. Your support, guidance, and confidence in me was exactly what I needed to grow into the scientist (and person) I am today. You lead by example – your tenacity, confidence, leadership, and perseverance were (and are) inspiring. Thank you for the times you pushed me, the times you were patient, and for your never-wavering positivity. I am excited to see the amazing things ahead for you and the Côté lab.

To my TAC members, Dr. Subash Saad, Dr. Robin Parks, Dr. Jean-Simon Diallo, and Dr. Morgan Fullerton, thank you for pushing me to think outside the box and challenge the conventional. Your "big picture" perspective was much needed when I was stuck in the nitty-gritty details.

To my friends and colleagues in the Côté lab, past and present, thank you for all the good times, laughs, and support. I would like to especially thank Yuxia Bo. Yuxia, you were truly the core of the lab. You were always there to help and support us whether it be teaching us new techniques or making sure that lab is organized and running well. Your support was paramount to my success. To Marie Ottenbrite and Salmaan Chummun – thank you for being awesome and for bearing with me as the first students I supervised! To Suresh, all I can say is "Cheers!" and I hope you continue to enjoy your Hennessy (oh, and thanks for all the laughs!). To all the other members of the Côté lab, thank you for all the good times and for tolerating me when I was running around doing a million things at once!

Shirley Qiu, I have not forgotten you in my Côté lab list as you deserve your own paragraph. We started the fellowship together, went through fire and water, from the lowest dungeon to the highest peak, and came out better for it. Thank you for always listening to my

rants, for always having my back, for reminding me of things when I forgot (as we all know how horrible my memory is), and for your friendship. Shirlz and Tempe for the win.

To my friends and colleagues at RGN, thank you for the laughs and good times. Tyler Smith and Nicholas LeBlond, thanks for always being willing to share your precious macrophages! To my office-mates Chantal, Shannon, and Dave, thank you for the great conversations and for keeping me sane. The “no science talk at lunch” rule really came in clutch.

And now to my family. To my Mom and Dad, thank you for everything you have done for me, for your encouragement, for your support in so many ways, and for always believing that I could do anything I set my mind to. To my brother and sister, Dan and Marlaena (and Bohee and Lee!) thank you for showing genuine interest in my research and for reminding me that I will always be “dummies” no matter what degree I get (haha)!

Finally, to my husband Kyle Stewart. I would not be where I am without you. Your love and support were paramount to my successes. You were (and are) my rock – you stood with me through all the complaining, the exhaustion, the stress, and the tears. Thank you for always knowing I had it in me to complete this PhD, even when times were tough.

And on a lighter note, to the Sneks (you know who you are), let’s go catch ourselves a mouse!

Table of Contents

List of Figures

List of Tables

List of Abbreviation

ADP: Adenosine diphosphate
AMPK: AMP-activated protein kinase
ARF: ADP-ribosylation factor
Arf6: ADP-ribosylation factor 6
ASGPRI: Asialoglycoprotein receptor 1
ATP: Adenosine-5'-triphosphate

BDBV: Bundibugyo virus

CatB: Cathepsin B
CatL: Cathepsin L
CCR5: C-C chemokine receptor type 5 (also known as CD195)
CD4: Cluster of differentiation 4
CD81: Cluster of differentiation 81
Cdc42: Cell division control protein 42 homolog
CLDN1: Claudin1
CLR: C-type lectin receptor
CXCR4: C-X-C chemokine receptor type 4 (also known as fusin or CD184)

DC-SIGN: Dendritic cell specific ICAM-3 grabbing non-integrin
DGK: Diacylglycerol kinase
DRC: Democratic Republic of the Congo

EBOV: Ebola virus
EIPA: 5-(N-ethyl-N-isopropyl)-amiloride
ESCRT: Endosomal sorting complex required for transport
EVD: Ebola virus disease
EVD: Ebola virus disease

FAK: Focal adhesion kinase
FDA: Food and Drug Administration
FRET: Förster resonance energy transfer

GAG: Glycosaminoglycan
Gas6: Growth arrest-specific protein 6
GM1: Monosialotetrahexosylganglioside
GP: Envelope glycoprotein
GP_0: Precursor full-length GP

$GP_{1,2}$: Post-translationally modified GP with GP1 and GP2 domains
GP_{20}: 20kDa GP intermediate (Cleaved by CatL only)
GP_{CL}: Fully primed 19kDa GP (Cleaved by CatB)
GPCR: G-protein coupled receptor
$GP_{\Delta muc}$: GP without the MLD
Grk2: G protein-coupled receptor kinase 2
GTP: Guanosine-5'-triphosphate

HA: Hemagglutinin
HCMV: Human cytomegalovirus
HCV: Hepatitis C virus
hMGL: Human macrophage galactose and acetylgalactosamine-specific C-type lectin
HOPS: Homotypic fusion and vacuole protein-sorting
HR1: Heptad repeat sequence 1
HR2: Heptad repeat sequence 2
HS: Heparan sulfate
HSV-1: Herpes simplex virus 1
HT1080: Human fibrosarcoma cell line

IAV: Influenza A Virus
IgG: immunoglobulin G

JAK: Janus kinases
JAK-STAT: Janus Kinase/Signal Transducer and Activator of Transcription
JUNV: Junin virus

L: RNA-dependent RNA polymerase
LASV: Lassa fever virus
LC3B: Microtubule-associated protein 1A/B light chain 3B
LSECTin: Lymph node sinusoidal endothelial cell C-type lectin
L-SIGN: Liver/lymph node specific ICAM-3 grabbing non-integrin

mAbs: Monoclonal antibodies
MAPK: Mitogen-activated protein kinase
MARV: Marburg virus
MERS: Middle eastern respiratory syndrome coronaviruses
MVD: Marburg virus disease

NFκ-B: Nuclear factor kappa B
NFκB: Nuclear factor kappa-light-chain-enhancer of activated B cells

NiV: Nipah virus
NP: Nucleoprotein
NPC1: Niemann-Pick C1

Pak1: p21-activated kinase
PAS: PIKfyve-ArPIKfyve-Sac3
PDGFR-α: platelet-derived growth factor receptor α
PI3K: Phosphatidylinositol-3-kinase
PIPs: Phosphorylated phosphatidylinositides
PKC: Protein kinase C
PLC: Phospholipase C
PTK: Protein tyrosine kinase

R_0: Reproductive number
Rab: Ras-related protein
Rac1: Ras-related C3 botulinum toxin substrate 1
RAVV: Ravn virus
HIV-1: Human immunodeficiency virus 1
RBD: Receptor binding domain
RGD: Arg-Gly-Asp
Rho: Ras homologues
RNP: Ribonucleoprotein
RTK: Receptor tyrosine kinase

S1P: Sphingosine-1-phosphate
S1PR: Sphingosine-1-phosphate G-protein coupled receptor
SARS-CoV-1: Severe acute respiratory syndrome coronavirus 1
SARS-CoV-2: Severe acute respiratory syndrome coronavirus 2
sGP: Soluble GP
SK1: Sphingosine kinase 1
SK2: Sphingosine kinase 2
ssGP: Small soluble GP
STAT: Signal transducer and activator of transcription proteins
SUDV: Sudan virus
SV40: Simian vacuolating virus 40

TAFV: Taï Forest virus
TAM: Tyro3-Axl-Mer
Tim-1 (or -4): T cell immunoglobulin and mucin receptor-1 or -4

UVRAG: Ultraviolet radiation resistance associated gene

Vero: African green monkey kidney epithelial cells
VLP: Virus-like particle
VP1: Viral protein 1
VP24: RNP-associated protein
VP30: Transcriptional activator
VP35: Polymerase co-factor
VP40: Matrix protein
VSV: Vesicular stomatitis virus

βlam: β-lactamase

Chapter 1: Introduction

1.1 FILOVIRUS IDENTIFICATION, CLASSIFICATION, AND GENERAL BIOLOGY

Filoviruses are enveloped, negative-sense, single-stranded RNA viruses of filamentous morphology that cause sporadic outbreaks of severe haemorrhagic fever diseases and originate primarily in West and Central Africa. The first documented filovirus outbreaks occurred in the Democratic Republic of the Congo (DRC) and southern Sudan in 1976, which resulted in the identification of the Zaire and Sudan Ebolaviruses respectively (1, 2). Since then, twelve filoviruses have been identified, six of which have been reported to cause human disease (3, 4). The continual discovery of new filoviruses in various geographic regions, such as the Měnglà virus identified in *Rousettes* bats in China, highlights the risk of future filovirus outbreaks occurring globally (5).

The *Filoviridae* family belongs to the order *Mononegavirales* and is most closely related to the P*aramyxoviridae, Pneumoviridae,* and *Sunviridae* families (3). Within the *Filoviridae* family there are 12 filoviruses belonging to 6 genera: *Cuevavirus*, *Dianlovirus*, *Ebolavirus*, *Marburgvirus*, *Striavirus*, and *Thamnovirus* (3). Ebolaviruses found to be pathogenic in humans are Bundibugyo virus (BDBV), Sudan virus (SUDV), Taï Forest virus (TAFV), and Ebola virus (EBOV, formally Zaire) species, while Marburgviruses known to cause disease in humans are Marburg virus (MARV) and Ravn virus (RAVV) species (Table 1.1) (3).

Filovirus genomes are approximately 15-19 kb of linear negative-sense non-segmented RNA. More specifically, fish-borne thamnoviruses are about 15 kb while Ebolaviruses, Marburgviruses, and Cuevaviruses are approximately 19 kb (3, 6, 7). Since only Ebolaviruses and Marburgviruses are known to be pathogenic in humans, and given that new filoviruses have only recently been identified with the advent of high-throughput sequencing technology, most of

what is known about filovirus biology is specific to Ebola and Marburgviruses and may or may not be applicable to the other filoviruses (8). Indeed, the finding that fish filoviruses belonging to the Striavirus and Thamnovirus genera have many differences in conserved motifs and even entire genes suggests that they may have evolved distinct mechanisms of replication and transcription (8, 9).

With respect to Ebola and Marburg viruses, the virions are filamentous or pleomorphic in shape with a diameter of approximately 80 nm and length generally ranging from 800-1000 nm (10, 11). Enclosing the core of the virion is a host-derived lipid envelope that is studded with the heterotrimeric viral glycoprotein (GP). After protein synthesis in the host cell, the GP precursor (GP_0) is cleaved by host furin proteases to form two covalently linked subunits, $GP_{1,2,}$ that are inserted as trimers into the viral envelope during egress (12). Lining the inner leaflet of the viral envelope is the matrix protein, VP40, which is the primary protein responsible for budding and forming the characteristic filamentous morphology of filoviruses (13-15). The core of the virion contains ribonucleoprotein (RNP) complexes composed of genomic RNA, the nucleoprotein (NP), RNA-dependent RNA polymerase (L), polymerase co-factor (VP35), transcriptional activator (VP30), and the RNP-associated protein (VP24) (Figure 1.1A) (15-18).

1.2 FILOVIRUS TRANSMISSION AND PATHOGENESIS

As zoonotic pathogens, filovirus infection in humans occurs after a spillover event from an animal reservoir into the human population. Similarly to other zoonotic viruses, the animal reservoir for EBOV and MARV is thought to be bats given that viral nucleotide sequences and immunoglobulin G (IgG) specific to both EBOV and MARV have been detected in bats from the *Pteropodidae* family, which are fruit bats local to Gabon and the DRC (19-21). Importantly, live

Table 1.1: Filovirus Taxonomy and Nomenclature.

Taxonomy based on an article published by Kuhn et al. (2019) (4).

Genus	Species
Ebolavirus	Bundibugyo virus
	Taï Forest virus
	Ebola virus
	Bombali virus
	Sudan virus
	Reston virus
Cuevavirus	Lloviu virus
Marburgvirus	Marburg virus
	Ravn virus
Dianlovirus	Měnglà virus
Striavirus	Xīlǎng virus
Thamnovirus	Huángjiāo virus

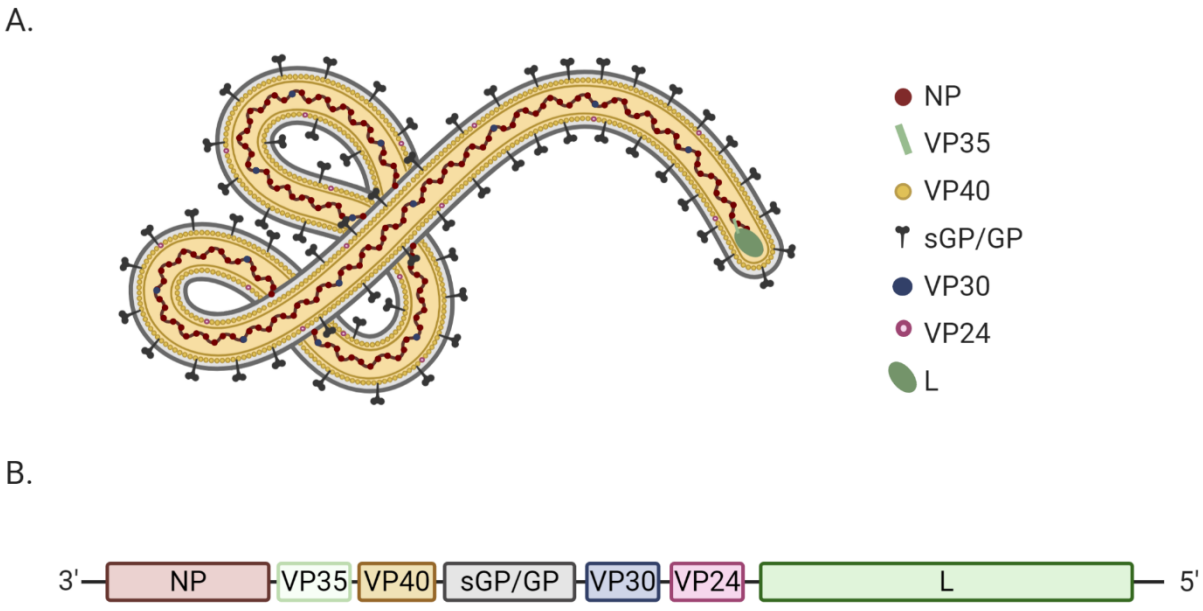

Figure 1.1: EBOV structure and genome organization

(A) Schematic of EBOV structure. (B) General schematic of EBOV genome organization. Created with BioRender.com.

MARV and RAVV has been isolated from the fruit bat *Rousettus aegyptiacus*, providing conclusive evidence that these bats are the natural reservoir species for Marburgviruses (22). However, in the case of the Ebolaviruses, researchers have yet been unable to isolate live virus from bats and therefore, while evidence strongly suggests that fruit bats are the natural reservoir for Ebolaviruses, ambiguity will remain until live virus is successfully isolated (21, 23, 24).

Historically, most filovirus outbreaks are believed to have occurred after a single spillover event from animals to humans. For example, genomic surveillance data from the 2013 to 2016 Ebola virus disease (EVD) outbreak in West Africa suggests that a single animal-to-human transmission event was responsible for the outbreak (25). Such spillover events typically occur after direct contact with infected bats or after consumption of bush meat from infected non-human primates (24, 26-29). Subsequent human-to-human transmission occurs mainly via direct contact with bodily fluids from an infected individual (21, 30, 31). While case-fatality rates for EBOV are high, typically ranging from 50 to 90%, infection control measures such as education and contact tracing are often enough to keep the reproductive number (R_0) below 1 (24, 32). However, employing these basic public health measures is often challenging given that outbreaks frequently occur in remote communities and in areas of high social and political unrest (33).

Following the 2-21 day incubation period, infection by filoviruses typically involves three phases (34). In the initial stages of filovirus infection in humans, symptoms are characteristic of non-specific viral syndrome and typically include fever, body aches, fatigue, and general malaise (34). Although early diagnosis is critical for favourable outcomes and infection control, due to the lack of specificity of early symptoms in addition to variances in clinical manifestations, initial infection by filoviruses is often hard to diagnose and is commonly misdiagnosed (35). In phase 2, patients progress to experience gastrointestinal symptoms such as vomiting and

diarrhoea; during this stage, some patients will begin to recover while some will progress to the third stage (34). During phase 3, symptoms include the characteristic haemorrhagic events, decline of liver and kidney function, convulsion, shock, and multi-organ failure, which often leads to death (21, 34). Since there are no FDA approved antiviral therapies for Ebola virus disease (EVD) or Marburg virus disease (MVD), aggressive supportive care administered as early as possible is currently the preferred treatment option for treating EVD and MVD (36).

Filoviruses enter the human body through breaks in the skin or mucosal surfaces (37). While filoviruses can infect almost all cell types, the virus preferentially first replicates in macrophages and dendritic cells (38). Since these cells are migratory, early infection of these cells allows the virus to be easily transported by the lymphatic system to other areas of the body including the liver, endothelium, spleen, lymph nodes, kidneys, adrenal glands, and pancreas (39, 40). In addition, filovirus infection also triggers the release of pro-inflammatory cytokines and chemokines from infected macrophages, resulting in a characteristic uncontrolled cytokine storm (41-44). The cytokine storm creates a perfect milieu for filoviruses to replicate – as more immune cells are recruited to the site of infection, more cells can inherently become infected (40). The consequences of such leads to tissue damage, loss of vascular integrity, and apoptosis of bystander lymphocytes, which in turn cumulatively favors enhanced filoviral replication (40). Additionally, infection of dendritic cells inhibits their maturation and prevents antigen presentation to T-cells, thereby impairing both the natural killer (NK) cell and T-cell responses to infection (34, 45, 46).

Filoviruses also impair type I interferon (IFN) production and employ many mechanisms to facilitate innate immune evasion (40, 47, 48). This is largely mediated by the viral protein, VP35, which effectively subverts cytosolic sensing of filoviruses by antagonizing signaling

pathways that lead to the expression of type 1 IFNs (49-52). Interestingly, when EBOV is engineered to express a mutant form of VP35 that is unable to antagonize type 1 IFN signaling pathways, there is reduced viral replication and non-lethality in animal models, providing evidence that VP35 is a crucial determinant of EVD *in vivo* (53, 54). In sum, the severity of filoviral infection in humans seems to result from excessive inflammatory responses, dysregulated immune function, and robust systemic viral replication that is virtually unimpeded by the innate immune response (40).

1.3 FILOVIRUS LIFE CYCLE

The filoviral life cycle is typical for negative-sense RNA viruses that replicate in the cytoplasm and consists of the following general steps: viral entry, genome replication, translation of viral genes, virion assembly, and budding. Due to sequence similarity, it is likely that all mammalian filoviruses follow the same general life cycle, however because the fish filoviruses are quite divergent, they may employ different mechanisms of entry, replication, and budding (8). The following section is based largely on what is known about the Ebolavirus lifecycle (summarized in Figure 1.2).

EBOV entry is quite complex, and since it is the topic of this thesis, it is described in more detail in section 1.4. In brief, entry begins with attachment of a viral particle to the cell surface via the viral GP and/or lipids on the viral envelope (55-57). Following attachment, EBOV is internalized via macropinocytosis and undergoes trafficking to late endosomes/lysosomes where the viral receptor, Niemann-Pick C1 (NPC1), is localized (58-63). Upon viral GP triggering, fusion occurs between the viral envelope and host cell membrane, resulting in the release of the viral RNP complex into the cytoplasm (62-68).

Once in the cytoplasm, RNP complex proteins NP, VP35, VP30, and L, facilitate the transcription of the viral genome (Figure 1.1B) (69, 70). Viral mRNAs are produced sequentially from the 3' end of the viral genome (69, 71). Transcription is terminated at conserved stop signals and may or may not reinitiate at conserved start signals (69, 71). This results in a gradient of mRNAs, all of which are translated by host machinery (71). In addition, transcriptional editing by L results in the production of various forms of GP: pre-cursor full length GP (GP_0) and two soluble forms known as soluble GP (sGP) and small soluble GP (ssGP) (72-74). In contrast to Ebolaviruses, Marburgviruses do not produce sGP or ssGP (75). For EBOV, sGP has multiple roles including anti-inflammatory functions to help sustain virus replication and transmission, as well as acting as a decoy to divert the humoral immune response away from GP on the viral envelope (43, 76). The role of ssGP in EBOV pathogenesis remains unknown (74). For both Ebolaviruses and Marburgviruses, GP_0 is post-translationally modified in the endoplasmic reticulum and golgi apparatus where it undergoes extensive *N*- glycosylation and *O*-glycosylation, in addition to furin-mediated cleavage, to form the mature GP_1 and GP_2 subunits (12, 73, 77). Mature $GP_{1,2}$ is then transported through the secretory pathway to VP40-rich regions of the plasma membrane (14, 78-80).

As viral proteins accumulate, NP drives the formation of cytoplasmic inclusion bodies that contain NP, VP35, VP40, and L, and are major sites of genome replication and transcription (81, 82). Newly formed RNP complexes condense into mature and transport competent nucleocapsids, a process that is mediated by the viral protein VP24 (83, 84). Mature nucleocapsids are then transported in an actin-dependent manner to sites of viral assembly for budding at the cell surface (84, 85). Through hijacking cellular endosomal sorting complex required for transport (ESCRT), VP40 drives budding from the plasma membrane where mature

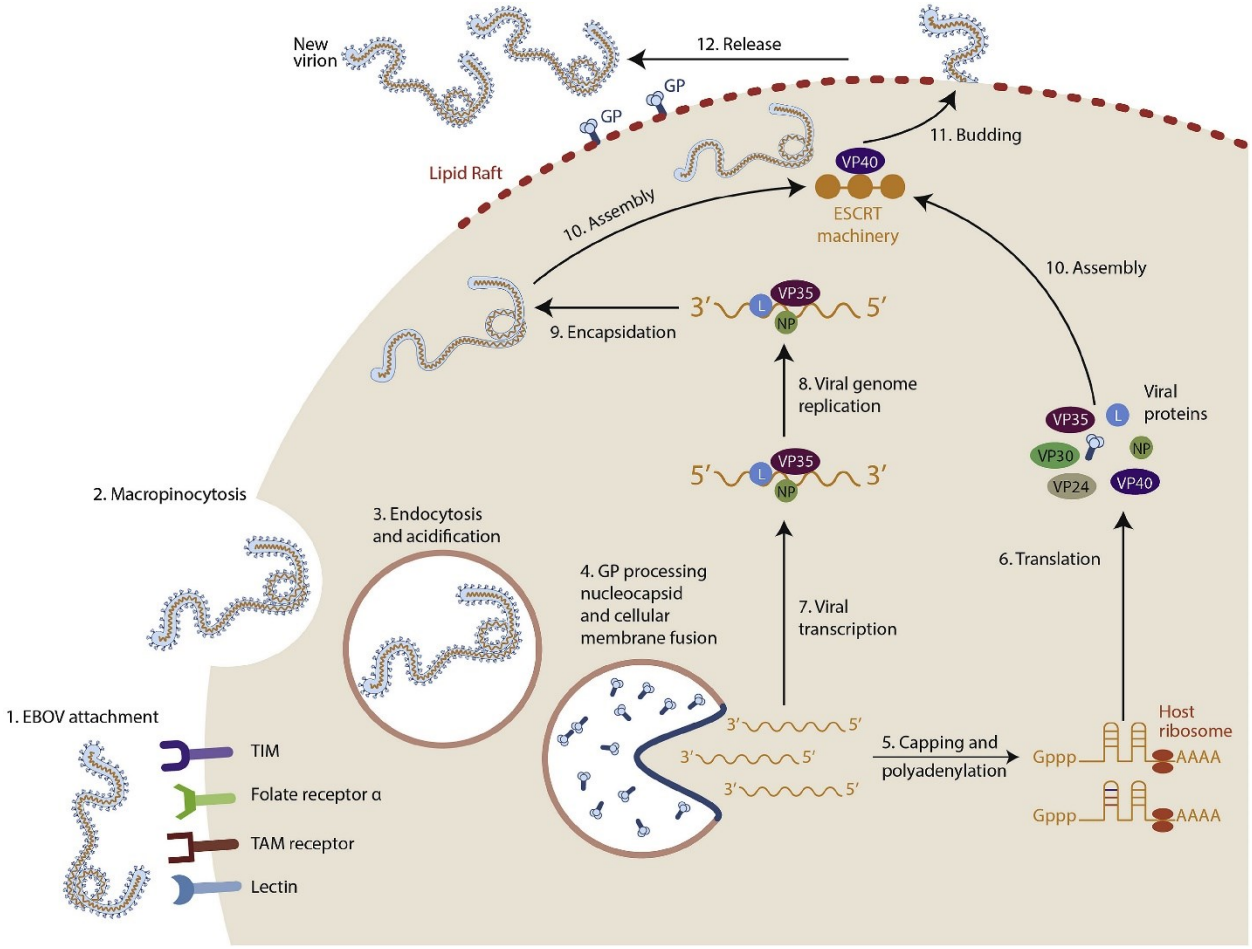

Figure 1.2: EBOV lifecycle

Schematic of the EBOV life cycle. Reprinted from Rojas et al. (2020) with permission in accordance with the Creative Commons Attribution-NonCommercial-NoDerivatives 4.0 International License (https://creativecommons.org/licenses/by-nc-nd/4.0/) (35).

$GP_{1,2}$ trimers are embedded (86, 87). In addition, interaction of $GP_{1,2}$ and/or VP40 with host cell scramblases results in the exposure of phosphatidylserine on the outer leaflet of the viral envelope, which has further implications for viral entry (56, 57, 88-91).

1.4 EBOLA VIRUS ENTRY

1.4.1 Ebola virus glycoprotein structure and function

For enveloped viruses to enter cells, fusion must occur between the viral envelope and the host cell membrane. This is mediated by a viral fusion protein that studs the viral envelope; the fusion protein needs to be both "primed" and "triggered" to transition from the pre-fusion to the post-fusion conformation (92). "Priming", which often involves proteolytic cleavage, makes the transition from the pre-fusion to post-fusion conformation possible. "Triggering" initiates this transition and involves ligand binding, such as binding a proton or a host-cell protein, the latter of which is known as a viral receptor (92). The transition from the activated, metastable pre-fusion conformation to the low energy post-fusion conformation of viral fusion proteins is generally irreversible, which is why viral fusion proteins have evolved to rely on priming and triggering to prevent premature fusion (93).

Viral fusion proteins are grouped into three classes (Class I, Class II, and Class III), each with characteristic structures and priming requirements (or lack thereof). The filovirus fusion protein, GP, is a Class I viral fusion protein that resembles the prototypical influenza A virus (IAV) hemagglutinin (HA) or the human immunodeficiency virus 1 (HIV-1) Env viral fusion proteins (94). As mentioned in section 1.3, the non-fusogenic precursor polypeptide, GP_0, is proteolytically processed by furin in viral producer cells to form GP1 (N-terminal region of GP_0) and GP2 (C-terminal region of GP_0), which are joined by a disulfide bond and non-covalent interactions, and assemble into the trimeric metastable prefusion conformation that is present on

the viral envelope (Figure 1.3) (64, 95-97). GP1 is divided into four distinct subdomains: the base, the receptor binding domain (RBD), the glycan cap, and the mucin-like domain (MLD) (Figure 1.3) (18). In brief, the base domain contains the intermolecular disulfide bond that links GP1 and GP2, and also acts as a clamp, stabilizing the prefusion conformation of GP2 (18). As the name suggests, the RBD contains residues that bind the host cell receptor, NPC1, which is essential for membrane fusion (62, 63, 77, 98-101). The glycan cap and MLD are heavily glycosylated with N and O-linked glycans that shield the ectodomain from neutralizing antibodies and are important for attachment of EBOV to the host cell (55, 95, 102). The MLD is often removed to increase entry efficiency of EBOV pseudotypes in cell culture. While the MLD has been shown to be dispensable for entry of EBOV pseudotypes, it does play roles in both cell adhesion and immune evasion *in vivo* (95, 103, 104). The transmembrane subunit, GP2, contains the fusion machinery including the hydrophobic internal fusion peptide, or 'fusion loop', and the alpha helical heptad repeat sequences (HR1 and HR2) that are characteristic of Class I viral fusion proteins (96, 105-107). After priming and triggering occurs, GP2 undergoes extensive conformational rearrangements, including formation of a 6-helix bundle and insertion of the fusion loop into the target cell membrane (68, 92, 108, 109). This drives the coalescence of the viral envelope and host cell membrane and results in delivery of the viral nucleocapsid into the cytoplasm (68, 92, 108, 109).

The priming and triggering requirements of viral fusion proteins is what ultimately determines the entry pathway for enveloped viruses. For some viruses, such as HIV-1, most of the triggering factors, including the receptor and co-receptor, are on the cell surface, therefore the entry pathway is less complex and requires fewer host factors (110). For other viruses, including filoviruses, the triggering factors are in endosomes and lysosomes; consequently, virus

internalization and subsequent endosomal trafficking are an absolute requirement for fusion. While the mechanism of EBOV GP-mediated fusion is assumed to mirror canonical class-I fusion proteins, requiring proteolytic cleavage, low pH, and receptor binding, a growing body of evidence suggests that EBOV GP-mediated fusion is more complex and requires additional cues (67, 68, 111, 112). For example, priming of class I fusion proteins typically requires a single proteolytic cleavage event in the secretory pathway of the viral producer cells, such as furin cleavage of HIV Env, to allow the glycoprotein to rearrange during fusion (113). For EBOV GP, however, furin cleavage of GP_0 to $GP_{1,2}$ in the viral producer cell is a) not sufficient to prime GP, which requires extensive proteolytic remodeling, and b) not required for infectivity (64, 114-116). Despite decades of research, the exact mechanism and triggering factors required for EBOV GP-mediated fusion remain to be fully elucidated.

During entry, $GP_{1,2}$ is cleaved by endosomal cysteine proteases, Cathepsin B (CatB) and Cathepsin L (Cat L), to form a smaller form of GP known as GP_{20}, which is then further cleaved to the smallest and fully cleaved form of GP, referred to as GP_{CL} (116-118). Interestingly, while thermostability drastically decreases from GP to GP_{CL}, there is no difference in thermostability between GP_{20} and GP_{CL}, suggesting that the function of the second cleavage event may not be to destabilize GP, but rather to prime GP for interaction with another, yet unidentified, host factor (118). Additionally, entry of VSV pseudotypes bearing GP_{CL} are still sensitive to the cysteine protease inhibitor E64D, but not the CatB inhibitor Ca074, therefore suggesting the existence of an additional cysteine protease-dependent entry step that is not mediated by CatB (116). Recent evidence suggests that this step occurs after lipids from the viral envelope and host cell membrane mix, suggesting that it may occur during fusion pore formation or expansion (67).

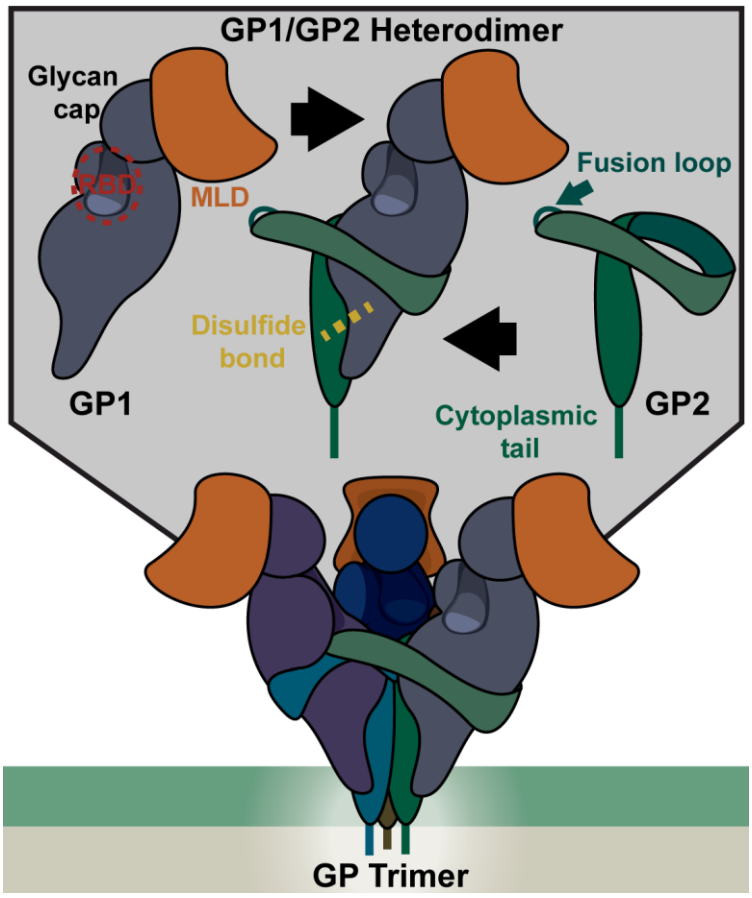

Figure 1.3: EBOV GP Structure

Schematic of EBOV GP structure. Each GP trimer consists of three GP_1/GP_2 heterodimers with each individual GP_1 and GP_2 monomer associating via a disulfide bond. The receptor binding domain (RBD) is protected by the glycan cap and mucin-like domain (MLD). The internal fusion loop is hidden until triggering induces conformational changes that facilitate fusion. Reprinted from Moller-Tank and Maury (2015) with permission in accordance with the Creative Commons Attribution License BY 4.0 (https://creativecommons.org/licenses/by/4.0/) (119).

In addition to cathepsin cleavage, low pH and Ca2+ have also been implicated as important triggering factors. While low pH was originally thought to destabilize GP_{CL} and act as a triggering factor, as is the case for many other viral fusion proteins, recent studies have shown that low pH stabilizes both GP and GP_{CL}, suggesting that acidic pH alone probably does not play a direct role in triggering GP_{CL} (92, 118). Spence et al. showed that fusion triggering can take up to 20 minutes after EBOV VLPs colocalize with NPC1, therefore it is plausible to speculate that the stabilization effect of low pH is an adaptive response to the harsh conditions of the late endosomes and lysosomes (67, 118). In addition to low pH, the endosomal two pore calcium channel 2 (TPC2) was identified to be a late entry factor for EBOV; knockdown of TPC2, small-molecule inhibitors of calcium channels, and calcium chelators all inhibit EBOV entry (120-123). Interestingly, two recent studies demonstrated that a combination of low pH and Ca2+ act synergistically to promote fusion (68, 123). Low pH promotes formation of an alpha-helical structure in the fusion loop, a conformational change that enhances membrane fusion, and calcium was shown to stabilize this structure, providing a possible mechanism for the roles of both calcium and low pH in promoting fusion (123). However, Ca2+, low pH, and the presence of NPC1 are still not sufficient to trigger fusion of GP_{CL}, indicating that additional triggering factor(s) are required for fusion (68, 112).

1.4.2 Attachment and Internalization

For EBOV to reach compartments that are conducive to fusion in late endosomes and lysosomes, it must first attach and be internalized into cells. Since EBOV has very broad cell tropism, it is able to utilize a wide variety of attachment factors, which bind to GP or lipids on the viral envelope. Namely, *N*- and *O*- linked glycans on EBOV GP can bind to cell surface

carbohydrate-binding receptors and phosphatidylserine (PS) exposed on the viral envelope can bind to cell surface PS receptors.

1.4.2.1 Carbohydrate-binding receptors

C-type lectins are a superfamily of over 1,000 proteins that are divided into 17 subgroups, all of which have one or more C-type lectin-like domains (124). They can bind carbohydrates in addition to other ligands including proteins and lipids, and exist as both transmembrane proteins and secreted molecules (124). Since the EBOV fusion protein is heavily glycosylated at both the MLD and glycan cap, it is not surprising that numerous C-type lectins, both the transmembrane and secreted forms, have been shown to bind EBOV GP and enhance infection in a variety of cell types including dendritic cells and macrophages (18).

Several transmembrane C-type lectin receptors (CLRs) have been implicated as attachment factors for EBOV because of their ability to bind GP and enhance entry (18). These include the dendritic cell specific ICAM-3 grabbing non-integrin (DC-SIGN), liver/lymph node specific ICAM-3 grabbing non-integrin (L-SIGN), lymph node sinusoidal endothelial cell C-type lectin (LSECTin), asialoglycoprotein receptor 1 (ASGPRI), human macrophage galactose and acetylgalactosamine-specific C-type lectin (hMGL), and likely additional CLRs that have yet to be identified (55, 125-128). CLRs bind EBOV GP through the *N*- and *O*- linked glycans present on the mucin domain, and/or the *N*- linked glycans on the glycan cap (77, 102). Interestingly, the *N*- linked glycan sites on the glycan cap are highly conserved among different Ebolaviruses despite poor sequence similarity within the rest of the glycan cap, suggesting important functional significance of these residues (102). This functional significance was demonstrated by genetically removing *N*- linked glycans and subsequently measuring entry (102). Genetic elimination of specific *N*- linked glycans revealed that entry mediated by DC-SIGN and L-SIGN

was highly dependent on *N*- linked glycans on both the MLD and glycan gap of GP1, while entry mediated by LSECtin was less dependent on *N*- linked glycans present on the glycan cap (102). In contrast, entry mediated by ASGPRI was partially dependent on *N*- glycans present on the MLD, while entry mediated by hMGL did not appear to be dependent on *N*- glycans at all (102). While the effect of *O*- glycan removal has not yet been studied, this finding suggests that the ligands for ASGPRI and hMGL are *O*- linked glycans on the MLD or *N*- linked glycans on GP2 (102).

In addition to CLRs, mannose binding lectin (MBL) and Ficolin-1, which are soluble C-type lectins and pattern recognition receptors, have also been implicated as attachment factors for EBOV. MBL, which binds to *N*- linked glycans on GP1, enhances EBOV infection in Vero cells and macrophages under low complement conditions (129, 130). Interestingly, MBL can also have an inhibitory effect on infection under high complement conditions due to MBL-dependent neutralization via the lectin complement pathway (129, 130). In contrast, binding of ficolin-1 to sialylated moieties present on *O*- liked glycans on the MLD was shown to enhance EBOV infection under low and high complement conditions, suggesting that the ficolin-1-GP interaction does not activate the lectin complement pathway (131).

Lastly, EBOV can utilize glycosaminoglycans (GAGs) such as heparan sulfate (HS) to mediate attachment to host cells (132). HS, heparin, and other GAGs, can bind to both GP and GP lacking the MLD ($GP_{\Delta muc}$), resulting in a block of viral entry (132, 133). In addition, knockdown of exostosin-1 (EXT1), which is involved in the biosynthesis of HS, was shown to reduce EBOV GP-mediated entry in A549 cells (133). In sum, EBOV attachment can be mediated, at least in part, by relatively non-specific GP-dependent interactions with cell surface carbohydrate-binding receptors.

1.4.2.2 PS Receptors and Apoptotic Mimicry

PS is a negatively charged lipid typically found on the inner leaflet of plasma membranes of healthy cells. However, during apoptosis, PS becomes exposed on the outer leaflet and functions to signal to phagocytic cells to internalize and degrade the apoptotic cell (134, 135). This signal is transmitted via PS receptors on phagocytic cells that either bind PS directly or via bridging molecules (136). Many enveloped viruses, including filoviruses, exploit this mechanism of apoptotic cell clearance to promote entry and subsequent infection; this is referred to as viral 'apoptotic mimicry' (136, 137).

During egress, EBOV GP and/or VP40 actively induce the flipping of PS to the outer leaflet in the localized region of the plasma membrane where budding occurs (88, 89). During entry, PS on the EBOV outer leaflet can bind directly to transmembrane PS receptors called T cell immunoglobulin and mucin receptor-1 and -4 (TIM-1 and TIM-4) to facilitate attachment and internalization of virions (57, 90, 138-141). The PS receptors of the Tyro3-Axl-Mer (TAM) family of receptor tyrosine kinases (RTK) have also been implicated as attachment and internalization factors for EBOV, presumably through PS-mediated binding of adaptor proteins, such as Gas6 and Protein S, which subsequently bind to the TAM RTKs (56, 139, 142, 143). While studies have shown indirect evidence of the EBOV-PS-Adaptor-TAM interaction, including competition assays demonstrating that addition of the Gas6 ligand reduces Axl mediated enhancement of infection, direct evidence of the EBOV-PS-Adaptor-TAM interaction has not yet been shown (142).

While it is well established that PS receptors TIM-1, TIM-4, and the TAM RTKs facilitate attachment of EBOV to host cells, the precise roles of these proteins for virus internalization is unclear (56, 90, 138). The TIM family of proteins, including TIM-1 and TIM-4,

share a similar structure. They possess an amino-terminal immunoglobulin-like variable (IgV)-like domain that contains the PS binding pocket, a heavily glycosylated MLD that extends from the plasma membrane, a transmembrane domain, and a short cytoplasmic tail through which signalling can be initiated (144, 145). The TAM proteins are RTKs that contain two N-terminal immunoglobulin-like domains, which interact with a PS-binding adaptor protein such as Gas6, followed by two fibronectin type III domains, a single transmembrane domain, and a cytoplasmic protein tyrosine kinase domain that is characteristic of the RTK superfamily (146-148). As is the case for all RTKs, homo-or-hetero-dimerization is required to initiate signaling through the cytoplasmic protein tyrosine kinase domain (149). It was first hypothesized that signaling through the cytoplasmic domains of these proteins is the mechanism by which they enhance EBOV internalization, as is the case for the uptake of apoptotic cells via PS receptors (135, 145). However, the transmembrane domain and cytoplasmic tail of TIM-1, and the protein tyrosine kinase (PTK) domain on Axl, were dispensable for the observed enhancement of virus internalization mediated by these PS receptors (138, 150). This raises the possibility that other proteins may interact with EBOV-PS bound TIM/TAM PS receptors to facilitate the enhancement of internalization and highlights the need for future studies to address such.

1.4.2.3 Internalization via Macropinocytosis

The major endocytic pathways that viruses use to enter cells are clathrin-mediated endocytosis, caveolin mediated endocytosis, macropinocytosis, phagocytosis, and adaptions of the classical routes, such as clathrin/caveolin independent endocytosis (151, 152). As is true of many viruses whose triggering factors are inside the cell, it was originally thought that EBOV is internalized through clathrin-mediated endocytosis. In support of this hypothesis, treatment with an inhibitor of clathrin-coated pit formation, chlorpromazine, partially blocked infection by

EBOV pseudoparticles, siRNA knockdown of the clathrin heavy chain reduced infection, and EBOV pseudoparticles were shown to associate with clathrin (56, 153, 154). However, in contrast, another study showed that EBOV pseudoparticles colocalized with caveolin-1, a marker of caveolin mediated endocytosis, but not transferrin, a marker of clathrin mediated endocytosis (155). Yet another study found that EBOV does not associate with markers of caveolae or clathrin-coated endosomes (59). These seemingly contradictory studies may be due to differences in cell types or the differential use of pseudoparticles, virus-like particles, or replication-competent virus.

While EBOV may utilize certain proteins involved in both clathrin and caveolin mediated endocytosis, many factors suggest that these are not the primary internalization routes. Some examples of such factors are: 1) cell lines lacking caveolae still support entry of EBOV pseudotypes, 2) chlorpromazine, which inhibits EBOV entry, is not a specific inhibitor of clathrin-mediated endocytosis and can also interfere with macropinocytosis and phagocytosis, 3) the clathrin heavy chain is also involved with other mechanisms of endocytosis, including phagocytosis, and, importantly, 4) the large size of EBOV particles makes uptake by clathrin and caveolin mediated endocytosis unlikely due to size constraints; clathrin-coated vesicles are 60-200 nm in diameter, caveolae are 50-100 nm, while EBOV is 80 nm in diameter and up to 1 μm in length (10, 156-161). Current evidence suggests that the primary entry route for EBOV is macropinocytosis, or a macropinocytosis-like mechanism (58, 59).

Macropinocytosis a process that involves large scale remodeling of the cell membrane and cytoskeleton, resulting in the uptake of extracellular fluid and particles into large vacuoles (152, 162). The size of macropinosomes can range from 0.2 μm to 10 μm in diameter, making them easily capable of carrying EBOV particles (163). Macropinocytosis is a highly coordinated

and tightly regulated process relying on numerous cellular kinases; in most cell types, macropinocytosis needs to be triggered by activating signaling cascades (162, 164). Such signaling cascades are complex and roles for kinases in macropinocytosis are continually emerging. Key regulators of macropinocytosis include the Rho GTPases Rac1 and Cdc42, the ARF GTPase Arf6, the kinases p21-activated kinase (Pak1) and protein kinase C (PKC), phospholipase C (PLC), and the lipid kinases phosphatidylinositol-3-kinase (PI3K) and diacylglycerol kinase (DGK) (165-175). Other factors thought to be important for macropinocytosis include Na+/H+ exchangers, which contribute to maintaining proper submembranous pH important for Rac1 signaling, AMP-activated protein kinase (AMPK), and cholesterol composition of the plasma membrane (172, 176-178).

To examine if EBOV utilizes macropinocytosis for internalization, both pharmacological and genetic approaches have been employed. Inhibitors of actin polymerization (cytochalasin D), NA+/H+ exchangers (EIPA), PI3K (Wortmannin, LY294002), AMPK (Compound C), and pharmacologically causing cholesterol depletion using methyl-β cyclodextrin, all result in a block of EBOV entry (58, 59, 154). In addition, knockdown of Cdc42 or Pak1, or expression of a dominant negative form of Rac1, all significantly reduce entry by EBOV VLPs (58, 59, 179). Colocalization studies found that EBOV VLPs co-localize with sorting nexin 5 (SNX 5), a component of newly formed macropinosomes, in addition to co-localizing with Arp2 complexes, which serve as actin nucleation sites (58, 59, 180). Furthermore, treatment of cells with EBOV induces fluid phase uptake of high molecular weight dextran, which can only be internalized through macropinocytosis; in fact, researchers saw a 2-3 fold increase in dextran positive vesicles per cell compared to incubation with VSV, a virus that utilizes clathrin-mediated endocytosis for internalization (59, 154). Additionally, recent studies have implicated several

autophagy-associated proteins, including microtubule-associated protein 1A/B light chain 3B (LC3B), to be important for the macropinocytosis of EBOV(181). Taken together, these studies provide strong evidence that EBOV induces macropinocytosis as its primary mode of internalization, however the mechanism by which EBOV triggers its macropinocytic uptake remains unknown.

1.4.3 Endolysosomal trafficking

Once particles, viruses or otherwise, are internalized into cells, endocytic vesicles deliver their cargo to early endosomes to be sorted. Most internalized cargo is recycled back to the plasma membrane, however certain cargo can also be sorted to the lysosome for degradation or sent to the trans-Golgi network via retrograde transport (182). These sorting and trafficking processes are tightly regulated in a spatio-temporal manner by a network of signaling lipids and proteins, including but not limited to phosphorylated phosphatidylinositides (PIPs) and Rab GTPases (182). For EBOV to efficiently enter host cells, it must be successfully sorted to the degradative route and trafficked to late-endosomes and lysosomes where its triggering factors are localized. Therefore, many proteins that are involved in regulating the maturation of early and late endosomes are essential for productive EBOV entry.

EBOV has been shown to colocalize with many markers of late endosomes, including Rab7 and Lamp1, and to kinetically experience a lag in fusion comparison to viruses that undergo fusion in earlier endocytic compartments, such as VSV. Other studies have demonstrated that functional Rab5 and Rab7, GTPases required for the maturation of early endosomes to late endosomes, are critical for entry as expressing dominant negative forms of these proteins in cells inhibits entry of EBOV. In addition, a genetic screen identified the homotypic fusion and vacuole protein-sorting (HOPS) complex and the PIKfyve-ArPIKfyve-

Sac3 (PAS) complex, both involved in regulating endolysosomal trafficking, to be critical for EBOV entry (63). Further work demonstrated that knockout of HOPS complex subunits or UV radiation resistance-associated gene (UVRAG), a protein that can bind to the HOPS complex and is known to positively regulate endocytic trafficking, reduced EBOV GP-mediated entry by preventing the virus from reaching NPC1+ compartments (61, 63). In addition, other work has demonstrated that PIKfyve kinase, which phosphorylates phosphatidylinositol (3) phosphate (PtIns3P) to phosphatidylinositol (3,5) bisphosphate (PtdIns(3,5)P_2), is critical for EBOV entry and that stimulation of cells with EBOV results in increased intracellular PtdIns(3,5)P_2 (60, 183). Interestingly, stimulating cells with EBOV also results in increased levels of phosphorylated Akt, and inhibiting Akt signaling interferes with endocytic trafficking of EBOV (184). Furthermore, one study demonstrated that phosphorylated Akt can activate PIKfyve, therefore it is plausible to speculate that EBOV may stimulate that activity of the PAS complex and regulate its endocytic trafficking through activating the PI3K/Akt pathway during entry (185).

An overall schematic of EBOV entry is summarized in Figure 1.4.

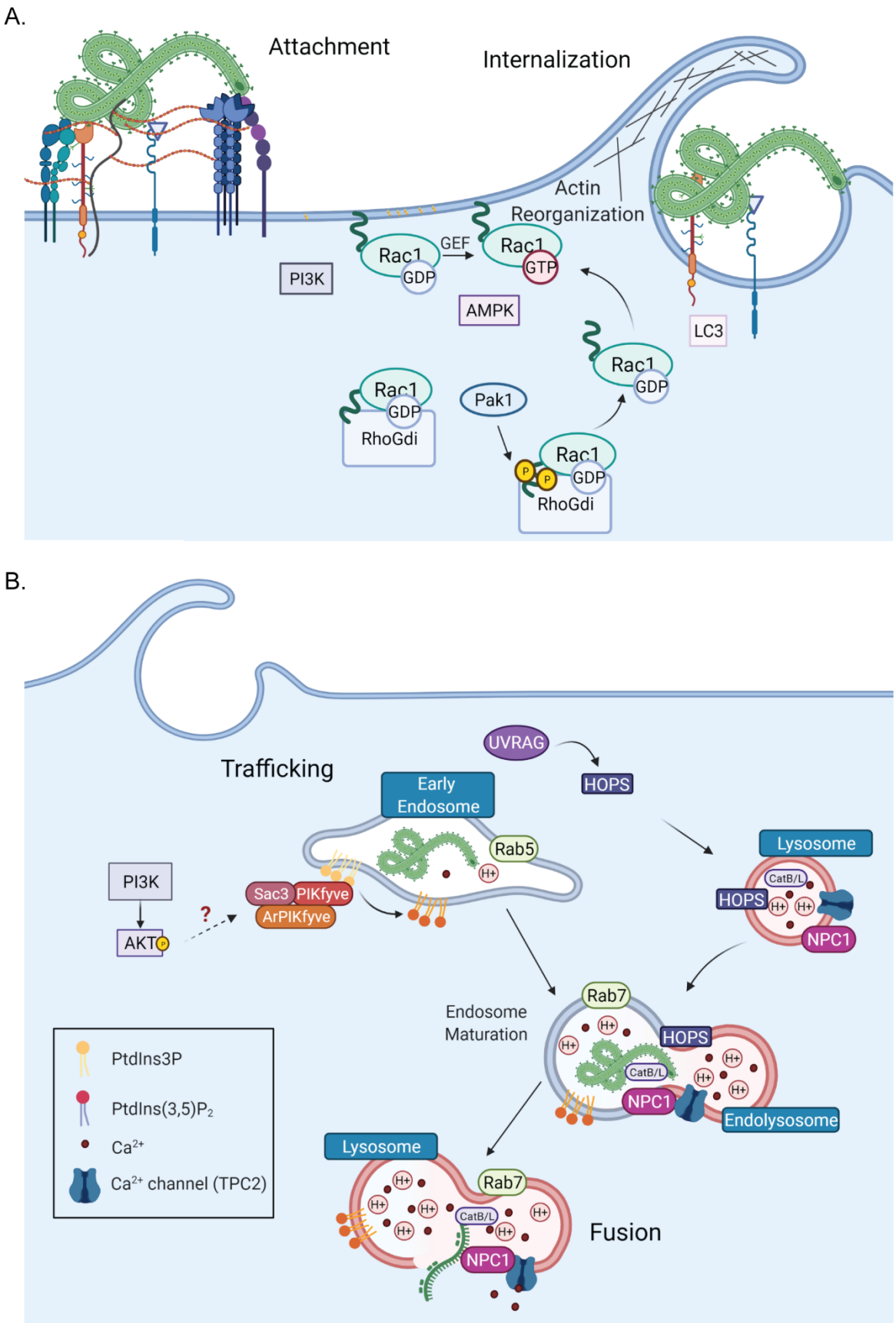
A.
Attachment
Internalization
Actin
Reorganization
Rac1
GDP
GEF
Rac1
GTP
PI3K
AMPK
LC3
Rac1
GDP
Rac1
GDP
RhoGdi
Pak1
Rac1
GDP
RhoGdi
B.
Trafficking
UVRAG
HOPS
Early
Endosome
Rab5
PI3K
AKT
Sac3
PIKfyve
ArPIKfyve
Lysosome
CatB/L
HOPS
NPC1
Endosome
Maturation
Rab7
HOPS
CatB/L
NPC1
Endolysosome
PtdIns3P
PtdIns(3,5)P2
Ca2+
Ca2+ channel (TPC2)
Lysosome
Rab7
CatB/L
NPC1
Fusion

Figure 1.4. Overall schematic of EBOV entry pathway.

(A) EBOV entry begins with binding of EBOV to the cell via cell surface attachemnt factors, followed by internalization via a macropinocytosis-like mechanism or phagocytosis. (B) The virus then undergoes endocytic trafficking to late endosomes and lysosomes where low-pH dependendent cathepsin proteases cleave EBOV GP. Following some yet to be determined fusion triggers and interaction with NPC1, fusion occurs and the viral nucleocapsid is released into the cytoplasm. Created using Biorender.com.

1.5 SIGNALING PATHWAYS REQUIRED FOR VIRAL ENTRY

Viral entry into host cells inevitably results in the activation of intracellular signaling cascades. These can be in the form of a cellular response to the incoming pathogen or can be induced by the incoming viral particle to promote efficient entry and establish a favorable intracellular environment for replication. During replication and translation, many viruses produce proteins that alter cell signaling pathways; however, viruses can also activate signaling pathways before replication, relying on attachment factors or receptors on the plasma membrane to initiate early signaling events (186). These include receptor tyrosine kinases (RTKs), integrins, and G-protein coupled receptors (GPCRs) (187-190). While some viruses penetrate the cellular membrane at the cell surface, most require internalization prior to membrane penetration and uncoating (191). In some instances, viruses are internalized via ongoing cellular endocytic processes, however many viruses can also induce their uptake by activating host-cell signaling pathways (192). Furthermore, signaling pathways activated by viruses during entry have also been implicated in post-internalization entry steps, such as facilitating intracellular virion transport to the site of genome replication (193).

1.5.1 Activation of signaling pathways via Receptor Tyrosine Kinases

RTKs are large family of cell-surface receptors, many of which have been implicated as important host factors for mediating viral entry. In humans, there are 58 RTKs that fall into 20 subfamilies, all existing as single protomers and containing an extracellular ligand binding domain, a single transmembrane helix, and a cytoplasmic region that contains a PTK domain through which signal transduction is initiated (149). Signal transduction occurs when single receptors homo-or-heterodimerize, which can be entirely ligand mediated, entirely receptor mediated due to clustering, or a of combination of the two extremes (149). RTKs are regulators

of many cellular processes including cell survival, proliferation, differentiation, cell cycle control, and cell migration, however evidence suggests that many viruses can hijack and activate RTK signaling to promote their entry and replication (149, 194). Activation of RTKs by viruses is thought to occur through direct interaction with viral glycoproteins, as is the case for human cytomegalovirus (HCMV) and platelet-derived growth factor receptor α (PDGFR-α)/epidermal growth factor receptor (EGFR), through interactions with lipids on the viral envelope, as is the case for many enveloped viruses via TAM RTKs, or through other indirect mechanisms that usually result in RTK activation via protomer clustering (195-198).

HCMV glycoprotein mediated binding and activation of PDGFR-α and EGFR is a well-characterized example of a virus that can activate signaling cascades via direct interaction of viral glycoproteins with RTKs. The key HMCV glycoproteins involved in entry are gB, gH, gL, gO, and HMCV proteins UL128-131; these exist in various glycoprotein complexes, the composition of which can differ between strains (199-202). According to the latest studies, gB dependent EGFR activation occurs in concert with a gH dependent β1 integrin interaction and activation of signaling occurs via EGFR-β1 integrin cross-talk (203). With regards to PDGFR-α, recent evidence suggests that the gB-PDGFR-α interaction only occurs in the presence of the gH/gL/gO trimer, which was shown to bind to PDGFR-α directly, seemingly via the N-terminal region of gO (197, 204). These studies highlight the complexities of virus-induced activation of signaling pathways, even when the activation mechanism is through direct interaction with viral proteins.

TAM RTKs, which bind to phosphatidylserine on viral envelopes via adaptor proteins Gas6 or ProteinS, have been broadly implicated in the entry of many different families of enveloped viruses (reviewed extensively in (91)). Studies originally found that expression of

these receptors enhanced entry of pseudotyped virus particles of filoviruses, flaviviruses, arenaviruses, and more (56, 205-209). Specifically, it is thought that TAM receptors help facilitate internalization of viral particles (56, 91, 205, 206). Interestingly, some studies suggest that while the PTK domain of TAM receptors is required for the observed enhancement of virus endocytosis, virus endocytosis can still occur if this domain is deleted (56, 206). While the PTK domain may be dispensable for endocytosis, virus-induced TAM signalling through the PTK domain is certainly important for dampening the cellular innate immune response, which provides a more favorable environment for viral replication (206, 208). In addition to enveloped viruses, the non-enveloped polyomavirus, SV40, can also interact with TAM receptors (210). The VP1 capsid protein of SV40 shares structural homology with Gas6 and can interact with Axl to initiate internalization events (210). Furthermore, Axl knockdown reduces SV40 infection to a greater extent than entry is reduced when virus-like particles are tested, suggesting that signaling may be induced upon interaction with Axl (210). Evidently, more work needs to be done to fully determine the role of virus-induced TAM signalling in facilitating viral entry and infection.

Many viruses employ other indirect mechanisms to activate RTKs, which include promoting heterodimerization with proteins/receptors of a different class or promoting the rather non-specific clustering of RTKs. For example, hepatitis C virus (HCV) can induce EGFR activation presumably via binding to the HCV co-receptor CD81, as CD81 cross-linking was shown to induce EGFR activation (211). Further, EGFR signaling to HRas is required for the lateral membrane diffusion of CD81 to promote its interaction with another HCV coreceptor, claudin1 (CLDN1), which is essential for virion endocytosis (212). Examples of viruses that induce RTK clustering are IAV and Herpes simplex virus 1 (HSV-1). With regards to IAV, attachment to the plasma membrane via sialic acid residues results in clustering of ganglioside

GM1 enriched membrane microdomains, which allows multiple RTKs to come into proximity intrinsically activate (198). Similarly, to IAV, HSV-1 infection induces lipid raft formation and EGFR clustering, which results in EGFR activation, induction of PI3K-Akt and mitogen-activated protein kinase (MAPK) signaling, and subsequent actin cytoskeletal rearrangements (213). For both IAV and HSV-1, activation of EGFR facilitated internalization of virions in the cell lines tested.

1.5.2 Activation of signaling pathways via Integrins

Many viruses also utilize integrins expressed on the cell surface to initiate signaling events. Integrins are heterodimeric cell adhesion molecules consisting of α and β subunits; structurally, they consist of a large extracellular domain, a transmembrane domain, and a smaller cytoplasmic domain (214). Some viruses such as adenoviruses can interact directly with integrins through the RGD (Arg-Gly-Asp) tripeptide motif on their envelope glycoproteins, however many other viruses utilize non-RGD binding domains for integrin interaction as well (188). Regardless of the integrin-binding motifs, virus-integrin interaction changes the quaternary structure of the integrin, resulting in induction of signaling cascades primarily through cytoplasmic focal adhesion kinase (FAK), which can transmit signals through both the PI3K and MAPK signaling pathways (188). Viruses that utilize integrin binding to mediate signal transduction include adenoviruses, echoviruses, rotaviruses, hantaviruses, herpesviruses and more; in these cases, physical interaction with integrins helps mediate virus endocytosis through eventual activation of Rho GTPases and also helps prepare the cell for subsequent replication through activation of the MAPK signaling pathway (193, 215-227). Interestingly, filoviruses have also been shown to require integrins for entry, albeit through regulating endosomal cathepsins rather than binding and internalization (228).

1.5.3 Activation of signaling pathways via GPCRs

G-protein coupled receptors (GPCRs) are a large family of seven-(pass)-transmembrane domain receptors that trigger signaling cascades through second messengers. Compared to integrins and RTKs, there have been few documented cases of virus activated GPCR signaling. However, one obvious example is HIV-1 and its GPCR coreceptors CCR5 and CXCR4 (229, 230). Activation of a cellular actin-depolymerizing factor, cofilin, via CXCR4 is required for HIV-1 entry in resting CD4+ T-cells (229). While signaling through CXCR4 and CCR5 is not required for HIV-1 entry in all cell types, it does appear to be ubiquitously important for the rest of the infectious cycle, including facilitating replication and enhancing virus propagation (231). With regards to other viruses, GPCR antagonists were shown to inhibit entry of filoviruses at a step post attachment but prior to membrane fusion, and G protein-coupled receptor kinase 2 (Grk2) was shown to promote entry of flaviviruses (189, 190). Whether filoviruses and flaviviruses directly activate GPCRs during entry remains to be determined.

1.5.4 Downstream signaling pathways and outcomes

Signaling pathways downstream of RTKs, integrins, and GPCRs overlap to a large extent as they transmit signals from the exterior to interior of the cell. Key signaling pathways activated include the Janus Kinase/Signal Transducer and Activator of Transcription (JAK-STAT) pathway, the nuclear factor kappa-light-chain-enhancer of activated B cells (NFκB) pathway, the PI3K pathway, the MAPK pathway, and the phospholipase C-γ (PLCγ) pathway (186, 188, 232). Activation of these pathways can result in different outcomes depending on many factors including cell type or crosstalk from other signaling pathways. While downstream signaling pathways activated by viruses to facilitate entry are incompletely characterized, and therefore difficult to tease out, a common theme are kinases involved in regulating actin dynamics, such as

Rho GTPase family members and the PI3K/Akt pathway (232). Many viruses also activate the p38 MAPK pathway to promote infection (233). However, while this pathway is often activated during entry, its activation is rarely required for entry (exceptions include certain adenoviruses and avian reovirus) (233-236).

1.6 RATIONALE, HYPOTHESIS, AND OBJECTIVES

Ebola virus entry is a multistep process requiring attachment to the host cell, internalization by macropinocytosis, and trafficking to late endosomes and lysosomes where fusion triggering factors are localized. Given that virus internalization by macropinocytosis needs to be triggered, in conjunction with the requirement for trafficking through the endosomal labyrinth, we hypothesize that EBOV hijacks host cell signaling pathways to ensure efficient entry into host cells. The overarching objective of this thesis was to identify signaling pathways that EBOV utilizes during entry and to determine if these are activated by the virus or if EBOV relies on steady state signaling in host cells. Furthermore, by employing a chemical biology approach, we aimed to identify small molecules that target host kinases involved in entry, a process that is highly conserved among filoviruses, to serve as a starting point for antiviral drug development.

The specific aims for each chapter are as follows:

<u>Chapter 2: Identify signaling pathways involved in entry through screening a kinase inhibitor library</u>

a) Screen a kinase inhibitor library to identify small molecules that modulate entry of EBOV and MARV
b) Determine the mechanism of action of receptor tyrosine kinase inhibitors (top screen hits)
c) Assess if EBOV activates RTK-dependent signaling pathways during entry

Chapter 3: Assess the role of sphingosine kinases in EBOV entry

a) Confirm the antiviral target of screen hits PF-543 and FTY720
b) Determine the mechanism of action of sphingosine kinase inhibitors
c) Further characterize the role of sphingosine-1-phosphate signaling for EBOV entry
d) Determine if the sphingosine kinase inhibitors block entry of other late penetrating viruses

Chapter 4: Further characterize the role of diacylglycerol kinases in EBOV entry using a chemical biology approach

a) Characterize the antiviral profile of diacylglycerol kinase inhibitor, R-59-022
b) Determine the mechanism of action of R-59-022

Chapter 2: Ebola virus triggers receptor tyrosine kinase-dependent signaling to promote the delivery of viral particles to entry-conducive intracellular compartments

Corina M. Stewart[1,2,3], Alexandra Phan[1,2,3], Yuxia Bo[1,2,3], Nicholas D. LeBlond[1,3], Tyler K.T. Smith[1,3], Geneviève Laroche[1], Patrick M. Giguère[1], Morgan D. Fullerton[1,3], Martin Pelchat[1], Darwyn Kobasa[4,5], Marceline Côté[1,2,3*]

[1] Department of Biochemistry, Microbiology and Immunology, University of Ottawa, Ottawa, Canada

[2] Ottawa Institute of Systems Biology, University of Ottawa, Ottawa, Canada

[3] Centre for Infection, Immunity, and Inflammation, University of Ottawa, Ottawa, Canada

[4] Special Pathogens Program, National Microbiology Laboratory, Public Health Agency of Canada, Winnipeg, Canada

[5] Department of Medical Microbiology, University of Manitoba, Winnipeg, Canada

* Corresponding author

This chapter has been previously published in PLoS Pathogens.

C. M. Stewart *et al.*, Ebola virus triggers receptor tyrosine kinase-dependent signaling to promote the delivery of viral particles to entry-conducive intracellular compartments. *PLoS Pathog* **17**, e1009275 (2021).

Author contributions: AP performed the flow virometry and Annexin V staining experiments. YB performed the MLV pseudotype virus panel experiments. NL and TS (supervised by MF) extracted, differentiated, and seeded murine BMDMs. GL (supervised by PG) planned and helped conduct calcium signaling experiments (data not incorporated). DK performed replication competent EBOV experiments. CS conducted all other experiments. MP performed data analysis for the screen. Figures were produced by CS. Manuscript was written by CS and MC and edited by CS, MC, PG, MF, MP, and DK.

2.1 ABSTRACT

Filoviruses, such as the Ebola virus (EBOV) and Marburg virus (MARV), are causative agents of sporadic outbreaks of hemorrhagic fevers in humans. To infect cells, filoviruses are internalized via macropinocytosis and traffic through the endosomal pathway where host cathepsin-dependent cleavage of the viral glycoproteins occurs. Subsequently, the cleaved viral glycoprotein interacts with the late endosome/lysosome resident host protein, Niemann-Pick C1 (NPC1). This interaction is hypothesized to trigger viral and host membrane fusion, which results in the delivery of the viral genome into the cytoplasm and subsequent initiation of replication. Some studies suggest that EBOV viral particles activate signaling cascades and host-trafficking factors to promote their localization with host factors that are essential for entry. However, the mechanism through which these activating signals are initiated remains unknown. By screening a kinase inhibitor library, we found that receptor tyrosine kinase inhibitors potently block EBOV and MARV GP-dependent viral entry. Inhibitors of epidermal growth factor receptor (EGFR), tyrosine protein kinase Met (c-Met), and the insulin receptor (InsR)/insulin like growth factor 1 receptor (IGF1R) blocked filoviral GP-mediated entry and prevented growth of replicative EBOV in Vero cells. Furthermore, inhibitors of c-Met and InsR/IGF1R also blocked viral entry in macrophages, the primary targets of EBOV infection. Interestingly, while the c-Met and InsR/IGF1R inhibitors interfered with EBOV trafficking to NPC1, virus delivery to the receptor was not impaired in the presence of the EGFR inhibitor. Instead, we observed that the NPC1 positive compartments were phenotypically altered and rendered incompetent to permit viral entry. Despite their different mechanisms of action, all three RTK inhibitors tested inhibited virus-induced Akt activation, providing a possible explanation for how EBOV may activate

signaling pathways during entry. In sum, these studies strongly suggest that receptor tyrosine kinases initiate signaling cascades essential for efficient post-internalization entry steps.

2.2 INTRODUCTION

In order for viruses to replicate, they must first deliver their genetic material into host cells. With regards to enveloped viruses specifically, this requires fusion of the viral membrane with the cellular membrane, a process that is mediated by viral fusion proteins that protrude from the viral envelope. Upon specific triggers, including but not limited to viral receptor interaction, these viral fusion proteins will undergo extensive conformational rearrangements to facilitate membrane fusion [1]. In the last few years, some enveloped viruses, such as Ebola virus (EBOV) and Lassa fever virus (LASV), have been found to require interaction with entry receptors localized in late endosomes and/or lysosomes [2-5]. In these instances, the viral particles must not only be endocytosed, but also require trafficking to the specific intracellular compartment containing host factors necessary for fusion triggering. However, it is still unclear whether these viruses use mechanisms to regulate their trafficking within the endosomal system or are passive passengers of intracellular vesicles.

Filoviruses, including EBOV and Marburg virus (MARV), are zoonotic pathogens that can cause severe hemorrhagic fevers in humans and non-human primates [6]. Previous studies have shown that the filovirus entry receptor is the late endosome/lysosome-resident protein Niemann-Pick C1 (NPC1) [2-4]. To reach NPC1, filoviral particles must be internalized via macropinocytosis and then undergo extensive trafficking through the endosomal labyrinth whereby endosomes transition from Rab5+ to Rab7+ compartments [7-9]. Also involved in filovirus trafficking to NPC1 are the homotypic fusion and protein sorting (HOPS) and PIKfyve/ArPIKfyve/Sac3 (PAS) tethering and trafficking complexes [2, 10-12]. These

complexes, along with the small GTPase Rab7, regulate vesicular fusion events required for specific trafficking of cargoes to late endosomes and lysosomes in cells [13, 14]. While the activity of Rab7, HOPS, and PAS can be modulated by various stimuli [15, 16], whether EBOV can also regulate these host trafficking proteins remains to be determined.

Using a probe that binds to phosphatidylinositol (3,5)bisphosphate (PtdIns(3,5)P_2), the product of PIKfyve within the PAS complex, we previously found that PtdIns(3,5)P_2 was increased during EBOV entry, suggesting that viral particles can stimulate the activity of the PAS complex [10]. Although the mechanism through which this occurs is still unknown, previous studies have shown that Akt, part of the phosphoinositide 3-kinase (PI3K)/Akt pathway, can activate PIKfyve [16]. Furthermore, Saeed et al. found that EBOV triggers Akt phosphorylation and that the PI3K/Akt pathway was required for EBOV trafficking [17]. Therefore, it is plausible that EBOV stimulates the activity of the PAS complex through activating the PI3K/Akt signaling pathway. However, the mechanism through which EBOV may activate Akt, a primarily cytosolic protein, is still unclear. We propose that EBOV activates host signaling pathways upon contact with the host cell that function to "prime" the cell for both entry and subsequent replication.

To identify signaling pathways important for filovirus entry, we screened a library of kinase inhibitors using pseudotypes harboring the EBOV, MARV or vesicular stomatitis virus (VSV) glycoproteins. We found that receptor tyrosine kinase (RTK) inhibitors potently block EBOV and MARV GP-dependent viral entry. More specifically, inhibitors of epidermal growth factor receptor (EGFR), c-Met, and the insulin receptor (InsR)/insulin like growth factor 1 receptor (IGF1R) blocked filoviral GP-mediated entry and growth of replicative EBOV. Interestingly, while the c-Met and InsR/IGFR inhibitors both interfered with EBOV trafficking

to NPC1, virus delivery to the receptor was not impaired in the presence of an EGFR inhibitor. However, the NPC1+ compartments were altered phenotypically and were rendered incompetent to permit viral entry. Interestingly, despite their different mechanisms of action, all three RTK inhibitors tested inhibited virus-induced Akt activation. These studies strongly suggest that receptor tyrosine kinases initiate signaling cascades that are essential for efficient EBOV post-internalization entry steps.

2.3 RESULTS

2.3.1 Screening of a kinase inhibitor library for the identification of signaling pathways required for filovirus GP-mediated entry.

To identify signaling pathways important for filovirus entry, we screened a library of small-molecule kinase inhibitors using murine leukemia virus (MLV) pseudotyped with the glycoproteins of EBOV, MARV, or VSV. Due to the toxicity inherent to the mucin domain of EBOV GP that leads to low virus yield, we used an EBOV GP construct with this region deleted (EBOV GPΔmuc, herein simply referred to as EBOV GP)[18]. Previous work has shown that this construct does not interfere with the overall EBOV entry pathway and likewise requires cathepsin cleavage and NPC1 binding to mediate infection [19]. In addition, to minimize the effect of signaling induced by growth factors found in the serum used to culture the cells, Vero cells were serum-starved during pre-incubation with 1μM of each inhibitor. MLV pseudotypes encoding β-galactosidase (LacZ) were then added for four hours, after which cells were placed in media containing ammonium chloride to stop entry. Twenty-four hours post-infection, media was replaced again, and cells incubated for another 48 hours to allow for the expression of the reporter gene. Transduction efficiency was measured using a luminescence-based substrate and normalized to vehicle-treated cells. Ratios of signals from EBOV or MARV pseudotypes over

that of VSV were then calculated. VSV pseudotypes were used as controls because the entry pathway of VSV is different than that of filoviruses; it is internalized via clathrin-dependent endocytosis and VSV G-mediated fusion occurs in early endosomes [20, 21]. In addition, inhibitors that exert effects on MLV reverse-transcription, integration, or reporter gene transcription are expected to have similar effects on all pseudotypes, including VSV, and as such will not be identified as hits in our analysis. We also assessed potential effects of inhibitor treatment on cellular proliferation and metabolic activity using CellTiter Glo 24 hours post-treatment. Transduction data from inhibitors that had metabolic activity lower than 80% of the vehicle controls were eliminated.

Volcano plots of the p-values versus ratios over VSV revealed 35 compounds that had a significant effect on EBOV and/or MARV GP-mediated infection when compared to VSV (Figure 2.1A and 2.1B, Table S2.1, Table S2.2, Appendix 2). Interestingly, none of the 35 compounds enhanced infection – all were found to be inhibitory. Of the 35 hits, 10 were shared by EBOV and MARV, while 12 and 13 were unique to EBOV or MARV GP-mediated infection respectively (Figure 2.1B), suggesting some overlap between the signaling pathways used by these filoviruses. Importantly, some hits and their targets were previously shown to have an effect on filovirus GP-mediated infection, including AMP-activated protein kinase (AMPK) (Dorsomorphin)[22] and Akt (MK-2206) [17, 22], thus validating our approach (Figure 2.1C). Some new pathways were also revealed, such as mammalian target of rapamycin (mTOR), mitogen-activated protein kinase (MAPK), and sphingosine-1-phosphate receptors (S1PRs) (Figure 2.1C and 2.1D). Interestingly, we also observed an enrichment of receptor tyrosine kinase (RTK) inhibitors in our hits compared to the overall proportion of RTK inhibitors in the library (Figure 2.1D), suggesting that RTK signaling is important

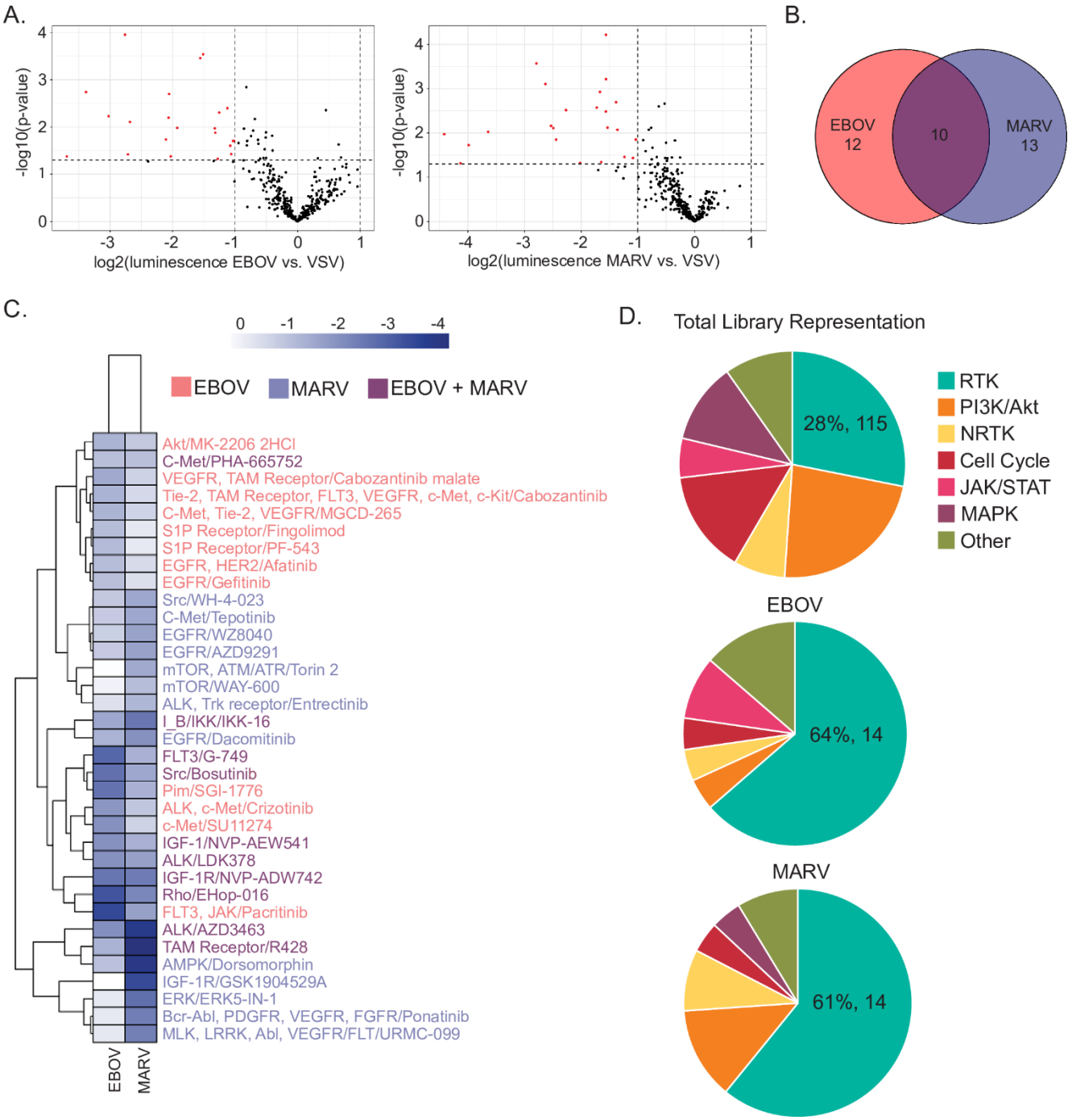
A.
-log10(p-value)
log2(luminescence EBOV vs. VSV)
log2(luminescence MARV vs. VSV)
B.
EBOV
12
10
MARV
13
C.
0 -1 -2 -3 -4
EBOV
MARV
EBOV + MARV
Akt/MK-2206 2HCl
C-Met/PHA-665752
VEGFR, TAM Receptor/Cabozantinib malate
Tie-2, TAM Receptor, FLT3, VEGFR, c-Met, c-Kit/Cabozantinib
C-Met, Tie-2, VEGFR/MGCD-265
S1P Receptor/Fingolimod
S1P Receptor/PF-543
EGFR, HER2/Afatinib
EGFR/Gefitinib
Src/WH-4-023
C-Met/Tepotinib
EGFR/WZ8040
EGFR/AZD9291
mTOR, ATM/ATR/Torin 2
mTOR/WAY-600
ALK, Trk receptor/Entrectinib
I_B/IKK/IKK-16
EGFR/Dacomitinib
FLT3/G-749
Src/Bosutinib
Pim/SGI-1776
ALK, c-Met/Crizotinib
c-Met/SU11274
IGF-1/NVP-AEW541
ALK/LDK378
IGF-1R/NVP-ADW742
Rho/EHop-016
FLT3, JAK/Pacritinib
ALK/AZD3463
TAM Receptor/R428
AMPK/Dorsomorphin
IGF-1R/GSK1904529A
ERK/ERK5-IN-1
Bcr-Abl, PDGFR, VEGFR, FGFR/Ponatinib
MLK, LRRK, Abl, VEGFR/FLT/URMC-099
EBOV
MARV
D.
Total Library Representation
28%, 115
RTK
PI3K/Akt
NRTK
Cell Cycle
JAK/STAT
MAPK
Other
EBOV
64%, 14
MARV
61%, 14

Figure 2.1 A kinase inhibitor screen to identify signaling pathways required for EBOV and MARV GP-mediated entry.

MLV pseudotypes encoding LacZ and harboring EBOV, MARV, or VSV glycoproteins were used to screen the Selleckchem L1200 kinase inhibitor library at 1μM in Vero cells (A) Volcano plots of the log2 values of the ratios of the means of biological replicates of EBOV (left panel) or MARV (right panel) vs VSV pseudotype transduction relative to the DMSO controls over the –log10 values of the p-value. Dots in red represent hits as determined with at least 2-fold ratio and $p<0.05$. Results are means of three independent experiments performed in duplicates. (B) Venn diagram of the hits for EBOV and MARV, with 22 total hits for EBOV, 23 total hits for MARV, and 10 hits shared between the two viruses. (C) Heat maps of the log2(normalized transduction efficiency of EBOV or MARV vs. that of VSV) for the total hits for both viruses. (D) Pie charts of the signaling pathways (grouped into the following categories: receptor tyrosine kinase (RTK) inhibitors, Janus kinase/signal transducers and activators of transcription (JAK/STAT) pathway inhibitors, mitogen-activated protein kinase (MAPK) pathway inhibitors, non-receptor tyrosine kinase (NRTK) inhibitors, and phosphatidylinositol-3-kinase (PI3K)/Akt inhibitors, or others) of the inhibitors in the library (top), EBOV hits (middle), and MARV (bottom). The representation in percentage and the number of the RTK inhibitors is indicated.

Table S2.1 Hits from small molecule kinase screen for EBOV.

Compound	Mean EBOV / Mean VSV	p-value [a]	Targets
Bosutinib (SKI-606)	0.14744	0.00011	Src
Cabozantinib malate (XL184)	0.35110	0.00029	VEGFR, TAM Receptor
IKK-16 (IKK Inhibitor VII)	0.33990	0.00035	IκB, IKK
Ehop-016	0.09569	0.00183	Rho
LDK378	0.24043	0.00201	ALK
PF-543	0.45908	0.00401	S1P Receptor, SK1
MK-2206 2HCl	0.41949	0.00494	Akt
G-749	0.12297	0.00590	FLT3
NVP-AEW541	0.23904	0.00635	IGF-1R
NVP-ADW742	0.15585	0.00781	IGF-1R, InsR
Crizotinib (PF-02341066)	0.26316	0.01045	ALK, c-Met
R428 (BGB324)	0.39924	0.01072	TAM Receptor
Cabozantinib (XL184, BMS-907351)	0.40127	0.01322	Tie-2, TAM Receptor, FLT3, VEGFR, c-Met, c-Kit
AZD3463	0.23228	0.01842	ALK
Gefitinib (ZD1839)	0.48905	0.01972	EGFR
PHA-665752	0.49418	0.01987	c-Met
Afatinib (BIBW2992)	0.47394	0.02491	EGFR, HER2
Fingolimod (FTY720) HCl	0.47949	0.03755	S1P Receptor
SGI-1776 free base	0.15245	0.03809	Pim
SU11274	0.24481	0.04192	c-Met
Pacritinib	0.07734	0.04214	FLT3, Jak
MGCD-265	0.41277	0.04714	c-Met, Tie-2, VEGFR

Src, proto-oncogene tyrosine-protein kinase Src; VEGFR, vascular endothelial growth factor receptor; TAM Receptor, Tyro3, Axl, and Mer Receptors; ALK, anaplastic lymphoma kinase; S1P Receptor, sphingosine-1-phosphate receptor; SK1, sphingosine kinase 1; Akt, protein kinase B; FLT3, fms-like tyrosine kinase 3; IGF-1R, insulin-like growth factor 1 receptor; InsR, insulin receptor; c-Met, tyrosine protein kinase Met; Tie-2, angiopoietin-1 receptor; c-Kit, mast/stem cell growth factor receptor; EGFR, epidermal growth factor receptor; HER2, human epidermal growth factor receptor 2; Pim, proto-oncogene serine/threonine-protein kinase; Jak, janus kinase.

[a] p-values were calculated using a two-tailed student's t test

Table S2.2 Hits from small molecule kinase screen for MARV.

Compound	Mean EBOV / Mean VSV	p-value[a]	Targets
Tepotinib (EMD 1214063)	0.33839	0.00006	c-Met
ERK5-IN-1	0.14453	0.00027	ERK
Bosutinib (SKI-606)	0.33863	0.00061	Src
IKK-16 (IKK Inhibitor VII)	0.16121	0.00078	IκB/IKK
AZD9291	0.31426	0.00118	EGFR
NVP-AEW541	0.38270	0.00201	IGF-1R
LDK378	0.30200	0.00268	ALK
EHop-016	0.20754	0.00305	Rho kinase
WH-4-023	0.33797	0.00329	Src
NVP-ADW742	0.17288	0.00688	IGF-1R, InsR
Torin 2	0.34467	0.00756	mTOR, ATM/ATR
Ponatinib (AP24534	0.17750	0.00775	Bcr-Abl, PDGFR, VEGFR, FGFR
G-749	0.38916	0.00843	FLT3
GSK1904529A	0.08005	0.00939	IGF-1R
R428 (BGB324)	0.04676	0.01063	TAM Receptors
PHA-665752	0.48744	0.01410	c-Met
URMC-099	0.18381	0.01412	MLK, LRRK, Abl, VEGFR
AZD3463	0.06306	0.01877	ALK
Entrectinib (RXDX-101	0.42418	0.03475	ALK, Trk receptor
WAY-600	0.47060	0.03693	mTOR
WZ8040	0.31926	0.04530	EGFR
Dacomitinib (PF299804, PF299)	0.24645	0.04779	EGFR
Dorsomorphin (Compound C	0.05700	0.04837	AMPK

c-Met, tyrosine protein kinase Met; ERK, extracellular signal-regulated kinases; Src, proto-oncogene tyrosine-protein kinase Src; EGFR, epidermal growth factor receptor; IGF-1R, insulin-like growth factor 1 receptor; ALK, anaplastic lymphoma kinase; Rho; InsR, insulin receptor; mTOR, mammalian target of rapamycin; ATM, ataxia telangiectasia mutated; ATR, ATM and RAD3-related; PDGFR, platelet-derived growth factor receptor; VEGFR, vascular endothelial growth factor receptor; FGFR, fibroblast growth factor receptor; FLT3, fms-like tyrosine kinase 3; TAM Receptor, Tyro3, Axl, and Mer Receptors; MLK, mixed-lineage kinase; LRRK, leucine-rich repeat kinase; Trk, tropomyosin receptor kinase; AMPK, AMP-activated protein kinase.

[a] p-values were calculated using a two-tailed student's t test

for EBOV and MARV entry. In sum, the results of this small molecule screen indicate that specific signaling pathways, particularly RTK signaling, are required for filovirus entry.

2.3.2 Receptor tyrosine kinase inhibitors block entry of multiple filoviruses and growth of replicative EBOV in Vero cells.

To confirm the effect of RTK inhibitors on EBOV GP-mediated entry, we used filoviral-like particles (VLPs) generated by co-expression of the EBOV nucleoprotein (NP), matrix protein (VP40), and the glycoprotein of interest [23]. These viral particles exhibit the characteristic filamentous morphology of filoviral particles, can enter target cells according to the entry pathway of the viral glycoproteins expressed on their surface, and allow measurement of membrane fusion in cells by using a VP40 construct that is fused with β-lactamase (βlam) [23]. Using this system, we first tested a panel of RTK inhibitors identified as screen hits and measured viral entry into Vero cells using VLPs bearing EBOV GP or VSV G (Figure S2.1). We found that RTK inhibitors of EGFR, c-Met, InsR/IGF1R, or multiple RTKs, blocked EBOV GP-mediated entry and had no significant effect on VSV G-mediated entry (Figure S2.1). To further investigate and dissect the RTK signaling requirements, we performed dose-response studies of the specific inhibitors of EGFR (Gefitinib), c-Met (SU11274), or InsR/IGF1R (NVP-ADW742) and found that all reduced EBOV GP-mediated entry (Gefitinib IC50=1.8 μM, SU11274 IC50=0.7 μM, NVP-ADW742 IC50=1 μM) (Figure 2.2A). Importantly, these had either no effect or slightly increased VSV G-mediated entry (Figure 2.2A). To confirm that the absence of the mucin domain did not influence the potency of the RTK inhibitors, we infected Vero cells with EBOV VLPs bearing EBOV ΔM GP or EBOV full length GP and did not observe a difference between the two GPs (Figure S2.2). Additionally, we tested entry mediated by two other highly pathogenic ebolaviruses, Bundibugyo (BDBV) and Sudan (SUDV). We found that

the three RTK inhibitors blocked entry mediated by all filovirus GPs tested in our panel, (Figure 2.2B), suggesting that they interfere with an entry step or steps required by all filoviruses.

To investigate the efficacy of the RTK inhibitors on native infection, we next tested their ability to block growth of GFP-expressing replicative EBOV. We found that all drugs were able to inhibit EBOV growth, albeit with different efficiency (Figure 2.2C). The InsR/IGF1R inhibitor, NVP-ADW742, was the most potent and completely blocked replicative EBOV infection at 5 μM, while the c-Met inhibitor, SU11274, required 10 μM for complete inhibition. Although viral replication was still observed in the presence of Gefitinib at 10 μM, the compound was able to reduce EBOV growth (Figure 2.2C). Taken together, these results indicate that RTK inhibitors can block entry by several pathogenic filoviruses and growth of replicative EBOV.

2.3.3 The antiviral effects of Gefitinib, SU11274, and NVP-ADW742 are specific to filoviral entry

To investigate the specificity of the RTK inhibitors on filoviral entry, we next tested entry of MLVs bearing glycoproteins from viruses that utilize a variety of different entry routes. Specifically, we used MLV pseudotypes of LASV, lymphocytic choriomeningitis virus (LCMV), and Junin virus (JUNV), which undergo fusion in late or early endosomes following internalization, in addition to Nipah virus (NiV), which utilizes the ephrin receptors for viral entry at the cell surface [24-26]. We found that entry mediated by the LCMV and JUNV glycoproteins was unchanged by the EGFR, InsR/IGF1R, and c-Met inhibitors despite their shared requirement for internalization and endosomal trafficking (Figure 2.3) [27, 28]. LASV entry, which requires low pH and LAMP1 in late endosomes [5], remained mostly unaffected by

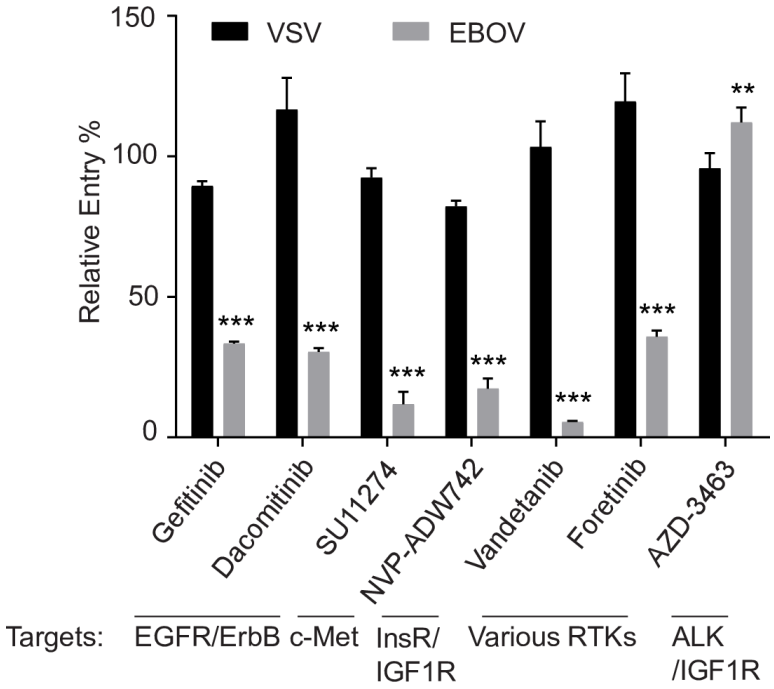

Figure S2.1 Effect of a panel of RTK inhibitors on EBOV GP-mediated entry.

Vero cells were exposed to βlam VLPs harboring the EBOV GP or VSV G in the presence of vehicle (DMSO, 0.1%) or the indicated RTK inhibitor at 1 μM. Viral entry was detected via flow cytometry after loading cells with the βlam substrate, CCF2, and quantifying the percentage of cells with cleaved CCF2. Data are expressed as percentages of inhibitor treated cells relative to vehicle alone. Data are representative of 3 independent experiments. * $p < 0.05$, ** $p < 0.01$, *** $p < 0.001$.

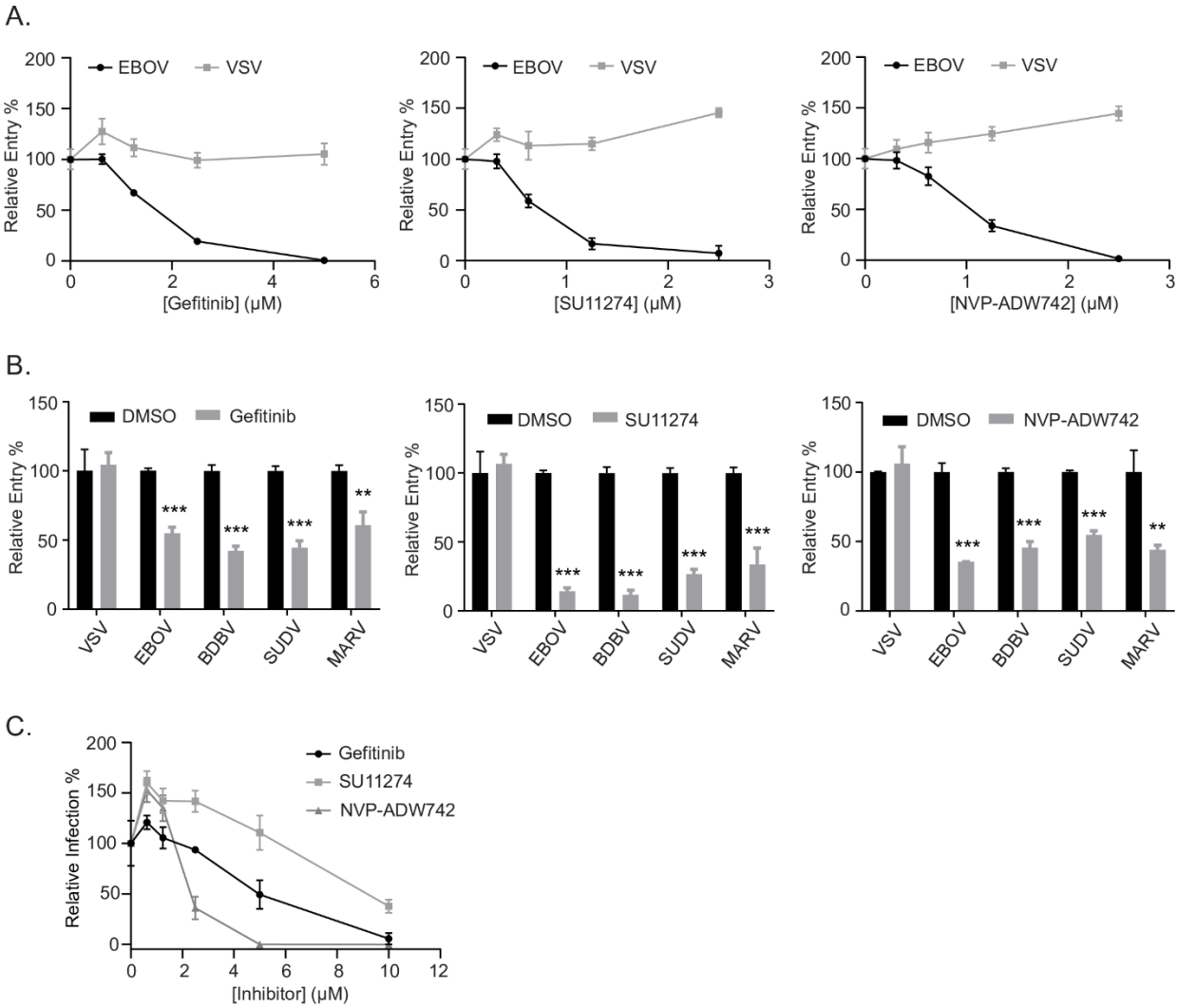

Figure 2.2 RTK inhibitors block filovirus entry in Vero cells.

(A) Entry of βlam VLPs harboring the EBOV GP or VSV G in Vero cells treated with vehicle (DMSO, 0.1%) or increasing concentrations of Gefitinib, SU11274, or NVP-ADW742. Entry was detected via flow cytometry after loading cells with βlam substrate (CCF2) and measuring the percentage of inhibitor treated cells with cleaved CCF2. Data are expressed as percentages relative to DMSO-treated cells. (B) Entry of βlam VLPs bearing the GPs of EBOV, SUDV, BDBV, MARV, or VSV G in the presence of 1 μM Gefitinib, 1 μM SU11274, 1 μM NVP-ADW742, or vehicle (DMSO, 0.1%). (C) Infection of Vero cells with replication-competent EBOV expressing GFP at increasing concentrations of the indicated inhibitor. Infection was measured by GFP fluorescence 3 days post-infection and normalized to vehicle-treated cells. Results are expressed as mean ± s.d. of triplicates and are representative of 3 experiments. * $p < 0.05$, ** $p < 0.01$, *** $p < 0.001$.

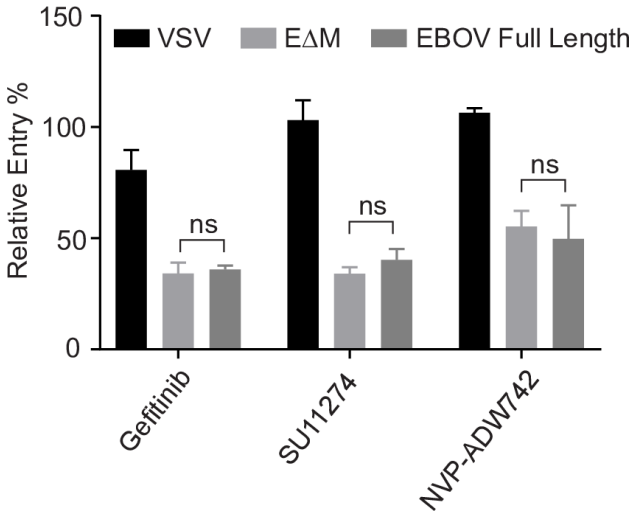

Figure S2.2 RTK inhibitors block entry of EBOV ΔM GP and EBOV Full Length GP to the same extent.

Vero cells were exposed to βlam VLPs harboring VSV-G, EBOV ΔM GP, or the EBOV Full Length GP in the presence of vehicle (DMSO, 0.1%), Gefitinib (1 μM), SU11274 (500 nM), or NVP-ADW742 (500 nM). Entry was detected via flow cytometry after loading cells with βlam substrate (CCF2) and measuring the percentage of cells with cleaved CCF2. Data are expressed as percentages of inhibitor treated cells relative to vehicle alone. Data are representative of 3 independent experiments. Students t-test was performed to compare % entry for EBOV ΔM GP and EBOV Full Length GP.

the inhibitors, although a slight decrease was observed in cells treated with the c-Met inhibitor, SU11274 (Figure 2.3). Interestingly, NiV entry, which occurs at the cell surface [24], was increased in the presence of the inhibitors (Figure 2.3). These results further support the notion that the RTK inhibitors block specific step(s) in filovirus entry.

2.3.4 The effect of RTK inhibitors on EBOV GP-mediated entry in bone marrow-derived macrophages

Previous studies have shown that one of the primary targets of filoviruses in vivo are macrophages [29]. Therefore, we assessed EBOV entry in bone marrow-derived macrophages (BMDMs) in the presence of the inhibitors. We found that while both SU11274 and NVP-ADW742 efficiently blocked EBOV GP-mediated entry, Gefitinib had no effect (Figure 2.4A). Entry of VSV G-bearing VLPs into BMDMs was also slightly reduced in the presence of SU11274 and NVP-ADW742 (Figure 2.4A). The lack of inhibitory effect in BMDMs after Gefitinib treatment prompted us to investigate the expression of the inhibitors' targets in both cell types. We found that c-Met and InsR, respective targets of SU11274 and NVP-ADW742, were expressed in both Vero cells and BMDMs (Figure 2.4B). However, expression of EGFR was undetectable in BMDMs (Figure 2.4B). Furthermore, this apparent absence of expression could not be attributed to an inability of the antibody to recognize mouse EGFR, since it could readily detect the protein in mouse embryonic fibroblasts (Figure 2.4B). Overall, these data suggest that RTK inhibitors can efficiently block EBOV entry in different cell types and that the effect is dependent on expression of the specific RTKs targeted by these inhibitors.

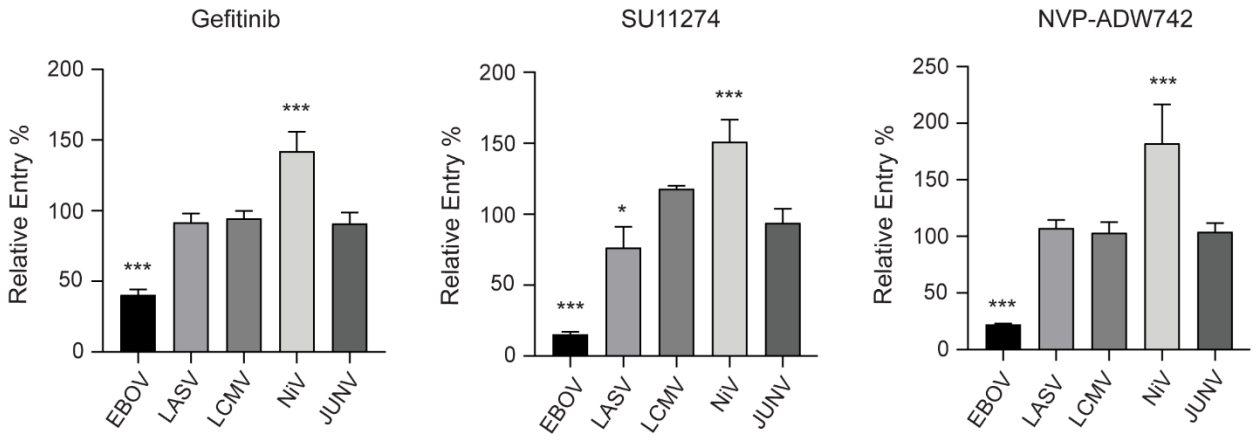

Figure 2.3 RTK inhibitors do not inhibit entry mediated by a panel of other viral GPs.

Vero cells were transduced with MLV pseudotypes encoding LacZ and harboring EBOV, LASV, LCMV, Nipah, or Junin glycoproteins in the presence of Gefitinib (1 μM), SU11274 (1 μM), NVP-ADW742 (1 μM) or vehicle (DMSO, 0.1%). Results are expressed as mean ± s.d. of triplicates and are representative of 3 experiments. * $p < 0.05$, ** $p < 0.01$, *** $p < 0.001$.

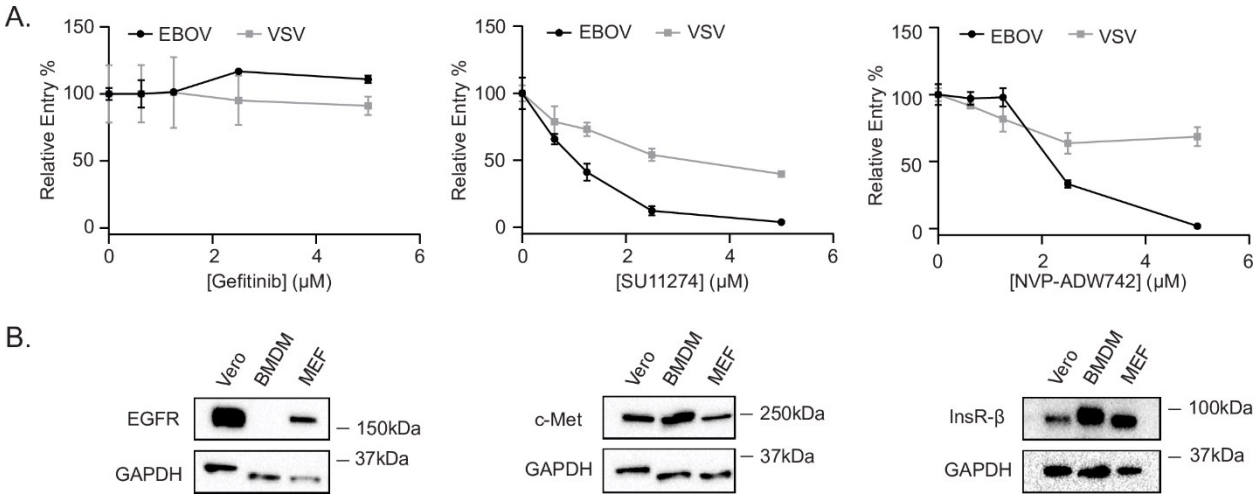

Figure 2.4 Effect of RTK inhibitor treatment on EBOV GP-mediated entry in BMDMs.
(A) Entry of βlam VLPs harboring EBOV GP or VSV G in BMDMs treated with vehicle (DMSO, 0.1%) or increasing concentrations of Gefitinib, SU11274, or NVP-ADW742. (B) Vero cells, BMDMs, and MEFs were serum-starved, lysed, and expression of EGFR, Met, InsR-β, and GAPDH was detected by immunoblotting. Results in (A) are expressed as mean ± s.d. of triplicates and are representative of 3 experiments. Results in (B) are representative blots of 3 independent experiments.

2.3.5 The c-Met and InsR/IGF1R inhibitors interfere with EBOV trafficking to NPC1+ intracellular compartments

Previous studies have shown that influenza A virus (IAV) activates EGFR signaling for internalization into host cells [30]. To test whether RTK signaling is also required for EBOV internalization, we used fluorescent EBOV VLPs containing VP40 fused to mCherry and spinoculated them onto Vero cells at 4°C to prevent internalization. Unbound VLPs were removed, pre-warmed media containing inhibitors or vehicle was added, and cells were incubated at 37°C for 1 hour to allow for VLP internalization. VLPs that were not internalized were then removed from the cell surface using trypsin and the level of fluorescent VLP internalization was measured by flow cytometry. For these experiments, we used the macropinocytosis inhibitor 5-(N-Ethyl-N-isopropyl)amiloride (EIPA) as a control [31]. We found that while EIPA reduced VLP internalization in cells, IC90 concentrations of Gefitinib, SU11274, or NVP-ADW742 did not interfere with EBOV internalization (Figure 2.5A). This indicates that, unlike IAV, EBOV requires RTK signaling for a post-internalization step or steps. To further investigate the mechanism by which RTK inhibitors block EBOV GP-mediated entry, we used fluorescent VLPs harboring the fusion deficient EBOV GP^{F535R} [32]. VLPs bearing EBOV GPF535R are internalized and trafficked similarly to those harboring the wt GP, and while EBOV GPF535R can also bind to NPC1 following cathepsin cleavage [33], it is unable to perform complete membrane fusion [9]. Therefore, these particles can be used to examine VLP accumulation at the site of fusion by microscopy. For these assays, we used HT1080 cells because their flat morphology allows for better visualization of VLPs in NPC1+ compartments. Importantly, EBOV entry into HT1080 cells is also blocked by the RTK inhibitors (Figure S2.3). To determine if the inhibitors interfere with EBOV trafficking to NPC1+ compartments, HT1080

cells were incubated with EBOV GPF535R VLPs in the presence of inhibitors or vehicle for 3 hours. Cells were fixed, immunostained for NPC1, and imaged by confocal microscopy. For these experiments, we used Akt Inhibitor VIII as a control because previous studies have shown an accumulation of EBOV in early endosomal compartments when Akt signaling was inhibited [17]. As we reported previously, we observed that a little over 10% of the VLPs colocalized with NPC1 in DMSO-treated cells (Figure 2.5B and 2.5C) [10]. However, when we blocked Akt signaling using Akt Inhibitor VIII, we found that colocalization of the VLPs with NPC1 was significantly reduced, indicating that they were not able to reach NPC1+ compartments (Fig 2.5C). Interestingly, when we compared the RTK inhibitors, we found that both SU11274 and NVP-ADW742 blocked VLP trafficking to NPC1 (Figure 2.5B and 2.5C). Surprisingly, however, Gefitinib treatment did not reduce VLP colocalization with NPC1, suggesting that the RTK inhibitors have different antiviral mode of actions. We also investigated colocalization of VLPs in vesicles that are NPC1+ and two-pore channel 2 (TPC2)+, which has been reported as the potential EBOV fusion-conducive compartment [9, 34, 35]; however, we did not observe a notable difference in VLP localization between vehicle- or Gefitinib-treated cells (Figure S2.4A and S2.4C). This further suggests that, unlike the other RTK inhibitors, Gefitinib does not block EBOV trafficking. Taken together, these data indicate that the RTK inhibitors have no effect on EBOV VLP internalization; instead, both SU11274 and NVP-ADW742 interfere with delivery of EBOV to its receptor.

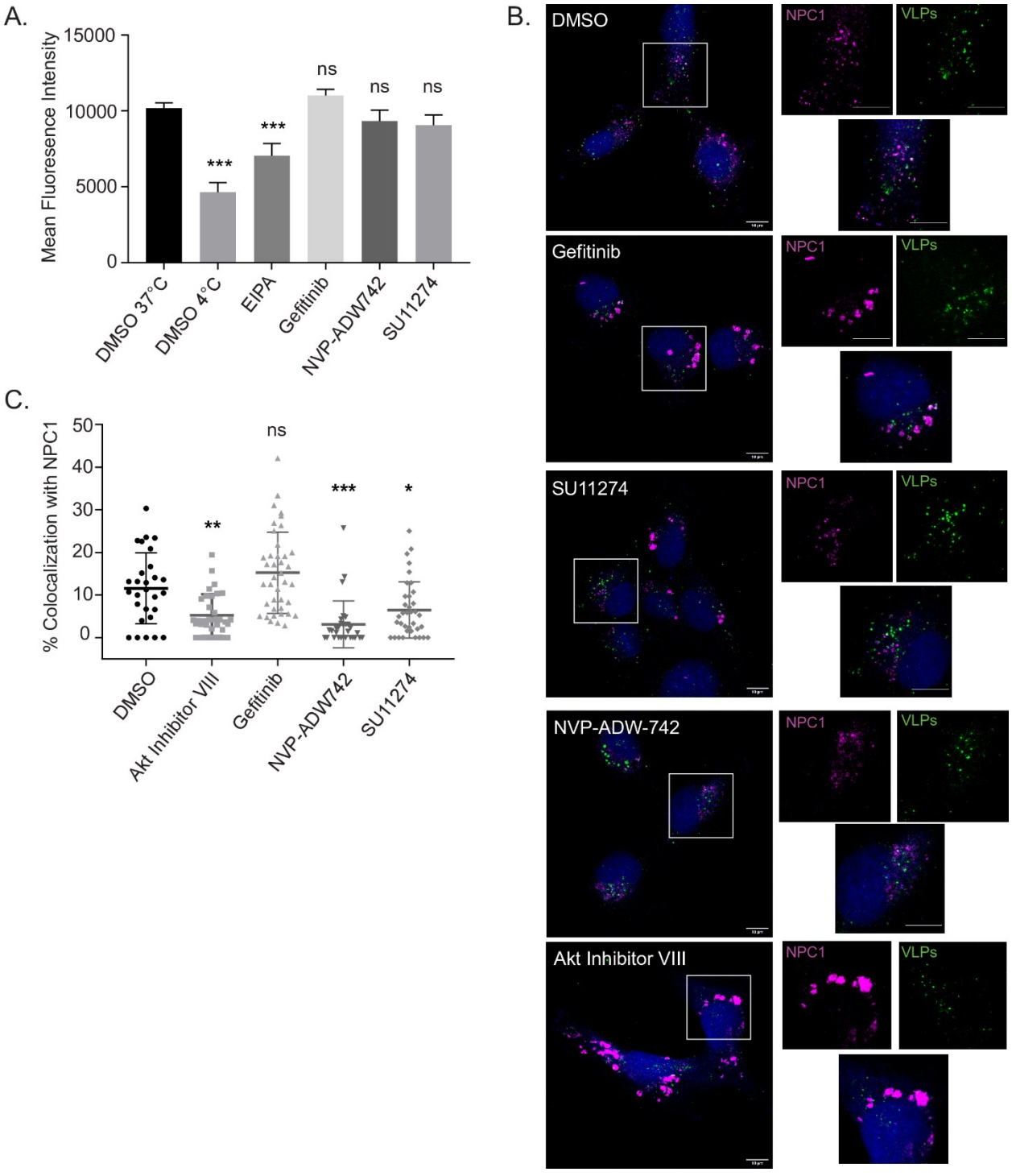
A.
Mean Fluorescence Intensity
15000
10000
5000
0
***
***
ns
ns
ns
DMSO 37°C
DMSO 4°C
EIPA
Gefitinib
NVP-ADW742
SU11274
C.
% Colocalization with NPC1
50
40
30
20
10
0
**
ns
***
*
DMSO
Akt Inhibitor VIII
Gefitinib
NVP-ADW742
SU11274
B.
DMSO
Gefitinib
SU11274
NVP-ADW-742
Akt Inhibitor VIII
NPC1
VLPs

Figure 2.5 RTK inhibitors do not block EBOV VLP internalization, but SU11274 and NVP-ADW742 interfere with trafficking to NPC1+ compartments.

(A) Fluorescent mCherry VLPs harboring EBOV ΔM GP were pre-bound to Vero cells by spinoculation at 4°C, followed by washing and incubation with vehicle (DMSO, 0.1%), EIPA (30 μM), Gefitinib (5 μM), SU11274 (2.5 μM), or NVP-ADW742 (2.5 μM) at 37°C for one hour, or vehicle (DMSO, 0.1%) at 4°C for one hour. Cells were then trypsinized with 0.5% trypsin and mCherry fluorescence analyzed by flow cytometry. (B) Infection of HT1080 cells pre-treated with DMSO (0.1%), Akt Inhibitor VIII (10 μM), Gefitinib (5 μM), SU11274 (2.5 μM), or NVP-ADW742 (2.5 μM) with fluorescent VLPs (Green) harboring the fusion deficient ΔM GP^{F535R} for 3 h. 30 min prior to fixation, CMAC cytoplasmic dye (Blue) was added. Cells were then fixed, permeabilized, and immunostained with rabbit anti-NPC1 and DY650-conjugated antiserum (Magenta). Cells were imaged on an LSM800 confocal microscope (Zeiss). Images are displayed as maximum intensity z-projections, bar = 10 μm. (C) Colocalization between VLPs and NPC1 (of a minimum of 25 cells per condition) were analyzed using Imaris software (Bitplane). Data are representative of 3 independent experiments. * $p < 0.05$, ** $p < 0.01$, *** $p < 0.001$.

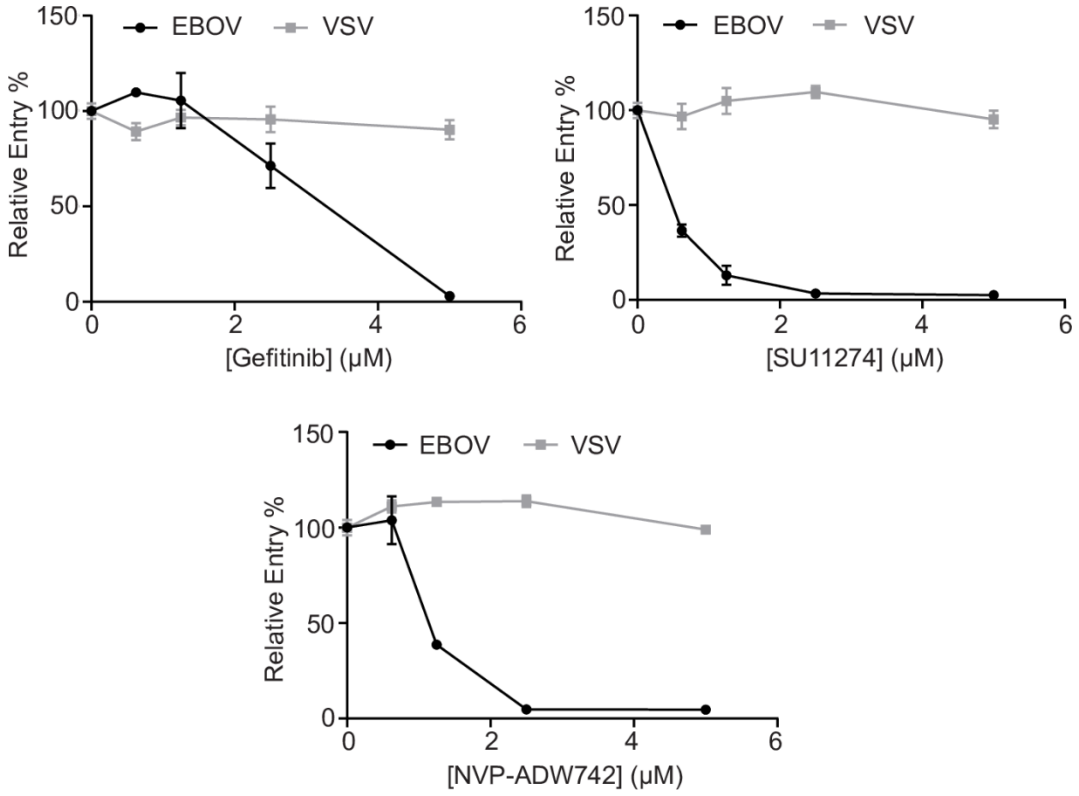

Figure S2.3 RTK inhibitors block filovirus entry in HT1080 cells.

HT1080 were exposed to βlam VLPs harboring the EBOV GP or VSV G in the presence of vehicle (DMSO, 0.1%) or increasing concentrations of Gefitinib, SU11274, or NVP-ADW742. Entry was detected via flow cytometry after loading cells with βlam substrate (CCF2) and measuring the percentage of cells with cleaved CCF2. Data are expressed as percentages of inhibitor treated cells relative to vehicle alone. Data are representative of 3 independent experiments.

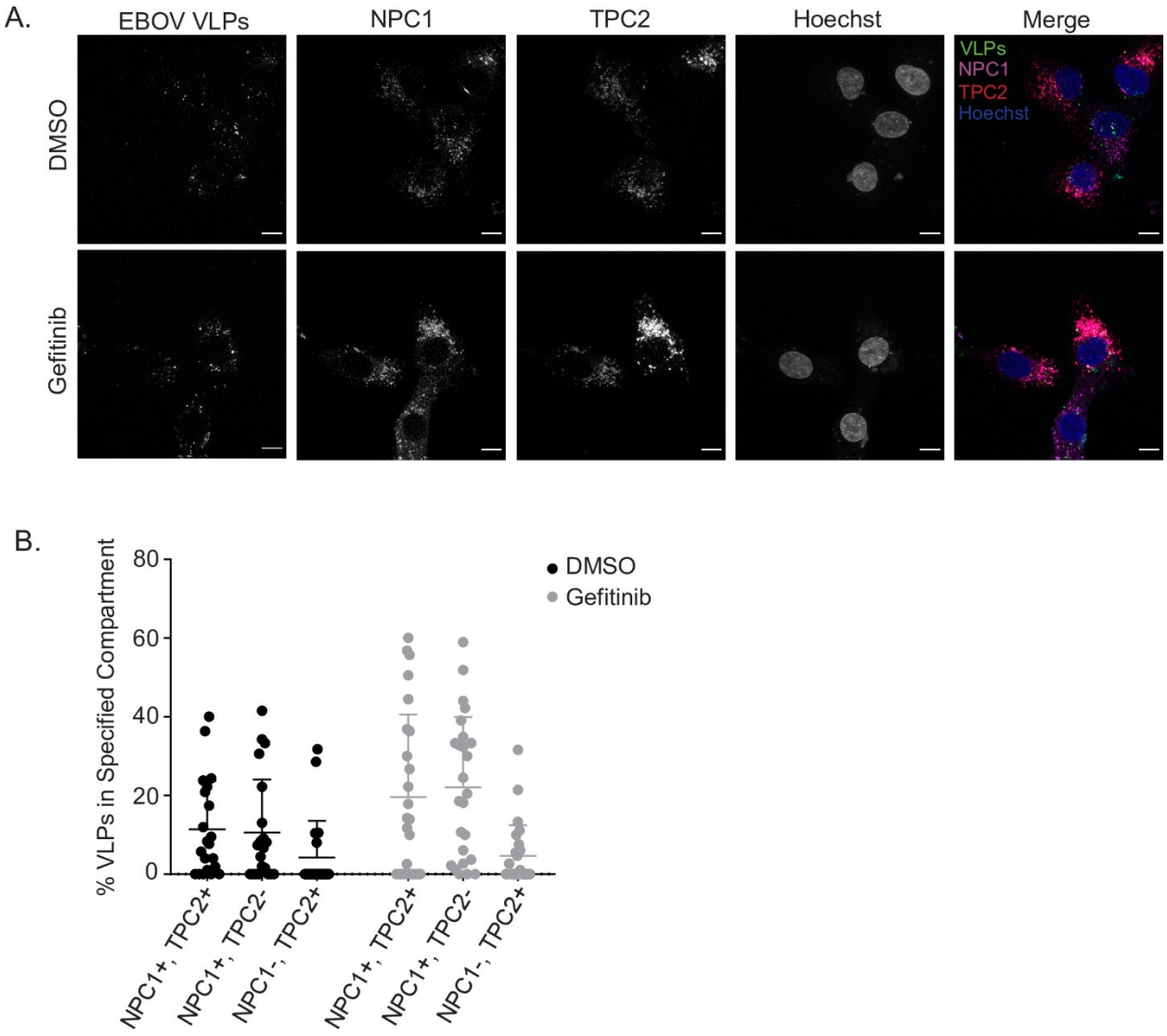

Figure S2.4 Localization of EBOV VLPs in NPC1+ TPC2- compartments does not explain the antiviral activity of Gefitinib.

(A-B) HT1080 cells that were transfected with GFP-TPC2 (Red) and pre-treated with vehicle (DMSO, 0.1%) or Gefitinib (5 μM) were exposed to fluorescent VLPs (Green) harboring the fusion deficient ΔM GP^{F535R} for 3 h. Cells were then fixed, permeabilized, immunostained with rabbit anti-NPC1 and DY650-conjugated antiserum (Magenta), and Hoechst (Blue). Cells were imaged on an LSM800 confocal microscope (Zeiss). Images in (A) are displayed as maximum intensity z-projections, bar = 10 μm. (B) Colocalization between VLPs and NPC1 and/or TPC2 were analyzed using Imaris software (Bitplane). Data are representative of 3 independent experiments. * $p < 0.05$, ** $p < 0.01$, *** $p < 0.001$.

2.3.6 EGFR inhibitor treatment alters the biology and subvesicular localization of NPC1, rendering these compartments non-conducive to EBOV entry

Because Gefitinib did not block EBOV trafficking to NPC1, we sought to analyze the NPC1+ compartment further. One striking phenotype observed in Gefitinib-treated cells was an enlargement of the NPC1+ compartments compared to those in vehicle-treated cells (Figure 2.5B, Figure 2.6A and 2.6B). Quantitative measurement of the volume of these compartments indeed revealed that Gefitinib treatment, as well as treatment with Akt inhibitor VIII, led to a significant increase in their size (Figure 2.6B). However, neither NVP-ADW742 nor SU11274 affected the volume of the NPC1+ compartments. These results indicate that, although EBOV VLPs are delivered to NPC1+ compartments in Gefitinib-treated cells, these compartments are modified and are not conducive to entry. Interestingly, the blunt effect of blocking Akt directly, which caused both an enlargement of NPC1+ compartments and an EBOV VLP trafficking defect, resembles a combination of the phenotypes of Gefitinib, which also causes an enlargement of NPC1+ compartments, and those of SU11274/NVP-ADW742, causing trafficking defects (Figure 2.5C and Figure 2.6B).

Previous studies have associated an enlargement of late endosomes/lysosomes with a decrease in cathepsin activity [36]. Because EBOV GP needs to be cleaved by cathepsin proteases to reveal its receptor binding domain [3, 4, 37, 38], we sought to test whether the mechanism by which Gefitinib blocks EBOV entry involves a decrease in GP cleavage by cathepsins. To investigate this, we experimentally mimicked cathepsin cleavage of GP by pre-treating EBOV VLPs with thermolysin (Figure S2.5A) [39, 40]. Entry of the uncleaved and cleaved VLPs was then measured in Vero cells treated with the RTK inhibitors or the cathepsin B inhibitor (Ca074-Me) as a control. As expected, Ca074-Me blocked entry of the uncleaved

VLPs but was unable to inhibit entry of the pre-cleaved VLPs (Figure S2.5B). In contrast, we found that Gefitinib and the other RTK inhibitors blocked entry of both the uncleaved and cleaved VLPs (Figure S2.5B). Although these results do not completely rule out a defect in cathepsin activity, they suggest that another critical EBOV entry step or steps are inhibited in Gefitinib-treated cells.

Another factor that can lead to enlarged late endosomes/lysosomes is the accumulation of lipids such as cholesterol [41]. To investigate this, we used filipin to test whether cholesterol build-up is induced in Gefitinib-treated cells compared to the other RTK inhibitors and U18666A, a molecule that blocks EBOV entry and induces cholesterol accumulation in cells characteristic of Niemann-Pick C disease [4]. Interestingly, while increased filipin staining in Gefitinib-treated cells was noticeable, we also observed a similar phenotype in SU11274 and NVP-ADW742-treated cells (Figure S2.6). This suggested that cholesterol build-up does not correlate with enlarged NPC1+ compartments nor the ability/inability of EBOV to traffic to NPC1. However, because there was no apparent trafficking defect in Gefitinib treated cells (Figure 2.5C), the accumulation of cholesterol in the presence of Gefitinib could be an indication that NPC1 function is altered. Therefore, we next sought to look more closely at the expression of NPC1 in intraluminal vesicle (ILV) containing endolysosomes, the typical site of cholesterol transport.

Normally, for low-density lipoprotein (LDL) associated cholesterol to be taken up by cells, it must be endocytosed and trafficked to NPC2+ and NPC1+ endolysosomes that are characterized by the presence of ILVs rich in the anionic lipid, lysobisphosphatitic acid (LBPA) [42, 43]. To transport cholesterol from the endolysosome to the endoplasmic reticulum, NPC2 shuttles the cholesterol from the ILVs to NPC1 localized at the limiting membrane of the

endolysosomes [42, 43]. Using LBPA and NPC1 specific antibodies, we examined cells treated with vehicle, Gefitinib, or other EBOV inhibitors (Figure 2.6C). As expected, we observed that irrespective of the drug treatment, NPC1 can be found in both LBPA+ and - compartments. However, the enlarged NPC1+ vesicles found in Gefitinib- and Akt Inhibitor VIII-treated cells were almost all exclusively LBPA+ (Figure 2.6C). By examining the subvesicular localization of NPC1, we found that NPC1 staining surrounded the LBPA-containing vesicles in vehicle treated cells, suggesting the expected presence of NPC1 at the limiting membrane of these intracellular compartments (Figure 2.6C). Interestingly, the localization of NPC1 was substantially changed in the Gefitinib-treated cells; NPC1 seemed to be localized both at the limiting membrane as well as within the vesicles (Figure 2.6C, Figure S2.7A). Further analysis revealed increased colocalization of NPC1 with LBPA (Figure S2.7B), suggesting that Gefitinib treatment causes a redistribution of NPC1 to intraluminal vesicles containing LBPA. Interestingly, this subvesicular localization of the EBOV receptor would presumably be incompatible with cytoplasmic delivery of the ribonucleocapsid. Taken together, our data suggest that treatment of cells with Gefitinib profoundly changes the biology of NPC1+ compartments, rendering them non-conducive to EBOV entry.

2.3.7 EBOV VLPs induce Akt activation in a GP-independent manner

Our findings indicate that the RTK inhibitors have important consequences on EBOV trafficking or the biology of the NPC1+ compartments. A remaining question is whether EBOV activates RTK signaling or if viral entry relies on steady state cell signaling. As mentioned previously, studies using irradiated replicative EBOV have shown that EBOV triggers Akt phosphorylation, a pathway that is activated downstream of RTK stimulation [17]. To investigate

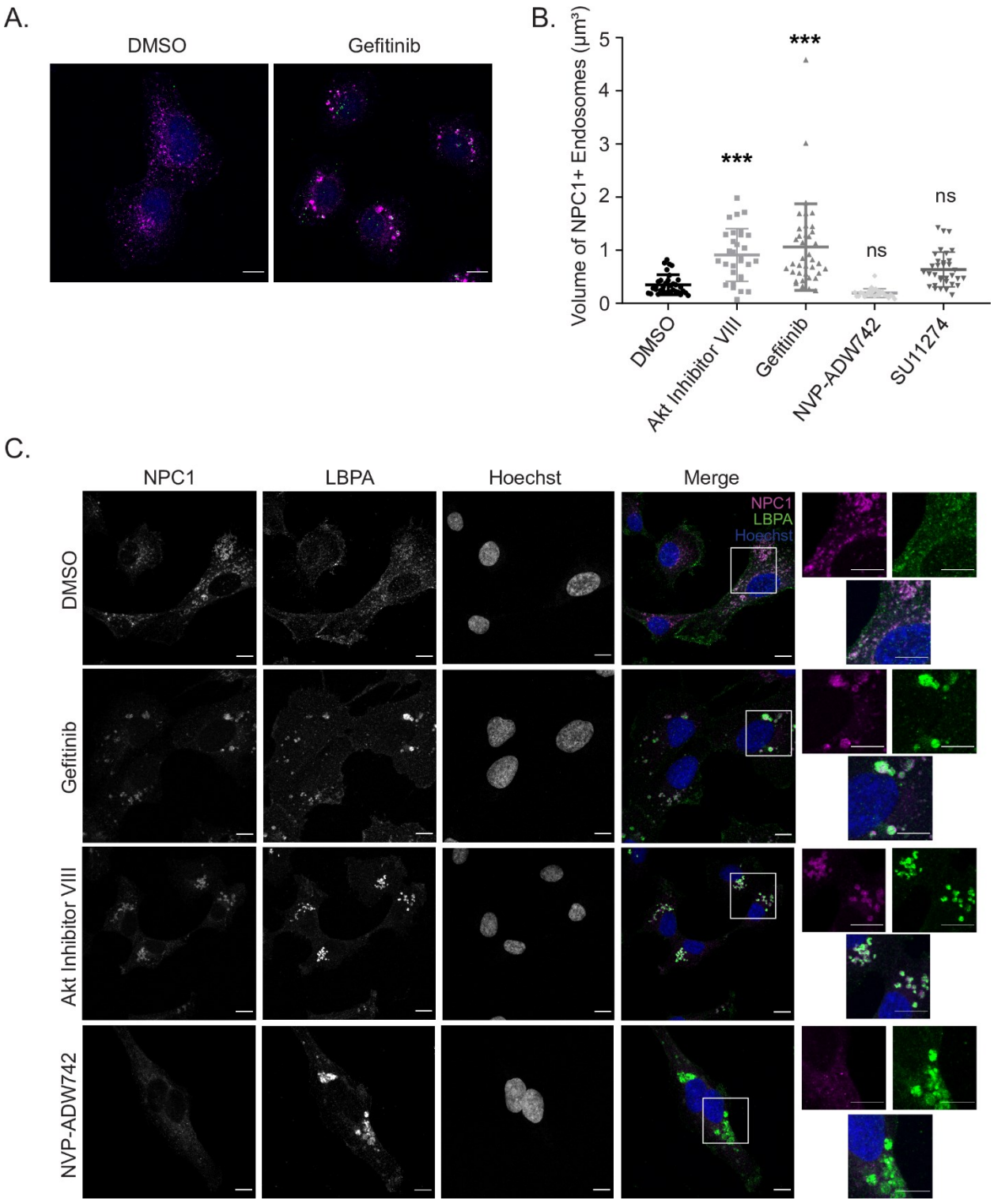
A.
DMSO
Gefitinib
B.
Volume of NPC1+ Endosomes (µm³)
0
1
2
3
4
5
***
***
ns
ns
DMSO
Akt Inhibitor VIII
Gefitinib
NVP-ADW742
SU11274
C.
NPC1
LBPA
Hoechst
Merge
NPC1
LBPA
Hoechst
DMSO
Gefitinib
Akt Inhibitor VIII
NVP-ADW742

Figure 2.6 Gefitinib interferes with the biology of NPC1+ compartments.

(A) Infection of HT1080 cells pre-treated with vehicle (DMSO, 0.1%) or Gefitinib (5 μM) with fluorescent VLPs (Green) harboring the fusion deficient EBOV GP^{F535R} for 3 h. 30 min prior to fixation, CMAC cytoplasmic dye (Blue) was added. Cells were then fixed, permeabilized, and stained for NPC1 (Magenta). Cells were imaged on an LSM800 confocal microscope (Zeiss). Images are displayed as maximum intensity z-projections, bar = 10 μm. (B) Average volume (μm^3) of NPC1+ compartments per cell (of a minimum of 25 cells per condition) was determined by modeling these compartments using Imaris software (Bitplane). (C) HT1080 cells were treated with DMSO (0.1%), Gefitinib (5 μM), Akt Inhibitor VIII (10 μM), or NVP-ADW742 (2.5 μM) for 4 h. Cells were then fixed, permeabilized, and immunostained with rabbit anti-NPC1 and mouse anti-LBPA, followed by DY650-conjugated antiserum (Magenta) or AF555-conjugated antiserum (Green). Following immunostaining, cells were stained with Hoechst (Blue) and imaged on an LSM800 confocal microscope (Zeiss). Images are displayed as maximum intensity z-projections, bar = 10 μm. Data are representative of 3 independent experiments. * $p < 0.05$, ** $p < 0.01$, *** $p < 0.001$.

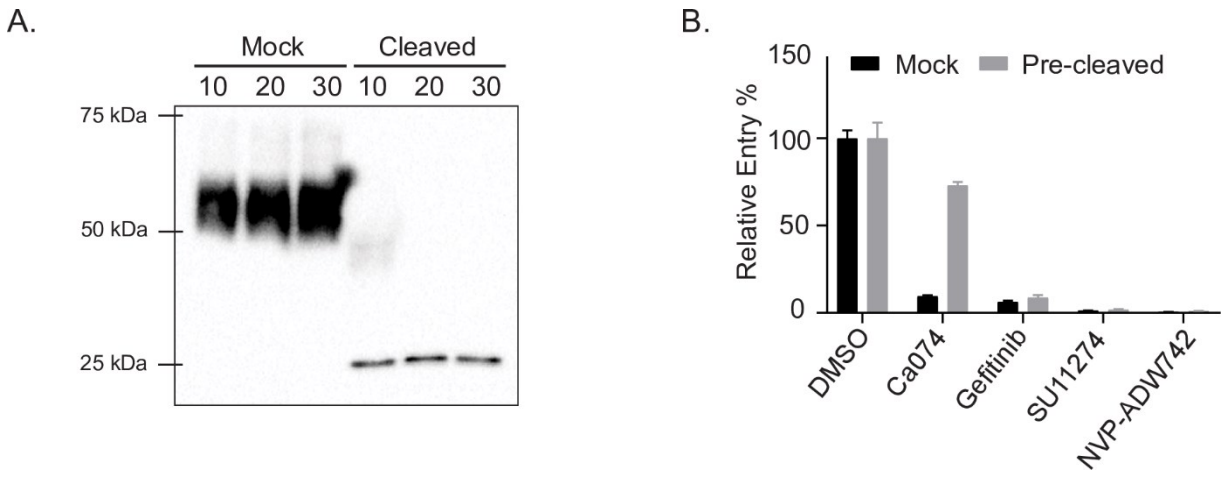

Figure S2.5 RTK inhibitors are sensitive to entry by pre-cleaved EBOV VLPs.

(A) βlam VLPs harboring the EBOV ΔM GP were incubated either with thermolysin (0.2 mg/mL) (Pre-cleaved) or PBS (Mock) for 10, 20, or 30 minutes prior to addition of phosphoramidon (500 μM). Lysates were prepared and immunoblotted for EBOV GP. (B) Pre-cleaved or mock virus that was incubated with thermolysin or PBS for 20 minutes was used to infect Vero cells treated with vehicle (DMSO, 0.1%), Ca074-Me (20 μM), Gefitinib (5 μM), SU11274 (2.5 μM), or NVP-ADW742 (2.5 μM). Entry was detected via flow cytometry after loading cells with βlam substrate (CCF2) and measuring the percentage of cells with cleaved CCF2. Data are expressed as percentages of inhibitor treated cells relative to vehicle alone. Data are representative of 3 independent experiments.

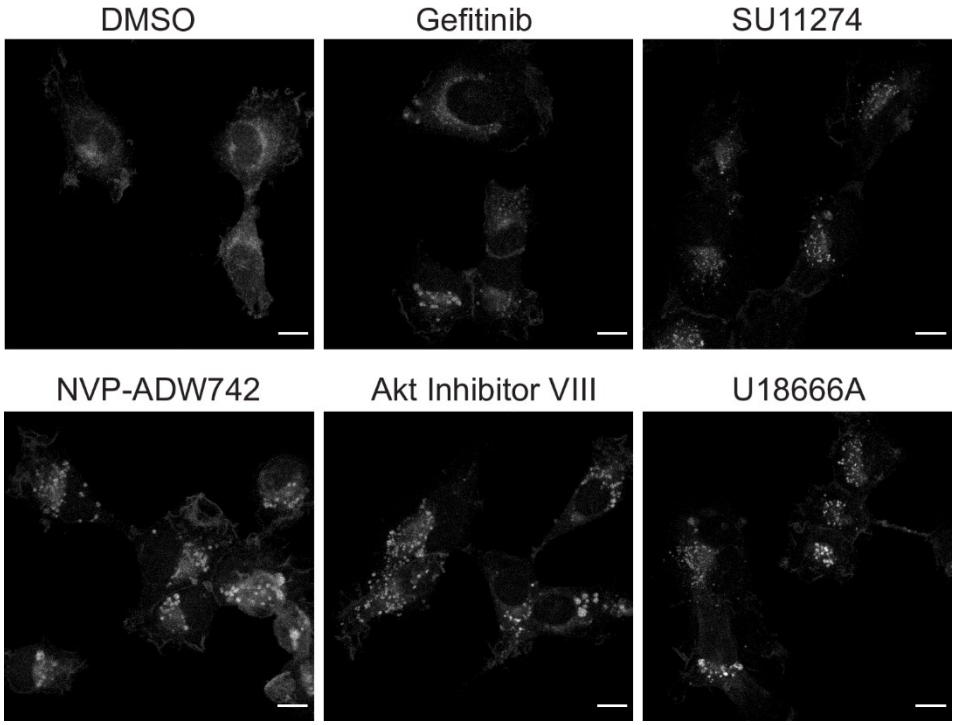

Figure S2.6 Treatment of cells with RTK inhibitors leads to cholesterol accumulation in cells. HT1080 cells were treated with vehicle (DMSO, 0.1%), Gefitinib (5 μM), SU11274 (2.5 μM), NVP-ADW742 (2.5 μM), Akt Inhibitor VIII (10 μM), or U18666A (5 μM) for 4 h. Cells were then fixed, stained with Filipin III, and imaged on an LSM800 confocal microscope (Zeiss). Images are displayed as maximum intensity z-projections, bar = 10 μm. Data are representative of 3 independent experiments.

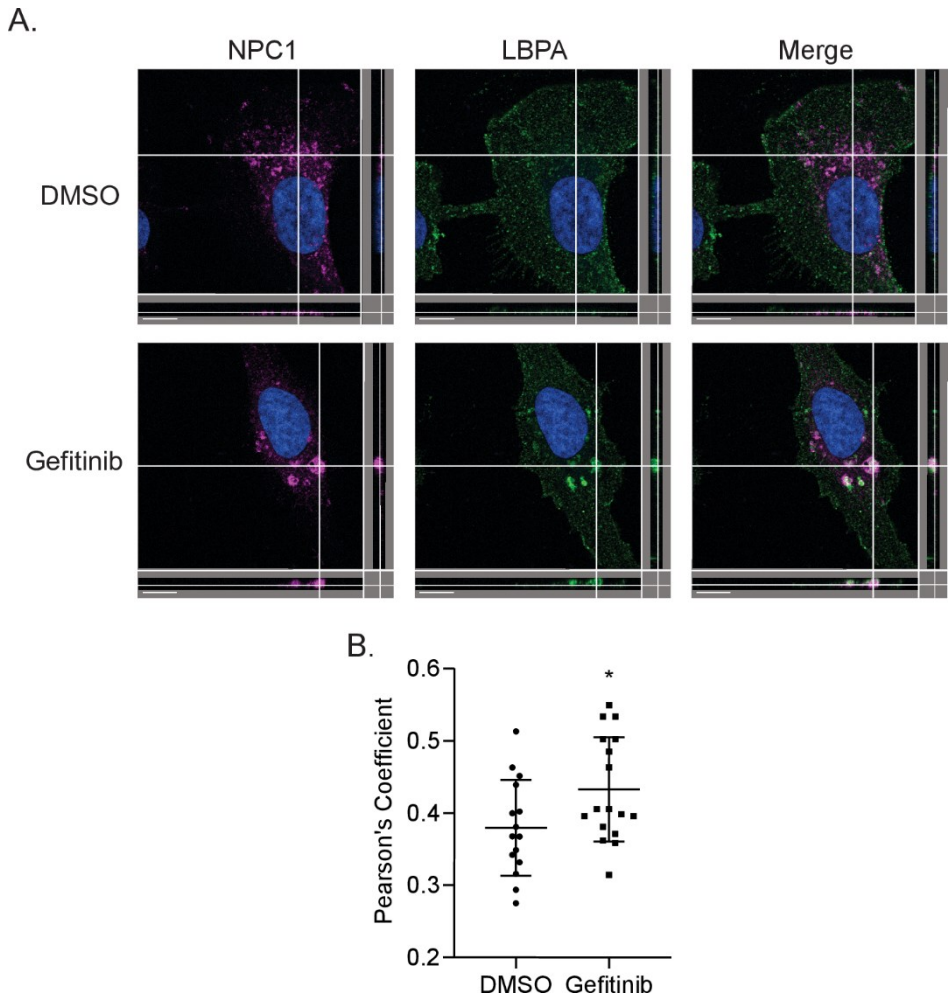

Figure S2.7 LBPA and NPC1 colocalize in Gefitinib treated cells.

(A) HT1080 cells were treated with vehicle (DMSO, 0.1%), Gefitinib (5 µM), or NVP-ADW742 (2.5 µM) for 4 h. Cells were then fixed, permeabilized, and immunostained with rabbit anti-NPC1 and mouse anti-LBPA, followed by DY650-conjugated antiserum (Magenta) or AF555-conjugated antiserum (Green). Following immunostaining, cells were stained with Hoechst (Blue) and imaged on an LSM800 confocal microscope (Zeiss). Images are a cross-sectional view to visualize the Z coordinate axis, bar = 10 µm. (B) Pearson's coefficient was determined per cell for each condition using Imaris (Bitplane) image analysis software. Data are representative of 3 independent experiments. * $p < 0.05$, ** $p < 0.01$, *** $p < 0.001$.

a link between RTKs and Akt during EBOV entry, we first tested whether VLPs harboring EBOV GP can recapitulate the activation observed with irradiated EBOV. We performed a time-course experiment and probed for phosphorylated Akt after Vero cells were exposed to sucrose cushion purified EBOV VLPs or purified supernatant from mock-transfected producer cells (Figure 2.7A). We found that while the mock-transfected cell supernatants induced slight Akt activation at early time points, EBOV VLP-induced Akt activation was stronger and sustained for at least 30 minutes (Figure 2.7A).

Next, we sought to characterize further how VLPs activate Akt phosphorylation in cells. First, we compared Akt activation following incubation with VLPs harboring the full length or mucin deleted EBOV GP and found that both induced Akt phosphorylation to a similar extent in Vero cells (Figure 2.7B) and BMDMs (Figure S2.8). In addition, the kinetics of Akt activation by full length EBOV GP VLPs followed closely that of its mucin-deleted counterpart (Figure 2.7A and Figure S2.9). While these data indicate that the mucin region is not responsible for Akt activation, it is still unclear whether signaling is GP-dependent. Previous studies have shown that EBOV particles have exposed phosphatidylserine (PS) on the outer leaflet of the viral envelope, which has been shown to be actively induced by EBOV via PS flipping mechanisms that can be dependent on GP or VP40 [44, 45]. To test whether induction of Akt phosphorylation can be GP-independent, we produced "bald" VLPs containing EBOV NP and GFP-VP40 but devoid of GP. These GFP+ VLPs can be readily detected by flow cytometry, and using fluorescently labeled annexin V, we confirmed exposure of PS at the surface of VLPs in the presence or absence of GP (Figure S2.10). Importantly, all VLPs were able to activate Akt in cells (Figure 2.7C), strongly suggesting that EBOV can induce Akt phosphorylation in a GP-independent manner.

2.3.8 The RTK inhibitors block EBOV-induced activation

Akt is known to be one of the signaling molecules downstream of RTK activation [46]. The resistance of EBOV GP-mediated entry to Gefitinib treatment in BMDMs, which do not express EGFR, provides evidence that the antiviral targets of these inhibitors are their respective RTKs (Figure 2.4A and 2.4B). To further confirm the specificity of the inhibitors at the concentrations used, we tested the effects of Gefitinib (EGFR inhibitor), NVP-ADW742 (IGF1R/InsR inhibitor), and SU11274 (c-Met inhibitor) on Akt activation induced by their respective growth factors. We found that at the EBOV IC90 concentrations, the c-Met and InsR/IGF1R inhibitors specifically blocked Akt phosphorylation when induced with the RTK growth factor ligand of their respective target (Figure 2.8A). Interestingly, while Gefitinib (the EGFR inhibitor), did abrogate EGF specific Akt phosphorylation, it reduced Akt phosphorylation to a lower level than the serum-starved control, suggesting that Gefitinib blocks both steady-state signaling in unstimulated cells as well as EGF-induced signaling (Figure 2.8A). In addition to EGF-, IGF-induced Akt phosphorylation was also reduced by Gefitinib (Figure 2.8A). Although this reduction could be due to EGFR transactivation by activated IGF1R [47], this potentially indicates that Gefitinib could have additional effects on downstream signaling following activation of other RTKs. Nonetheless, this experiment suggests that, at the concentrations used to block EBOV GP-mediated entry, the RTK inhibitors block Akt signaling in a target specific manner.

Given that RTK inhibitors block EBOV entry and that EBOV VLPs induce Akt phosphorylation, a straightforward hypothesis is that RTK activation is responsible for Akt signaling induced by EBOV. To test this, we exposed Vero cells to EBOV VLPs in the presence or absence of the RTK inhibitors and found that all inhibitors were able to block EBOV VLP-

induced Akt phosphorylation (Figure 2.8B). These results suggest that EBOV VLPs can indeed activate Akt phosphorylation during entry via RTK-dependent signaling cascades. Taking our conclusions in conjunction with the findings of Saeed et al. [17] examining the role of Akt in EBOV trafficking, these results serve to further suggest that EBOV VLPs can induce RTK-dependent activation of Akt to promote trafficking to entry-conducive NPC1+ compartments.

2.4 DISCUSSION

EBOV entry into host cells is a multistep process that requires internalization by macropinocytosis and trafficking through the endosomal pathway to reach vesicular compartments containing triggering factors such as cathepsin proteases and NPC1 [2-4, 7, 8, 10, 37, 48]. While the specific host factors involved in regulating EBOV trafficking, such as the HOPS and PAS complexes, are becoming increasingly well-characterized, it is still unclear whether EBOV particles are passive passengers of the endolysosomal system or hijackers – actively directing their delivery to entry-conducive compartments. In this study, we show that EBOV uses and activates signaling pathways to promote its delivery to NPC1+ compartments that can facilitate delivery of the ribonucleocapsid to the cytoplasm.

By screening a library of kinase inhibitors, we identified specific and common signaling pathways required for EBOV and/or MARV entry (Figure 2.1C). Previous studies have also uncovered the importance of cellular kinases in the different steps of the EBOV entry. For example, studies have suggested that AMPK [22] and diacylglycerol (DAG) kinases [31] play a role in the macropinocytic uptake of EBOV. Interestingly, the AMPK inhibitor, Dorsomorphin, was also identified in our screen; although it mostly affected MARV GP-mediated entry, it also slightly reduced transduction by EBOV pseudotypes (Figure 2.1C).

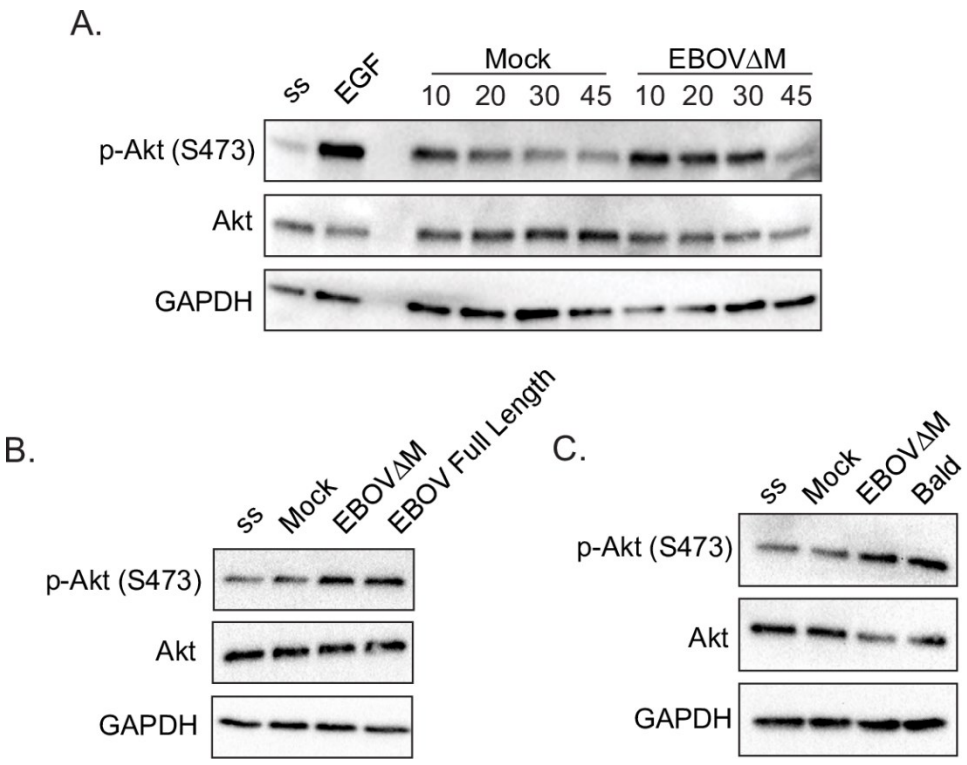

Figure 2.7 EBOV ΔM GP, EBOV Full Length GP, and Bald EboV VLPs all stimulate Akt phosphorylation in Vero cells.

Vero cells were serum starved in HBSS for 1h, followed by stimulation with (A) EGF (50 ng/mL), Mock, or βlam EBOV ΔM GP VLPs for 10, 20, 30, or 45 min, (B) Mock, βlam EBOV ΔM GP, or βlam EBOV Full Length GP VLPs for 20 min., or (C) Mock, βlam EBOV ΔM GP VLPs, or Bald EBOV VLPs for 20min. Cells were lysed and phosphorylated Akt (p-Akt - S473), total Akt (Akt), and GAPDH were detected by immunoblot. Abbreviations are serum starved (ss), βlam EBOV ΔM GP VLPs (EBOV), βlam EBOV Full Length GP VLPs (Full Length). Data are representative of 3 independent experiments.

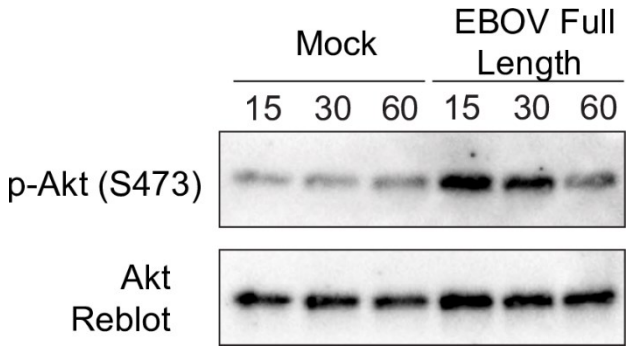

Figure S2.8 Kinetics of full-length EBOV GP VLP-induced Akt phosphorylation in Vero cells. Vero cells were serum-starved in HBSS for 1h followed by exposure to purified Mock supernatants or βlam VLPs harboring the full-length EBOV GP for 15, 30, or 60 min. Cells were washed, lysed, and immunoblotted for phosphorylated Akt (p-Akt S473). The membrane was then stripped and re-probed for total Akt. Data are representative of 2 independent experiments.

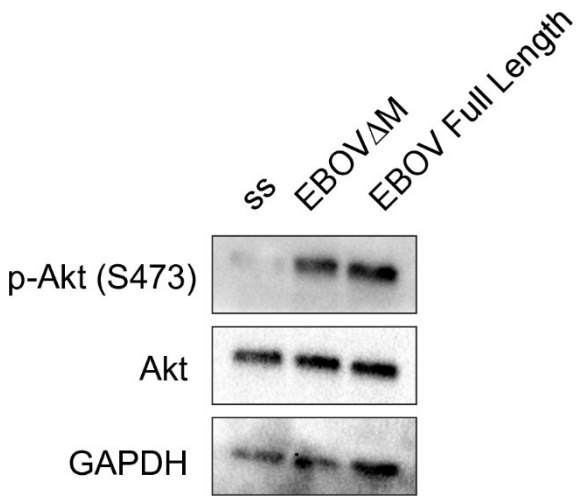

Figure S2.9 Viral particles harboring full-length EBOV GP and EBOV ΔM GP activate Akt in BMDMs.

Murine bone-marrow derived macrophages were serum starved in serum-free RPMI for 1h followed by exposure to purified Mock, βlam EBOV ΔM GP, or βlam EBOV Full Length GP VLPs for 20 min. Cells were lysed and phosphorylated Akt (p-Akt - S473), total Akt (Akt), and GAPDH were detected by immunoblot. Data are representative of 3 independent experiments.

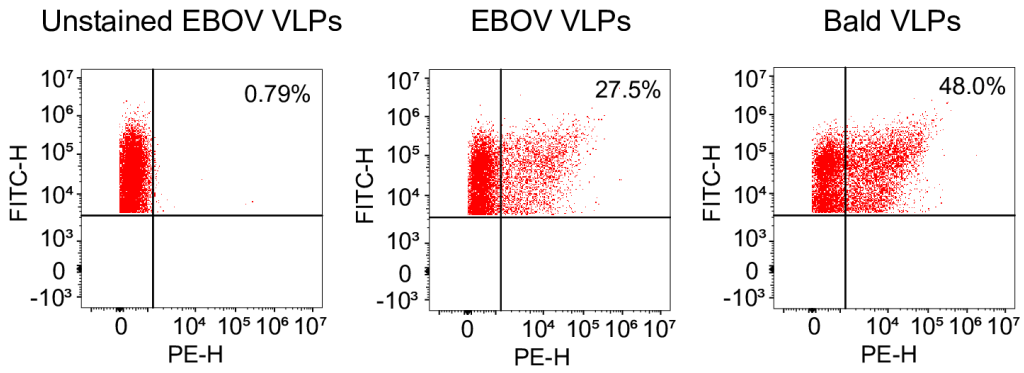

Figure S2.10 Phosphatidylserine is present on the viral envelope of both EBOV ΔM GP VLPs and Bald VLPs.

GFP EBOVΔM GP VLPs and GFP Bald VLPs were stained with Annexin V-PE in ABB and analyzed using nanoscale flow cytometry (CytoFLEX S, Beckman Coulter). Unstained GFP EBOVΔM GP VLPs were run as a negative control (left). Data is representative of 3 independent experiments.

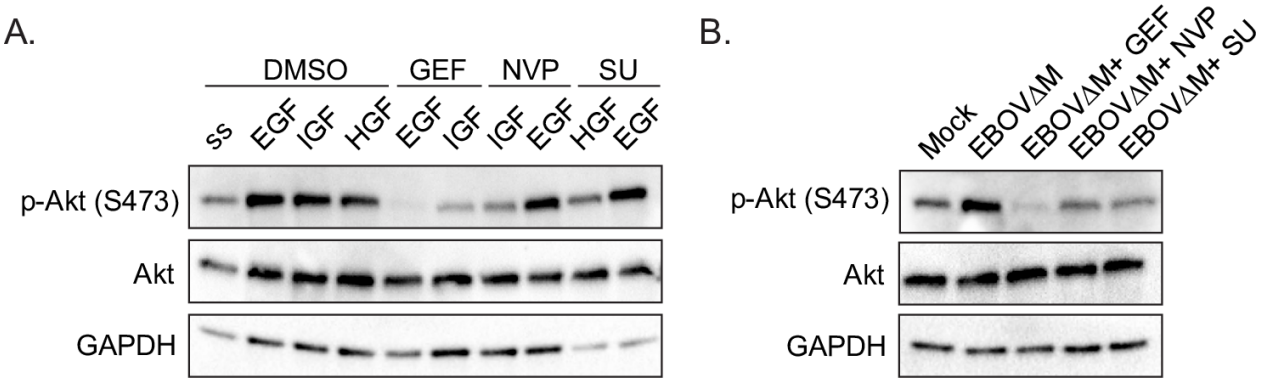

Figure 2.8 RTK inhibitors block EBOV VLP-induced Akt phosphorylation.

Vero cells were pre-treated with Gefitinib (5 µM), SU11274 (2.5 µM), NVP-ADW742 (2.5 µM) or vehicle (DMSO, 0.1%) in serum-free HBSS for 1h. Cells were then stimulated with (A) EGF (50 ng/mL), IGF (50 ng/mL), or HGF (200 ng/mL) for 10, 20, 30, or 45 min, or (B) with Mock, βlam EBOV ΔM GP VLPs (MOI = 100) for 20 min. Cells were lysed and phosphorylated Akt (p-Akt - S473), total Akt (Akt), and GAPDH were detected by immunoblot. Abbreviations are serum starved (ss), βlam EBOV ΔM GP VLPs (EBOV), Gefitinib (GEF), NVP-ADW742 (NVP), and SU11274 (SU). Data are representative of 3 independent experiments.

Whether AMPK or DAG kinases are activated during entry or if the virus relies on steady state signaling through these kinases for macropinocytic uptake remains to be determined. However, because small-molecule inhibitors of both AMPK and DAG kinases are also capable of blocking high molecular weight dextran, it is likely that treatment with these inhibitors results in a general block of the macropinocytic uptake process, whether EBOV is present or not. In addition to AMPK and DAG kinases, a previous study utilized G-protein-coupled receptor (GPCR) antagonists to reveal that GPCR signaling might be involved in a post-attachment entry step [49]. However, it is unclear if the antiviral target of these GPCR inhibitors is a host factor or if the inhibitors act via direct binding to EBOV GP [50]. Interestingly, in our study, EBOV GP-mediated entry was blocked by FTY720 (Figure 2.1C), an antagonist of the sphingosine-1-phosphate (S1P) receptor GPCR [51]. S1P, the GPCR ligand, is generated through phosphorylation of sphingosine by sphingosine kinases; interestingly, we also identified a sphingosine kinase inhibitor (PF-543) in our screen (Figure 2.1C) [52]. The identification of both FTY720 and PF-543 raises the interesting hypothesis that the SK-S1PR axis may also play a role in EBOV GP-mediated entry. More work needs to be done to test this hypothesis and to elucidate whether these signaling pathways are activated by the virus to promote entry.

In our small-molecule screen, we also identified RTKs as a common and overrepresented signaling pathway among our hits (Figure 2.1D). Inhibitors of EGFR, c-Met, or InsR/IGF1R blocked EBOV GP-mediated entry in multiple cell lines in addition to replicative EBOV growth. While previous studies have suggested that EGFR and Ephrin receptor signaling is important for Ebola virus infection, our study was the first to provide a detailed mechanism of action [53-55]. Since RTKs have been reported to facilitate the macropinocytosis of other viruses, we sought to determine if this is true for Ebola virus as well [56]. Interestingly, we found that the RTK

inhibitors did not interfere with internalization, but rather, the c-Met and InsR/IGFR inhibitors prevented the delivery of viral particles to NPC1+ compartments (Figure 2.5B and 2.5C). Each of these inhibitors also blocked EBOV-induced Akt signaling during entry (Figure 2.8B). Since Akt signaling has also been characterized to be important for EBOV trafficking [17], our data suggests that Akt signaling may be initiated through RTK dependent signaling pathways. Additionally, production of PtdIns(3,5)P_2 via PIKfyve is also enhanced by EBOV, and previous work has shown that EGF stimulation leads to an increase in PIKfyve activity via Akt-mediated phosphorylation [16]. Interestingly, chemical inhibition of Akt or PIKfyve leads to a block in EBOV VLP trafficking to NPC1+ compartments [10, 11, 17]. While a link between Akt and PIKfyve is implied by the literature, the mechanisms by which these pathways are activated by EBOV remain unknown. It is tempting to speculate that one of the roles of the EBOV induced RTK-Akt signaling is to activate PIKfyve for efficient delivery to NPC1+ endolysosomes. More work needs to be done to test this hypothesis.

Similar to the c-Met and IGF1R/InsR inhibitors, the EGFR inhibitor also led to a block in EBOV-induced Akt activation (Figure 2.8B). Surprisingly, however, treatment with this inhibitor did not impair the delivery of EBOV VLPs to NPC1+ compartments (Figure 2.5B and 2.5C). Since EBOV was able to reach the NPC1+ compartments following inhibitor treatment but was unable to successfully enter cells, this implied that Gefitinib treatment renders the NPC1+ compartments non-conducive to entry. Interestingly, we observed that Gefitinib-treated cells had enlarged NPC1+ endosomes (Figure 2.6A and 2.6B) and exhibited a distinctive NPC1 expression pattern, with NPC1 appearing inside the endosomes in addition to its expected localization at the limiting membrane (Figure 2.6C). The redistribution of NPC1 also explains the apparent accumulation of cholesterol in these vesicles (Figure S2.6), since it must be shuttled

from LBPA rich intraluminal vesicles by NPC2 to NPC1 localized at the limiting membrane of the endolysosomes for transport to the endoplasmic reticulum [42, 43]. Because EBOV VLPs were observed to colocalize with NPC1 inside the enlarged endosomes of Gefitinib-treated cells (Figure 2.5B and 2.5C), we speculate that, in Gefitinib-treated cells, fusion may occur in these NPC1+ intraluminal vesicles instead of at the limiting membrane of the endosome, thus preventing the ribonucleocapsid from reaching the cytoplasm. Interestingly, our studies also revealed that, in addition to blocking EGF- and EBOV-induced Akt activation, Gefitinib reduced Akt phosphorylation below that observed in serum-starved cells (Figure 2.8A and 2.8B). This finding suggests that the biology of the NPC1 compartment is modulated by steady state signaling and may not be dependent on EBOV entry. Future studies will aim to further characterize the NPC1+ compartments after Gefitinib treatment.

To begin dissecting how signaling pathways are activated during filoviral entry, here we provide evidence that EBOV-induced Akt activation is RTK dependent and can occur in the absence of GP (Figure 2.7C and Figure 2.8B). With regards to filovirus induced signaling pathways, previous studies have shown that cells, especially immune cells, can become activated after exposure of EBOV [57-59]. For instance, in dendritic cells, EBOV VLPs activate NFκ-B and MAPK signaling in a EBOV GP-dependent manner, and that this requires the mucin domain for full activation [58]. Additionally, other studies have shown that the presence of EBOV GP on VLPs was required to engage TLR4 in multiple cell lines [57]. Further, EBOV can also activate lymphocytes via binding to TIM-1, presumably via virus exposed PS [59, 60]. While these studies clearly demonstrate that signaling pathways can be activated in response to EBOV, we chose to focus on identifying pathways that are activated by EBOV to promote entry. We demonstrated that EBOV can activate Akt both in the presence or absence of GP on VLPs

(Figure 2.7), suggesting that a lipid on the envelope may be required. It is well-established in the literature that PS on the surface of enveloped viruses, including EBOV, can bind to cell surface PS receptors and mediate attachment and internalization of virions [61, 62]. The receptor tyrosine kinases Tyro3, Axl, and Mer (TAM family) are three examples of such PS receptors; for these, binding of PS is mediated by Protein S or Gas6 [60, 63]. RTKs, including those of the TAM family, can undergo unconventional heterodimerization among their different classes. More specifically, it has been shown in multiple cell lines that Axl and EGFR can heterodimerize and that interaction with Axl can drive EGFR signaling through the PI3K/Akt pathway, even in the presence of an EGFR blocking antibody [64, 65]. Interestingly, for other enveloped viruses that utilize the TAM family of RTKs during entry, evidence suggests that the protein tyrosine kinase domain of Axl is dispensable for enhancement of virus attachment and internalization; however, it has also been shown that subsequent infection is impaired when there is no kinase activity [66, 67]. In conjunction with our data, it is tempting to speculate that heterodimerization of RTKs of different classes, driven by PS on the viral envelope and the TAM RTKs, may activate signaling cascades through the PI3K/Akt pathway and promote viral entry. Notably, a model requiring hetero-oligomerization of multiple RTKs would explain the dominant negative effect of each RTK inhibitor on viral entry. More work needs to be done to test this hypothesis and to determine if c-Met, IGF1R, and InsR can also heterodimerize with the TAM family of RTKs.

While this manuscript was in peer-review, Kuroda et al. reported a role for HER2 and other RTKs in EBOV infection. Interestingly, they also came to a similar model for Akt activation via TAM RTKs. Their study mainly focused on the role of HER2 in entry and proposed that it is involved in macropinocytic uptake. This proposed mechanism of action was

based off the findings that overexpression of HER2 leads to increased dextran uptake and that viral particles colocalized with HER2/TYRO3 complexes at the cell surface but not once virions were internalized. In our study, inhibition of RTK signaling had no effect on EBOV internalization. This discrepancy could be explained by the use of HT1080 cells for many of our experiments, which are known to be HER2 negative or express a very low level of this RTK [68, 69]. Collectively, the two studies highlight differential usage of RTK signaling for entry depending on the expression profiles in the target cells. Future work will aim at dissecting the contribution of each RTK on the different steps of the filovirus entry pathway.

In conclusion, the characterization of host trafficking factors and signaling pathways activated during viral entry are important to further our understanding of EBOV infection and provide potential targets for antiviral therapies. In our study, we identified RTK inhibitors, some of which are FDA-approved drugs, that could be used to block entry by all known pathogenic filoviruses. Since all filoviruses known to date, even Měnglà virus recently discovered in bats in China [70], use NPC1 as their entry receptor, these inhibitors have the potential to be effective antiviral agents against all filoviruses and development of such therapies may allow us to be prepared for future outbreaks sparked by emerging filoviruses.

2.5 MATERIALS AND METHODS

Ethics Statement

All animal procedures were approved by the University of Ottawa Animal Care Committee (protocol number BMI-1863), which are in compliance with the standards of the Canadian Council on Animal Care (CCAC), and Ontario's Animals for Research Act and its regulations.

Cell lines and cell culture

Vero cells (ATCC) and HT1080 cells (ATCC) were cultured in Minimum Essential Medium (MEM, Sigma,) and Human Embryonic Kidney HEK293T (ATCC) cells were cultured in Dulbecco's Modified Eagle Medium (DMEM, Wisent). All culture media were supplemented with 10% Fetal Bovine Serum (FBS, Sigma), 0.3 mg/mL L-glutamine, 100 U/mL penicillin, and 100µg/mL streptomycin (Wisent). Cells were maintained at 37˚C in 5% CO2 at 100% relative humidity.

BMDMs were isolated from C57Bl/6J mice (stock no. 00064, originally purchased from Jackson Laboratories and maintained as a colony at the University of Ottawa) and differentiated as previously described [71]. Briefly, bone marrow cells were seeded in DMEM supplemented with 10% FBS (Wisent), penicillin, and streptomycin (Hyclone, GE healthcare). L929-conditioned media (20%) was utilized for macrophage differentiation, and Roswell Park Memorial Institute (RPMI, Wisent) media supplemented with 10% FBS (Sigma-Aldrich), 0.3mg/mL L-glutamine, 100 U/mL penicillin, and 100 µg/mL streptomycin (Wisent) was utilized for seeding and subsequent experiments.

Small Molecule Inhibitors, Antibodies and Plasmids

SU11274, NVP-ADW742, Akt Inhibitor VIII, and 5-(N-ethyl-N-isopropyl)-Amiloride (EIPA) were all purchased from Cayman Chemical and Gefitinib was purchased from ApexBio. Stock solutions were prepared in DMSO, aliquoted, and stored at -80ºC until use. Filipin III from Streptomyces filipinensis (F 4767) was purchased from Sigma and resuspended in DMSO prior to use.

Anti-Akt (9272S), anti-phospho-Akt S473 (92721S), and anti-mouse IgG HRP-linked (7076S) antibodies were purchased from Cell Signaling Technology. GAPDH (ab8245), EGFR (ab52894), Met (ab51067), NPC1 (ab134113), InsR (ab69508), and DY650 sheep anti-rabbit

(ab96926) antibodies were purchased from Abcam. The LBPA (Z-PLBPA) antibody was purchased from Echelon Biosciences. The goat anti-Rabbit IgG HRP-linked (31460) and donkey anti-mouse Alexa Fluor 555 antibodies (A-31570) were purchased from ThermoFisher. The pan-filovirus anti-GP antibody (21D10) was purchased from IBT Bioservices.

Plasmids encoding the different virus glycoproteins (EBOV Δmucin GP, BDBV Δmucin GP, SUDV Δmucin GP, MARV GP, EBOV full-length GP, EBOV Δmucin GPF535R, and VSV G), pCAGGS, MLV gag/pol packaging plasmid, and the MLV retroviral vector encoding LacZ were kind gifts of Dr. James Cunningham, Brigham and Women's Hospital. Plasmids encoding the EBOV NP and EBOV VP40-β-lactamase were kind gifts of Dr. Lijun Rong, University of Illinois. The EBOV VP40-mCherry plasmid was a gift from Dr. Judith White, University of Virginia (Addgene plasmid #74421) [72]. The GFP-TPC2 plasmid was a gift from Dr. Santiago Di Pietro, Colorado State University (Addgene plasmid #80153).

Murine leukemia virus pseudotypes and viral-like particles production

Murine leukemia virus (MLV) pseudotypes were prepared by co-transfecting 293T cells with the MLV packaging plasmid gag-pol, a MLV retroviral vector encoding LacZ, and a plasmid encoding the glycoprotein of interest (EBOV Δmucin GP, MARV GP, or VSV G) at a 1:1:1.25 ratio respectively. Similarly, EBOV viral-like particles (VLPs) were prepared by co-transfecting 293T cells with plasmids encoding the EBOV nucleoprotein (NP), EBOV VP40 fused to β-lactamase (βlam), mCherry or GFP, and pCAGGS (Bald VLPs) or the viral glycoprotein of interest (EBOV Δmucin GP, EBOV Δmucin GPF535R, EBOV Full Length GP, SUDV Δmucin GP, BDBV Δmucin GP, MARV GP, or VSV G) at a 1:1:1.25 ratio. For the mock control, the pCAGGS plasmid was transfected instead. Transfections were performed using the jetPRIME transfection reagent (Polyplus Transfection) according to the manufacturers protocol.

For MLV pseudotypes, VLPs, and mock, supernatants were harvested 48, 72, and 96 h post-transfection followed by concentration by ultracentrifugation (20,000 RPM, 4 ºC, 1.5h, Beckman Coulter Optima XPN-100, SW32Ti rotor) through a 20% (w/v) sucrose cushion. Pellets were re-suspended in PBS, aliquoted, and stored at -80 ºC.

MLV transduction and VLP entry assays

For MLV pseudotype transduction assays, Vero cells were seeded and grown to 60% confluency in white 96 well plates. 30 minutes prior to infection with MLV pseudotypes, the cells were pre-treated with inhibitors or vehicle (DMSO) in serum-free MEM containing 5 μg/mL polybrene. Four hours post-infection, the media was replaced with phenol-red free DMEM containing 15 mM NH4Cl and supplemented with 10% FBS (Sigma), 0.3 mg/mL L-glutamine, 100 U/mL penicillin, and 100μg/mL streptomycin (Wisent). Twelve hours later, the media was again replaced with phenol red free DMEM as described above, but without NH_4Cl, and cells were incubated an additional 48 hours. LacZ+ cells were quantified using the Beta-Glo Assay System (Promega) following the manufacturers protocol. Luminescence was measured using a Synergy Neo2 Multi-Mode plate reader (BioTek).

For VLP infection assays, Vero, HT1080 or BMDMs were seeded and grown to 90% confluency in 48 well plates. Prior to virus addition, the cells were pre-treated with inhibitor or vehicle in serum-free MEM (for Vero and HT1080 cells) or serum-free RPMI (for BMDMs). 30 minutes later, βlam VLPs were added at a MOI between 0.2 and 0.4. Three hours post-infection, cells were loaded with a β-lactamase cleavable FRET substrate, CCF2-AM (ThermoFisher), according to manufacturer's protocol and supplemented with 15 mM NH4Cl. One to two hours later, cells were trypsinized and prepared for analysis by flow cytometry (FACSCelesta, BD Biosciences). Analysis was performed using FlowJo software (BD Biosciences) and infection

was quantified by using uninfected controls to assess the percentage of cells that underwent a shift from 530 nm to 460 nm emission, representing cleaved CCF2.

Small molecule inhibitor screen

The small molecule inhibitor screen was performed using MLV pseudotypes (as described above) on a 418 compound L1200 kinase inhibitor library (Selleckchem). Metabolic activity was assessed in parallel at the equivalent time point of 12 hours post infection (cells were not infected for metabolic activity measurement) using the CellTiter-Glo assay system (Promega) according to manufacturer's protocol. Luminescence was measured for infection and metabolic activity assays using a Synergy Neo2 Multi-Mode plate reader (BioTek). Relative percent infection or relative percent viability was then calculated based on luminescence from wells that were infected with virus but contained vehicle alone.

The mean of each technical duplicate was calculated and, from these, the mean of each biological triplicate was calculated. Using the mean metabolic activity normalized to that of the vehicle treated cells, we set a cutoff of 80% and eliminated the data from these compounds (9 compounds). Data from the compounds with negative mean values were also eliminated (10 compounds). The ratio between the mean of each virus versus the mean of VSV was then determined. Using the triplicates, p-values (t-test) between EBOV/MARV and VSV were calculated. Using the ratio and the p-value, volcano plots were generated. Cutoffs of 2-fold and 0.05 for the ratios and p-values, respectively, were used. Heatmaps were also generated using log2 ratios.

Replication-competent virus growth assay

Vero cells were seeded in clear bottom, black well tissue culture plates (Corning). Cells at 80% confluence were treated with different concentrations of the RTK inhibitors and infected

with EBOV (strain Mayinga), expressing enhanced-GFP, at a multiplicity of infection of 0.1. Virus growth was assessed by measurement of GFP at different time-points using a BioTek Synergy/HTX plate reader with excitation at 485nm and emission at 516nm. Experiments with replication-competent EBOV were performed in the Biosafety Level 4 facility at the National Microbiology Laboratory at the Public Health Agency of Canada in Winnipeg.

Pre-cleaved virus assay

βlam VLPs harboring EBOV Δmucin GP were incubated in 0.2 mg/mL thermolysin (Sigma) or PBS for 10, 20, and 30 minutes at 37ºC to determine the optimal length of thermolysin incubation. Thermolysin activity was quenched by incubation in phosphoramidon (Sigma, 500 μM) on ice for 10 minutes. A portion of the samples were aliquoted and stored at -80ºC for future use, while another portion was used to prepare lysates for immunoblotting. The resulting PVDF membrane was probed with a pan-filovirus anti-GP antibody. The 20 minute time point was selected to be optimal and VLP entry experiments were performed with the pre-cleaved virus as described above.

Internalization assay

Vero cells were seeded and grown to 90% confluency in 48 well plates. Cells were pre-treated with serum-free MEM (Vero) or RPMI (BMDM) containing inhibitor or vehicle (DMSO) for 30 minutes at 37 ºC followed by 15 minutes at 4 ºC. The mCherry VLPs were added on ice and attached to the surface of the cells by centrifugation at 300 x g for 30 minutes at 4 ºC. Following centrifugation, cells were washed 3 times with ice-cold PBS, pre-warmed serum-free media containing inhibitor or vehicle was added, and cells were then incubated at 37 ºC for 1 h. In parallel, one set of vehicle alone samples was not moved to 37 ºC but rather kept at 4 ºC following the cold PBS washes to serve as a no internalization control. After 1 h, the cells were

washed with cold PBS and incubated at 4 ºC with 0.5% Trypsin-EDTA (Gibco) for 30 min. Samples were prepared and analyzed by flow cytometry (Celesta, BD Biosciences). Analysis was performed using FlowJo (BD Biosciences) and mCherry mean fluorescence intensity was determined for each sample.

NPC1/VLP and NPC1/TPC2 Colocalization Assays

HT1080 cells were seeded onto coverslips and grown to 50% confluency. Cells were pre-treated in serum-free MEM with inhibitor or vehicle for 1 h followed by addition of mCherry VLPs harboring the fusion deficient EBOV Δmucin GP^{F535R} and incubated at 37 ºC for 3 h. 30 minutes before fixation, CellTracker Blue CMAC dye (ThermoFisher) was added according to manufacturer's protocol. 3h post infection, cells were fixed with formalin, permeabilized with 0.5% triton X-100, and blocked with 20% FBS in PBS for 30 minutes. Cells were incubated with a NPC1 primary antibody (1:70) followed by a DY650 secondary antibody (1:400), and mounted with PermaFluor Aqueous Mounting medium (ThermoFisher). Cells were imaged by confocal microscopy (LSM800 AxioObserver Z1, Zeiss) using a 63x / 1.4NA oil Plan Apochromat objective. Fifteen z-stacks were acquired per image, with a pixel size of 0.1 µm.

Image analysis was performed using Imaris software v. 8.4.2 (Bitplane). In brief, VLPs were modelled as spots and each cell was modeled as a surface based on the CMAC cytoplasmic stain. Then, the number of spots per cell was determined and the modeled spots were assigned colocalization values based on intensity correlation to NPC1. Colocalization thresholds were set manually by determining the minimum mean fluorescence intensity value in the NPC1 channel that corresponded to a colocalized VLP, modeled as a spot. Intensity thresholds were set for each experiment but kept constant between experimental conditions. The percentage of VLPs

colocalizing with NPC1 was then determined by dividing the number of spots above the colocalization threshold by the total number of spots per cell.

To analyze NPC1+ compartment size, the far-red channel (NPC1) was modelled as a surface with thresholds manually set per image. To avoid bias, image files were re-named, and the surface modeling was performed blind. The surfaces were then divided into cells based on the cells that were modeled previously for the NPC1 colocalization analysis. The statistics for surface volume was exported and the average volume of NPC1+ compartments per cell was determined.

For the NPC1/TPC2 colocalization assay, HT1080 cells were transfected with a GFP-TPC2-encoding plasmid prior to re-seeding and infection with EBOV VLPs as described above. NPC1 immunofluorescence was performed as described above with the exception that cells were stained with Hoechst (Invitrogen) instead of CMAC. Similar to the NPC1 colocalization assays, image analysis was performed using Imaris software v. 8.4.2 (Bitplane). VLPs were modeled as spots and each cell was modeled as a surface based on background immunofluorescence seen by bumping up the intensity threshold for the NPC1 channel. Intensity thresholds were set for NPC1 and TPC2 (with a certain intensity rating representing the presence of either marker), and the number of VLPs in [NPC1+, TPC2+], [NPC1-, TPC2+], or [NPC1+, TPC2-] were determined and expressed as percentages compared to the total number of VLPs in each cell.

LBPA Assay

HT1080 cells were seeded onto coverslips, grown to 50% confluency, and incubated at 37 ºC for 4h with inhibitor or vehicle in serum free MEM. Cells were fixed with formalin and blocked with 20% FBS in 0.05% saponin-PBS (Saponin, EMD Millipore). Cells were incubated in 0.05% saponin-PBS with a LBPA primary antibody (1:100) and NPC1 primary antibody

(1:70), followed by an AF555 (1:400) and DY650 secondary antibody (1:400). Cells were stained with Hoechst and then mounted with PermaFluor Aqueous mounting medium (ThermoFisher). Imaging was performed by confocal microscopy (LSM800 AxioObserver Z1, Zeiss) using a 63x / 1.4NA oil Plan Apochromat objective. An average of twenty z-stacks were acquired per image, with a pixel size of 0.1 μm. Image analysis was performed using Imaris software v. 9.6.0 (Bitplane). In brief, cells were modeled as surfaces and masks were created to separate each cell into a channel. Intensity based thresholds for the NPC1 and LBPA channels were determined manually (and kept consistent for each experiment across conditions) and Pearson's coefficient was calculated for each cell using the colocalization module.

Filipin III Staining

HT1080 cells were seeded onto coverslips, grown to 50% confluency, and incubated at 37 ºC for 4h with inhibitor or vehicle in serum free MEM. Cells were fixed with formalin, incubated with Filipin III (50 μg/mL in PBS) for 2h at RT, and coverslips mounted with PermaFluor Aqueous mounting medium. Cells were imaged by confocal microscopy (LSM800 AxioObserver Z1, Zeiss) using a 63x / 1.4NA oil Plan Apochromat objective. An average of twenty z-stacks were acquired per image, with a pixel size of 0.1 μm.

Immunoblots

Vero cells in growth phase were seeded and grown to 50% confluency in 12 well plates. Cells were washed 3 times with pre-warmed Hanks' Balanced Salt Solution (HBSS, Sigma) and pre-treated for 1h in serum-free HBSS containing the appropriate RTK inhibitor or vehicle (DMSO). After one hour, cells were stimulated in serum-free HBSS for either the indicated time point or 20 min with EGF (50 ng/mL), IGF (50 ng/mL), HGF (200 ng/mL), βlam VLPs harboring EBOV GP at a MOI of 100, or mock at the same volume as the volume of VLPs. Cells

were then washed once with cold PBS and lysed in cold lysis buffer (1% Triton X-100, 0.1% IGEPAL CA-630, 150mM NaCl, 50mM Tris-HCl, pH 7.5) containing protease and phosphatase inhibitors (Cell Signaling). Proteins in cell lysates were resolved on SDS-polyacrylamide gels (Bio-Rad) and transferred to polyvinylidenedifluoride (PVDF) membranes. Membranes were blocked for 1h at RT with blocking buffer (5% skim milk powder dissolved in 25mM Tris, pH 7.5, 150mM NaCl, and 0.1% Tween-20 [TBST]) containing sodium orthovanadate (Na_3VO_4, 1mM, Alfa Aesar) and sodium fluoride (NaF, 10mM, VWR). PVDF membranes were then incubated overnight at 4ºC with the appropriate primary antibody in 5% bovine serum albumin (BSA, Sigma) in TBST containing Na3VO4 and NaF. Blots were then washed in TBST and incubated with HRP-conjugated secondary antibody for 1h at room temperature. PVDF membranes were washed again, incubated in chemiluminescence substrate and imaged using the ChemiDoc XRS+ imaging system (Bio-Rad). In some instances, the same membrane was stripped and re-probed for total Akt.

Annexin V staining and flow cytometry analysis of VLPs

EBOV VLPs were produced as described above. VLP concentration was determined using a Zetaview nanoparticle tracking instrument (ParticleMatrix). Then, the VLPs were diluted to a concentration of 109 particles/mL in Annexin V Binding Buffer (10mM Hepes pH 7.4, 140mM NaCl, 2.5mM $CaCl_2$, filtered with a 0.1µm pore). To stain VLPs, 5uL of Annexin V-PE (BD Biosciences) was added to 100uL of VLP in ABB and incubated in the dark for 30 minutes at 4ºC. The stained sample was then diluted in ABB at a 1:500 ratio in preparation for sample acquisition using a CytoFLEX S (Beckman Coulter). The FITC channel (525/40) and PE channel (585/42) were used to detect VLPs and AnnexinV, respectively. Samples were collected at a

flow rate of 10uL/min with cytometer calibration and settings previously described [73]. Data analysis was performed using FlowJo (Version 10.7.0).

Acknowledgements

We would like to acknowledge technical support from the uOttawa Cell Biology and Image Acquisition Core staff, Chloë van Oostende and Skye Green, and Vera A. Tang from the uOttawa Flow Cytometry & Virometry Core Facility. We would also like to acknowledge Shirley Qiu for her experimental and technical support.

2.6 REFERENCES

1. Harrison, S.C., Viral membrane fusion. Virology, 2015. 479-480: p. 498-507.
2. Carette, J.E., et al., Ebola virus entry requires the cholesterol transporter Niemann-Pick C1. Nature, 2011. 477(7364): p. 340-3.
3. Miller, E.H., et al., Ebola virus entry requires the host-programmed recognition of an intracellular receptor. EMBO J, 2012. 31(8): p. 1947-60.
4. Cote, M., et al., Small molecule inhibitors reveal Niemann-Pick C1 is essential for Ebola virus infection. Nature, 2011. 477(7364): p. 344-8.
5. Jae, L.T., et al., Virus entry. Lassa virus entry requires a trigger-induced receptor switch. Science, 2014. 344(6191): p. 1506-10.
6. Messaoudi, I., G.K. Amarasinghe, and C.F. Basler, Filovirus pathogenesis and immune evasion: insights from Ebola virus and Marburg virus. Nat Rev Microbiol, 2015. 13(11): p. 663-76.
7. Saeed, M.F., et al., Cellular entry of ebola virus involves uptake by a macropinocytosis-like mechanism and subsequent trafficking through early and late endosomes. PLoS Pathog, 2010. 6(9): p. e1001110.
8. Mulherkar, N., et al., The Ebola virus glycoprotein mediates entry via a non-classical dynamin-dependent macropinocytic pathway. Virology, 2011. 419(2): p. 72-83.
9. Spence, J.S., et al., Direct Visualization of Ebola Virus Fusion Triggering in the Endocytic Pathway. MBio, 2016. 7(1): p. e01857-15.
10. Qiu, S., et al., Ebola virus requires phosphatidylinositol (3,5) bisphosphate production for efficient viral entry. Virology, 2018. 513: p. 17-28.
11. Nelson, E.A., et al., The phosphatidylinositol-3-phosphate 5-kinase inhibitor apilimod blocks filoviral entry and infection. PLoS Negl Trop Dis, 2017. 11(4): p. e0005540.
12. Bo, Y., et al., Filoviruses Use the HOPS Complex and UVRAG To Traffic to Niemann-Pick C1 Compartments during Viral Entry. J Virol, 2020. 94(16).
13. Behnia, R. and S. Munro, Organelle identity and the signposts for membrane traffic. Nature, 2005. 438(7068): p. 597-604.
14. Balderhaar, H.J. and C. Ungermann, CORVET and HOPS tethering complexes - coordinators of endosome and lysosome fusion. J Cell Sci, 2013. 126(Pt 6): p. 1307-16.
15. Sun, Q., et al., Rubicon controls endosome maturation as a Rab7 effector. Proc Natl Acad Sci U S A, 2010. 107(45): p. 19338-43.
16. Er, E.E., et al., AKT facilitates EGFR trafficking and degradation by phosphorylating and activating PIKfyve. Sci Signal, 2013. 6(279): p. ra45.
17. Saeed, M.F., et al., Phosphoinositide-3 kinase-Akt pathway controls cellular entry of Ebola virus. PLoS Pathog, 2008. 4(8): p. e1000141.
18. Yang, Z.Y., et al., Identification of the Ebola virus glycoprotein as the main viral determinant of vascular cell cytotoxicity and injury. Nat Med, 2000. 6(8): p. 886-9.
19. Manicassamy, B., et al., Comprehensive analysis of ebola virus GP1 in viral entry. J Virol, 2005. 79(8): p. 4793-805.

20. Cureton, D.K., et al., Vesicular stomatitis virus enters cells through vesicles incompletely coated with clathrin that depend upon actin for internalization. PLoS Pathog, 2009. 5(4): p. e1000394.
21. Sieczkarski, S.B. and G.R. Whittaker, Differential requirements of Rab5 and Rab7 for endocytosis of influenza and other enveloped viruses. Traffic, 2003. 4(5): p. 333-43.
22. Kondratowicz, A.S., et al., AMP-activated protein kinase is required for the macropinocytic internalization of ebolavirus. J Virol, 2013. 87(2): p. 746-55.
23. Noda, T., et al., Ebola virus VP40 drives the formation of virus-like filamentous particles along with GP. J Virol, 2002. 76(10): p. 4855-65.
24. Diederich, S., L. Thiel, and A. Maisner, Role of endocytosis and cathepsin-mediated activation in Nipah virus entry. Virology, 2008. 375(2): p. 391-400.
25. Bonaparte, M.I., et al., Ephrin-B2 ligand is a functional receptor for Hendra virus and Nipah virus. Proc Natl Acad Sci U S A, 2005. 102(30): p. 10652-7.
26. Negrete, O.A., et al., EphrinB2 is the entry receptor for Nipah virus, an emergent deadly paramyxovirus. Nature, 2005. 436(7049): p. 401-5.
27. Pasqual, G., et al., Old world arenaviruses enter the host cell via the multivesicular body and depend on the endosomal sorting complex required for transport. PLoS Pathog, 2011. 7(9): p. e1002232.
28. Martinez, M.G., S.M. Cordo, and N.A. Candurra, Characterization of Junin arenavirus cell entry. J Gen Virol, 2007. 88(Pt 6): p. 1776-84.
29. Geisbert, T.W., et al., Pathogenesis of Ebola hemorrhagic fever in cynomolgus macaques: evidence that dendritic cells are early and sustained targets of infection. Am J Pathol, 2003. 163(6): p. 2347-70.
30. Eierhoff, T., et al., The epidermal growth factor receptor (EGFR) promotes uptake of influenza A viruses (IAV) into host cells. PLoS Pathog, 2010. 6(9): p. e1001099.
31. Stewart, C.M., et al., A Diacylglycerol Kinase Inhibitor, R-59-022, Blocks Filovirus Internalization in Host Cells. Viruses, 2019. 11(3).
32. Brecher, M., et al., Cathepsin cleavage potentiates the Ebola virus glycoprotein to undergo a subsequent fusion-relevant conformational change. J Virol, 2012. 86(1): p. 364-72.
33. Wang, M.K., et al., Biochemical Basis for Increased Activity of Ebola Glycoprotein in the 2013-16 Epidemic. Cell Host Microbe, 2017. 21(3): p. 367-375.
34. Simmons, J.A., et al., Ebolavirus Glycoprotein Directs Fusion through NPC1+ Endolysosomes. J Virol, 2016. 90(1): p. 605-10.
35. Sakurai, Y., et al., Ebola virus. Two-pore channels control Ebola virus host cell entry and are drug targets for disease treatment. Science, 2015. 347(6225): p. 995-8.
36. Cermak, S., et al., Loss of Cathepsin B and L Leads to Lysosomal Dysfunction, NPC-Like Cholesterol Sequestration and Accumulation of the Key Alzheimer's Proteins. PLoS One, 2016. 11(11): p. e0167428.

37. Chandran, K., et al., Endosomal proteolysis of the Ebola virus glycoprotein is necessary for infection. Science, 2005. 308(5728): p. 1643-5.
38. Wang, H., et al., Ebola Viral Glycoprotein Bound to Its Endosomal Receptor Niemann-Pick C1. Cell, 2016. 164(1-2): p. 258-268.
39. Kaletsky, R.L., G. Simmons, and P. Bates, Proteolysis of the Ebola virus glycoproteins enhances virus binding and infectivity. J Virol, 2007. 81(24): p. 13378-84.
40. Schornberg, K., et al., Role of endosomal cathepsins in entry mediated by the Ebola virus glycoprotein. J Virol, 2006. 80(8): p. 4174-8.
41. van der Kant, R., et al., Cholesterol-binding molecules MLN64 and ORP1L mark distinct late endosomes with transporters ABCA3 and NPC1. J Lipid Res, 2013. 54(8): p. 2153-65.
42. McCauliff, L.A., et al., Intracellular cholesterol trafficking is dependent upon NPC2 interaction with lysobisphosphatidic acid. Elife, 2019. 8.
43. Hoglinger, D., et al., NPC1 regulates ER contacts with endocytic organelles to mediate cholesterol egress. Nat Commun, 2019. 10(1): p. 4276.
44. Adu-Gyamfi, E., et al., Host Cell Plasma Membrane Phosphatidylserine Regulates the Assembly and Budding of Ebola Virus. J Virol, 2015. 89(18): p. 9440-53.
45. Nanbo, A., et al., Ebola virus requires a host scramblase for externalization of phosphatidylserine on the surface of viral particles. PLoS Pathog, 2018. 14(1): p. e1006848.
46. Manning, B.D. and A. Toker, AKT/PKB Signaling: Navigating the Network. Cell, 2017. 169(3): p. 381-405.
47. Roudabush, F.L., et al., Transactivation of the EGF receptor mediates IGF-1-stimulated shc phosphorylation and ERK1/2 activation in COS-7 cells. J Biol Chem, 2000. 275(29): p. 22583-9.
48. Nanbo, A., et al., Ebolavirus is internalized into host cells via macropinocytosis in a viral glycoprotein-dependent manner. PLoS Pathog, 2010. 6(9): p. e1001121.
49. Cheng, H., et al., Inhibition of Ebola and Marburg Virus Entry by G Protein-Coupled Receptor Antagonists. J Virol, 2015. 89(19): p. 9932-8.
50. Schafer, A., et al., Repurposing potential of 1st generation H1-specific antihistamines as anti-filovirus therapeutics. Antiviral Res, 2018. 157: p. 47-56.
51. Oo, M.L., et al., Immunosuppressive and anti-angiogenic sphingosine 1-phosphate receptor-1 agonists induce ubiquitinylation and proteasomal degradation of the receptor. J Biol Chem, 2007. 282(12): p. 9082-9.
52. Strub, G.M., et al., Extracellular and intracellular actions of sphingosine-1-phosphate. Adv Exp Med Biol, 2010. 688: p. 141-55.
53. Kolokoltsov, A.A., et al., Identification of novel cellular targets for therapeutic intervention against Ebola virus infection by siRNA screening. Drug Dev Res, 2009. 70(4): p. 255-265.

54. Kolokoltsov, A.A., et al., Inhibition of Lassa virus and Ebola virus infection in host cells treated with the kinase inhibitors genistein and tyrphostin. Arch Virol, 2012. 157(1): p. 121-7.
55. Kouznetsova, J., et al., Identification of 53 compounds that block Ebola virus-like particle entry via a repurposing screen of approved drugs. Emerg Microbes Infect, 2014. 3(12): p. e84.
56. Mercer, J. and A. Helenius, Virus entry by macropinocytosis. Nat Cell Biol, 2009. 11(5): p. 510-20.
57. Okumura, A., et al., Interaction between Ebola virus glycoprotein and host toll-like receptor 4 leads to induction of proinflammatory cytokines and SOCS1. J Virol, 2010. 84(1): p. 27-33.
58. Martinez, O., C. Valmas, and C.F. Basler, Ebola virus-like particle-induced activation of NF-kappaB and Erk signaling in human dendritic cells requires the glycoprotein mucin domain. Virology, 2007. 364(2): p. 342-54.
59. Younan, P., et al., Ebola Virus Binding to Tim-1 on T Lymphocytes Induces a Cytokine Storm. mBio, 2017. 8(5).
60. Moller-Tank, S., et al., Role of the phosphatidylserine receptor TIM-1 in enveloped-virus entry. J Virol, 2013. 87(15): p. 8327-41.
61. Jemielity, S., et al., TIM-family proteins promote infection of multiple enveloped viruses through virion-associated phosphatidylserine. PLoS Pathog, 2013. 9(3): p. e1003232.
62. Brunton, B., et al., TIM-1 serves as a receptor for Ebola virus in vivo, enhancing viremia and pathogenesis. PLoS Negl Trop Dis, 2019. 13(6): p. e0006983.
63. Morizono, K. and I.S. Chen, Role of phosphatidylserine receptors in enveloped virus infection. J Virol, 2014. 88(8): p. 4275-90.
64. Vouri, M., et al., Axl-EGFR receptor tyrosine kinase hetero-interaction provides EGFR with access to pro-invasive signalling in cancer cells. Oncogenesis, 2016. 5(10): p. e266.
65. Brand, T.M., et al., AXL mediates resistance to cetuximab therapy. Cancer Res, 2014. 74(18): p. 5152-64.
66. Meertens, L., et al., The TIM and TAM families of phosphatidylserine receptors mediate dengue virus entry. Cell Host Microbe, 2012. 12(4): p. 544-57.
67. Moller-Tank, S. and W. Maury, Phosphatidylserine receptors: enhancers of enveloped virus entry and infection. Virology, 2014. 468-470: p. 565-580.
68. Li, R., et al., Single-Cell Intravital Microscopy of Trastuzumab Quantifies Heterogeneous in vivo Kinetics. Cytometry A, 2020. 97(5): p. 528-539.
69. Parihar, R., et al., IL-12 enhances the natural killer cell cytokine response to Ab-coated tumor cells. J Clin Invest, 2002. 110(7): p. 983-92.
70. Yang, X.L., et al., Characterization of a filovirus (Mengla virus) from Rousettus bats in China. Nat Microbiol, 2019.
71. LeBlond, N.D. and M.D. Fullerton, Methods to Evaluate AMPK Regulation of Macrophage Cholesterol Homeostasis. Methods Mol Biol, 2018. 1732: p. 477-493.

72. Shoemaker, C.J., et al., Multiple cationic amphiphiles induce a Niemann-Pick C phenotype and inhibit Ebola virus entry and infection. PLoS One, 2013. 8(2): p. e56265.
73. Welsh, J.A., J.C. Jones, and V.A. Tang, Fluorescence and Light Scatter Calibration Allow Comparisons of Small Particle Data in Standard Units across Different Flow Cytometry Platforms and Detector Settings. Cytometry A, 2020. 97(6): p. 592-601.

Chapter 3: Ebola virus requires sphingosine kinase 1 and 2 activity for host cell entry

Corina M. Stewart[1,2,3], Yuxia Bo[1,2,3], Kathy Fu[1,2,3], Mable Hagan.[4,5], Robert Kozak[4], Gary Kobinger[4], Darwyn Kobasa[4,5], Marceline Côté[1,2,3]*

[1] Department of Biochemistry, Microbiology and Immunology, University of Ottawa, Ottawa, Canada

[2] Ottawa Institute of Systems Biology, University of Ottawa, Ottawa, Canada

[3] Centre for Infection, Immunity, and Inflammation, Ottawa, Canada

[4] Special Pathogens Program, National Microbiology Laboratory, Public Health Agency of Canada, Winnipeg, Canada

[5] Department of Infectious Diseases and Medical Microbiology, University of Manitoba, Winnipeg, Canada

* Corresponding author

This chapter is currently being prepared for journal submission.

Author contributions: CS, YB, and KF contributed to MLV and Lentivirus pseudotype assays. CS and KF contributed to the DsiRNA experiments. CL-4 experiments were performed by RK and GK. CL-3 experiments were performed by MH and DK. All other experiments were performed by CS. Manuscript was written and edited by CS and MC.

3.1 ABSTRACT

Entry of enveloped viruses into host cells requires fusion between the viral envelope and host cell membrane, a process that is facilitated by viral fusion proteins protruding from the viral envelope. For this to occur, viral fusion proteins need to be triggered by host factors. For many enveloped viruses, including Ebola virus (EBOV) and SARS-CoV-2 in some cell types, triggering occurs inside endosomes and/or lysosomes. Therefore, these 'late-penetrating viruses' must be internalized and undergo extensive intracellular trafficking through endosomes to reach their triggering factors. Previously, we hypothesized that late-penetrating viruses require host-cell signaling to facilitate entry and screened a library of kinase inhibitors to identify such kinases that are important for EBOV entry. Among our hits was an inhibitor of sphingosine kinase 1 (SK1), PF-543, and an inhibitor of sphingosine-1-phosphate receptors (S1PRs), FTY720, which suggested that the SK-S1PR axis may pla a role in EBOV entry. In this study, we found that chemical inhibition of SK1 and/or SK2 and knockdown of SK1 or SK2, inhibited entry of EBOV into host cells. Mechanistically, we found that inhibition of SK1 and/or SK2 prevented EBOV from reaching late-endosomes and lysosomes containing the EBOV intracellular receptor. We also demonstrated that the trafficking defect caused by SK1/2 inhibition occurs independently of S1P signaling through cell-surface S1PRs. Lastly, we found that treatment of cells with SK inhibitors prevents entry of other late-penetrating viruses, including arenaviruses and coronaviruses, in addition to inhibiting infection of replication competent EBOV and SARS-CoV-2. Therefore, these molecules could serve as candidates for the development of broad-spectrum antiviral therapeutics.

3.2 INTRODUCTION

For enveloped viruses to deliver their genome into the cytoplasm of host cells, fusion must occur between the viral and cellular membranes, a process mediated by viral fusion proteins. For fusion to occur, these proteins need to be both primed and triggered (1). Priming, which often involves proteolytic cleavage in the viral producer cells, makes the transition from pre-fusion to post-fusion conformation possible (1). Triggering initiates the transition and often involves protonation of residues within the fusion protein, viral receptor binding, or further proteolytic cleavage (1). In the case of some viruses, including Ebola virus (EBOV) and Lassa fever virus (LASV), the viral fusion protein, which is a glycoprotein (GP) that protrudes from the viral envelope, is triggered by factors localized in late endosomes and lysosomes (2). Therefore, these viruses must internalize and undergo endolysosomal trafficking to enter cells (3). For other viruses, including the severe acute respiratory syndrome coronaviruses 1 and 2 (SARS-CoV-1 and SARS-CoV-2), the location of fusion triggering depends on the expression of cell surface serine proteases, such as TMPRSS2, that are required for priming and/or triggering (4-8). In the absence of such expression, SARS-CoV-1 and SARS-CoV-2 require internalization and trafficking to cathepsin proteases in late endosomes (5, 8, 9). Although the triggering factors of late penetrating viruses differ, one commonality is a need for internalization and endosomal trafficking in host cells (2).

Given that the EBOV entry receptor, cholesterol transporter Niemann-Pick C1 (NPC1), is a late endosome/lysosome resident protein, EBOV entry inherently is a multistep process that involves attachment, internalization, and endosomal trafficking (10, 11). Attachment of EBOV to host cells is mediated by nonspecific interactions between GP and cell surface carbohydrate binding proteins, and/or between phosphatidylserine (PS) on the viral envelope and cell surface

PS receptors, such as TIM-1 or Axl (12-14). Once attached to the cell surface, EBOV triggers its internalization via macropinocytosis or phagocytosis, followed by extensive endosomal trafficking to late endosomes and lysosomes (15-20). Here, low pH-dependent cathepsin proteases, cathepsins L and B, cleave EBOV GP, which exposes the receptor binding domain and allows GP to bind NPC1 binding (10, 11, 21, 22). Once bound to NPC1, the activity of another endosomal protease, and possibly other triggering factors, are required to facilitate the conformational change in GP necessary to mediate virus-host membrane fusion (23-25).

Many host proteins have been identified to be important for endosomal trafficking of EBOV, such as the small GTPase Rab7, the homotypic fusion and protein sorting (HOPS) complex, and the PIKfyve-ArPIKfyve-Sac3 (PAS) complex (16, 26, 27). In addition, increasing evidence suggests that EBOV particles can stimulate signaling cascades such as the PI3K/Akt pathway (28). In a previous study, we screened a library of kinase inhibitors and identified 35 compounds that inhibited EBOV entry (30). Included in these hits were inhibitors of kinases that were already known to be important for EBOV internalization or trafficking, such AMP-activated protein kinase (AMPK), and Akt, however many novel inhibitors were also identified (28-31). In this study, we further characterized inhibitors of sphingosine kinases and sphingosine-1-phosphate G-protein coupled receptors (S1PR) that were identified in the screen.

Sphingosine kinases 1 and 2 (SK1/2) catalyze the phosphorylation of sphingosine to sphingosine-1-phosphate (S1P). Despite their polypeptide sequence similarity, SK1 and 2 appear to have distinct physiological functions; generally, SK1 promotes cell survival and proliferation while SK2 is pro-apoptotic (32). S1P has both extracellular and intracellular targets. Extracellular S1P activates signaling pathways through a family of five S1P GPCRs (S1PR1-5), while intracellular S1P has been shown to modulate the activity of multiple enzymes including p-

21 activated kinase 1 (Pak1), which is an important regulator of macropinocytosis (33-36). In addition, recent studies have also demonstrated a link between SK1, levels of sphingosine, and regulation of endocytic membrane trafficking (37, 38). Their putative roles in macropinocytosis and trafficking indicate that SK1 and SK2 may be entry host factors for EBOV and potential druggable targets for antiviral therapy.

Here, we investigated the role of sphingosine kinases in the entry of EBOV and other late penetrating viruses. We found that treatment with sphingosine kinase inhibitors and knockdown of sphingosine kinase 1 and 2 reduced EBOV growth and/or EBOV GP-mediated entry. More specifically, the sphingosine kinase inhibitors blocked trafficking of EBOV viral-like particles (VLPs) to NPC1 independently of S1P signaling through S1PRs. Lastly, we found that treatment with the SK inhibitors reduced entry of other late penetrating viruses and blocked surface serine protease-independent infection of SARS-CoV-2. Our results suggest that SKs play a critical role in regulating endosomal trafficking and that inhibition of SK activity results in trafficking defects that prevent late-penetrating viruses from reaching their triggering factors.

3.3 RESULTS

3.3.1 Sphingosine kinase inhibitors reduce entry of EBOV VLPs

Previously, we conducted a kinase inhibitor screen and identified inhibitors of SKs and S1PRs that blocked entry of murine leukemia virus (MLV) pseudotypes harbouring EBOV GP (30). One such inhibitor, PF-543, is a competitive inhibitor of SK1 and is over 100 times more selective to SK1 (reported IC50 = 2.7 nM) compared to SK2 (reported IC50 = 356 nM) (39, 40). In the screen, we also identified the S1PR agonist, FTY720 (fingolimod, 2-amino-2-(2-(4-octylphenyl)-ethyl)-1,3-propanediol). FTY720 is a sphingosine analogue that, once taken up by cells, is phosphorylated by SK1 or 2 prior to export out of the cell where it can bind to and

activate S1PR1,3,4 and/or 5 to induce S1PR proteasomal degradation and downregulation (41-43). In addition to its inhibitory effect on S1PRs, FTY720 has also been reported to induce the proteasomal degradation of SK1 and has been shown to competitively inhibit SK1 and 2 (42, 44, 45). We also investigated the antiviral activity of SK1-I, which is a sphingosine analogue that is highly specific to SK1 (46). The unique characteristics of each SK inhibitor were critical to teasing out the role of the SK-S1PR signaling axis in viral entry.

To confirm the antiviral activity of PF-543, FTY720, and SK1-I, we used filoviral-like particles (VLPs) generated by the co-expression of the EBOV nucleoprotein (NP), matrix protein (VP40) fused to a β-lactamase (βlam) reporter, and the glycoprotein of interest. These particles are advantageous over MLV pseudotypes as they exhibit the characteristic filamentous morphology of filoviruses and allow for a more direct measure of viral entry as reporter gene integration is not required. We found that treatment with all three inhibitors reduced entry mediated by VLPs harbouring EBOV GP (Figure 3.1 A-C). Importantly, entry mediated by vesicular stomatitis virus (VSV) G protein, which undergoes fusion in early endosomes, was not significantly reduced after inhibitor treatment, suggesting that the inhibitory effects of these inhibitors are not due to cytotoxicity or a general defect in cellular processing (Figure 3.1 A-C). In sum, these results suggest that EBOV requires SK1/2 activity for entry and may require S1P signaling through S1PRs.

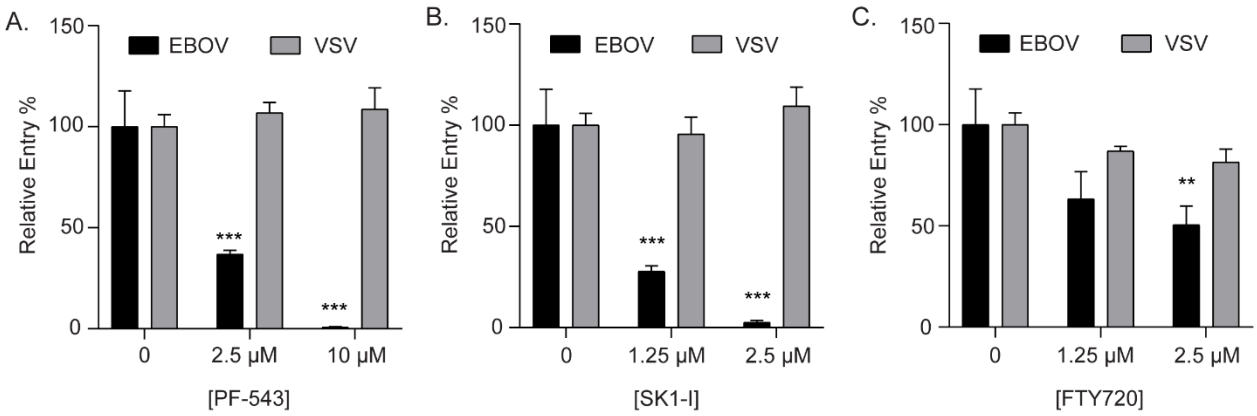

Figure 3.1 Sphingosine kinase inhibitors block EBOV GP-mediated entry

Entry of βlam VLPs harbouring EBOV GP or VSV G in HT1080 cells treated with (A) PF-543, (B) SK1-I, (C) FTY720, or vehicle (DMSO, 0.1%). Relative entry % was determined by measuring the percentage of inhibitor-treated cells with cleaved βlam substrate (CCF2) compared to vehicle-treated cells. Results in are expressed as mean ± s.d. of triplicates and are representative of three experiments. * $p < 0.05$, ** $p < 0.01$, *** $p < 0.001$.

3.3.2 Knockdown of sphingosine kinase 1 and 2 reduces EBOV GP-mediated entry

The inhibitory activity of PF-543, SK1-I, and FTY720 strongly suggests that SK1, SK2, or both are playing a role in EBOV entry. To dissect their potential roles, we specifically targeted each SK using mRNA silencing. SK1 or SK2 targeted DsiRNAs or a scrambled control were transfected in HT1080 cells. Immunoblot analysis confirmed that SK1 and SK2 expression was substantially knocked down when the respective DsiRNA was transfected (Figure 3.2 A). These cells were then used to assess entry of VLPs harboring EBOV GP or VSV G (Figure 3.2 B). Importantly, knockdown of SK1/2 did not interfere with VSV G-mediated entry, however both resulted in a decrease in EBOV GP-mediated entry. Interestingly, although expression of each SK was undetectable after DsiRNA knockdown, the SK2 knockdown had a slightly greater inhibitory effect on EBOV entry (Figure 3.2 B). To test whether SK1 and 2 play redundant roles in viral entry, we attempted a double knockdown. Unfortunately, cell viability was severely compromised (data not shown). Nevertheless, these results suggest EBOV GP-mediated entry requires SK1 and/or SK2 activity (Figure 3.2 B).

3.3.3 PF-543 inhibits growth of replication-competent EBOV

We next sought to confirm that SK1/2 activity is required for bonafide EBOV infection. Given that both SK1 and SK2 seem to be involved in entry, we investigated the effect of PF-543, which inhibits both SKs (albeit with reduced efficacy against SK2), on infection by replication-competent EBOV. Vero cells were infected with GFP-expressing replicative EBOV in the presence or absence of PF-543 and EBOV growth was assessed by measuring GFP fluorescence. We found that PF-543 significantly inhibited growth of replicative EBOV at 5μM and

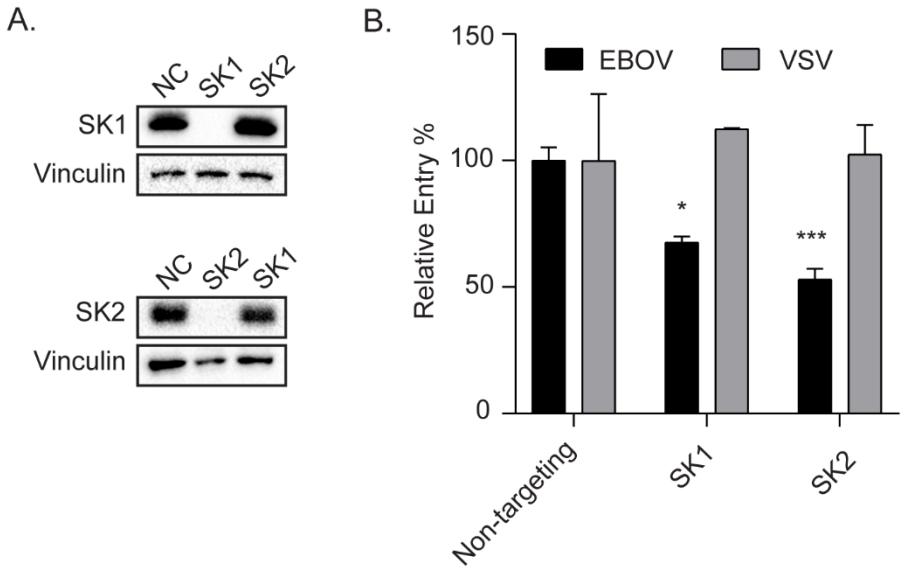

Figure 3.2 Knockdown of sphingosine kinase 1 or 2 reduces EBOV VLP entry

HT1080 cells transfected with nontargeting control DsiRNA or DsiRNA targeting SK1 or SK2 were either (A) lysed and expression of SK1 or SK2 (upper) and Vinculin (lower) detected by immunoblot, or (B) infected with βlam VLPs harbouring EBOV GP or VSV G. Relative entry % was determined by measuring the percentage of inhibitor-treated cells with cleaved βlam substrate (CCF2) compared to vehicle-treated cells. Results in are expressed as mean ± s.d. of triplicates and are representative of three experiments. * $p < 0.05$, ** $p < 0.01$, *** $p < 0.001$.

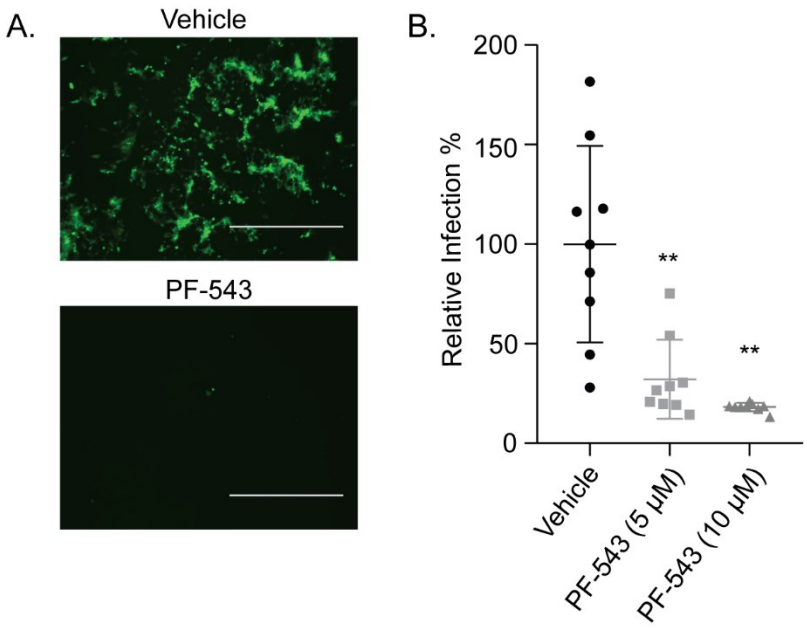

Figure 3.3 PF-543 inhibits infection of replication-competent EBOV

Infection of Vero cells with replication-competent EBOV expressing GFP and treated with vehicle or PF-543. Images in (A) were acquired for vehicle or PF-543 (5 µM) treated wells, bar=1mm. Relative infection % in (B) was determined by measuring mean GFP fluorescence intensity for PF-543 treated cells compared to vehicle alone. Results are expressed as mean ± s.d. of three experiments. * $p < 0.05$, ** $p < 0.01$, *** $p < 0.001$.

completely inhibited growth at 10μM (Figure 3.3 A-B). These results further indicate that SKs play a role in EBOV infection.

3.3.4 Sphingosine kinase inhibitors do not interfere with EBOV attachment or internalization

EBOV entry begins with attachment of the viral particle to the cell surface, followed by virion internalization via a macropinocytosis-like mechanism (16). To further elucidate the role of sphingosine kinases in EBOV entry, we first assessed whether the SK inhibitors had an effect on EBOV attachment. We exposed inhibitor treated cells to fluorescent EBOV VLPs at 4ºC to allow for virion attachment but not internalization, and assessed the resulting VLP fluorescence by flow cytometry. We found that none of our inhibitor treatments resulted in a reduction in VLP fluorescence, indicating that none significantly blocked attachment of EBOV VLPs (Figure 3.4 A).

To assess if the SK inhibitors blocked macropinocytic uptake of EBOV, we incubated cells with VLPs 4˚C as described above, but then shifted the temperature to 37˚C to allow for internalization. As controls, some samples were not shifted to 37ºC such that no internalization was permitted, and some samples were incubated with 5-(N-Ethyl-N-isopropyl)amiloride (EIPA), a known inhibitor of macropinocytosis (Figure 4 B) (47). We found that while PF-543 did partially block internalization of fluorescent EBOV VLPs, the effect was not nearly as pronounced as that of EIPA (Figure 3.4B). Notably, SK1-I and FTY720 had no effect on EBOV VLP internalization (Figure 3.4B). Taken together, these results suggested that SK activity is required at an entry step after attachment and internalization.

3.3.5 Sphingosine kinase inhibitors block entry of pre-cleaved EBOV VLPs

A critical post-internalization EBOV entry step is the cleavage of EBOV GP by endosomal cathepsin proteases such as cathepsin B (21). Interestingly, a previous study

suggested that SK1-I treatment results in enlarged vacuoles that lack cathepsin B activity, therefore we also assessed if the SK inhibitors may prevent GP-mediated cleavage by cathepsins (38). To investigate this, we experimentally mimicked cathepsin cleavage by pre-cleaving EBOV VLPs with thermolysin. These cleaved VLPs will still require attachment, internalization, and trafficking to NPC1, but should no longer require cleavage by endosomal cathepsins. We assessed entry of uncleaved and cleaved VLPs in HT1080 cells treated with the cathepsin B inhibitor, Ca074, in addition to the SK inhibitors. As expected, Ca074 had reduced potency on cleaved VLPs compared to the uncleaved VLPs (Figure S3.1). In contrast, the SK inhibitors were equally potent at inhibiting entry of uncleaved and cleaved VLPs, suggesting that their primary mechanism of action is not to inhibit Cathepsin B-mediated cleavage of EBOV GP (Figure S3.1).

3.3.6 Sphingosine kinase inhibitors block trafficking of EBOV to NPC1+ intracellular compartments

Since the SK inhibitors did not significantly prevent attachment or internalization, and did block entry of pre-cleaved VLPs, we next sought to assess whether they had an effect on endolysosomal trafficking to the EBOV receptor, NPC1. For these experiments, we utilized fluorescent VLPs harbouring EBOV GP^{F535R}, which can bind to NPC1 following cathepsin cleavage but cannot undergo fusion, allowing us to visualize accumulation of VLPs in NPC1+ compartments (48). As a control, we treated cells with Akt Inhibitor VIII, which has previously been shown to result in the accumulation of EBOV in early endosomal compartments (28). We determined the percentage of fluorescent VLPs that colocalized with immunostained NPC1 in inhibitor treated cells compared to vehicle alone and found a decrease in the percentage of VLPs per cell that colocalized with NPC1 for all three SK inhibitors (Figure 3.4 C and D), suggesting that the SK inhibitors interfere with endosomal trafficking. We also observed dilated intracellular

vesicles in SK1-I and FTY720 treated cells that were not present in vehicle or PF-543 treated cells (Figure 3.4 C). This is consistent with recent studies demonstrating that treatment with sphingosine or sphingosine analogs, including SK1-I and FTY720, induce rapid formation of enlarged intracellular vesicles in cells (37, 38). Since such vesicles are often indicative of defects in endosomal trafficking, their presence also supports our hypothesis that treatment with the SK inhibitors result in endosomal trafficking defects.

3.3.7 The endolysosomal trafficking defect induced by the SK inhibitors is independent of S1PR signaling

S1P, the product of SKs, is a bioactive sphingolipid involved in regulating cell growth, survival, and migration (49). It is well-characterized to exert this function by binding to cell surface S1PRs and thus activating downstream signaling cascades such as the PI3K-Akt pathway (33, 50, 51). Consistent with this, treatment with SK1-I has previously been shown to inhibit Akt phosphorylation (52). Given this and the fact that Akt signaling is also important for EBOV trafficking, we hypothesized that the SK inhibitors block EBOV trafficking by preventing S1P activation of S1PRs, thereby preventing subsequent Akt activation (28). To test this hypothesis, we evaluated the antiviral activity of FTY720-Phosphate, which inhibits S1PR signaling by inducing S1PR degradation (41-43). However, unlike FTY720, FTY720-Phosphate cannot enter cells and therefore cannot inhibit SKs (41-43). Cells were pre-treated for one hour with FTY720 or FTY720-Phosphate and entry of VLPs harbouring EBOV GP or VSV G was evaluated. We found that FTY720-Phosphate had no effect on EBOV GP-mediated entry while FTY720 drastically blocked EBOV GP-mediated entry at the same concentration (Figure 3.5 A). This

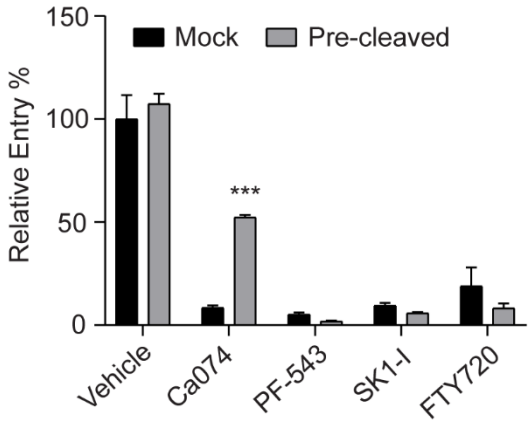

Figure S3.1 Sphingosine kinase inhibitors block entry of pre-cleaved EBOV VLPs

Pre-treated cells were infected with thermolysin cleaved (pre-cleaved) and mock cleaved βlam VLPs. Relative entry % was determined by measuring the percentage of inhibitor-treated cells with cleaved βlam substrate (CCF2) compared to vehicle-treated cells. Results in are expressed as mean ± s.d. and are representative of three experiments. * $p < 0.05$, ** $p < 0.01$, *** $p < 0.001$.

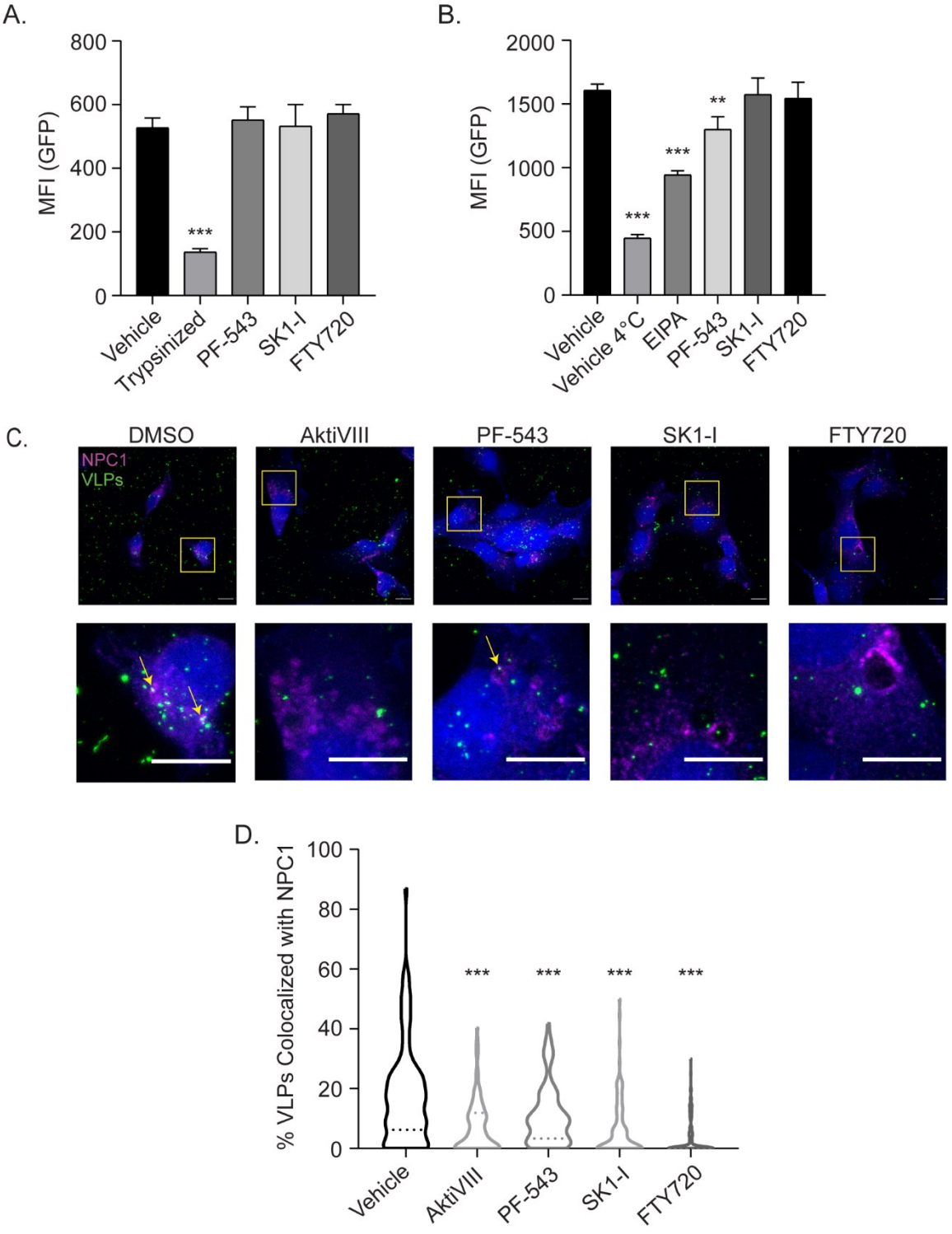
A.
MFI (GFP)
800
600
400
200
0
***
Vehicle
Trypsinized
PF-543
SK1-I
FTY720
B.
MFI (GFP)
2000
1500
1000
500
0
***
***
**
Vehicle
Vehicle 4°C
EIPA
PF-543
SK1-I
FTY720
C.
DMSO
AktiVIII
PF-543
SK1-I
FTY720
NPC1
VLPs
D.
% VLPs Colocalized with NPC1
100
80
60
40
20
0
***
***
***
***
Vehicle
AktiVIII
PF-543
SK1-I
FTY720

Figure 3.4 Sphingosine kinase inhibitors block trafficking of EBOV VLPs to NPC1

HT1080 cells were treated with vehicle (DMSO, 0.1%), PF-543 (10 μM), SK1-I (2.5 μM), FTY720 (2.5 μM), and either EIPA (30 μM) (B), or AktiVIII (10 μM) (C-D). In (A), cells were then detached and incubated with GFP VLPs harbouring EBOV GP at 4 ºC. Cells were washed and a subset of cells were trypsinized remove bound virions as a negative control. Cells were incubated with SYTOX red dead cell stain and fluorescence analyzed by flow cytometry. (B) GFP VLPs harbouring EBOV GP were pre-bound to treated cells by spinoculation at 4 ºC, washed, and either incubated again with vehicle or inhibitor at 37 ºC or vehicle alone at 4 ºC. Cells were then trypsinized to remove bound virions, washed, incubated with SYTOX red dead cell stain, and fluorescence analyzed by flow cytometry. (C-D) Pre-treated cells were incubated for 3 hours with GFP VLPs (Green) harbouring the fusion deficient ΔM GP^{F535R}. 30 minutes prior to fixation, cells were treated with CMAC cytoplasmic dye (Blue). Cells were then fixed, permeabilized, and immunostained with anti-NPC1 and DY-650 conjugated antiserum (Magenta). Cells were imaged on a LSM800 confocal microscope (Zeiss). Displayed images are maximum intensity Z-projections, arrows indicate colocalization of VLPs and NPC1, bar = 10 μm. (B) Colocalization between VLPs and NPC1 was analyzed using Imaris software (Bitplane). Results in are expressed as mean ± s.d. and are representative of three experiments. * $p < 0.05$, ** $p < 0.01$, *** $p < 0.001$.

provided the first evidence that the observed trafficking defect after treatment with the SK inhibitors is not a result of reduced signaling through S1PRs.

To further explore if FTY720 and FTY720-Phosphate reduce S1PR mediated PI3K-Akt pathway activation, we treated cells with the inhibitors and assessed Akt phosphorylation by immunoblot. As a positive control, we added S1P to vehicle treated cells and found that S1P treatment did indeed increase levels of phosphorylated Akt in cells. Interestingly, while there was no difference in phosphorylated Akt levels after treatment with FTY720 compared to vehicle, treatment with FTY720-Phosphate increased Akt phosphorylation to a similar extent as S1P treated cells (Figure 3.5 B). This suggests that FTY720-Phosphate induces activation of S1PRs prior to inducing their degradation, a result that is consistent with previous reports in the literature (43). Therefore, the lack of entry inhibition seen after FTY-720-Phosphate treatment does not fully rule out the possibility that the antiviral activity of the SK inhibitors is due to a reduction in S1P signaling through cell surface S1PRs.

To address this, we performed an add-back experiment where S1P was added to inhibitor treated cells prior to virus addition. If the entry and trafficking defects observed after SK inhibitor treatment are due to a decrease in S1P signaling through S1PRs, adding extracellular S1P should rescue the inhibitory entry effects mediated by the SK inhibitors. Importantly, we found that S1P addition did not rescue EBOV entry in the presence of PF-543, SK1-I, or FTY720 (Figure 3.5 C). This result suggested that the trafficking defect observed after treatment with the SK inhibitors was not due to reduced S1P signaling through S1PRs. Further work needs to be done to elucidate the precise molecular mechanism underlying the EBOV entry defect observed after treatment with SK inhibitors.

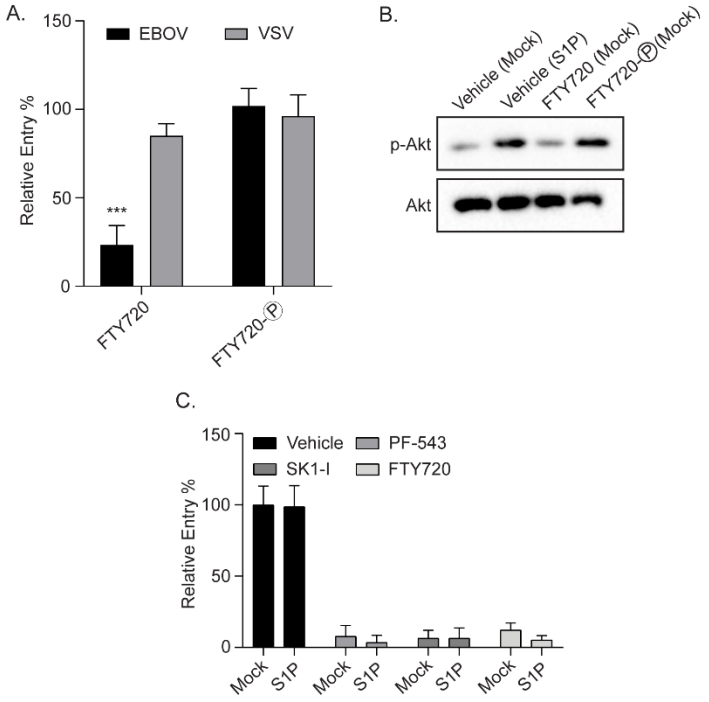

Figure 3.5 S1PR agonist, FTY720-Phosphate, does not reduce EBOV entry and S1PR activation by S1P does not rescue EBOV infection in inhibitor treated cells

(A-B) HT1080 cells were pre-treated with vehicle (DMSO, 0.1%), FTY720 (2.5 μM), or FTY720-Phosphate (2.5 μM) and infected with βlam VLPs harbouring EBOV GP or VSV G (A) or stimulated with S1P or mock (B). In (A), relative entry % was determined by measuring the percentage of inhibitor-treated cells with cleaved βlam substrate (CCF2) compared to vehicle-treated cells. In (B), cells were lysed and immunoblotted for phosphorylated Akt (p-Akt S473) or total Akt. (C) HT1080 cells were pre-treated with vehicle (DMSO, 0.1%), PF-543 (10 μM), SK1-I (2.5 μM), or FTY720 (2.5 μM), stimulated with S1P (125 nM) or mock, and infected with βlam VLPs harbouring EBOV GP. Relative entry % was determined by measuring the percentage of inhibitor-treated cells with cleaved βlam substrate (CCF2) compared to vehicle-treated cells. Results are expressed as mean ± s.d. of triplicates and are representative of three experiments. * $p < 0.05$, ** $p < 0.01$, *** $p < 0.001$.

3.3.8 Sphingosine kinase inhibitors block entry of other late-penetrating viruses

The requirement for intracellular trafficking is shared among other viruses whose entry receptor or other triggering factors are in late endosomes. Therefore, it is plausible that entry mediated by the GP of these viruses may also be inhibited by the SK inhibitors. To investigate this, we utilized MLV pseudotypes harbouring the viral fusion proteins of a related filovirus, Marburg virus (MARV), the Old World arenavirus, LASV, the New World arenavirus, Junin virus (JUNV), and Influenza A virus (IAV). The entry pathway of MARV is similar to that of EBOV, although studies have suggested that the cathepsin requirements differ between the two viruses (53, 54). In addition to their entry receptors, LASV, JUNV, and IAV all require low pH for fusion and therefore must traffic to early/late endosomes (3, 55-60). As controls, we also included VSV, which undergoes fusion in early endosomes, and Nipah virus (NiV), which requires entry receptor ephrinB2 to mediate fusion at the cell surface (61-64). We found that the SK inhibitors blocked entry of MARV and to a lesser extent, LASV and JUNV, however they were the most potent at inhibiting EBOV entry (Figure 3.6 A). Unexpectedly, PF-543 and SK1-I enhanced entry of IAV, while FTY720 had no effect (Figure 3.6 A). PF-543 and SK1-I did not reduce VSV or NiV entry, and while FTY720 slightly reduced entry mediated by MLV pseudotypes harbouring VSV G, it was not to the same extent as the other viruses (Figure 3.6 A). In addition, we also used lentivirus pseudotypes to examine entry mediated by the spike protein of the coronaviruses SARS-CoV-1 and middle eastern respiratory syndrome coronavirus (MERS). We found that all SK inhibitors drastically inhibited entry mediated by SARS-CoV-1, while only PF-543 had a significant effect on MERS (Figure 3.6 B). For these experiments, coronavirus entry was presumed to follow the endosomal route as Camostat, a TMPRSS2 inhibitor, did not inhibit SARS-CoV-1 entry in this cell type (Figure S3.2). Lastly, we tested

whether the most potent inhibitor for inhibiting SARS-CoV-1 entry, SK1-I, also inhibited infection of replication competent SARS-CoV-2. We found that SK1-I inhibited infection of SARS-CoV-2 in Huh7.5 cells in a dose-dependent manner (Figure 3.6C). These results suggest that SK inhibitors reduce infection of viruses that enter cells through late endosomes and that SKs could be potential targets for broad spectrum antiviral therapies.

3.4 DISCUSSION

Entry of enveloped viruses into host cells requires viral glycoprotein-mediated fusion between the viral and host cell membranes. For EBOV and many other viruses, cellular proteins important for the priming and/or triggering of viral glycoproteins are localized in late-endosomes and lysosomes, therefore EBOV entry requires internalization and extensive endolysosomal trafficking. To determine if EBOV particles are passive passengers of the endolysosomal system or if they actively direct their delivery to late endosomes and lysosomes through altering host cell signaling pathways, we previously screened a library of kinase inhibitors and identified several signaling pathways that are important for EBOV entry (30). Through this screen, we identified SK and S1PR inhibitors that block EBOV entry (30). Here, we further characterized the role of SK and S1PRs in EBOV entry, investigated the mechanism of action of the SK inhibitors, and explored if these inhibitors block entry of other viruses that require endolysosomal trafficking.

In this study, we investigated the antiviral activity of three SK inhibitors and found that they all inhibited entry of EBOV VLPs, which suggested that SKs are the antiviral target of the inhibitors (Figure 3.1). To confirm this, we used DsiRNAs to knockdown SK1 or SK2 in cells and found that indeed EBOV GP-mediated entry was reduced (Figure 3.2). We also attempted to

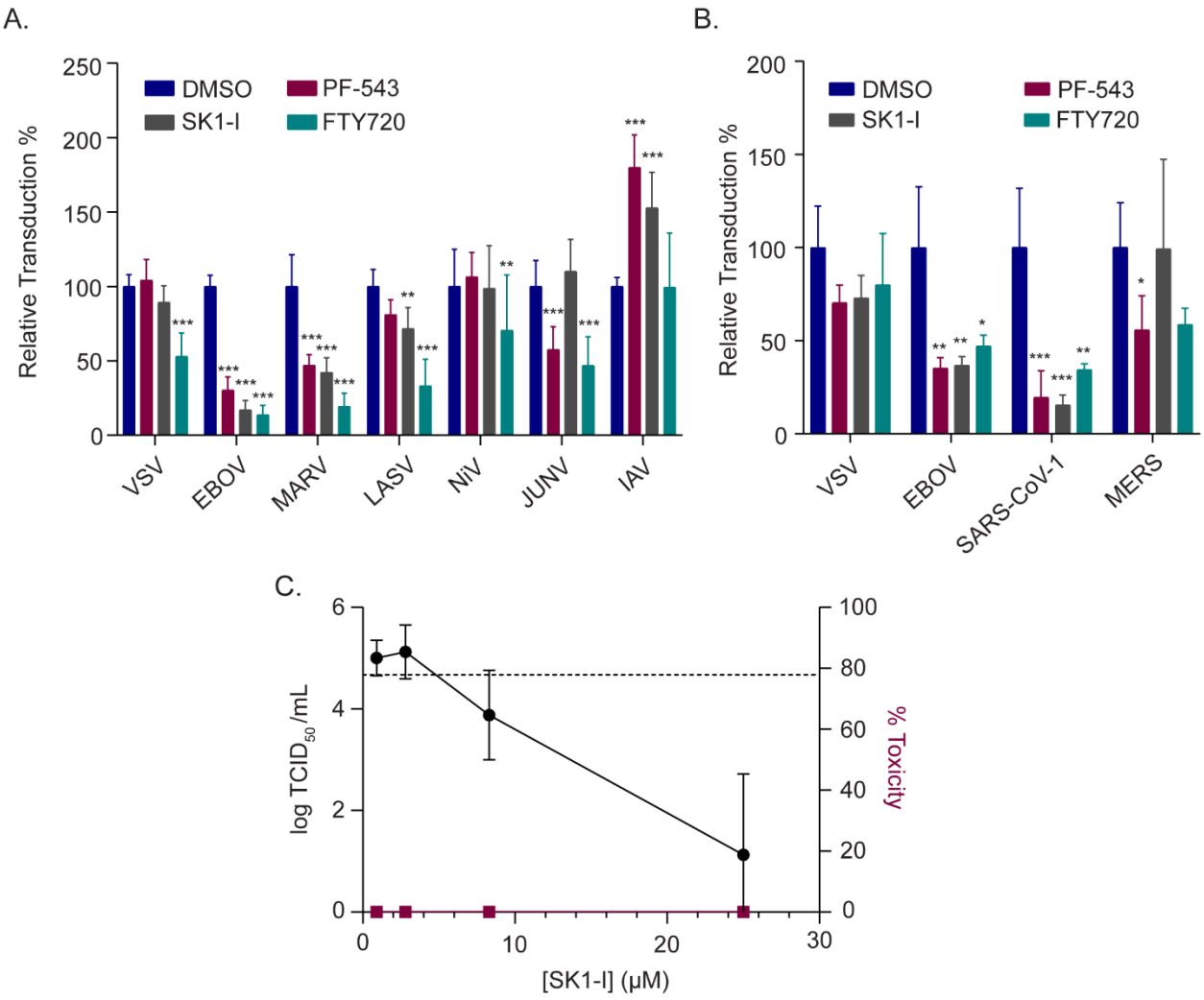

Figure 3.6 Sphingosine kinase inhibitors block entry of late-penetrating viruses and infection mediated by SARS-CoV-2

(A-B) HT1080 cells treated with vehicle (DMSO, 0.1%), PF-543 (10 μM), SK1-I (2.5 μM), or FTY720 (2.5 μM) were transduced with MLV pseudotypes (A) or lentiviral pseudotypes (B) encoding lacZ harbouring the fusion proteins of the indicated viruses. Relative transduction % was determined by quantifying LacZ positive inhibitor treated cells compared to vehicle treated cells. (C) Huh7.5 cells treated with vehicle or increasing concentrations of SK1-I were infected with replication-competent SARS-CoV-2. 48 hpi, supernatant was collected and used directly to measure the TCID50 in Vero cells. Results in are expressed as mean ± s.d. of triplicates and are representative of three experiments. * $p < 0.05$, ** $p < 0.01$, *** $p < 0.001$.

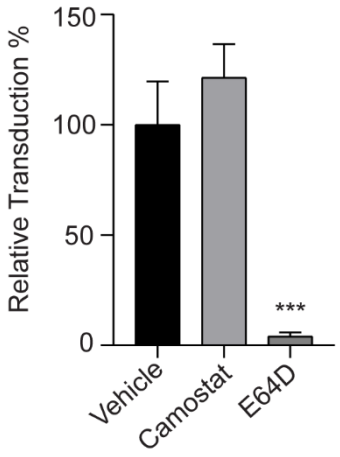

Figure S3.2 Cathepsin inhibitor, E64D, blocks entry of SARS-CoV-1 in HT1080 cells

HT1080 cells treated with vehicle (DMSO, 0.1%), Camostat (25 μM), or E64D (10 μM) were transduced lentiviral pseudotypes encoding lacZ and harbouring the SARS-CoV-1 Spike protein. Relative transduction % was determined by quantifying LacZ positive inhibitor treated cells compared to vehicle treated cells. Results in are expressed as mean ± s.d. and are representative of three experiments. * $p < 0.05$, ** $p < 0.01$, *** $p < 0.001$.

knockdown both SK1 and SK2, however cell viability was severely compromised. Previous studies have demonstrated that there is some degree of functional redundancy between SK1 and SK2, as SK1 or SK2 null mice are viable and phenotypically unremarkable, but a double knockout is embryonically lethal (65). Whether SK1 and SK2 play redundant roles for EBOV entry remains to be determined.

We then sought to further characterize the mechanism of action of the SK inhibitors – that is, to determine the entry step that the inhibitors act on and block. We found that the SK inhibitors have little or no effect on binding and internalization of EBOV particles, but rather, all prevent EBOV from trafficking to late-endosomes and/or lysosomes containing NPC1 (Figure 3.4). Interestingly, other studies have also implicated SKs to be important for proper endosomal maturation and fusion (37, 38). Consistent with our study, treatment with the sphingosine analogues SK1-I and FTY720 resulted in the formation of dilated intracellular vesicles positive for Rab7a and Lamp1, which are markers of late endosomes and therefore suggests that the trafficking block occurs at the late endosome step (37, 38). Further, Young et al. found that the vacuolization is independent of S1P signaling as pre-treatment with FTY720-Phosphate did not alter SK1-I/FTY720 induced vacuole formation (38). Moreover, they showed that overloading endosomal membranes with sphingosine results in similar vacuole formation and that treatment with PF-543 delays clearance (38). Our data indicates that while PF-543, a SK inhibitor that is not a sphingosine analogue, does not induce formation of dilated vesicles, it does induce a similar endocytic trafficking defect (Figure 3.4 C and D). This not only sheds light on the mechanism of action of our SK inhibitors but also points to some potential areas for future investigations with regards to the role of sphingosine, SKs, and S1P in the regulation of endolysosomal trafficking.

Other lipid modifying enzymes have also been implicated to be important for EBOV entry such as PIKfyve and acid sphingomyelinases (ASMase) (27, 66). Of particular interest to this study is the role of ASMase; EBOV was found to associate with lipid rafts rich in sphingomyelin (SM) and ASMases, and knockdown of ASMase inhibited EBOV entry (66). ASMase hydrolyses SM to ceremide, which can be converted to sphingosine and subsequently S1P via SKs. Ceramide has also been implicated in lipid raft expansion and is more favorable compared to SM to promote membrane curvature and macropinocytosis (67). Interestingly, Shen et al. demonstrated that SK1 associates with membranes of high curvature including macropinosomes and speculate that endocytosis may correlate with the conversion of SM to sphingosine, which can flip across the membrane and be converted to S1P by SKs (68). In our study, we also found that treatment with the SK1 inhibitor, PF-543, slightly reduced internalization of EBOV, suggesting that SK1 may be involved in macropinocytosis as well as endosomal trafficking (Figure 3.4 B). More work needs to be done to fully elucidate the roles of lipid signaling and lipid modifying enzymes in EBOV entry.

In addition to blocking EBOV entry, the SK inhibitors tested also inhibited entry of other late penetrating viruses. For example, MARV, a related filovirus, was sensitive to the inhibitory effects of the SK inhibitors, although not to the same extent as EBOV (Figure 3.6 A). Similarly, LASV entry was slightly blocked by the SK inhibitors, however it was significantly less sensitive to their inhibition in comparison to EBOV (Figure 3.6 A). These differences may be attributed to the ability of both MARV, and even more so, LASV, to undergo fusion in earlier endocytic compartments. Studies have shown that although MARV does require NPC1 for fusion, the MARV GP is significantly less stable than EBOV GP, and although proteolytic triggering of MARV GP is required for entry, MARV is less dependent on cathepsins B and L

(53, 54, 69). This suggests that MARV GP-mediated fusion may be able to occur in earlier endocytic compartments compared to EBOV. Similarly, a recent study suggested that LASV fusion may be able to occur in early endosomes that contain only a small amount of the entry receptor Lamp1 (57). With regards to the human coronaviruses tested, the location of fusion depends on the presence of proteases required to cleave the Spike protein (5). In our study, we tested the effects of the SK inhibitors in cell types lacking proteases that allow for surface fusion, forcing entry via a route that requires endosomal trafficking. It is not surprising, then, that the SK inhibitors inhibited entry and/or infection of SARS-CoV-1, SARS-CoV-2, and to a lesser extent, MERS coronaviruses (Figure 3.6 B and C). Together, our data suggests that the SK inhibitors block a late trafficking entry step and that the efficacy of these inhibitors as antiviral agents will correspond to the location of viral triggering factors.

In this study, we identified sphingosine kinases as host factors required for EBOV entry and entry of other late-penetrating viruses. We found that inhibition of sphingosine kinases impairs endosomal trafficking and that this occurs independently of S1P signaling through S1PRs at the cell surface. Since entry of many enveloped viruses requires endosomal trafficking, small molecule inhibitors of sphingosine kinases may be promising candidates for the development of broad-spectrum antiviral therapeutics that could prevent infection of both existing and emerging viruses.

3.5 MATERIALS AND METHODS

Cell lines, antibodies, and inhibitors

HEK293T cells (ATCC) were cultured in Dulbecco's Modified Eagle Medium (DMEM, Wisent), while HT1080 and Vero cells (ATCC) were cultured in Minimum Essential Medium (MEM, Sigma). Both were supplemented with 10% Fetal Bovine Serum (FBS, Sigma), 0.3

mg/mL L-glutamine, 100 U/mL penicillin, and 100 µg/mL streptomycin (Wisent). Cells were maintained at 37 ºC in 5% CO2 at 100% relative humidity.

Primary antibodies used were NPC1 (ab134113, Abcam), Akt (9272S, Cell Signaling Technology), phospho-Akt S473 (92721S, Cell Signaling Technology), GAPDH (ab8245, Abcam), SK1 (12071S, Cell Signaling Technology), SK2 (32346S, Cell Signaling Technology) and pan-filovirus anti-GP antibody (21D10, IBT Bioservices). Secondary antibodies used were goat anti-rabbit IgG HRP-linked (7074S, Cell Signaling Technology), anti-mouse IgG HRP-linked (7076S, Cell Signaling Technology) and DY650 sheep anti-rabbit (ab96926, Abcam).

PF-543 (Cayman Chemical), SK1-I (BML-258, Enzo Life Sciences Inc.), FTY720 (Cayman Chemical), FTY720-Phosphate (Cayman Chemical), 5-(N-ethyl-N-isopropyl)-Amiloride (EIPA, Cayman Chemical), and Akt Inhibitor VIII (Cayman Chemical) were prepared in DMSO, aliquoted, and stored at -20 ºC prior to use. Sphingosine-1-phosphate (d18:1, Cayman Chemical) was prepared in methanol:water (95:5), mixture heated and sonicated to dissolve, and stored in glass vials at -20 ºC. Prior to use, the methanol:water solution was evaporated under a N2 stream and a 125 µM stock solution prepared in 4 mg/mL fatty acid free Bovine Serum Albumin (Sigma) in PBS and stored at -20 ºC for up to 3 months.

Plasmids and dsiRNA

Plasmids encoding several of the different virus glycoproteins (EBOV Δmucin GP, EBOV Δmucin GPF535R, MARV GP, VSV G, LASV GP, SARS-CoV-1 Spike, MERS Spike, NiV F and G fusion proteins, IAV Vict HA and 1918 NA, MLV packaging plasmid, MLV retroviral vector encoding LacZ, lentiviral packaging plasmid psPAX2, and the lentiviral vector encoding LacZ were all kind gifts of Dr. James Cunningham, Brigham and Women's Hospital. Plasmids encoding the EBOV NP and EBOV VP40-β-lactamase or GFP were kind gifts of Dr.

Lijun Rong, University of Illinois. The plasmid encoding Ace2 was a kind gift of Dr. Hyeryun Choe (The Scripps Research Institute, Jupiter, Florida). Predesigned DsiRNAs for SK1 (hs.Ri.SPHK1.13.1; duplex sequences:
5'-rGrCrGrUrCrArUrGrCrArUrCrUrGrUrUrCrUrArCrGrUrGCG -3';
3'- rCrGrCrArCrGrUrArGrArArCrArGrArUrGrCrArUrGrArCrGrCrCrA-5'), SK2 (hs.Ri.SPHK213.1; duplex sequences:
5'-rCrCrCrUrGrArArArCrUrArArArCrArArGrCrUrUrGrGrUAC-3',
3'-rGrUrArCrCrArArGrCrUrUrGrUrUrUrArGrUrUrUrCrArGrGrGrCrU-5'), and negative control dsiRNA (51-01-14-04) were purchased from IDT, Inc.

Virus pseudotype and virus-like particle production

Murine leukemia virus and lentivirus pseudotypes were prepared by co-transfecting HEK293T cells with three plasmids: 1) MLV packaging plasmid gag-pol or psPAX2, 2) MLV retroviral or lentiviral vector encoding LacZ, and 3) a plasmid encoding the glycoprotein of interest (EBOV Δmucin GP, MARV GP, LASV GP, NiV F and G (1:1), Junin GP, IAV envelope proteins (Vict HA, 1918 NA), SARS-CoV-1 spike, MERS spike, or VSV G) at a 1:1:1.25 ratio respectively. Similarly, EBOV viral-like particles (VLPs) were prepared by co-transfecting HEK293T cells with plasmids encoding the EBOV nucleoprotein (NP), EBOV VP40 fused to β-lactamase (βlam) or GFP, and the viral glycoprotein of interest (EBOV Δmucin GP, EBOV Δmucin GPF535R, or VSV G) at a 1:1:1.25 ratio. Transfections were performed using the jetPRIME transfection reagent (Polyplus transfection) according to the manufacturers protocol. Cell supernatants were harvested at 48, 72, and 96 h post-transfection. MLVs and lentiviruses were passed through a 0.45μm filter, but VLPs were not due to their larger size. The filtered pseudotypes or VLPs were then concentrated by ultracentrifugation (20,000 RPM, 4 ºC,

1.5h, Beckman Coulter Optima XPN-100, SW32Ti rotor) through a 20% (w/v) sucrose cushion. Pellets were re-suspended in PBS, aliquoted, and stored at -80 ºC.

Virus entry assays

For MLV and lentivirus pseudotype transduction assays, HT1080 cells were seeded and grown to approximately 60% confluency in white 96-well pates. Cells were pre-incubated with inhibitor or vehicle (DMSO) in serum-free MEM containing 5 µg/mL polybrene. MLV or lentivirus pseudotypes encoding LacZ and harbouring the viral fusion protein of interest were added to the media. 4-6 hours after virus addition, the media was replaced with MEM containing 15 mM NH_4Cl and supplemented with 10% FBS (Sigma), 0.3 mg/mL L-glutamine, 100 U/mL penicillin, and 100µg/mL streptomycin (Wisent). Approximately 12 hours later, the media was replaced with complete MEM (without NH_4Cl) and cells incubated an additional 48 hours. Transduced (LacZ+) cells were quantified using the Beta-Glo Assay System (Promega) following the manufacturers protocol. Luminescence was measured using a Synergy Neo2 multi-mode plate reader (BioTek).

For the VLP entry assays, HT1080 cells were seeded and grown to 90% confluency. For inhibitor experiments, cells were pre-treated with inhibitor or vehicle (DMSO) for 1 hour in serum-free MEM. For S1P experiments, cells were pre-treated in serum-free MEM with inhibitor or vehicle, and S1P (125 nM) was added 10 minutes prior to virus addition. VP40-βlam VLPs harbouring EBOVΔM or VSV G were added at a MOI between 0.2 and 0.4. 3 hours post infection, cells were loaded with a β-lactamase cleavable FRET substrate, CCF2-AM (ThermoFisher), according to manufacturer's protocol and supplemented with 15 mM NH_4Cl and 250 µM probenecid (Sigma). Cells were then incubated for 1h at room temperature in the dark. Following this, cells were washed with PBS, trypsinized, and resuspended in 2% FBS in

PBS prior to analysis by flow cytometry (FACSCelesta or LSRFortessa, BD Biosciences). Analysis was performed using FlowJo software (BD Biosciences) and infection was quantified by using uninfected controls to assess the percentage of cells that underwent a shift from 530 nm to 460 nm emission, representing cleaved CCF2.

Pre-cleaved virus assay

βlam VLPs harboring EBOV Δmucin GP were incubated in 0.2 mg/mL thermolysin (Sigma) or PBS for 30 minutes at 37ºC. Phosphoramidon (Sigma) was then added to a final concentration of 500 μM and the mixture was incubated on ice for 10 minutes. Pre-cleaved (thermolysin treated) and mock cleaved (PBS treated) samples were aliquoted and stored at -80 37ºC prior to analysis by flow cytometry.

DsiRNA Assay

Dicer-substrate short interfering RNAs (DsiRNAs) were transfected into HT1080 cells grown to 90% confluency in using Lipofectamine RNAiMAX (ThermoFisher) according to the manufactures protocol. 24 hours post-transfection, cells were re-seeded for VLP entry assays and immunoblot lysate preparation. VLP entry assays were conducted 48 hours post-transfection as described earlier with the exception that cells were pre-incubated in serum-free MEM that did not contain any inhibitor or vehicle. In addition, 48 hours post-transfection, cells seeded for lysate preparation were washed once with PBS followed by the addition of lysis buffer (1% Triton X-100, 0.1% IGEPAL CA-630, 150mM NaCl, 50mM Tris-HCl, pH 7.5) containing protease inhibitors (Cell Signaling). Proteins in cell lysates were resolved on SDS-polyacrylamide gels and transferred to polyvinylidenedifluoride (PVDF) membranes. Membranes were blocked for 1h at RT with blocking buffer (5% skim milk powder dissolved in 25mM Tris, pH 7.5, 150mM NaCl, and 0.1% Tween-20 [TBST]). PVDF membranes were then

incubated overnight at 4ºC with the appropriate primary. The following day, blots were washed in TBST and incubated with HRP-conjugated secondary antibody for 1h at room temperature. PVDF membranes were washed again, incubated in chemiluminescence substrate, and imaged using the ChemiDoc XRS+ imaging system (Bio-Rad).

Infection assays

For infection assays with replication-competent EBOV, Vero cells were seeded onto black 96 well plates with glass bottom wells. After 48 hours, cells were pre-treated for 1 hour with vehicle (DMSO) or PF-543 in DMEM supplemented with 1% FBS. Ebola virus (Mayinga) expressing GFP was added to media containing inhibitors or vehicle and incubated together for 15 minutes prior to addition of the mixture to the cells at a final MOI of 1. Control wells containing no virus were also included. After infection, GFP expression was monitored daily using a BioTk Synergy/HTX plate reader. These experiments were performed at the CL-4 facility at the National Microbiology Laboratory of the Public Health Agency of Canada.

For infection assays with replication-competent SARS-CoV-2, Huh7.5 cells were seeded and once adhered, inhibitor or vehicle was incubated with the cells at 2x concentration for 1 hour. SARS-CoV-2 was then added to each well at an MOI of 0.01 and to give a final inhibitor concentration of 1x. The inoculum + drug mixture was incubated on cells for 2-3 hours at 37 ºC, cells were then washed with MEM and media containing inhibitor or vehicle was added back to cells and incubated for an additional 48h at 37 ºC. Cellular CPE was observed at 24 and 48 hours post infection (hpi); virus only infected wells showed no CPE, which suggests that any CPE observed is due to drug toxicity. 48 hpi, supernatant was collected and used directly to measure the TCID50. These experiments were performed at the CL-3 facility at the National Microbiology Laboratory of the Public Health Agency of Canada.

S1PR downstream signaling assay

HT1080 cells were seeded and grown to 50% confluency, washed with PBS, and pre-treated for 1 hour with inhibitor or vehicle (DMSO) in serum-free MEM. Cells were then stimulated for 30 minutes with S1P prepared in 4 mg/mL fatty acid free Bovine Serum Albumin (Sigma) in PBS or mock treated for 30 minutes with 4 mg/mL fatty acid free Bovine Serum Albumin (Sigma) in PBS. After this, cells were washed once with cold PBS and lysed in cold lysis buffer (1% Triton X-100, 0.1% IGEPAL CA-630, 150mM NaCl, 50mM Tris-HCl, pH 7.5) containing protease and phosphatase inhibitors (Cell Signaling). Proteins were resolved on SDS-polyacrylamide gels (Bio-Rad) and transferred to polyvinylidenedifluoride (PVDF) membranes. Membranes were blocked at RT with blocking buffer (5% skim milk powder in TBST containing sodium orthovanadate (Na_3VO_4, 1mM, Alfa Aesar) and sodium fluoride (NaF, 10mM, VWR)). After 1 hour of blocking, membranes were incubated overnight at 4ºC with either the pAkt antibody in 5% bovine serum albumin (BSA, Sigma) in TBST containing Na3VO4 and NaF, or Akt antibody in 5% skim milk powder in TBST. The following day, blots were washed in TBST and incubated with HRP-conjugated secondary antibody for 1h at room temperature. After 3 more washes in TBST, the membranes were incubated in chemiluminescence substrate and imaged using the ChemiDoc XRS+ imaging system (Bio-Rad).

Attachment and internalization assays

For the attachment assay, HT1080 cells were seeded and grown to 90% confluency. Cells were pre-treated with serum-free MEM containing inhibitor or vehicle (DMSO) for 1 hour at 37 ºC. The cells were detached with 5 mM EDTA and resuspended in 2% FBS in PBS containing inhibitor or vehicle. After incubation at 4 ºC for 15 minutes, VP40-GFP EBOVΔM VLPs were added on ice and incubated for 1 h at 4 ºC to allow the virus to attach to the cell surface. The cell

and virus mixtures were spun down and washed three times with cold PBS prior to resuspension in 2% FBS in PBS containing SYTOX Red dead cell stain (ThermoFisher) and analysis by flow cytometry.

For the internalization experiments, HT1080 cells were seeded and grown to 90% confluency. Cells were pre-treated with serum-free MEM containing inhibitor or vehicle (DMSO) for 1 hour at 37ºC. The cells were then incubated at 4ºC for 15 minutes prior to spinoculation of VP40-GFP EBOVΔM VLPs at 300g for 30 minutes. Cells were then washed 3x with cold PBS to removed unbound virions, pre-warmed media containing inhibitor or vehicle was added, and cells were moved to 37ºC for 1 hour to allow for internalization. Cells were then washed again with cold PBS and incubated with 0.5% trypsin-EDTA (Gibco) at 4ºC for 30 minutes. Cells were then distributed into flow tubes containing cold PBS, spun down and washed twice with cold PBS, and finally resuspended in 2% FBS in PBS containing SYTOX Red dead cell stain (ThermoFisher) prior to analysis by flow cytometry.

Fluorescence microscopy and image analysis

HT1080 cells were seeded onto coverslips that were coated with Poly-D-lysine (Sigma) and grown to approximately 50% confluency. Cells were then pre-treated with inhibitors or vehicle (DMSO) in serum-free MEM for 1 h followed by addition of VP40-GFP VLPs harboring the fusion deficient EBOV Δmucin GP^{F535R}. Cells were incubated for 2.5 hours at 37 ºC, CellTracker Blue CMAC dye (ThermoFisher) was added according to manufacturer's protocol, and cells were incubated for an additional 30 minutes. Cells were then washed with PBS, fixed with formalin, permeabilized with 0.5% triton X-100, and blocked with 20% FBS in PBS for 30 minutes. Cells were then incubated with a NPC1 primary antibody (1:70) followed by a DY650 secondary antibody (1:400), and mounted with PermaFluor Aqueous Mounting medium

(ThermoFisher). Imaging was performed with a LSM800 confocal microscope (AxioObserver Z1, Zeiss) using a 63x / 1.4NA oil Plan Apochromat objective. Approximately fifteen z-stacks were acquired per image with a pixel size of 0.1 µm.

Image analysis was performed using Imaris software v. 8.4.2 (Bitplane). In brief, each cell was modeled based on the CMAC cytoplasmic stain using the surfaces module and VLPs were modelled as spots. The number of spots per cell was then determined and the modeled spots were assigned colocalization values based on intensity correlation to NPC1. Intensity thresholds were manually set for each experiment but kept constant between experimental conditions. By dividing the number of spots above the colocalization threshold by the total number of spots per cell, the percentage of VLPs colocalizing with NPC1 was determined.

Acknowledgements

We would like to thank the uOttawa CBIA core staff, Chloë van Oostende, Skye Green, and Redaet Daniel, for their technical support. We would also like to thank and acknowledge Shirley Qiu for her experimental guidance and contribution to editing the manuscript.

3.6 REFERENCES

1. Harrison SC (2015) Viral membrane fusion. Virology 479-480:498-507.
2. Lozach PY, Huotari J, & Helenius A (2011) Late-penetrating viruses. Current opinion in virology 1(1):35-43.
3. Jae LT & Brummelkamp TR (2015) Emerging intracellular receptors for hemorrhagic fever viruses. Trends Microbiol 23(7):392-400.
4. Hoffmann M, et al. (2020) SARS-CoV-2 Cell Entry Depends on ACE2 and TMPRSS2 and Is Blocked by a Clinically Proven Protease Inhibitor. Cell 181(2):271-280.e278.
5. Shang J, et al. (2020) Cell entry mechanisms of SARS-CoV-2. Proceedings of the National Academy of Sciences 117(21):11727-11734.
6. Ou X, et al. (2020) Characterization of spike glycoprotein of SARS-CoV-2 on virus entry and its immune cross-reactivity with SARS-CoV. Nature Communications 11(1):1620.
7. Glowacka I, et al. (2011) Evidence that TMPRSS2 Activates the Severe Acute Respiratory Syndrome Coronavirus Spike Protein for Membrane Fusion and Reduces Viral Control by the Humoral Immune Response. Journal of Virology 85(9):4122-4134.
8. Simmons G, et al. (2005) Inhibitors of cathepsin L prevent severe acute respiratory syndrome coronavirus entry. Proceedings of the National Academy of Sciences of the United States of America 102(33):11876-11881.
9. Tang T, Bidon M, Jaimes JA, Whittaker GR, & Daniel S (2020) Coronavirus membrane fusion mechanism offers a potential target for antiviral development. Antiviral Res 178:104792.
10. Cote M, et al. (2011) Small molecule inhibitors reveal Niemann-Pick C1 is essential for Ebola virus infection. Nature 477(7364):344-348.
11. Carette JE, et al. (2011) Ebola virus entry requires the cholesterol transporter Niemann-Pick C1. Nature 477(7364):340-343.
12. Alvarez CP, et al. (2002) C-type lectins DC-SIGN and L-SIGN mediate cellular entry by Ebola virus in cis and in trans. J Virol 76(13):6841-6844.
13. Kondratowicz AS, et al. (2011) T-cell immunoglobulin and mucin domain 1 (TIM-1) is a receptor for Zaire Ebolavirus and Lake Victoria Marburgvirus. Proceedings of the National Academy of Sciences 108(20):8426-8431.
14. Hunt CL, Kolokoltsov AA, Davey RA, & Maury W (2011) The Tyro3 receptor kinase Axl enhances macropinocytosis of Zaire ebolavirus. J Virol 85(1):334-347.
15. Nanbo A, et al. (2010) Ebolavirus is internalized into host cells via macropinocytosis in a viral glycoprotein-dependent manner. PLoS Pathog 6(9):e1001121.
16. Saeed MF, Kolokoltsov AA, Albrecht T, & Davey RA (2010) Cellular entry of ebola virus involves uptake by a macropinocytosis-like mechanism and subsequent trafficking through early and late endosomes. PLoS Pathog 6(9):e1001110.
17. Mulherkar N, Raaben M, de la Torre JC, Whelan SP, & Chandran K (2011) The Ebola virus glycoprotein mediates entry via a non-classical dynamin-dependent macropinocytic pathway. Virology 419(2):72-83.

18. Shtanko O, Reyes AN, Jackson WT, & Davey RA (2018) Autophagy-Associated Proteins Control Ebola Virus Internalization Into Host Cells. J Infect Dis 218(suppl_5):S346-S354.
19. Stewart CM, et al. (2019) A Diacylglycerol Kinase Inhibitor, R-59-022, Blocks Filovirus Internalization in Host Cells. Viruses 11(3):206.
20. Dahlmann F, et al. (2015) Analysis of Ebola Virus Entry Into Macrophages. J Infect Dis 212 Suppl 2:S247-257.
21. Chandran K, Sullivan NJ, Felbor U, Whelan SP, & Cunningham JM (2005) Endosomal Proteolysis of the Ebola Virus Glycoprotein Is Necessary for Infection. Science 308(5728):1643-1645.
22. Brindley MA, et al. (2007) Ebola virus glycoprotein 1: identification of residues important for binding and postbinding events. J Virol 81(14):7702-7709.
23. Wong AC, Sandesara RG, Mulherkar N, Whelan SP, & Chandran K (2010) A Forward Genetic Strategy Reveals Destabilizing Mutations in the Ebolavirus Glycoprotein That Alter Its Protease Dependence during Cell Entry. Journal of Virology 84(1):163-175.
24. Spence JS, Krause TB, Mittler E, Jangra RK, & Chandran K (2016) Direct Visualization of Ebola Virus Fusion Triggering in the Endocytic Pathway. MBio 7(1):e01857-01815.
25. Das DK, et al. (2020) Conformational changes in the Ebola virus membrane fusion machine induced by pH, Ca2+, and receptor binding. PLoS Biol 18(2):e3000626.
26. Bo Y, Qiu S, Mulloy RP, & Cote M (2020) Filoviruses Use the HOPS Complex and UVRAG To Traffic to Niemann-Pick C1 Compartments during Viral Entry. J Virol 94(16): e01002-01020.
27. Qiu S, et al. (2018) Ebola virus requires phosphatidylinositol (3,5) bisphosphate production for efficient viral entry. Virology 513:17-28.
28. Saeed MF, Kolokoltsov AA, Freiberg AN, Holbrook MR, & Davey RA (2008) Phosphoinositide-3 kinase-Akt pathway controls cellular entry of Ebola virus. PLoS Pathog 4(8):e1000141.
29. Kondratowicz AS, Hunt CL, Davey RA, Cherry S, & Maury WJ (2013) AMP-activated protein kinase is required for the macropinocytic internalization of ebolavirus. J Virol 87(2):746-755.
30. Stewart CM, et al. (2021) Ebola virus triggers receptor tyrosine kinase-dependent signaling to promote the delivery of viral particles to entry-conducive intracellular compartments. PLoS Pathog 17(1):e1009275.
31. Kuroda M, Halfmann P, & Kawaoka Y (2020) HER2-mediated enhancement of Ebola virus entry. PLOS Pathogens 16(10):e1008900.
32. Pitson SM (2011) Regulation of sphingosine kinase and sphingolipid signaling. Trends Biochem Sci 36(2):97-107.
33. Bryan AM & Del Poeta M (2018) Sphingosine-1-phosphate receptors and innate immunity. Cell Microbiol 20(5):e12836.

34. Hait NC, et al. (2009) Regulation of Histone Acetylation in the Nucleus by Sphingosine-1-Phosphate. Science 325(5945):1254-1257.
35. Maceyka M, Alvarez SE, Milstien S, & Spiegel S (2008) Filamin A links sphingosine kinase 1 and sphingosine-1-phosphate receptor 1 at lamellipodia to orchestrate cell migration. Mol Cell Biol 28(18):5687-5697.
36. Dharmawardhane S, et al. (2000) Regulation of macropinocytosis by p21-activated kinase-1. Mol Biol Cell 11(10):3341-3352.
37. Lima S, Milstien S, & Spiegel S (2017) Sphingosine and Sphingosine Kinase 1 Involvement in Endocytic Membrane Trafficking. J Biol Chem 292(8):3074-3088.
38. Young MM, et al. (2016) Sphingosine Kinase 1 Cooperates with Autophagy to Maintain Endocytic Membrane Trafficking. Cell Rep 17(6):1532-1545.
39. Schnute ME, et al. (2012) Modulation of cellular S1P levels with a novel, potent and specific inhibitor of sphingosine kinase-1. Biochem J 444(1):79-88.
40. Schnute ME, et al. (2017) Discovery of a Potent and Selective Sphingosine Kinase 1 Inhibitor through the Molecular Combination of Chemotype-Distinct Screening Hits. J Med Chem 60(6):2562-2572.
41. Brinkmann V, et al. (2002) The immune modulator FTY720 targets sphingosine 1-phosphate receptors. J Biol Chem 277(24):21453-21457.
42. Paugh SW, Payne SG, Barbour SE, Milstien S, & Spiegel S (2003) The immunosuppressant FTY720 is phosphorylated by sphingosine kinase type 2. FEBS Lett 554(1-2):189-193.
43. Oo ML, et al. (2007) Immunosuppressive and anti-angiogenic sphingosine 1-phosphate receptor-1 agonists induce ubiquitinylation and proteasomal degradation of the receptor. J Biol Chem 282(12):9082-9089.
44. Tonelli F, et al. (2010) FTY720 and (S)-FTY720 vinylphosphonate inhibit sphingosine kinase 1 and promote its proteasomal degradation in human pulmonary artery smooth muscle, breast cancer and androgen-independent prostate cancer cells. Cellular Signalling 22(10):1536-1542.
45. Lim KG, et al. (2011) FTY720 analogues as sphingosine kinase 1 inhibitors: enzyme inhibition kinetics, allosterism, proteasomal degradation, and actin rearrangement in MCF-7 breast cancer cells. J Biol Chem 286(21):18633-18640.
46. Paugh SW, et al. (2008) A selective sphingosine kinase 1 inhibitor integrates multiple molecular therapeutic targets in human leukemia. Blood 112(4):1382-1391.
47. Koivusalo M, et al. (2010) Amiloride inhibits macropinocytosis by lowering submembranous pH and preventing Rac1 and Cdc42 signaling. J Cell Biol 188(4):547-563.
48. Brecher M, et al. (2012) Cathepsin cleavage potentiates the Ebola virus glycoprotein to undergo a subsequent fusion-relevant conformational change. J Virol 86(1):364-372.

49. Rosen H, Stevens RC, Hanson M, Roberts E, & Oldstone MB (2013) Sphingosine-1-phosphate and its receptors: structure, signaling, and influence. Annual review of biochemistry 82:637-662.
50. Bonnaud S, et al. (2010) Sphingosine-1-phosphate activates the AKT pathway to protect small intestines from radiation-induced endothelial apoptosis. Cancer Res 70(23):9905-9915.
51. Wang H, Huang H, & Ding S-F (2018) Sphingosine-1-phosphate promotes the proliferation and attenuates apoptosis of Endothelial progenitor cells via S1PR1/S1PR3/PI3K/Akt pathway. Cell Biology International 42(11):1492-1502.
52. Kapitonov D, et al. (2009) Targeting Sphingosine Kinase 1 Inhibits Akt Signaling, Induces Apoptosis, and Suppresses Growth of Human Glioblastoma Cells and Xenografts. Cancer Research 69:6915-6923.
53. Misasi J, et al. (2012) Filoviruses require endosomal cysteine proteases for entry but exhibit distinct protease preferences. J Virol 86(6):3284-3292.
54. Gnirß K, et al. (2012) Cathepsins B and L activate Ebola but not Marburg virus glycoproteins for efficient entry into cell lines and macrophages independent of TMPRSS2 expression. Virology 424(1):3-10.
55. Sieczkarski SB & Whittaker GR (2003) Differential requirements of Rab5 and Rab7 for endocytosis of influenza and other enveloped viruses. Traffic 4(5):333-343.
56. Torriani G, Galan-Navarro C, & Kunz S (2017) Lassa Virus Cell Entry Reveals New Aspects of Virus-Host Cell Interaction. Journal of Virology 91(4):e01902-01916.
57. Hulseberg CE, Fénéant L, Szymańska KM, & White JM (2018) Lamp1 Increases the Efficiency of Lassa Virus Infection by Promoting Fusion in Less Acidic Endosomal Compartments. mBio 9(1):e01818-01817.
58. Martinez MG, Cordo SM, & Candurra NA (2007) Characterization of Junín arenavirus cell entry. Journal of General Virology 88(6):1776-1784.
59. Martinez MG, Forlenza MB, & Candurra NA (2009) Involvement of cellular proteins in Junin arenavirus entry. Biotechnology Journal 4(6):866-870.
60. York J & Nunberg JH (2009) Intersubunit Interactions Modulate pH-Induced Activation of Membrane Fusion by the Junín Virus Envelope Glycoprotein GPC. Journal of Virology 83(9):4121-4126.
61. Cureton DK, Massol RH, Saffarian S, Kirchhausen TL, & Whelan SP (2009) Vesicular stomatitis virus enters cells through vesicles incompletely coated with clathrin that depend upon actin for internalization. PLoS Pathog 5(4):e1000394.
62. Johannsdottir HK, Mancini R, Kartenbeck J, Amato L, & Helenius A (2009) Host cell factors and functions involved in vesicular stomatitis virus entry. J Virol 83(1):440-453.
63. Bonaparte MI, et al. (2005) Ephrin-B2 ligand is a functional receptor for Hendra virus and Nipah virus. Proc Natl Acad Sci U S A 102(30):10652-10657.
64. Negrete OA, et al. (2005) EphrinB2 is the entry receptor for Nipah virus, an emergent deadly paramyxovirus. Nature 436(7049):401-405.

65. Mizugishi K, et al. (2005) Essential role for sphingosine kinases in neural and vascular development. Mol Cell Biol 25(24):11113-11121.
66. Miller ME, Adhikary S, Kolokoltsov AA, & Davey RA (2012) Ebolavirus requires acid sphingomyelinase activity and plasma membrane sphingomyelin for infection. J Virol 86(14):7473-7483.
67. Gulbins E & Li PL (2006) Physiological and pathophysiological aspects of ceramide. American journal of physiology. Regulatory, integrative and comparative physiology 290(1):R11-26.
68. Shen H, et al. (2014) Coupling between endocytosis and sphingosine kinase 1 recruitment. Nat Cell Biol 16(7):652-662.
69. Bortz RH, 3rd, et al. (2020) A Virion-Based Assay for Glycoprotein Thermostability Reveals Key Determinants of Filovirus Entry and Its Inhibition. J Virol 94(18): e00336-00320.

Chapter 4: A Diacylglycerol Kinase Inhibitor, R-59-022, Blocks Filovirus Internalization in Host Cells

Corina M. Stewart [1,2,3], Stephanie S. Dorion [1], Marie A.F. Ottenbrite [1], Nicholas D. LeBlond [1,3], Tyler K.T. Smith [1,3], Shirley Qiu [1,2,3], Morgan D. Fullerton [1,3], Darwyn Kobasa [4,5] and Marceline Côté [1,2,3*]

[1] Department of Biochemistry, Microbiology and Immunology, University of Ottawa, Ottawa, ON K1H 8M5, Canada
[2] Ottawa Institute of Systems Biology, University of Ottawa, Ottawa, ON K1H 8M5, Canada
[3] Centre for Infection, Immunity and Inflammation, University of Ottawa, Ottawa, ON K1H 8M5, Canada
[4] Special Pathogens Program, National Microbiology Laboratory, Public Health Agency of Canada, Winnipeg, MB R3E 3R2, Canada
[5] Department of Medical Microbiology, University of Manitoba, Winnipeg, MB R3E 0J9, Canada
*Corresponding author

This chapter appears as published in Viruses.
C. M. Stewart *et al.*, A Diacylglycerol Kinase Inhibitor, R-59-022, Blocks Filovirus Internalization in Host Cells. *Viruses* **11**, (2019).

Author Contributions: CS, SD, and MO contributed to the MLV pseudotype entry assays. NL and TS (supervised by MF) extracted, differentiated, and seeded BMDMs. CS and SQ contributed to the microscopy experiments. CL-4 experiments were performed by DK. All other experiments were performed by CS. Manuscript was written by CS and MC. Manuscript review and editing was performed by CS, SQ, MF, DK, and MC.

4.1 ABSTRACT

Filoviruses, such as Ebola virus (EBOV) and Marburg virus, are causative agents of unpredictable outbreaks of severe hemorrhagic fevers in humans and non-human primates. For infection, filoviral particles need to be internalized and delivered to intracellular vesicles containing cathepsin proteases and the viral receptor Niemann-Pick C1. Previous studies have shown that EBOV triggers macropinocytosis of the viral particles in a glycoprotein (GP)-dependent manner, but the molecular events required for filovirus internalization remain mostly unknown. Here we report that the diacylglycerol kinase inhibitor, R-59-022, blocks EBOV GP-mediated entry into Vero cells and bone marrow-derived macrophages. Investigation of the mode of action of the inhibitor revealed that it blocked an early step in entry, more specifically, the internalization of the viral particles via macropinocytosis. Finally, R-59-022 blocked viral entry mediated by a panel of pathogenic filovirus GPs and inhibited growth of replicative Ebola virus. Taken together, our studies suggest that R-59-022 could be used as a tool to investigate macropinocytic uptake of filoviruses and could be a starting point for the development of pan-filoviral therapeutics.

4.2 INTRODUCTION

Filoviruses, which include Ebola virus (EBOV) and Marburg virus (MARV), are zoonotic pathogens that can cause unpredictable outbreaks of severe hemorrhagic fevers in humans and non-human primates [1]. The virions are enveloped filamentous particles, of about 80nm in diameter and an average length of 800-1000nm, which enclose the negative single-stranded RNA genome of approximately 19,000 nucleotides [2]. The Filoviridae family contains three distinct genera: Ebolavirus that comprises five viruses (Bundibugyo (BDBV), EBOV, Reston (RESTV), Sudan (SUDV), and Taï Forest (TAFV)), Marburgvirus, and Cuevavirus [3].

While most outbreaks occurred in Central and West Africa, recent studies have uncovered the high diversity and large geographical distributions of filoviruses including the discovery of new bat-borne filoviruses in China [4]. Although several EBOV vaccines are being developed and the rVSV-EBOV was shown to be efficacious in a phase 3 clinical trial [5,6], these do not protect from infection by all filoviruses. Furthermore, there is currently no FDA-approved antiviral against any of these highly pathogenic viruses.

As enveloped viruses, filoviruses require the fusion of the viral membrane with that of the host cell to deliver its genome into the cell cytoplasm and initiate replication. Membrane fusion is accomplished by the viral glycoprotein (GP) that protrudes from the viral membrane [7]. In the current model of GP triggering for membrane fusion, GP needs to be cleaved by pH-dependent host cathepsin proteases to expose the receptor binding domain, followed by cleaved-GP interaction with the endosome/lysosome resident protein Niemann-Pick C1 (NPC1) [8–11]. Direct involvement of acidic pH on GP-mediated membrane fusion is still unclear [12,13]. These requirements of a low pH environment and presence host proteins located within intracellular vesicles indicate that a first step in filovirus entry is internalization of the viral particles.

Previous studies have shown that EBOV and potentially all filoviruses use a macropinocytosis or macropinocytosis-like mechanism for internalization [14–17]. Uptake of EBOV was found to be dependent on Rho GTPases including RhoC, Rac1, and Cdc42 [15,17], p53-activated kinase 1 [14,15], and protein kinase C [15], which are all known to be required for macropinocytosis [18]. While macropinocytosis can be constitutive in some cell types such as macrophages and dendritic cells, it needs to be triggered in others [18]. Interestingly, macropinocytosis was shown to be stimulated by EBOV in a GP-dependent manner as well as by phosphatidylserine molecules present in the viral membrane that can bind to phosphatidylserine

receptors expressed by some host cells [14–16,19]. The signaling cascades required for filovirus uptake by macropinocytosis remain to be determined.

Macropinocytosis requires large-scale organized movements of the actin cytoskeleton and results in the formation of macropinosomes of diameter varying from 0.2 to 10 μm, which can accommodate the size of filoviral particles [18]. Macropinosome formation requires the generation of membrane ruffles that extend from the cell surface by the assembly of actin filaments [20]. Most ruffles will retract, yet some will bend into cups that will close to form macropinosomes [18]. The lipid composition of the membrane during macropinocytosis - from ruffling, cup formation, to cup closure - is spatio-temporally regulated. For instance, macropinocytosis often requires activation of PI3K for the production of phosphatidylinositol(3,4,5)triphosphate (PtdIns(3,4,5)P_3) and PtdIns(3,4)P_2. These lipids can be visualized at the early stages of cup formation [21]. The synthesis of Ins(1,4,5)P_3 and diacylglycerol (DAG) from PtdIns(4,5)P_2 by the phospholipase Cγ (PLCγ) are also required. DAG is present in the membrane of the cup at later stages of formation and activates protein kinase Cα [21,22].

DAG kinases (DGKs) are lipid kinases that phosphorylate DAG to generate phosphatidic acid (PA) [23]. In mammals, there are ten isoforms of DGKs. Of these, most of them are localized, at least in part, at the plasma membrane [23]. Recent studies have suggested a role for DGKs in macropinocytosis; DGKζ was required for efficient macropinocytosis following growth factor stimulation [24] and loss of DGKζ expression decreased infection by vaccinia virus, which similarly to EBOV, requires macropinocytosis for viral entry [25]. Whether DGKs are implicated in filovirus entry is currently unknown.

Here we investigated a role for DGK activity in filovirus entry using a specific inhibitor of DGKs, R-59-022. We found that entry of pseudotypes and viral-like particles bearing the EBOV GP, but not those harboring the vesicular stomatitis virus (VSV)-G protein was blocked by R-59-022 in Vero cells. The small-molecule also inhibited EBOV GP-mediated entry in bone marrow-derived macrophages (BMDMs). Further analysis revealed that treatment of cells with R-59-022 led to a drastic inhibition of both virus and high molecular weight dextran internalization. Importantly, R-59-022 blocked entry mediated by multiple filoviral GPs and growth of replication competent EBOV. Our studies suggest that R-59-022 could be used as a tool to dissect the molecular events required for filoviral particle uptake and be a starting point for the development of pan-filoviral inhibitors.

4.3 RESULTS

4.3.1 R-59-022 Efficiently Blocks EBOV GP-Mediated Entry into Vero Cells

To investigate a potential role for DAG kinases in filovirus entry, we first tested the effect of a commercially available DAG kinase inhibitor R-59-022 on EBOV GP-mediated entry (Figure 1A). Because previous studies have shown that the mucin region of GP is not required for uptake via macropinocytosis or for cathepsin/NPC1 dependence, we used a mucin-deleted version of EBOV GP, which allows higher viral particle yields [8,9,16]. Vero cells were treated with increasing concentrations of R-59-022 and exposed for 4 hours to MLV pseudotypes encoding LacZ and bearing EBOV GP or VSV G in the presence of the drug. Media was then replaced with media containing ammonium chloride to stop further viral entry. Successful entry and provirus integration were then assessed by measurement of β-galactosidase activity using a luminescent substrate. We found that the inhibitor blocked entry of EBOV pseudotypes in a concentration-dependent manner (IC50: ~5μM, Figure 1B), but had no significant inhibitory

effect on VSV pseudotypes even at the highest concentration tested (Figure 1B). Instead, a slight increase in VSV pseudotype infection was observed at low R-59-022 concentrations. These results strongly suggested that R-59-022 blocked an entry step specific to EBOV GP.

To directly test for a potential role of R-59-022 in blocking viral entry, we used viral-like particles (VLPs) produced by co-transfection of EBOV NP and VP40 in cells. Expression of these viral proteins leads to the production of filoviral-like particles of similar morphology and size to those of native filoviral particles. To allow and measure virus-cell fusion of these particles into target cells, VLPs were produced by co-transfection of plasmids encoding EBOV NP, an EBOV VP40 construct fused with β-lactamase (βlam), and EBOV GP or VSV-G. The entry of these βlam VLPs leads to the delivery of VP40-βlam into the target cell cytoplasm which can be detected by loading cells with the βlam FRET substrate CCF2-AM. Vero cells were treated with increasing concentrations of R-59-022 and exposed to VLPs bearing EBOV GP or VSV G in the presence of the drug for 3 h. Delivery of VP40- βlam into the target cell cytoplasm was then assessed by labeling with CCF2-AM and analyzed by flow cytometry. Using this assay, we observed a R-59-022 dose-dependent decrease in entry by the VLPs harboring the EBOV GP (IC50: ~2 μM, Figure 1C). Interestingly, unlike the results of the experiments using MLV pseudotypes, a slight decrease in VSV G-mediated entry could also be observed. However, the decrease in entry of the VLPs bearing VSV-G was not dose-dependent (Figure 1C). This decrease can potentially be attributed to the large size some of the filoviral-like particles can exhibit, especially when compared to the size of MLV particles. Importantly, the inhibitor treatment did not have a detectable effect on the viability of Vero cells even at the highest concentration (Figure 1C). These results demonstrate that R-59-022 is an inhibitor of EBOV-GP mediated entry.

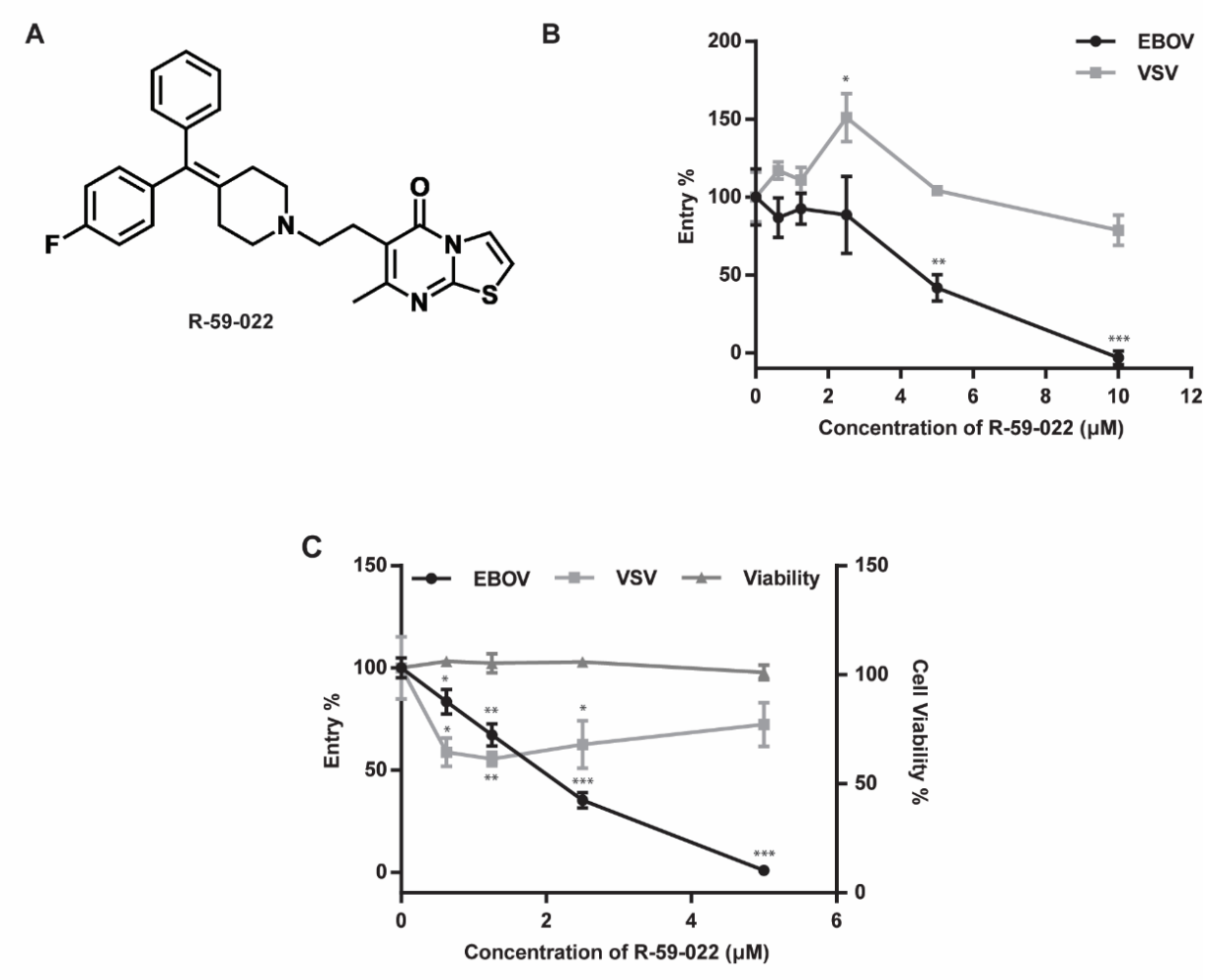

Figure 4.1 R-59-022 blocks EBOV GP-mediated entry in Vero cells.

(A) Chemical structure of R-59-022; (B, C) Measurement of GP-mediated entry in Vero cells. Vero cells were pre-treated for 1 h with increasing concentrations of R-59-022 or vehicle and exposed to (B) MLV pseudotypes encoding LacZ or (C) βlam VLPs harbouring the indicated viral glycoproteins in the presence of the drug for 4 and 3 h respectively. Infection was measured by (B) quantifying β-galactosidase activity using a luminescent substrate or (C) determining the percentage of cells with cytoplasmic βlam by CCF2-AM staining and flow cytometry analysis. Data are expressed as percentages relative to vehicle-treated cells; (C) Metabolic activity of the inhibitor-treated cells was measured in parallel and values were normalized to vehicle-treated cells. Data are representative of 3 independent experiments. * $p < 0.05$, ** $p < 0.01$, *** $p < 0.001$.

4.3.2 EBOV GP-Mediated Entry in Bone Marrow-Derived Macrophages is Inhibited by R-59-022

One of the primary targets of EBOV in vivo is macrophages. Therefore, we next sought to test if R-59-022 could also block EBOV GP-mediated entry in bone marrow-derived macrophages (BMDMs). Because BMDMs are terminally differentiated and do not proliferate, MLV pseudotypes could not be used for these experiments as MLV requires actively dividing cells for integration. Thus, we directly assessed EBOV GP-mediated entry in the presence of the inhibitor using the βlam VLP bearing EBOV GP or VSV-G. BMDMs were treated with increasing concentrations of R-59-022 and exposed to the βlam VLPs in the presence of the drug for 3 hours before staining and analysis by flow cytometry. Similarly to the results obtained with Vero cells, we found that entry of EBOV VLPs was significantly inhibited by R-59-022 in a dose-dependent manner (Figure 2). A reduction in the entry of the VSV-G VLPs could also be observed, albeit at a lesser extent when compared to the EBOV GP VLPs. Unlike the decrease obtained in the Vero cells, the slight decrease of VSV-G VLPs in the BMDMs was dose-dependent suggesting that VSV-G entry in those cells is in part sensitive to R-59-022 (Figure 2). Again, the drug treatment had no noticeable effect on cell viability when using Cell-Titer Glo to measure metabolic activity of the cells (Figure 2). Taken together, our data suggest that R-59-022 can inhibit EBOV GP-mediated entry in multiple cell types.

4.3.3 R-59-022 Interferes with Virus Internalization

EBOV entry involves multiple steps including attachment to the target cell, internalization by a macropinocytosis or macropinocytosis-like mechanism, trafficking, cleavage of GP by acid-dependent cathepsin proteases, and GP interaction with NPC1 [30]. To identify the step at which R-59-022 inhibits EBOV GP-mediated entry, we first performed kinetics

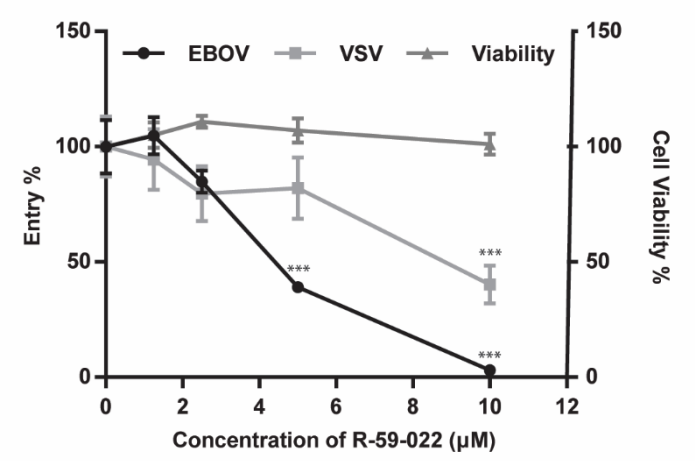

Figure 4.2 R-59-022 inhibits EBOV GP-mediated entry in bone marrow-derived macrophages. BMDMs were pre-treated for 1 hour with increasing concentrations of R-59-022 or vehicle and exposed to βlam VLPs harbouring EBOV GP or VSV G. Infection was measured by determining the percentage of cells with cytoplasmic βlam by CCF2-AM staining and flow cytometry analysis. Data are expressed as percentages relative to vehicle-treated cells. Metabolic activity was measured in parallel and was also normalized to vehicle-treated cells. Data are representative of 3 independent experiments. * $p < 0.05$, ** $p < 0.01$, *** $p < 0.001$.

experiments to determine if the drug acted at an early or late step of viral entry. Vero cells were exposed to βlam VLPs bearing EBOV GP and R-59-022 was added at different time-points during infection. Ammonium chloride (NH_4Cl) was used as a control as this lysosomotropic agent neutralizes the pH of the endosomes and lysosomes and therefore inhibits cathepsin activity and potentially downstream membrane fusion events. Using this assay, we found that the inhibitory activity of R-59-022 was lost at earlier time points when compared to that of NH_4Cl (Figure 3A). This result suggested that R-59-022 blocked an early step of EBOV GP-mediated viral entry.

The first steps in EBOV entry are virus attachment and internalization. To assess the ability of R-59-022 to interfere with virus attachment, we produced fluorescent VLPs, by the co-expression of a VP40 construct fused with mCherry. Vero cells were incubated with mCherry VLPs in the presence or absence of the inhibitor at 4°C to prevent internalization. Cells were washed to remove unbound viral particles, and the attached VLPs were measured using flow cytometry. Using the IC90 concentration of R-59-022, no significant difference in the extent of virus attachment was observed in the presence drug when compared to vehicle-treated cells (Figure 3B). To determine if R-59-022 blocked internalization, cells were incubated with mCherry VLPs at 4°C, unbound particles were removed, and cells with mCherry VLPs were incubated at 37°C to allow for internalization. For these experiments, 5-(N-Ethyl-N-isopropyl)amiloride (EIPA), a known inhibitor of macropinocytosis, was used as a control. We found that R-59-022 significantly inhibited VLP internalization at levels similar to that of EIPA treatment (Figure 3C). To confirm that the inhibitor has the same mode of action in different cell types, we also tested internalization of VLPs in the presence of R-59-022 in BMDMs. Again, internalization of VLPs was significantly blocked by the inhibitor (Figure 3D). Interestingly, R-

59-022 was even more potent than EIPA at inhibiting VLP internalization in these cells. Taken together, our results indicate that R-59-022 interferes with EBOV VLP internalization.

4.3.4 R-59-022 Blocks Macropinocytosis in Vero Cells

Since VLPs with EBOV GP are internalized via macropinocytosis or a macropinocytosis-like mechanism, we hypothesized that R-59-022 inhibits macropinocytosis. To test this, we incubated Vero cells with high molecular weight fluorescently labeled dextran, known to enter cells via macropinocytosis, in the presence or absence of R-59-022 or EIPA. As expected, treatment with R-59-022 and EIPA reduced the number of dextran positive vesicles in cells (Figure 4A,4B). These results indicate that R-59-022 inhibits macropinocytosis.

Our results suggest that R-59-022 blocks macropinocytic uptake of viral particles in cells. In an attempt to determine the fate of the VLPs in the presence of R-59-022, we used live-cell imaging to visualize the behavior of fluorescent VLPs. In addition, we sought to monitor actin filaments using GFP-utrophin as actin rearrangements are required for macropinocytosis. GFP-Utrophin transfected Vero cells were treated with vehicle or R-59-022 and mCherry VLPs bearing EBOV GP were added immediately prior to imaging. Interestingly, we observed significantly less movements of VLPs on/in the cell in the presence of R-59-022 treated cells compared to vehicle alone (Figure 4C,4D, Videos S1–S4). While VLPs were able to attach to the surface of the R-59-022 treated cell, these VLPs appeared to be ‘stuck’ and fewer actin cups were observed (Videos S1–S4). In sum, we observed a defect in macropinocytic uptake of high molecular weight dextran and reduced movements of VLPs in the presence of R-59-022.

4.3.5 R-59-022 Blocks Viral Entry of Pathogenic Filoviruses

Our data suggest that R-59-022 blocks macropinocytic uptake of EBOV VLPs. Given the large size of all filoviruses and the dependence on triggering factors such as NPC1 located in

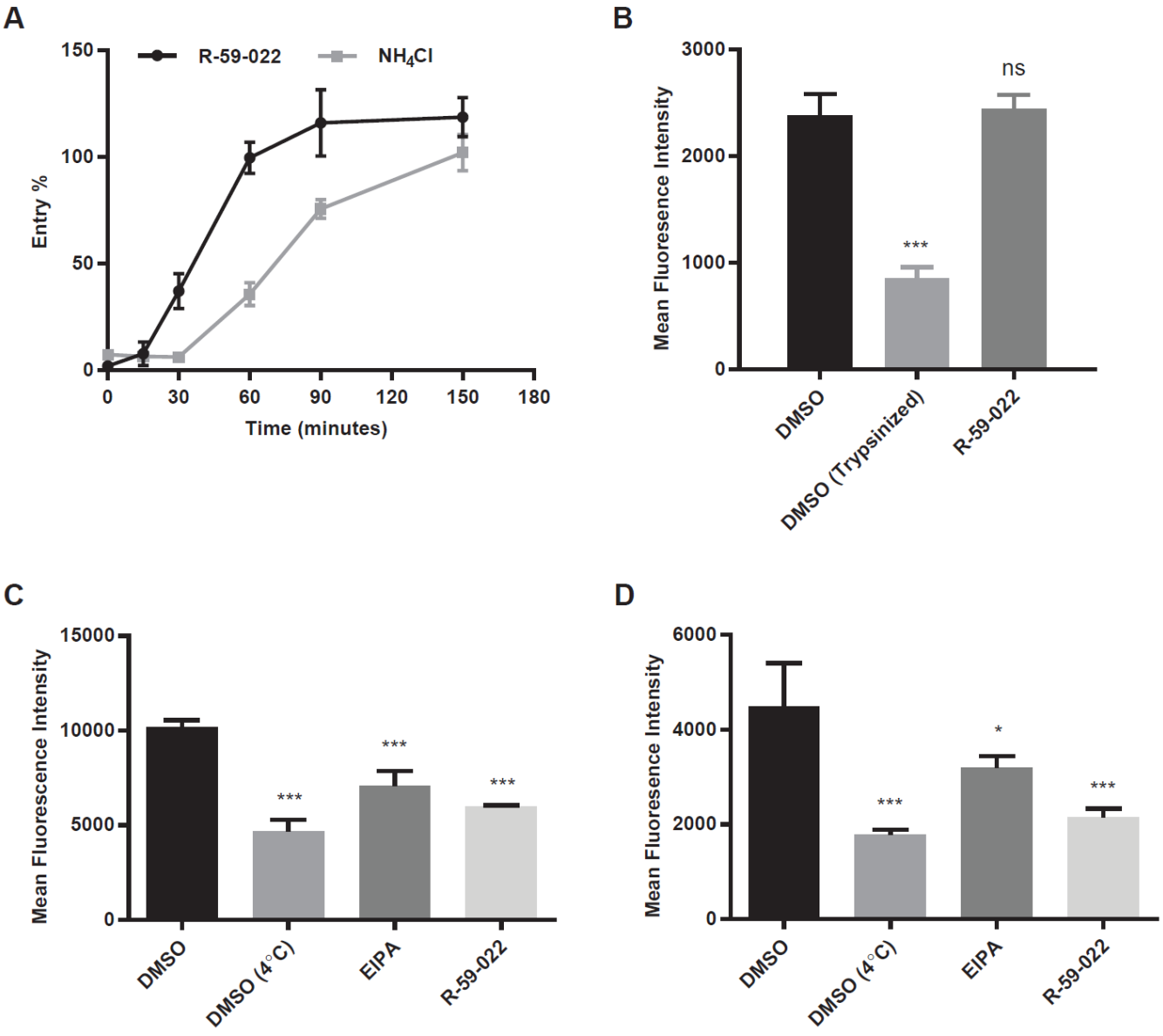
A
150
100
50
0
Entry %
R-59-022
NH4Cl
0
30
60
90
120
150
180
Time (minutes)
B
3000
2000
1000
0
Mean Fluoresence Intensity
ns
***
DMSO
DMSO (Trypsinized)
R-59-022
C
15000
10000
5000
0
Mean Fluorescence Intensity
***
***
***
DMSO
DMSO (4°C)
EIPA
R-59-022
D
6000
4000
2000
0
Mean Fluorescence Intensity
***
*
***
DMSO
DMSO (4°C)
EIPA
R-59-022

Figure 4.3 R-59-022 blocks internalization of EBOV VLPs into the host cell.

(A) Time of addition assay in Vero cells with βlam VLPs harboring EBOV GP. Cells were infected at t = 0 and R-59-022 (5 μM) or NH4Cl (15 mM) were added at indicated time points post-infection. Viral entry was measured by determining the percentage of cells with cleaved CCF2 compared to vehicle; (B) Attachment assay in Vero cells using mCherry VLPs harbouring EBOV GP. Vero cells were pre-treated with 5 μM R-59-022 or vehicle followed by a 1-hour incubation at 4°C with EBOV VLPs. One set of DMSO samples was trypsinized to remove bound VLPs. Fluorescence of mCherry VLPs was measured by flow cytometry and mean fluorescence intensity (MFI) for each sample determined using the FlowJo software; (C, D) Internalization assay in (C) Vero cells and (D) BMDMs using mCherry EBOV VLPs. Cells were pre-treated with 5 μM R-59-022, 30 μM EIPA, or vehicle followed by addition of VLPs and spinoculation at 4°C. Cells were washed with cold PBS and pre-warmed media containing inhibitor or vehicle was added. Cells with attached VLPs were incubated at 37°C for 1 h to allow for internalization and were then moved to 4°C for 15 min. Cells were then trypsinized at 4°C for 30 min to remove non-internalized VLPs. Fluorescence of internalized mCherry VLPs was measured by flow cytometry and mean fluorescence intensity determined using the FlowJo software. Data are representative of 3 independent experiments. * $p < 0.05$, ** $p < 0.01$, *** $p < 0.001$, ns: not significant.

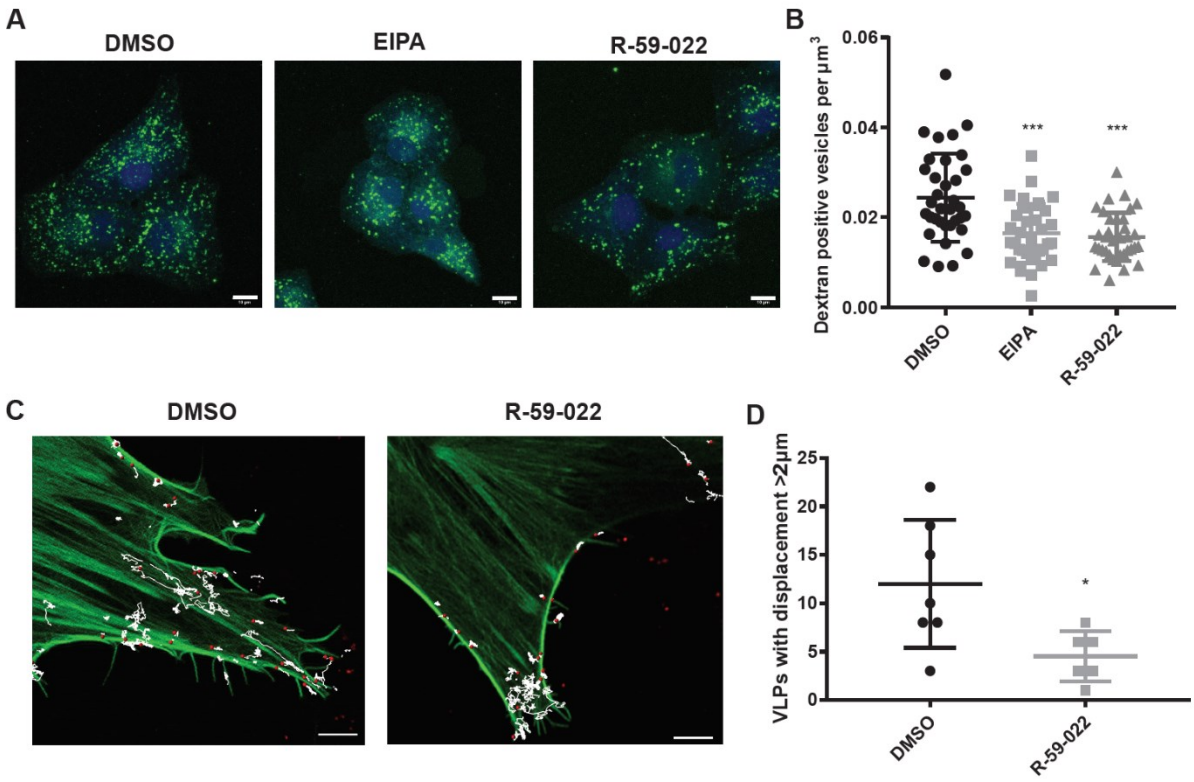

Figure 4.4 R-59-022 inhibits macropinocytosis in Vero cells.

(A) Vero cells were pre-treated with R-59-022 (5 µM), EIPA (30 µM), or vehicle for 30 min followed by addition of high molecular weight fluorescein dextran and incubation at 37°C for another 30 min. Cells were stained with Cell Tracker Blue CMAC fluorescent dye, which was added concomitantly with the fluorescent dextran. Cells were fixed and imaged with a LSM 800 confocal microscope (Zeiss). Images are displayed as maximum intensity z-projections, bar = 10 µm; (B) Number of dextran-positive puncta per cell volume (µm3) was determined using the Imaris software (Bitplane). (C) GFP-Utrophin transfected Vero cells were pre-treated with R-59-022 (5 µM) or vehicle for at least 30 min. The cells were then placed in an environmental chamber (37°C, 5% CO2) and mCherry EBOV VLPs added. Immediately after VLP addition, cells were imaged with a LSM 880 confocal microscopy (Zeiss) using AiryScan FAST on a single z plane. Images were analyzed using tracking algorithms on Imaris software (Bitplane). Each track represents the movement of VLPs over time. Bar = 5 µm; (D) Track length and displacement were measured (per VLP) and the number of VLPs with a displacement greater than 2 µM were counted per time lapse image. Data are representative of 3 independent experiments. *$p < 0.05$, $p < 0.01$, *** $p < 0.001$.

intracellular vesicles, it is expected that all filoviruses will require uptake by macropinocytosis or a macropinocytosis-like mechanism. Therefore, the prediction is that entry of all filoviruses will be blocked by R-59-022. To test this, we produced βlam VLPs harboring the GP of a panel of pathogenic filoviruses; EBOV, BDBV, SUDV, and MARV. Vero cells were exposed to the different VLPs in the presence of R-59-022 and entry efficiency was measured by CCF2-AM staining and flow cytometry analysis. As expected, entry by the VLPs harboring the filovirus GPs were potently blocked by R-59-022, while entry mediated by VSV G was not affected at the concentration used (Figure 5A). These data indicate that R-59-022 blocks a step used by all pathogenic filoviruses, presumably macropinocytosis, and could therefore be a pan-filovirus inhibitor.

4.3.6 EBOV Growth is Inhibited by R-59-022

As a preliminary assessment of R-59-022 potential as an anti-filovirus therapeutic, we tested the inhibitor for activity against replication-competent EBOV. Vero cells were treated with different concentrations of R-59-022 and infected with EBOV Mayinga expressing GFP. Virus growth was assessed by measurement of GFP at different time-points. Using this assay, we found that R-59-022 could indeed block EBOV growth, although it required higher concentrations then those used for single round infections (Figure 5B). Taken together, our results suggest that R-59-022 can inhibit native EBOV and potentially other filoviruses.

4.4 DISCUSSION

The entry mechanism of filoviruses involves a complex series of events that culminates with the fusion of the viral membrane with the endosomal membrane of the cell. Viral particles need to be internalized via macropinocytosis and trafficked to endosomal compartments containing cathepsin proteases and the viral receptor NPC1. While the molecular details of how

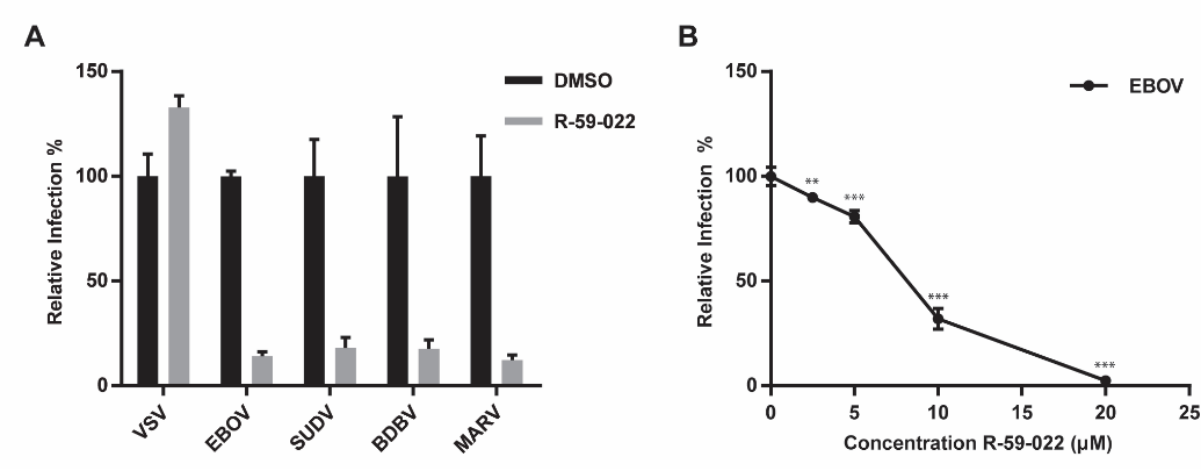

Figure 4.5 R-59-022 blocks entry of pathogenic filoviruses and growth of replication-competent EBOV

(A) Infection of Vero cells with βlam VLPs harbouring the GPs of EBOV, SUDV, BDBV, MARV, or VSV G in the presence of 5 μM R-59-022 or vehicle. Infection was measured using flow cytometry by determining the percentage of cells with cleaved CCF2. Data are expressed as percentages relative to vehicle-treated cells; (B) Infection of Vero cells with replication-competent EBOV expressing GFP at increasing concentrations of R-59-022 or vehicle. Infection was measured by GFP fluorescence 3 days post-infection and normalized to vehicle treated cells. Data is representative of 3 independent experiments. * $p < 0.05$, ** $p < 0.01$, *** $p < 0.001$.

each step is regulated remain to be investigated, we report here the discovery of R-59-022, a small-molecule inhibitor of filovirus entry. Analysis of the inhibitory mechanism of R-59-022 revealed that it prevented the macropinocytic uptake of filoviral particles, inhibited entry mediated by multiple filovirus GPs, and blocked replicative EBOV growth.

Several lines of evidence indicate that R-59-022 is an inhibitor of macropinocytosis. First, investigation of the kinetics of action of the inhibitor revealed that it specifically interfered with an early step in entry (Figure 3A). Second, further analysis of attachment and internalization of filoviral particles indicated that virus uptake was prevented in the presence of the drug (Figure 3C,3D) and live-imaging of viral particles in R-59-022 treated cells showed that viruses remained mostly static at the surface of the cells (Figure 4C,4D). Third, internalization of high molecular weight dextran, which is known to be primarily mediated by macropinocytosis [14], was also inhibited in the presence of the drug (Figure 4A,4B). Finally, while R-59-022 blocked entry mediated by all filovirus GPs tested (Figure 5A), it had no striking effect on VSV G-mediated entry which was shown to be internalized via clathrin-dependent endocytosis [31]. Interestingly, low concentrations of R-59-022 caused a small increase in VSV MLV pseudotype infection (Figure 1B). Whether low concentrations of R-59-022 can increase clathrin-mediated endocytosis remains to be determined. In contrast, we did observe a slight reduction in the entry of filoviral-like particles harbouring VSV G (Figure 1C). Given that these particles will exhibit the characteristic heterogenous filamentous morphology of EBOV, which can reach 1000 nm in length, it is expected that vesicles formed by clathrin-coated pits will be unable to accommodate the viral particles with larger sizes. Indeed, the biggest particles should only be able to enter cells via macropinocytosis or phagocytosis regardless of the viral glycoprotein expressed at their surface. Consequently, the slight decrease in VSV G-mediated entry of filoviral-like particles can

be explained by a block of internalization of a small fraction of the heterogenous particle population that comprises particles that are too large and require uptake by macropinocytosis. Therefore, our studies identify R-59-022 as a macropinocytosis inhibitor.

R-59-022 adds to the known repertoire of macropinocytosis-targeting EBOV inhibitors. Commonly used macropinocytosis inhibitors for viral entry include EIPA and Latrunculin A (Lat A). Each, however, have their own limitations and drawbacks. For example, EIPA, an analogue of the prototypical amiloride, is an inhibitor of Na+/H+ exchange that must be used at high concentrations of at least 25 μM, increasing off-target effects and reducing specificity. In addition, a study using sensitive pH nanosensors has also showed that amiloride treatment leads to change in endosomal pH [32]. With regards to Lat A, being a natural product that sequesters monomeric actin, it interferes with cell morphology and cytoskeletal homeostasis in addition to blocking macropinocytosis [33]. Although more characterization of the mode of action R-59-022 is required, R-59-022 has the potential to be a useful tool for the study of macropinocytosis. Our results show that R-59-022 inhibited the uptake of filoviral particles in both Vero cells and BMDMs. Interestingly, BMDMs can potentially also internalize the VLPs by phagocytosis which is a process that closely resembles macropinocytosis [18]. Analysis of EBOV GP-mediated entry of VLPs in the presence of R-59-022 revealed that the drug inhibited entry completely at 10 μM. While more work needs to be done, these results indicate that R-59-022 can inhibit macropinocytosis in multiple cell types and can also potentially interfere with phagocytosis. In addition, since R-59-022 blocked high molecular weight dextran uptake, this suggest that R-59-022 could also inhibit other viruses in addition to large molecules and complexes. Future studies will be needed to determine if R-59-022 can also inhibit other intracellular pathogens that utilize macropinocytosis and/or phagocytosis to enter the host cell.

Previous studies have demonstrated that EBOV triggers signaling cascades during viral entry. Cellular signaling proteins, such as Akt, PI3K, and the PIKfyve/ArPIKfyve/Sac3 complex, were shown to be activated during EBOV entry and involved in the intracellular trafficking and delivery of viral particles to vesicles containing NPC1 [34,35]. However, how EBOV regulates and/or induces macropinocytic uptake remain to be fully elucidated. Previous studies have shown that AMP-activated protein kinase is required for uptake of EBOV in multiple cell types [36]. More recently, the exchange protein directly activated by cAMP was also shown to be important for EBOV uptake in endothelial cells [37]. R-59-022 targets DGKs, which are relatively uncharacterized regulators of macropinocytosis, and represents to our knowledge the first evidence that EBOV could require these host enzymes. Future studies will be focused on the validation of the antiviral target of R-59-022 and investigation into a possible role for the ten different DGK isozymes in filovirus entry.

In this study, we have identified a small-molecule that blocks filovirus infection. To date, there are no FDA-approved antiviral therapies for EBOV or other filoviruses, highlighting the need for the identification of new small- molecule inhibitors of infection. We have found that R-59-022 is an inhibitor of filovirus internalization, therefore representing a potential starting point for the development of a pan-filovirus therapy.

4.5 MATERIALS AND METHODS

Cell Culture

HEK293T and Vero cells (ATCC) were cultured in Dulbecco's Modified Eagle Medium (DMEM, Wisent Bioproducts, Saint-Bruno, QC, Canada) and Minimum Essential Medium (MEM, Sigma-Aldrich, St. Louis, MO, USA) respectively, and supplemented with 10% Fetal Bovine Serum (FBS, Sigma-Aldrich), 0.3 mg/mL L-glutamine, 100 U/mL penicillin, and 100

μg/mL streptomycin (Wisent). Cells were maintained at 37°C in 5% CO2 at 100% relative humidity. Bone marrow-derived macrophages (BMDMs) were isolated and differentiated as described previously [26]. Briefly, mice were euthanized, musculature and connective tissue removed from the tibia and femur, and the bones cut at each end. The bones were placed in a tube containing a hole at the bottom, centrifuged, bone marrow cells re-suspended in DMEM supplemented with 10% FBS (Wisent), penicillin and streptomycin (Hyclone, GE Healthcare, Chicago, IL, USA), and were filtered through a 40 μm filter. Cells were differentiated into macrophages in 20% L929-conditioned media and plated for 7 days. On day 8, cells were seeded into 48-well plates and were placed in Roswell Park Memorial Institute medium (RPMI, Wisent), supplemented with 10% FBS (Sigma-Aldrich), 0.3 mg/mL L-glutamine, 100 U/mL penicillin, and 100 μg/mL streptomycin. All animal procedures were approved by the University of Ottawa Animal Care Committee.

Inhibitors and Plasmids

5-(N-ethyl-N-isopropyl)-Amiloride (EIPA, Cayman chemical, Ann Arbor, MI, USA) and R-59-022 (Cayman chemical) were prepared in DMSO, aliquoted, and stored at −80°C. Ammonium chloride (Sigma-Aldrich) stock solutions of 1.5M were prepared in water and filtered with 0.22 μm syringe filters.

All plasmids encoding the different virus envelope proteins (EBOV Δmucin GP, BDBV Δmucin GP, SUDV Δmucin GP, or MARV GP and VSV G) described previously [27], the packaging plasmid MLV gag/pol, and the MLV retroviral vector encoding LacZ were kind gifts of Dr. James Cunningham, Brigham and Women's Hospital. Plasmids encoding EBOV NP and EBOV VP40-β-lactamase were kind gifts of Dr. Lijun Rong, University of Illinois. The

mCherry-EBOV VP40 plasmid was a gift from Dr. Judith White (Addgene plasmid # 74421) [28].

Virus Pseudotype and Viral-Like Particle Production

To prepare murine leukemia virus (MLV) pseudotypes, 293T cells were co-transfected with a MLV retroviral vector encoding LacZ, the packaging plasmid MLV gag/pol, and a plasmid encoding the viral glycoprotein of interest (filoviral GP or VSV G). Transfection was performed using the jetPRIME transfection reagent (Polyplus transfection, Illkirch, France) according to the manufacturer's protocol and at a 1:1:1.15 (LacZ:GagPol:GP) ratio. Supernatants were harvested at 48, 72, and 96h post-transfection followed by virus concentration by ultracentrifugation (20,000 RPM, 4°C, 1.5h, Beckman Coulter Optima XPN-100, SW32Ti rotor) through a 20% (w/v) sucrose cushion. Concentrated virus was resuspended in PBS, aliquoted, and stored at −80°C.

To prepare EBOV viral-like particles (VLPs), 293T cells were co-transfected with plasmids encoding the EBOV nucleoprotein (NP), EBOV VP40 fused to β-lactamase (□lam) or mCherry, and the viral glycoprotein of interest (EBOV Δmucin GP, BDBV Δmucin GP, SUDV Δmucin GP, or MARV GP) at a 1:1:1.15 ratio. Transfection and virus concentration was performed as described above.

Virus Entry and Cell Viability Assays

For MLV infection assays, Vero cells were seeded onto white 96-well plates and grown to approximately 60% confluency. Cells were pre-treated for 1h with inhibitor or vehicle (DMSO, 0.01%) in serum-free MEM containing 5 μg/mL polybrene. Virus was added to pre-treated cells and infection allowed to proceed. Four hours post-infection, the media was replaced with phenol-red free complete DMEM containing 15 mM NH_4Cl and incubated overnight. Cells

were then grown for an additional 48h in phenol-red free complete DMEM without NH_4Cl. LacZ+ cells were quantified 72 h post-infection using the Beta-Glo Assay System (Promega, Madison, WI, USA) following the manufacturer's protocol. Luminescence was read using a Synergy Neo2 Multi-Mode plate reader (BioTek, Winooski, VT, USA).

For VLP entry assays, Vero cells or BMDMs were seeded onto clear 48-well plates and grown to approximately 90% confluency. Cells were pre-treated for 1h with inhibitor or vehicle in serum-free MEM (for Vero cells) or serum-free RPMI (for BMDMs) followed by the addition of VLPs. Three hours post-infection, cells were stained for 2 h at room temperature. Staining solution was prepared using the CCF2-AM kit (ThermoFisher, Waltham, MA, USA) according to the manufacturer's protocol and supplemented with 15 mM NH4Cl and 250 μM probenecid (Sigma-Aldrich). After staining, cells were washed, trypsinized, and prepared for analysis by flow cytometry (FACSCelesta, BD Biosciences, Franklin Lakes, NJ, USA). Infection was quantified using the FlowJo software by assessing the percentage of cells with cleaved CCF2 (shift from 530 nm to 460 nm emission) compared to uninfected samples. Cell viability/metabolic activity was also measured 4h post-inhibitor incubation using the CellTitre-Glo assay system (Promega) according to the manufacturer's protocol. Luminescence was read using a Synergy Neo2 Multi-Mode plate reader (BioTek).

Time of Addition Assay

Vero cells were seeded onto clear 48-well plates and grown to approximately 90% confluency. Media was changed to cold serum-free MEM and cells incubated at 4°C for 15 min. βlam VLPs were added on ice and attached to the surface of the cells by centrifugation at 300 × g for 30 min at 4°C. Inhibitors or NH_4Cl were added at the time of infection (0 h) or various time points post-infection (15 min, 30 min, 60 min, 120 min, 150 min). For the DMSO control,

vehicle was added at the 0 h time point. The infection was allowed to proceed and samples analyzed by flow cytometry as described above.

Virus Attachment Assay

Vero cells were detached using 0.5 mM EDTA in phosphate buffered saline (PBS), counted, and 100,000 cells were aliquoted into tubes. Cells were spun down, re-suspended in 2% FBS in PBS containing inhibitor or vehicle, and incubated at 37°C for 30 min. Cells were then incubated at 4°C for 15 min, followed by addition of mCherry VLPs and incubation at 4°C for 1 h. Cells were washed twice with cold PBS, re-suspended in cold 2% FBS in PBS, and mCherry fluorescence analyzed by flow cytometry (Celesta, BD Biosciences). In the trypsinized condition, 0.05% trypsin was added after the cold PBS washes and incubated for 5 min at room temperature prior to centrifugation and resuspension in cold 2% FBS in PBS.

Virus Internalization Assay

Vero cells or BMDMs were seeded onto clear 48-well plates and grown to approximately 90% confluency. Cells were pre-treated for 30 min with inhibitor or vehicle in serum-free MEM (for Vero cells) or serum-free RPMI (for BMDMs). Cells were incubated at 4°C for 15 min and mCherry VLPs added and attached to the surface of the cells by centrifugation at 300 × g for 30 min at 4°C. Unbound VLPs were washed with cold PBS followed by the addition of media containing pre-warmed inhibitor or vehicle and cells were incubated at 37°C for 1 h. For the 4°C control, cold media was added after the PBS wash instead of pre-warmed media and the incubation was maintained at 4°C for the duration of the assay. After 1h, the cells were again washed with cold PBS and incubated at 4°C with 0.5% trypsin for 30 min. Samples were prepared and mCherry fluorescence analyzed by flow cytometry (Celesta, BD Biosciences).

Dextran Internalization Assay

Vero cells were seeded onto coverslips and grown to approximately 60% confluency. Cells were pre-treated for 1 h with inhibitor or vehicle in serum-free MEM, followed by a 30 min incubation with Dextran-Fluorescein (10,000 MW, Anionic, 1 mg/mL, ThermoFisher) and CellTracker Blue CMAC Dye (ThermoFisher). Cells were washed, fixed, and imaged by confocal microscopy (LSM800 AxioObserver Z1, Zeiss, Oberkochen, Germany). Image analysis was performed using Imaris image analysis software (Bitplane, Zurich, Switzerland) whereby dextran containing vesicles were modeled as spots and counted for each cell.

Live-Cell Imaging of VLPs and Actin

Vero cells were seeded to approximately 70% confluency and transfected with a plasmid encoding GFP-Utrophin, a gift from William Bement (Addgene plasmid # 26737) [29], using jetPRIME transfection reagent (Polyplus transfection) according to the manufacturer's protocol. Twenty-four hours post-transfection, cells were re-seeded onto chamber slides (Lab-Tek, Scotts Valley, California, USA) to about 60% confluency. The next day, cells were pre-incubated with inhibitor or vehicle and mCherry EBOV VLPs were added. Live-cell imaging was performed immediately after addition of VLPs and proceeded for no longer than 30 min. The live imaging was performed on a Zeiss LSM 880 AxioObserver Z1 confocal microscope using AiryScan FAST mode on a single z plane. The environmental control chamber was set to 37°C, 5% CO2 and a 63x/1.4NA oil objective was used. Image analysis was performed using Imaris software (Bitplane) by tracking modeled VLPs as spots over time using the Brownian motion tracking algorithm.

Replication-Competent Virus Growth Assay

VeroE6 cells were seeded in clear bottom, black well tissue culture plates (Corning, Kennebunk, ME, USA) to be 80% confluent at the time of infection. The cells were treated with

different concentrations of R-59-022 and infected with EBOV (strain Mayinga), expressing enhanced-GFP, at a multiplicity of infection of 0.1. Virus growth was assessed by measurement of GFP at different time-points using a BioTek Synergy/HTX plate reader with excitation at 485 nm and emission at 516 nm. Experiments with replication-competent EBOV were performed in the Biosafety Level 4 facility at the National Microbiology Laboratory at the Public Health Agency of Canada.

Statistical Analysis

Statistical analysis was performed using Prism (GraphPad Software, San Diego, CA, USA). T-tests were performed for figures 1,2 and 4D and one-way ANOVA was used for figures 3B–D. Data in all figures are means ± standard deviation.

Supplementary Materials: The following are available online at www.mdpi.com/xxx/s1, Video S1: DMSO A, Video S2: DMSO B, Video S3: R-59-022 A, Video S4: R-59-022 B.

Funding: This research was funded by the Canadian Institutes of Health Research: grant number ER1-143489 to M.C., PJT148634 to M.D.F., and PJT155984 to M.C. and D.K.; C.M.S. was supported by a graduate scholarship from the Natural Sciences and Engineering Research Council of Canada and an Ontario Graduate Scholarship. S.Q. was supported by a graduate scholarship from the Natural Sciences and Engineering Research Council of Canada. M.C. is a Canada Research Chair in Molecular Virology and Antiviral Therapeutics. Additional support is provided to D.K. by the Public Health Agency of Canada. M.D.F. is supported by a CIHR New Investigator Award (MSH141981) and is recipient of an Ontario Ministry of Research, Innovation and Science Early Researcher Award.

Acknowledgments: We would like to acknowledge technical support from the uOttawa CBIA core staff, Chloë van Oostende and Skye McBride.

Conflicts of Interest: The authors declare no conflict of interest.

4.6 REFERENCES

1. Feldmann, H., Geisbert, T.W. Ebola haemorrhagic fever. Lancet 2011, 377, 849–862.
2. Peters, C.J., Sanchez, A., Feldmann, H., Rollin, P.E., Nichol, S., Ksiazek, T.G. Filoviruses as Emerging Pathogens. Seminars in Virology 1994, 5, 147–154.
3. Bao, Y., Amarasinghe, G.K., Basler, C.F., Bavari, S., Bukreyev, A., Chandran, K., Dolnik, O., Dye, J.M., Ebihara, H., Formenty, P., et al. Implementation of Objective PASC-Derived Taxon Demarcation Criteria for Official Classification of Filoviruses. Viruses 2017, 9, 106, https://doi.org/10.3390/v9050106.
4. Yang, X.L., Tan, C.W., Anderson, D.E., Jiang, R.D., Li, B., Zhang, W., Zhu, Y., Lim, X.F., Zhou, P., Liu, X.L., et al. Characterization of a filovirus (Mengla virus) from Rousettus bats in China. Nat. Microbiol. 2019, 4, 390–395.
5. Henao-Restrepo, A.M., Camacho A., Longini, I.M., Watson, C.H., Edmunds, W.J., Egger, M., Carroll, M.W., Dean, N.E., Diatta, I., Doumbia, M., et al. Efficacy and effectiveness of an rVSV-vectored vaccine in preventing Ebola virus disease: Final results from the Guinea ring vaccination, open-label, cluster-randomised trial (Ebola Ca Suffit!). Lancet 2017, 389, 505–518.
6. Wong, G., Mendoza, E.J., Plummer, F.A., Gao, G.F., Kobinger, G.P., Qiu, X. From bench to almost bedside: the long road to a licensed Ebola virus vaccine. Expert. Opin. Biol. Ther. 2018, 18, 159–173.
7. Harrison, S.C. Viral membrane fusion. Virology 2015, 479–480, 498-507.
8. Chandran, K., Sullivan, N.J., Felbor, U., Whelan, S.P., Cunningham, J.M. Endosomal proteolysis of the Ebola virus glycoprotein is necessary for infection. Science 2005, 308, 1643–1645.
9. Côté, M., Misasi, J., Ren, T., Bruchez, A., Lee, K., Filone, C.M., Hensley, L., Li, Q., Ory, D., Chandran, K., Cunningham, J.M. Small molecule inhibitors reveal Niemann-Pick C1 is essential for Ebola virus infection. Nature 2011, 477, 344–348.
10. Carette, J.E., Raaben, M., Wong, A.C., Herbert, A.S., Obernosterer, G., Mulherkar, N., Kuehne, A.I., Kranzusch, P.J., Griffin, A.M., Ruthel, G., et al. Ebola virus entry requires the cholesterol transporter Niemann-Pick C1. Nature 2011, 477, 340–343.
11. Miller, E.H., Obernosterer, G., Raaben, M., Herbert, A.S., Deffieu, M.S., Krishnan, A., Ndungo, E., Sandesara, R.G., Carette, J.E., Kuehne, A.I., et al. Ebola virus entry requires the host-programmed recognition of an intracellular receptor. EMBO J. 2012, 31, 1947–1960.
12. Markosyan, R.M., Miao, C., Zheng, Y.M., Melikyan, G.B., Liu, S.L., Cohen, F.S. Induction of Cell-Cell Fusion by Ebola Virus Glycoprotein: Low pH Is Not a Trigger. PLoS Pathog. 2016, 12, e1005373.
13. Harrison, J.S., Higgins, C.D., Chandran, K., Lai, J.R. Designed protein mimics of the Ebola virus glycoprotein GP2 alpha-helical bundle: stability and pH effects. Protein Sci. 2011, 20, 1587–1596.

14. Saeed, M.F., Kolokoltsov, A.A., Albrecht, T., Davey, R.A. Cellular entry of ebola virus involves uptake by a macropinocytosis-like mechanism and subsequent trafficking through early and late endosomes. PLoS Pathog. 2010, 6, e1001110.
15. Nanbo, A., Imai, M., Watanabe, S., Noda, T., Takahashi, K., Neumann, G., Halfmann, P., Kawaoka, Y. Ebolavirus is internalized into host cells via macropinocytosis in a viral glycoprotein-dependent manner. PLoS Pathog. 2010, 6, e1001121.
16. Mulherkar, N., Raaben, M., de la Torre, J.C., Whelan, S.P., Chandran, K. The Ebola virus glycoprotein mediates entry via a non-classical dynamin-dependent macropinocytic pathway. Virology 2011, 419, 72–83.
17. Quinn, K., Brindley, M.A., Weller, M.L., Kaludov, N., Kondratowicz, A., Hunt, C.L., Sinn, P.L., McCray, P.B. Jr., Stein, C.S., Davidson, B.L., et al. Rho GTPases modulate entry of Ebola virus and vesicular stomatitis virus pseudotyped vectors. J. Virol. 2009, 83, 10176–10186.
18. Swanson, J.A. Shaping cups into phagosomes and macropinosomes. Nat. Rev. Mol. Cell. Biol. 2008, 9, 639–649.
19. Hunt, C.L., Kolokoltsov, A.A., Davey, R.A., Maury, W. The Tyro3 receptor kinase Axl enhances macropinocytosis of Zaire ebolavirus. J. Virol. 2011, 85, 334–347.
20. Condon, N.D., Heddleston, J.M., Chew, T.L., Luo, L., McPherson, P.S., Ioannou, M.S., Hodgson, L., Stow, J.L., Wall, A.A. Macropinosome formation by tent pole ruffling in macrophages. J. Cell Biol. 2018, 217, 3873–3885.
21. Botelho, R.J., Teruel, M., Dierckman, R., Anderson, R., Wells, A., York, J.D., Meyer, T., Grinstein, S. Localized biphasic changes in phosphatidylinositol-4,5-bisphosphate at sites of phagocytosis. J. Cell Biol. 2000, 151, 1353–1368.
22. Cheeseman, K.L., Ueyama, T., Michaud, T.M., Kashiwagi, K., Wang, D., Flax, L.A., Shirai, Y., Loegering, D.J., Saito, N., Lennartz, M.R. Targeting of protein kinase C-epsilon during Fcgamma receptor-dependent phagocytosis requires the epsilonC1B domain and phospholipase C-gamma1. Mol. Biol. Cell 2006, 17, 799–813.
23. Shulga, Y.V., Topham, M.K., Epand, R.M. Regulation and functions of diacylglycerol kinases. Chem. Rev. 2011, 111, 6186–6208.
24. Abramovici, H., Mojtabaie, P., Parks, R.J., Zhong, X.P., Koretzky, G.A., Topham, M.K., Gee, S.H. Diacylglycerol kinase zeta regulates actin cytoskeleton reorganization through dissociation of Rac1 from RhoGDI. Mol. Biol. Cell 2009, 20, 2049–2059.
25. Ard, R., Mulatz, K., Pomoransky, J.L., Parks, R.J., Trinkle-Mulcahy, L., Bell, J.C., Gee, S.H. Regulation of Macropinocytosis by Diacylglycerol Kinase zeta. PLoS ONE 2015, 10, e0144942.
26. LeBlond, N.D., Fullerton, M.D. Methods to Evaluate AMPK Regulation of Macrophage Cholesterol Homeostasis. Methods Mol. Biol. 2018, 1732, 477–493.
27. Misasi, J., Chandran, K., Yang, J.Y., Considine, B., Filone, C.M., Côté, M., Sullivan, N., Fabozzi, G., Hensley, L., Cunningham, J. Filoviruses require endosomal cysteine

proteases for entry but exhibit distinct protease preferences. J. Virol. 2012, 86, 3284–3292.
28. Shoemaker, C.J., Schornberg, K.L., Delos, S.E., Scully, C., Pajouhesh, H., Olinger, G.G., Johansen, L.M., White, J.M. Multiple cationic amphiphiles induce a Niemann-Pick C phenotype and inhibit Ebola virus entry and infection. PLoS ONE 2013, 8, e56265.
29. Burkel, B.M., von Dassow, G., Bement, W.M. Versatile fluorescent probes for actin filaments based on the actin-binding domain of utrophin. Cell Motil. Cytoskeleton 2007, 64, 822–832.
30. Moller-Tank, S., Maury, W. Ebola virus entry: A curious and complex series of events. PLoS Pathog. 2015, 11, e1004731.
31. Cureton, D.K., Massol, R.H., Saffarian, S., Kirchhausen, T.L., Whelan, S.P. Vesicular stomatitis virus enters cells through vesicles incompletely coated with clathrin that depend upon actin for internalization. PLoS Pathog. 2009, 5, e1000394.
32. Nowak-Lovato, K.L., Wilson, B.S., Rector, K.D. SERS nanosensors that report pH of endocytic compartments during FcepsilonRI transit. Anal. Bioanal. Chem. 2010, 398, 2019–2029.
33. Spector, I., Shochet, N.R., Blasberger, D., Kashman, Y. Latrunculins--novel marine macrolides that disrupt microfilament organization and affect cell growth: I. Comparison with cytochalasin D. Cell Motil. Cytoskeleton 1989, 13, 127–144.
34. Saeed, M.F., Kolokoltsov, A.A., Freiberg, A.N., Holbrook, M.R., Davey, R.A. Phosphoinositide-3 kinase-Akt pathway controls cellular entry of Ebola virus. PLoS Pathog. 2008, 4, e1000141.
35. Qiu, S., Leung, A., Bo, Y., Kozak, R.A., Anand, S.P., Warkentin, C., Salambanga, F.D.R., Cui, J., Kobinger, G., Kobasa, D., Côté, M. Ebola virus requires phosphatidylinositol (3,5) bisphosphate production for efficient viral entry. Virology 2018, 513, 17–28.
36. Kondratowicz, A.S., Hunt, C.L., Davey, R.A., Cherry, S., Maury W.J. AMP-activated protein kinase is required for the macropinocytic internalization of ebolavirus. J. Virol. 2013, 87, 746–755.
37. Drelich, A., Judy, B., He, X., Chang, Q., Yu, S., Li, X., Lu, F., Wakamiya, M., Popov, V., Zhou, J., Ksiazek, T., Gong, B. Exchange Protein Directly Activated by cAMP Modulates Ebola Virus Uptake into Vascular Endothelial Cells. Viruses 2018, 10, 563, https://doi.org/10.3390/v10100563.

Chapter 5: General Discussion and Future Directions

5.1 SUMMARY OF FINDINGS AND FUTURE DIRECTIONS

EBOV entry is a multistep process requiring attachment, internalization, and trafficking to late endosomes and lysosomes where the EBOV GP fusion triggering factors are localized. Since EBOV can infect almost all cell types, it must employ mechanisms to trigger its internalization and facilitate its endolysosomal trafficking. The overarching goal of this thesis was to identify signaling pathways that EBOV activates or otherwise utilizes during entry to ensure delivery of the ribonucleocapsid to the cytosol. The work described in this thesis outlines the identification of several kinases, namely RTKs, SKs, and DGKs, whose activities are critical for EBOV entry and as such, can be targeted and inhibited by small molecules. Notably, two small molecule inhibitors identified and characterized in our studies, Gefitinib and FTY720, are already FDA-approved for cancer and multiple sclerosis respectively, and thus serve as valuable candidates for antiviral development.

In Chapter 2, we employed a chemical biology approach and screened a kinase inhibitor library to identify kinases and signaling pathways required for EBOV and/or MARV entry, and to identify novel inhibitors of EBOV entry. In addition to identifying kinases already known to be required for EBOV entry, we also identified some kinase inhibitors and their targets that were not previously implicated to be involved in filovirus entry. In the remainder of Chapter 2, we further characterized a set of RTK inhibitors identified in the screen, while in Chapter 3 we investigated a different set of hits – inhibitors of sphingosine kinases and sphingosine-1-phosphate receptors.

Our small molecule screen sits among a long list of others and with our kinase inhibitor library consisting only of 418 compounds, it was far from an exhaustive study of all possible

host kinases that could be involved in EBOV entry (62, 63, 120, 237-244). Despite this, our approach did allow for the identification of novel host factors involved in EBOV entry and by only targeting kinase inhibitors, we were able to strategically set the experimental conditions of our screen. For example, we screened in the absence of serum to minimize the effect of signaling induced by growth factors used to culture cells and we chose a screening concentration of 1 μM because most of the kinase inhibitors in our screen were already optimized to be highly specific to their target, with IC50 values in the low nanomolar range. This was in contrast to many other large-scale screens, even those of FDA approved drugs (eg. Lee et al. (243), or Basu et al. (239)), that are conducted at concentrations of 10 μM or higher. Additionally, many of the kinase inhibitors in our screen were developed to treat cancer, and thus developed to induce cell death. Therefore, screening at a lower concentration may have allowed us to identify compounds or groups of compounds that may be missed in other screens due to inherent cytotoxicity. While some of the signaling pathways identified in our screen were identified by other groups, such as Lee et al.'s identification of the EGFR signaling pathway, we were able to see an enrichment of RTK inhibitors as a whole in our hits and this lead to a clear line of further investigation (243). It is also relevant to note that our screen did not cover all of the 538 protein and lipid kinases in the human kinome and thus further exploration is recommended to identify other signaling pathways involved in EBOV entry (245).

In addition to the small size of our screen, another major limitation is off target effects and the possibility that the antiviral target is not the same as the known target of the compound. While screening using a genetic approach may have solved this problem, none of the genetic screens conducted by other groups have identified RTKs or SKs as hits (63, 120, 242, 244, 246, 247). This may be due to the deleterious effects of knocking down kinases important for cell

growth but may also be due to built-in redundancy. For example, we saw that the RTK inhibitors exerted a dominant negative effect and therefore simply knocking out or knocking down a single RTK would be unlikely to result in a reduction in infection because other RTKs can likely compensate. In the case of the SKs, SK1 and SK2 are known to compensate for one another – while a double knockout is embryonic lethal in mice, a single knockout has no obvious phenotype (248). In our follow up studies, we did attempt to verify the antiviral targets using genetic approaches, however we were only successful with the SKs. More work needs to be done to confirm the antiviral targets of our other screen hits.

In the remainder of Chapter 2, we investigated the role of RTK signaling in EBOV entry and further characterized select RTK hits by determining their mode of action and antiviral profiles. We found that the RTK inhibitors blocked entry mediated by the GPs of other pathogenic filoviruses by preventing trafficking of virions to entry conducive intracellular compartments. Furthermore, treatment with RTK inhibitors abrogated EBOV VLP induced Akt phosphorylation, a kinase known to be downstream of RTKs and that was previously reported to regulate endosomal trafficking of EBOV (184). Interestingly, another study proposed that phosphorylation of the host trafficking factor, PIKfyve, by EGF-activated Akt, promotes degradation of EGFR, thus suggesting a possible feedback mechanism for terminating RTK signaling (185). By activating RTKs during entry, EBOV may exploit this mechanism to promote its delivery to degradative endosomal compartments where its triggering factors are localized. We also found that EBOV-induced Akt activation can occur in the absence of EBOV GP. This led us to hypothesize that RTK activation could occur via PS binding to TAM RTKs and subsequent hetero-or-oligomerization of TAM RTKs with other RTKs, such as EGFR. This could also help explain why each RTK inhibitor can almost completely block EBOV entry, as

inhibiting one RTK would have the dominant negative effect of inhibiting both RTKs in the heterodimer.

A major caveat of this study is that we did not directly demonstrate that RTKs are activated by EBOV. Although we did attempt this through immunoblotting and proximity ligation assay, the signal to noise ratio between mock and VLPs, in addition to the limited sensitivities of these assays, proved very problematic. Furthermore, according to our model it is unlikely that EBOV discriminates among different RTKs, lowering even further the probability of detecting phosphorylation of a given RTK at a given time. By examining a downstream kinase, we were able to take advantage of signal amplification, increasing our signal to noise ratio in addition to solving the problem of choosing one specific RTK to probe. Whether EBOV may preferentially activate certain RTKs, for example if a given RTK is more likely than another to heterodimerize with TAM RTKs, is a question that remains unanswered.

Our study was not the first to identify inhibitors of RTKs, particularly EGFR, as anti-EBOV agents (eg. (243, 249, 250)). In addition, while our manuscript presented in Chapter 2 was under review, Kuroda et al. published a complementary article whereby they screened a library of RTK inhibitors, demonstrated that knockdown of RTKs in Huh7 cells reduced infection by EBOVΔVP30 and showed that stimulation with EBOVΔVP30 increases phosphorylation of the RTK HER2 and Akt (251). They also found that HER2 and TAM receptors colocalize during EBOV entry, and therefore suggested that this interaction stimulates macropinocytosis of EBOV since the TAM receptors were previously shown to enhance EBOV internalization (56, 251). While other viruses such as IAV and HSV-1 may utilize RTKs to promote macropinocytosis, our results specifically demonstrate that EBOV internalization is not affected by the RTK inhibitors (198, 213). Rather, we propose that EBOV activates RTK signaling through interaction with PS

on the viral envelope and TAM RTKs, which promotes endocytic trafficking of the virion to degradative compartments that contain NPC1 at the limiting membrane. Our study, in conjunction with Kuroda et al., demonstrates that EBOV activates RTK signaling during entry to promote activation of the PI3K/Akt pathway, which is required to facilitate endocytic trafficking of EBOV to entry conducive intracellular compartments.

In Chapter 3, we followed up on inhibitors of SKs and S1PRs that were identified in the kinase screen and further characterized the role of SK signaling in EBOV entry. We found that knockdown of SK1 or SK2 reduces entry of EBOV VLPs, suggesting that the antiviral targets of the inhibitors are indeed SKs. Mechanism of action studies suggested that the SK inhibitors prevented trafficking of EBOV to NPC1, with the SK1 inhibitor, PF-543, slightly reducing virion internalization as well. We also found that addition of extracellular S1P does not rescue inhibition of entry mediated by the SK inhibitors, suggesting that S1PR signaling is not required for EBOV entry. This finding was somewhat surprising as FTY720 is touted as a S1PR inhibitor, however studies also suggest that FTY720 acts as a competitive inhibitor of SK2 (252, 253). Notably, other studies have also implicated SKs in regulating endocytosis and endocytic membrane trafficking independent of S1PR signaling, however mechanistic details remain largely uncharacterized (254-256).

While our study and others show a clear connection between SKs and the regulation of endocytic membrane trafficking, many questions remain to be answered. For example, are there intracellular targets of S1P that are involved in regulating endocytic membrane trafficking or do SKs help regulate the lipid composition of endosomes, such as levels of sphingosine, which may be important for regulating endosome maturation and trafficking? Interestingly, Lima et al. found that treatment of cells with sphingosine or sphingosine mimetics, such as SK1-I or FTY720,

results in the accumulation of enlarged Rab7a positive late endosomes and that treatment with PF-543 delays clearance of sphingosine induces vacuoles (255). We can infer similar results as infection mediated by IAV HA, which undergoes fusion in Rab7 positive late endosomes, was increased in the presence of SK1 inhibitors (257). These data suggest that SK activity and maintaining certain concentrations of sphingosine in endosomes may be important for regulating late endosome-lysosome fusion. Interestingly, Lima et al. also demonstrated that increasing levels of sphingosine resulted in recruitment of endophilin B1, which others have shown can bind to and activate ultraviolet radiation resistance associated gene (UVRAG), a protein that is known to both be important for EBOV entry and regulating late endosome/lysosome fusion (61, 255, 258, 259). Therefore, it is possible that through regulating the activity of UVRAG, SKs can regulate late endosome/lysosome fusion.

The results from the virus panel also raise an interesting question with regards to whether SK1 and 2 play redundant roles in regulating endocytosis and trafficking. SK1-I did not reduce infection mediated by Junin GP, while PF-543 and FTY720 inhibited entry by about 50% at EBOV IC90 concentrations. Junin is known to enter cells via clathrin coated pits and undergo fusion in early and late endosomes (260). Interestingly, while PF-543 is fairly specific to SK1, it can also inhibit SK2, however SK1-I does not inhibit SK2 (261-263). It is possible that Junin virus can utilize either SK1 or SK2, therefore only an inhibitor that can target both, such as PF-543 or FTY720, would have an effect. Alternatively, Junin virus entry may be dependent on SK2 but not SK1. If this is the case, it may suggest that SK1/2 play differing roles in regulating endocytosis and/or endocytic membrane trafficking.

In Chapter 4, we investigated the mechanism of action of diacylglycerol kinase inhibitor, R-59-022. Our results from Chapters 2 and 3 further characterize how EBOV regulates endocytic

membrane trafficking, however the signaling cascades required for filovirus uptake by macropinocytosis remain largely uncharacterized. While R-59-022 was not a kinase inhibitor present in our screen, studies performed by Abramovici et al. and Ard et al., demonstrated that diacylglycerol kinase ζ (DGKζ) functioned upstream of Pak1 and Rac1, kinases previously implicated to be important for macropinocytosis of EBOV (264-266). They found that knockdown of DGKζ in fibroblosts resulted in defective growth factor induced macropinocytosis and reduced macropinocytosis of vaccinia virus (266). Similarly, we found that inhibition of DGKs by R-59-022 drastically reduced internalization of EBOV in both Vero cells and macrophages. Live cell imaging studies demonstrated decreased actin rearrangements in the presence of the inhibitor and fewer macropinocytic cups were observed following addition of EBOV VLPs. Whether EBOV activates or promotes DGK activity during entry remains to be determined. Additionally, since humans have 10 DGK isoforms, future studies with knockdown or knockout of DGKs would be prudent to both confirm the antiviral target and delineate which isoforms are required for regulating macropinocytosis (267, 268).

Taking these studies together, we propose a model for EBOV entry whereby host cell kinases and virus-induced signaling cascades act in concert to promote macropinocytosis and delivery of EBOV VLPs to entry conducive intracellular compartments (Figure 5.1). In this model, the catalysis of DG to PA by DGKs promote macropinocytosis of EBOV. Furthermore, SKs are known to associate with PA rich membranes, therefore the presence of PA also likely promotes the recruitment of SKs to macropinosomes or early endosomes. Here, SK activity is required to regulate late endosome-lysosome fusion and ensure delivery of EBOV to entry-conducive intracellular compartments. Furthermore, EBOV activates RTK signaling during entry to promote activation of the PI3K/Akt pathway, which directs EBOV trafficking to degradative

compartments. In sum, we found that EBOV can activate host cell signaling pathways during entry but also depends on functional steady-state signaling to ensure efficient delivery of the ribonucleocapsid to the cytoplasm.

5.2 POTENTIAL FOR ANTIVIRAL DRUG DEVELOPMENT

Today in 2021, the emergence of SARS-CoV-2 and the COVID-19 pandemic painfully highlights the undisputed need for broad-spectrum, host directed antiviral therapies. Despite the fact that in the last decade alone, two other epidemics caused by new emerging viruses have occurred – MERS in 2012 and Zika virus in 2016 – 89% of antiviral therapies approved for use are direct acting antivirals, and therefore unlikely to be effective against future emerging pathogens (269). This is because direct acting antivirals are developed to antagonize viral proteins and are therefore highly specific to the virus in question. While direct acting antivirals are generally very well tolerated and have been revolutionary in the treatment of viruses such as HIV and HCV, they take years to develop and are not a practical solution to treat emerging viruses efficiently (270). As is true for the development of any drug, concerns surrounding host-directed antiviral therapies are generally centered around balancing toxicity and efficacy. However, one needs to also consider that infections by emerging pathogens such as Ebola often cause acute but severe disease, and in some cases concerns over short-term toxicity may have to be weighed against the lack of other treatment options if said therapeutic is proven efficacious (270). Furthermore, while host-directed antivirals may not be as potent as virus-directed antivirals, evidence suggests that reducing the viral load gives patients a better chance at survival and could be critical to increasing survival rates in situations such as the current COVID-19 pandemic (271-274).

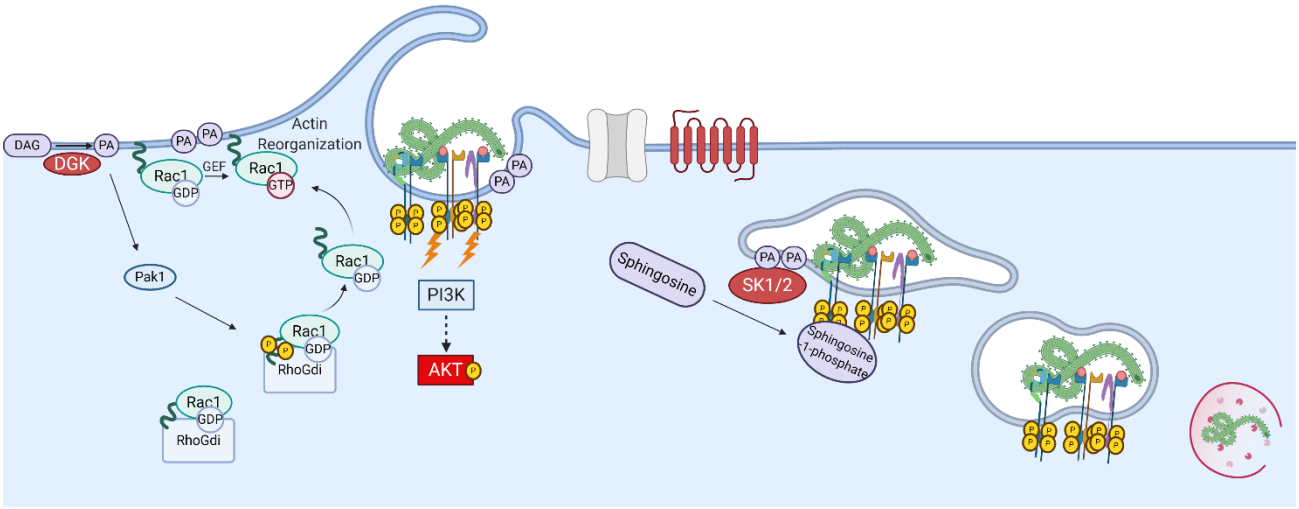

Figure 5.1 Proposed model of signaling pathways involved in EBOV entry presented in this thesis

Proposed role of diacylglycerol kinases, sphingosine kinases, and receptor tyrosine kinases in EBOV entry. Created using Biorender.com.

Host proteins involved in viral entry are attractive targets for the development of host-directed antivirals because viruses from different families often utilize similar host proteins and pathways to gain access to cells. Furthermore, targeting host proteins also decreases the likelihood that resistant viruses will arise. A few attempts have been made to develop host-directed viral entry antivirals, however most have been deemed too cytotoxic; examples of these include small molecules such as chloroquine that reduce acidification of endocytic vesicles or cytochalasin B which interferes with actin polymerization (270). A possible solution to this may be to identify synergistic drug combinations whereby the individual dose of each drug required to inhibit infection is reduced due to antiviral synergy (275). In addition, developments in research on viral entry over the past decade have identified other compounds or therapies, such as Bavituximab – a monoclonal antibody targeting PS – that may be more promising and pose fewer side effects (276). In this thesis, we describe some small molecules, several of which are already FDA-approved, that could be pursued in the development of host-directed antiviral therapies.

Since many viruses have been shown to utilize RTK signaling during entry – to promote internalization, trafficking, and to prepare the cell for subsequent infection – targeting RTKs has the potential to be a viable antiviral strategy. Furthermore, there are many RTK targeting monoclonal antibodies and small molecule inhibitors that are already FDA approved for other uses. For example, one of the small molecules discussed in this thesis, Gefitinib, which is sold under the brand name Iressa, is FDA-approved for treatment of certain cancers and since many viruses have already been shown to utilize EGFR signaling during entry, it could be an viable option to test in animal models (195, 198, 211, 213, 277-279). Many monoclonal antibodies against RTKs, including EGFR, are FDA-approved for use in cancer, however due to the

mechanism by which most viruses activate RTK signaling – that is via directly or indirectly inducing relatively non-specific RTK clustering – it is unlikely that targeting the extracellular domain of one RTK will be an effective treatment (280). Rather, we have shown that, at least for filoviruses, small molecules that target the intracellular tyrosine kinase domains exert a dominant negative effect by preventing cross-activation. Targeting RTKs likely will not completely inhibit infection *in vivo*, however they may be effective at reducing viral load and could potentially be used in combination with other antiviral drugs.

In this thesis, we also identified inhibitors of SKs and DGKs that are effective at preventing infection EBOV and other late penetrating viruses. Interestingly, FTY720, which is sold under the name Gilenya®, is FDA-approved for treatment of multiple sclerosis due to its immunomodulatory effects (252, 281, 282). In the early stages of the COVID-19 pandemic, a clinical trial (NCT04280588) was announced for FTY720 after a patient who was taking it for MS had a very favourable outcome for COVID-19 despite its immunomodulatory effects; unfortunately, the trial was recently withdrawn due to lack of participants (283, 284). This said, we show that FTY720 inhibits the entry of many late penetrating viruses, and other work has shown that it inhibits multiple stages of the HIV life cycle, suggesting that it may be a good candidate for antiviral development (285). In addition to FTY720, another sphingosine kinase 2 inhibitor, ABC294640, marketed under the brand name Opaganib, is under phase II clinical trials for COVID-19 (NCT04414618 and NCT04467840) and preclinical data have suggested both antiviral and anti-inflammatory effects for both SARS-CoV-2 and IAV (286, 287). Our lab has also shown that ABC294640 inhibits EBOV GP-mediated entry (data not shown). The antiviral and anti-inflammatory effects observed with SK2 inhibition may uniquely make SK2 inhibitors useful for treating viruses that trigger cytokine storms and dysregulated immune responses, such

as SARS-CoV-2 and EBOV. The results of these clinical trials will provide valuable insight into whether targeting SKs are an effective treatment strategy for COVID-19, and if so, it is likely that targeting SKs would be an effective treatment for other viruses as well.

5.3 CONCLUDING REMARKS

Today in the year 2021, in the face of the COVID-19 pandemic, researchers and clinicians around the world have scrambled to rapidly develop effective therapeutics against SARS-CoV-2; furthermore, the overwhelming socioeconomic and public health impacts are a grim reminder of our general lack of preparedness for treatment of emerging pathogens. Because many viruses utilize similar host factors during their infectious cycle, identifying and characterizing these host factors is critical for the development of antiviral therapeutics. In this thesis, we describe and characterize multiple kinases that EBOV and other late-penetrating viruses utilize to enter host cells. We demonstrate that EBOV can regulate its endolysosomal trafficking through RTK signaling during entry and speculate that activation of these pathways also prepares the cell for subsequent viral replication. Furthermore, we found that inhibiting SKs and DGKs prevents entry of EBOV by disrupting endolysosomal trafficking and macropinocytosis respectively. Through carefully elucidating the mechanism of action of these kinase inhibitors, we hope that this work may serve to support the development of broad-spectrum antiviral therapeutics to help prevent the catastrophic outcomes caused by emerging and re-emerging viruses.

References

1. **Anonymous.** 1978. Ebola haemorrhagic fever in Zaire, 1976. World Health Organ **56:**271-293.
2. **Anonymous.** 1978. Ebola haemorrhagic fever in Sudan, 1976. Report of a WHO/International Study Team. Bull World Health Organ **56:**247-270.
3. **Kuhn JH, Amarasinghe GK, Basler CF, Bavari S, Bukreyev A, Chandran K, Crozier I, Dolnik O, Dye JM, Formenty PBH, Griffiths A, Hewson R, Kobinger GP, Leroy EM, Mühlberger E, Викторович) SVNHC, Palacios G, Pályi B, Pawęska JT, Smither SJ, (高田礼人) AT, Towner JS, Wahl V, Consortium IR.** 2019. ICTV Virus Taxonomy Profile: Filoviridae. Journal of General Virology **100**.
4. **Kuhn JH, Adachi T, Adhikari NKJ, Arribas JR, Bah IE, Bausch DG, Bhadelia N, Borchert M, Brantsaeter AB, Brett-Major DM, Burgess TH, Chertow DS, Chute CG, Cieslak TJ, Colebunders R, Crozier I, Davey RT, de Clerck H, Delgado R, Evans L, Fallah M, Fischer WA, 2nd, Fletcher TE, Fowler RA, Grunewald T, Hall A, Hewlett A, Hoepelman AIM, Houlihan CF, Ippolito G, Jacob ST, Jacobs M, Jakob R, Jacquerioz FA, Kaiser L, Kalil AC, Kamara RF, Kapetshi J, Klenk HD, Kobinger G, Kortepeter MG, Kraft CS, Kratz T, Bosa HSK, Lado M, Lamontagne F, Lane HC, Lobel L, Lutwama J, Lyon GM, 3rd, et al.** 2019. New filovirus disease classification and nomenclature. Nat Rev Microbiol **17:**261-263.
5. **Yang XL, Tan CW, Anderson DE, Jiang RD, Li B, Zhang W, Zhu Y, Lim XF, Zhou P, Liu XL, Guan W, Zhang L, Li SY, Zhang YZ, Wang LF, Shi ZL.** 2019. Characterization of a filovirus (Mengla virus) from Rousettus bats in China. Nat Microbiol **4:**390-395.
6. **Feldmann H, Mühlberger E, Randolf A, Will C, Kiley MP, Sanchez A, Klenk HD.** 1992. Marburg virus, a filovirus: messenger RNAs, gene order, and regulatory elements of the replication cycle. Virus Res **24:**1-19.
7. **Sanchez A, Kiley MP, Holloway BP, Auperin DD.** 1993. Sequence analysis of the Ebola virus genome: organization, genetic elements, and comparison with the genome of Marburg virus. Virus Res **29:**215-240.
8. **Hume AJ, Muhlberger E.** 2019. Distinct Genome Replication and Transcription Strategies within the Growing Filovirus Family. J Mol Biol **431:**4290-4320.
9. **Shi M, Lin X-D, Chen X, Tian J-H, Chen L-J, Li K, Wang W, Eden J-S, Shen J-J, Liu L, Holmes EC, Zhang Y-Z.** 2018. The evolutionary history of vertebrate RNA viruses. Nature **556:**197-202.
10. **Geisbert TW, Jahrling PB.** 1995. Differentiation of filoviruses by electron microscopy. Virus Res **39:**129-150.
11. **Bharat TA, Riches JD, Kolesnikova L, Welsch S, Krahling V, Davey N, Parsy ML, Becker S, Briggs JA.** 2011. Cryo-electron tomography of Marburg virus particles and their morphogenesis within infected cells. PLoS Biol **9:**e1001196.
12. **Volchkov VE, Feldmann H, Volchkova VA, Klenk H-D.** 1998. Processing of the Ebola virus glycoprotein by the proprotein convertase furin. Proceedings of the National Academy of Sciences **95:**5762.
13. **Harty RN, Brown ME, Wang G, Huibregtse J, Hayes FP.** 2000. A PPxY motif within the VP40 protein of Ebola virus interacts physically and functionally with a ubiquitin

ligase: Implications for filovirus budding. Proceedings of the National Academy of Sciences **97:**13871.
14. **Noda T, Sagara H, Suzuki E, Takada A, Kida H, Kawaoka Y.** 2002. Ebola Virus VP40 Drives the Formation of Virus-Like Filamentous Particles Along with GP. Journal of Virology **76:**4855.
15. **Makino A, Yamayoshi S, Shinya K, Noda T, Kawaoka Y.** 2011. Identification of Amino Acids in Marburg Virus VP40 That Are Important for Virus-Like Particle Budding. The Journal of Infectious Diseases **204:**S871-S877.
16. **Becker S, Rinne C, Hofsäss U, Klenk HD, Mühlberger E.** 1998. Interactions of Marburg virus nucleocapsid proteins. Virology **249:**406-417.
17. **Groseth A, Charton JE, Sauerborn M, Feldmann F, Jones SM, Hoenen T, Feldmann H.** 2009. The Ebola virus ribonucleoprotein complex: a novel VP30-L interaction identified. Virus Res **140:**8-14.
18. **Davey RA, Shtanko O, Anantpadma M, Sakurai Y, Chandran K, Maury W.** 2017. Mechanisms of Filovirus Entry, p 323-352. *In* Mühlberger E, Hensley LL, Towner JS (ed), Marburg- and Ebolaviruses: From Ecosystems to Molecules doi:10.1007/82_2017_14. Springer International Publishing, Cham.
19. **Leroy EM, Kumulungui B, Pourrut X, Rouquet P, Hassanin A, Yaba P, Délicat A, Paweska JT, Gonzalez J-P, Swanepoel R.** 2005. Fruit bats as reservoirs of Ebola virus. Nature **438:**575-576.
20. **Towner JS, Pourrut X, Albarino CG, Nkogue CN, Bird BH, Grard G, Ksiazek TG, Gonzalez JP, Nichol ST, Leroy EM.** 2007. Marburg virus infection detected in a common African bat. PLoS One **2:**e764.
21. **Malvy D, McElroy AK, de Clerck H, Günther S, van Griensven J.** 2019. Ebola virus disease. The Lancet **393:**936-948.
22. **Towner JS, Amman BR, Sealy TK, Carroll SA, Comer JA, Kemp A, Swanepoel R, Paddock CD, Balinandi S, Khristova ML, Formenty PB, Albarino CG, Miller DM, Reed ZD, Kayiwa JT, Mills JN, Cannon DL, Greer PW, Byaruhanga E, Farnon EC, Atimnedi P, Okware S, Katongole-Mbidde E, Downing R, Tappero JW, Zaki SR, Ksiazek TG, Nichol ST, Rollin PE.** 2009. Isolation of genetically diverse Marburg viruses from Egyptian fruit bats. PLoS Pathog **5:**e1000536.
23. **Mühlberger E, Hensley LL, Towner JS.** 2017. Marburg- and Ebolaviruses From Ecosystems to Molecules, 1 ed, vol 1. Springer International Publishing.
24. **Jacob ST, Crozier I, Fischer WA, 2nd, Hewlett A, Kraft CS, Vega MA, Soka MJ, Wahl V, Griffiths A, Bollinger L, Kuhn JH.** 2020. Ebola virus disease. Nat Rev Dis Primers **6:**13.
25. **Gire SK, Goba A, Andersen KG, Sealfon RSG, Park DJ, Kanneh L, Jalloh S, Momoh M, Fullah M, Dudas G, Wohl S, Moses LM, Yozwiak NL, Winnicki S, Matranga CB, Malboeuf CM, Qu J, Gladden AD, Schaffner SF, Yang X, Jiang P-P, Nekoui M, Colubri A, Coomber MR, Fonnie M, Moigboi A, Gbakie M, Kamara FK, Tucker V, Konuwa E, Saffa S, Sellu J, Jalloh AA, Kovoma A, Koninga J, Mustapha I, Kargbo K, Foday M, Yillah M, Kanneh F, Robert W, Massally JLB, Chapman SB, Bochicchio J, Murphy C, Nusbaum C, Young S, Birren BW, Grant DS, Scheiffelin JS, et al.** 2014. Genomic surveillance elucidates Ebola virus origin and transmission during the 2014 outbreak. Science **345:**1369-1372.

26. **Chippaux J-P.** 2014. Outbreaks of Ebola virus disease in Africa: the beginnings of a tragic saga. Journal of Venomous Animals and Toxins including Tropical Diseases **20:**44.
27. **Azarian T, Lo Presti A, Giovanetti M, Cella E, Rife B, Lai A, Zehender G, Ciccozzi M, Salemi M.** 2015. Impact of spatial dispersion, evolution and selection on Ebola Zaire Virus epidemic waves. Scientific Reports **5:**10170.
28. **Olson SH, Reed P, Cameron KN, Ssebide BJ, Johnson CK, Morse SS, Karesh WB, Mazet JAK, Joly DO.** 2012. Dead or alive: animal sampling during Ebola hemorrhagic fever outbreaks in humans. Emerging Health Threats Journal **5:**9134.
29. **Emanuel J, Marzi A, Feldmann H.** 2018. Chapter Nine - Filoviruses: Ecology, Molecular Biology, and Evolution, p 189-221. *In* Kielian M, Mettenleiter TC, Roossinck MJ (ed), Advances in Virus Research, vol 100. Academic Press.
30. **Mate SE, Kugelman JR, Nyenswah TG, Ladner JT, Wiley MR, Cordier-Lassalle T, Christie A, Schroth GP, Gross SM, Davies-Wayne GJ, Shinde SA, Murugan R, Sieh SB, Badio M, Fakoli L, Taweh F, de Wit E, van Doremalen N, Munster VJ, Pettitt J, Prieto K, Humrighouse BW, Ströher U, DiClaro JW, Hensley LE, Schoepp RJ, Safronetz D, Fair J, Kuhn JH, Blackley DJ, Laney AS, Williams DE, Lo T, Gasasira A, Nichol ST, Formenty P, Kateh FN, De Cock KM, Bolay F, Sanchez-Lockhart M, Palacios G.** 2015. Molecular Evidence of Sexual Transmission of Ebola Virus. New England Journal of Medicine **373:**2448-2454.
31. **Diallo B, Sissoko D, Loman NJ, Bah HA, Bah H, Worrell MC, Conde lS, Sacko R, Mesfin S, Loua A, Kalonda JK, Erondu NA, Dahl BA, Handrick S, Goodfellow I, Meredith LW, Cotten M, Jah U, Guetiya Wadoum RE, Rollin P, Magassouba NF, Malvy D, Anglaret X, Carroll MW, Aylward RB, Djingarey MH, Diarra A, Formenty P, Keïta S, Günther S, Rambaut A, Duraffour S.** 2016. Resurgence of Ebola Virus Disease in Guinea Linked to a Survivor With Virus Persistence in Seminal Fluid for More Than 500 Days. Clinical Infectious Diseases **63:**1353-1356.
32. **Chowell G, Hengartner NW, Castillo-Chavez C, Fenimore PW, Hyman JM.** 2004. The basic reproductive number of Ebola and the effects of public health measures: the cases of Congo and Uganda. Journal of Theoretical Biology **229:**119-126.
33. **Bell BP, Damon IK, Jernigan DB, Kenyon TA, Nichol ST, O'Connor JP, Tappero JW.** 2016. Overview, Control Strategies, and Lessons Learned in the CDC Response to the 2014-2016 Ebola Epidemic. MMWR Suppl **65:**4-11.
34. **Furuyama W, Marzi A.** 2019. Ebola Virus: Pathogenesis and Countermeasure Development. Annu Rev Virol **6:**435-458.
35. **Rojas M, Monsalve DM, Pacheco Y, Acosta-Ampudia Y, Ramirez-Santana C, Ansari AA, Gershwin ME, Anaya JM.** 2020. Ebola virus disease: An emerging and re-emerging viral threat. J Autoimmun **106:**102375.
36. **Organization WH.** 2016. Clinical Management of Patients with Viral Haemorrhagic Fever: A Pocket Guide for Front-line Health Workers. Interim Emergency Guidance for Country Adaption. World Health Organization.
37. **Dowell SF, Mukunu R, Ksiazek TG, Khan AS, Rollin PE, Peters CJ.** 1999. Transmission of Ebola hemorrhagic fever: a study of risk factors in family members, Kikwit, Democratic Republic of the Congo, 1995. Commission de Lutte contre les Epidémies à Kikwit. J Infect Dis **179 Suppl 1:**S87-91.

38. **Geisbert TW, Hensley LE, Larsen T, Young HA, Reed DS, Geisbert JB, Scott DP, Kagan E, Jahrling PB, Davis KJ.** 2003. Pathogenesis of Ebola hemorrhagic fever in cynomolgus macaques: evidence that dendritic cells are early and sustained targets of infection. Am J Pathol **163:**2347-2370.
39. **Geisbert TW, Young HA, Jahrling PB, Davis KJ, Larsen T, Kagan E, Hensley LE.** 2003. Pathogenesis of Ebola hemorrhagic fever in primate models: evidence that hemorrhage is not a direct effect of virus-induced cytolysis of endothelial cells. Am J Pathol **163:**2371-2382.
40. **Messaoudi I, Amarasinghe GK, Basler CF.** 2015. Filovirus pathogenesis and immune evasion: insights from Ebola virus and Marburg virus. Nature Reviews Microbiology **13:**663-676.
41. **Hensley LE, Young HA, Jahrling PB, Geisbert TW.** 2002. Proinflammatory response during Ebola virus infection of primate models: possible involvement of the tumor necrosis factor receptor superfamily. Immunol Lett **80:**169-179.
42. **Ströher U, West E, Bugany H, Klenk H-D, Schnittler H-J, Feldmann H.** 2001. Infection and Activation of Monocytes by Marburg and Ebola Viruses. Journal of Virology **75:**11025.
43. **Wahl-Jensen V, Kurz S, Feldmann F, Buehler LK, Kindrachuk J, DeFilippis V, da Silva Correia J, Früh K, Kuhn JH, Burton DR, Feldmann H.** 2011. Ebola Virion Attachment and Entry into Human Macrophages Profoundly Effects Early Cellular Gene Expression. PLOS Neglected Tropical Diseases **5:**e1359.
44. **Gupta M, Mahanty S, Ahmed R, Rollin PE.** 2001. Monocyte-Derived Human Macrophages and Peripheral Blood Mononuclear Cells Infected with Ebola Virus Secrete MIP-1α and TNF-α and Inhibit Poly-IC-Induced IFN-α in Vitro. Virology **284:**20-25.
45. **Bosio CM, Aman MJ, Grogan C, Hogan R, Ruthel G, Negley D, Mohamadzadeh M, Bavari S, Schmaljohn A.** 2003. Ebola and Marburg Viruses Replicate in Monocyte-Derived Dendritic Cells without Inducing the Production of Cytokines and Full Maturation. The Journal of Infectious Diseases **188:**1630-1638.
46. **Mahanty S, Hutchinson K, Agarwal S, McRae M, Rollin PE, Pulendran B.** 2003. Cutting Edge: Impairment of Dendritic Cells and Adaptive Immunity by Ebola and Lassa Viruses. The Journal of Immunology **170:**2797.
47. **Harcourt BH, Sanchez A, Offermann MK.** 1998. Ebola virus inhibits induction of genes by double-stranded RNA in endothelial cells. Virology **252:**179-188.
48. **Harcourt BH, Sanchez A, Offermann MK.** 1999. Ebola virus selectively inhibits responses to interferons, but not to interleukin-1beta, in endothelial cells. J Virol **73:**3491-3496.
49. **Basler CF, Mikulasova A, Martinez-Sobrido L, Paragas J, Mühlberger E, Bray M, Klenk HD, Palese P, García-Sastre A.** 2003. The Ebola virus VP35 protein inhibits activation of interferon regulatory factor 3. J Virol **77:**7945-7956.
50. **Cárdenas WB, Loo YM, Gale M, Jr., Hartman AL, Kimberlin CR, Martínez-Sobrido L, Saphire EO, Basler CF.** 2006. Ebola virus VP35 protein binds double-stranded RNA and inhibits alpha/beta interferon production induced by RIG-I signaling. J Virol **80:**5168-5178.
51. **Leung DW, Prins KC, Borek DM, Farahbakhsh M, Tufariello JM, Ramanan P, Nix JC, Helgeson LA, Otwinowski Z, Honzatko RB, Basler CF, Amarasinghe GK.** 2010.

Structural basis for dsRNA recognition and interferon antagonism by Ebola VP35. Nat Struct Mol Biol **17:**165-172.

52. **Luthra P, Ramanan P, Mire CE, Weisend C, Tsuda Y, Yen B, Liu G, Leung DW, Geisbert TW, Ebihara H, Amarasinghe GK, Basler CF.** 2013. Mutual antagonism between the Ebola virus VP35 protein and the RIG-I activator PACT determines infection outcome. Cell Host Microbe **14:**74-84.
53. **Hartman AL, Bird BH, Towner JS, Antoniadou ZA, Zaki SR, Nichol ST.** 2008. Inhibition of IRF-3 activation by VP35 is critical for the high level of virulence of ebola virus. J Virol **82:**2699-2704.
54. **Prins KC, Delpeut S, Leung DW, Reynard O, Volchkova VA, Reid SP, Ramanan P, Cárdenas WB, Amarasinghe GK, Volchkov VE, Basler CF.** 2010. Mutations abrogating VP35 interaction with double-stranded RNA render Ebola virus avirulent in guinea pigs. J Virol **84:**3004-3015.
55. **Alvarez CP, Lasala F, Carrillo J, Muniz O, Corbi AL, Delgado R.** 2002. C-type lectins DC-SIGN and L-SIGN mediate cellular entry by Ebola virus in cis and in trans. J Virol **76:**6841-6844.
56. **Hunt CL, Kolokoltsov AA, Davey RA, Maury W.** 2011. The Tyro3 receptor kinase Axl enhances macropinocytosis of Zaire ebolavirus. J Virol **85:**334-347.
57. **Kondratowicz AS, Lennemann NJ, Sinn PL, Davey RA, Hunt CL, Moller-Tank S, Meyerholz DK, Rennert P, Mullins RF, Brindley M, Sandersfeld LM, Quinn K, Weller M, McCray PB, Chiorini J, Maury W.** 2011. T-cell immunoglobulin and mucin domain 1 (TIM-1) is a receptor for Zaire Ebolavirus and Lake Victoria Marburgvirus. Proceedings of the National Academy of Sciences **108:**8426-8431.
58. **Nanbo A, Imai M, Watanabe S, Noda T, Takahashi K, Neumann G, Halfmann P, Kawaoka Y.** 2010. Ebolavirus is internalized into host cells via macropinocytosis in a viral glycoprotein-dependent manner. PLoS Pathog **6:**e1001121.
59. **Saeed MF, Kolokoltsov AA, Albrecht T, Davey RA.** 2010. Cellular entry of ebola virus involves uptake by a macropinocytosis-like mechanism and subsequent trafficking through early and late endosomes. PLoS Pathog **6:**e1001110.
60. **Qiu S, Leung A, Bo Y, Kozak RA, Anand SP, Warkentin C, Salambanga FDR, Cui J, Kobinger G, Kobasa D, Cote M.** 2018. Ebola virus requires phosphatidylinositol (3,5) bisphosphate production for efficient viral entry. Virology **513:**17-28.
61. **Bo Y, Qiu S, Mulloy RP, Cote M.** 2020. Filoviruses Use the HOPS Complex and UVRAG To Traffic to Niemann-Pick C1 Compartments during Viral Entry. J Virol **94:** e01002-01020.
62. **Cote M, Misasi J, Ren T, Bruchez A, Lee K, Filone CM, Hensley L, Li Q, Ory D, Chandran K, Cunningham J.** 2011. Small molecule inhibitors reveal Niemann-Pick C1 is essential for Ebola virus infection. Nature **477:**344-348.
63. **Carette JE, Raaben M, Wong AC, Herbert AS, Obernosterer G, Mulherkar N, Kuehne AI, Kranzusch PJ, Griffin AM, Ruthel G, Dal Cin P, Dye JM, Whelan SP, Chandran K, Brummelkamp TR.** 2011. Ebola virus entry requires the cholesterol transporter Niemann-Pick C1. Nature **477:**340-343.
64. **Chandran K, Sullivan NJ, Felbor U, Whelan SP, Cunningham JM.** 2005. Endosomal Proteolysis of the Ebola Virus Glycoprotein Is Necessary for Infection. Science **308:**1643-1645.

65. **Misasi J, Chandran K, Yang JY, Considine B, Filone CM, Cote M, Sullivan N, Fabozzi G, Hensley L, Cunningham J.** 2012. Filoviruses require endosomal cysteine proteases for entry but exhibit distinct protease preferences. J Virol **86:**3284-3292.
66. **Brecher M, Schornberg KL, Delos SE, Fusco ML, Saphire EO, White JM.** 2012. Cathepsin cleavage potentiates the Ebola virus glycoprotein to undergo a subsequent fusion-relevant conformational change. J Virol **86:**364-372.
67. **Spence JS, Krause TB, Mittler E, Jangra RK, Chandran K.** 2016. Direct Visualization of Ebola Virus Fusion Triggering in the Endocytic Pathway. MBio **7:**e01857-01815.
68. **Das DK, Bulow U, Diehl WE, Durham ND, Senjobe F, Chandran K, Luban J, Munro JB.** 2020. Conformational changes in the Ebola virus membrane fusion machine induced by pH, Ca2+, and receptor binding. PLoS Biol **18:**e3000626.
69. **Mühlberger E, Weik M, Volchkov VE, Klenk H-D, Becker S.** 1999. Comparison of the Transcription and Replication Strategies of Marburg Virus and Ebola Virus by Using Artificial Replication Systems. Journal of Virology **73:**2333-2342.
70. **Sugita Y, Matsunami H, Kawaoka Y, Noda T, Wolf M.** 2018. Cryo-EM structure of the Ebola virus nucleoprotein–RNA complex at 3.6 Å resolution. Nature **563:**137-140.
71. **Mühlberger E.** 2007. Filovirus replication and transcription. Future Virol **2:**205-215.
72. **Volchkov VE, Becker S, Volchkova VA, Ternovoj VA, Kotov AN, Netesov SV, Klenk HD.** 1995. GP mRNA of Ebola virus is edited by the Ebola virus polymerase and by T7 and vaccinia virus polymerases. Virology **214:**421-430.
73. **Sanchez A, Trappier SG, Mahy BW, Peters CJ, Nichol ST.** 1996. The virion glycoproteins of Ebola viruses are encoded in two reading frames and are expressed through transcriptional editing. Proc Natl Acad Sci U S A **93:**3602-3607.
74. **Mehedi M, Falzarano D, Seebach J, Hu X, Carpenter MS, Schnittler HJ, Feldmann H.** 2011. A new Ebola virus nonstructural glycoprotein expressed through RNA editing. J Virol **85:**5406-5414.
75. **Anthony SM, Bradfute SB.** 2015. Filoviruses: One of These Things is (not) Like the Other. Viruses **7:**5172-5190.
76. **Mohan GS, Li W, Ye L, Compans RW, Yang C.** 2012. Antigenic subversion: a novel mechanism of host immune evasion by Ebola virus. PLoS Pathog **8:**e1003065.
77. **Feldmann H, Nichol ST, Klenk HD, Peters CJ, Sanchez A.** 1994. Characterization of filoviruses based on differences in structure and antigenicity of the virion glycoprotein. Virology **199:**469-473.
78. **Licata JM, Johnson RF, Han Z, Harty RN.** 2004. Contribution of Ebola Virus Glycoprotein, Nucleoprotein, and VP24 to Budding of VP40 Virus-Like Particles. Journal of Virology **78:**7344-7351.
79. **Mittler E, Kolesnikova L, Strecker T, Garten W, Becker S.** 2007. Role of the transmembrane domain of marburg virus surface protein GP in assembly of the viral envelope. J Virol **81:**3942-3948.
80. **Lee JE, Saphire EO.** 2009. Ebolavirus glycoprotein structure and mechanism of entry. Future Virol **4:**621-635.
81. **Hoenen T, Shabman RS, Groseth A, Herwig A, Weber M, Schudt G, Dolnik O, Basler CF, Becker S, Feldmann H.** 2012. Inclusion Bodies Are a Site of Ebolavirus Replication. Journal of Virology **86:**11779-11788.

82. **Lier C, Becker S, Biedenkopf N.** 2017. Dynamic phosphorylation of Ebola virus VP30 in NP-induced inclusion bodies. Virology **512:**39-47.
83. **Banadyga L, Hoenen T, Ambroggio X, Dunham E, Groseth A, Ebihara H.** 2017. Ebola virus VP24 interacts with NP to facilitate nucleocapsid assembly and genome packaging. Sci Rep **7:**7698.
84. **Takamatsu Y, Kolesnikova L, Becker S.** 2018. Ebola virus proteins NP, VP35, and VP24 are essential and sufficient to mediate nucleocapsid transport. Proc Natl Acad Sci U S A **115:**1075-1080.
85. **Schudt G, Dolnik O, Kolesnikova L, Biedenkopf N, Herwig A, Becker S.** 2015. Transport of Ebolavirus Nucleocapsids Is Dependent on Actin Polymerization: Live-Cell Imaging Analysis of Ebolavirus-Infected Cells. J Infect Dis **212 Suppl 2:**S160-166.
86. **Martin-Serrano J, Zang T, Bieniasz PD.** 2001. HIV-1 and Ebola virus encode small peptide motifs that recruit Tsg101 to sites of particle assembly to facilitate egress. Nat Med **7:**1313-1319.
87. **Licata JM, Simpson-Holley M, Wright NT, Han Z, Paragas J, Harty RN.** 2003. Overlapping motifs (PTAP and PPEY) within the Ebola virus VP40 protein function independently as late budding domains: involvement of host proteins TSG101 and VPS-4. J Virol **77:**1812-1819.
88. **Adu-Gyamfi E, Johnson KA, Fraser ME, Scott JL, Soni SP, Jones KR, Digman MA, Gratton E, Tessier CR, Stahelin RV.** 2015. Host Cell Plasma Membrane Phosphatidylserine Regulates the Assembly and Budding of Ebola Virus. J Virol **89:**9440-9453.
89. **Nanbo A, Maruyama J, Imai M, Ujie M, Fujioka Y, Nishide S, Takada A, Ohba Y, Kawaoka Y.** 2018. Ebola virus requires a host scramblase for externalization of phosphatidylserine on the surface of viral particles. PLoS Pathog **14:**e1006848.
90. **Moller-Tank S, Kondratowicz AS, Davey RA, Rennert PD, Maury W.** 2013. Role of the phosphatidylserine receptor TIM-1 in enveloped-virus entry. J Virol **87:**8327-8341.
91. **Moller-Tank S, Maury W.** 2014. Phosphatidylserine receptors: enhancers of enveloped virus entry and infection. Virology **468-470:**565-580.
92. **Harrison SC.** 2015. Viral membrane fusion. Virology **479-480:**498-507.
93. **Rey FA, Lok SM.** 2018. Common Features of Enveloped Viruses and Implications for Immunogen Design for Next-Generation Vaccines. Cell **172:**1319-1334.
94. **Miller EH, Chandran K.** 2012. Filovirus entry into cells - new insights. Curr Opin Virol **2:**206-214.
95. **Jeffers SA, Sanders DA, Sanchez A.** 2002. Covalent modifications of the ebola virus glycoprotein. J Virol **76:**12463-12472.
96. **Lee JE, Fusco ML, Hessell AJ, Oswald WB, Burton DR, Saphire EO.** 2008. Structure of the Ebola virus glycoprotein bound to an antibody from a human survivor. Nature **454:**177-182.
97. **Dias JM, Kuehne AI, Abelson DM, Bale S, Wong AC, Halfmann P, Muhammad MA, Fusco ML, Zak SE, Kang E, Kawaoka Y, Chandran K, Dye JM, Saphire EO.** 2011. A shared structural solution for neutralizing ebolaviruses. Nat Struct Mol Biol **18:**1424-1427.
98. **Kuhn JH, Radoshitzky SR, Guth AC, Warfield KL, Li W, Vincent MJ, Towner JS, Nichol ST, Bavari S, Choe H, Aman MJ, Farzan M.** 2006. Conserved receptor-binding

domains of Lake Victoria marburgvirus and Zaire ebolavirus bind a common receptor. J Biol Chem **281:**15951-15958.
99. **Brindley MA, Hughes L, Ruiz A, McCray PB, Jr., Sanchez A, Sanders DA, Maury W.** 2007. Ebola virus glycoprotein 1: identification of residues important for binding and postbinding events. J Virol **81:**7702-7709.
100. **Dube D, Brecher MB, Delos SE, Rose SC, Park EW, Schornberg KL, Kuhn JH, White JM.** 2009. The primed ebolavirus glycoprotein (19-kilodalton GP1,2): sequence and residues critical for host cell binding. J Virol **83:**2883-2891.
101. **Wang H, Shi Y, Song J, Qi J, Lu G, Yan J, Gao GF.** 2016. Ebola Viral Glycoprotein Bound to Its Endosomal Receptor Niemann-Pick C1. Cell **164:**258-268.
102. **Lennemann NJ, Rhein BA, Ndungo E, Chandran K, Qiu X, Maury W.** 2014. Comprehensive functional analysis of N-linked glycans on Ebola virus GP1. mBio **5:**e00862-00813.
103. **Reynard O, Borowiak M, Volchkova VA, Delpeut S, Mateo M, Volchkov VE.** 2009. Ebolavirus glycoprotein GP masks both its own epitopes and the presence of cellular surface proteins. J Virol **83:**9596-9601.
104. **Francica JR, Varela-Rohena A, Medvec A, Plesa G, Riley JL, Bates P.** 2010. Steric shielding of surface epitopes and impaired immune recognition induced by the ebola virus glycoprotein. PLoS Pathog **6:**e1001098.
105. **Weissenhorn W, Carfí A, Lee KH, Skehel JJ, Wiley DC.** 1998. Crystal structure of the Ebola virus membrane fusion subunit, GP2, from the envelope glycoprotein ectodomain. Mol Cell **2:**605-616.
106. **Malashkevich VN, Schneider BJ, McNally ML, Milhollen MA, Pang JX, Kim PS.** 1999. Core structure of the envelope glycoprotein GP2 from Ebola virus at 1.9-A resolution. Proc Natl Acad Sci U S A **96:**2662-2667.
107. **Koellhoffer JF, Malashkevich VN, Harrison JS, Toro R, Bhosle RC, Chandran K, Almo SC, Lai JR.** 2012. Crystal structure of the Marburg virus GP2 core domain in its postfusion conformation. Biochemistry **51:**7665-7675.
108. **Gregory SM, Harada E, Liang B, Delos SE, White JM, Tamm LK.** 2011. Structure and function of the complete internal fusion loop from Ebolavirus glycoprotein 2. Proceedings of the National Academy of Sciences **108:**11211-11216.
109. **Lee J, Nyenhuis DA, Nelson EA, Cafiso DS, White JM, Tamm LK.** 2017. Structure of the Ebola virus envelope protein MPER/TM domain and its interaction with the fusion loop explains their fusion activity. Proc Natl Acad Sci U S A **114:**E7987-E7996.
110. **Wilen CB, Tilton JC, Doms RW.** 2012. HIV: cell binding and entry. Cold Spring Harb Perspect Med **2**.
111. **Stegmann T, Hoekstra D, Scherphof G, Wilschut J.** 1985. Kinetics of pH-dependent fusion between influenza virus and liposomes. Biochemistry **24:**3107-3113.
112. **Fénéant L, Szymańska-de Wijs KM, Nelson EA, White JM.** 2019. An exploration of conditions proposed to trigger the Ebola virus glycoprotein for fusion. PLoS One **14:**e0219312.
113. **McCune JM, Rabin LB, Feinberg MB, Lieberman M, Kosek JC, Reyes GR, Weissman IL.** 1988. Endoproteolytic cleavage of gp160 is required for the activation of human immunodeficiency virus. Cell **53:**55-67.
114. **Wool-Lewis RJ, Bates P.** 1999. Endoproteolytic processing of the ebola virus envelope glycoprotein: cleavage is not required for function. J Virol **73:**1419-1426.

115. **Neumann G, Geisbert TW, Ebihara H, Geisbert JB, Daddario-DiCaprio KM, Feldmann H, Kawaoka Y.** 2007. Proteolytic processing of the Ebola virus glycoprotein is not critical for Ebola virus replication in nonhuman primates. J Virol **81:**2995-2998.
116. **Wong AC, Sandesara RG, Mulherkar N, Whelan SP, Chandran K.** 2010. A Forward Genetic Strategy Reveals Destabilizing Mutations in the Ebolavirus Glycoprotein That Alter Its Protease Dependence during Cell Entry. Journal of Virology **84:**163-175.
117. **Chandran K, Sullivan NJ, Felbor U, Whelan SP, Cunningham JM.** 2005. Endosomal Proteolysis of the Ebola Virus Glycoprotein Is Necessary for Infection. Science **308:**1643.
118. **Bortz RH, 3rd, Wong AC, Grodus MG, Recht HS, Pulanco MC, Lasso G, Anthony SJ, Mittler E, Jangra RK, Chandran K.** 2020. A Virion-Based Assay for Glycoprotein Thermostability Reveals Key Determinants of Filovirus Entry and Its Inhibition. J Virol **94:** e00336-00320.
119. **Moller-Tank S, Maury W.** 2015. Ebola Virus Entry: A Curious and Complex Series of Events. PLOS Pathogens **11:**e1004731.
120. **Kolokoltsov AA, Saeed MF, Freiberg AN, Holbrook MR, Davey RA.** 2009. Identification of novel cellular targets for therapeutic intervention against Ebola virus infection by siRNA screening. Drug Dev Res **70:**255-265.
121. **Sakurai Y, Kolokoltsov AA, Chen C-C, Tidwell MW, Bauta WE, Klugbauer N, Grimm C, Wahl-Schott C, Biel M, Davey RA.** 2015. Two-pore channels control Ebola virus host cell entry and are drug targets for disease treatment. Science **347:**995-998.
122. **Simmons JA, D'Souza RS, Ruas M, Galione A, Casanova JE, White JM.** 2016. Ebolavirus Glycoprotein Directs Fusion through NPC1+ Endolysosomes. J Virol **90:**605-610.
123. **Nathan L, Lai AL, Millet JK, Straus MR, Freed JH, Whittaker GR, Daniel S.** 2020. Calcium Ions Directly Interact with the Ebola Virus Fusion Peptide To Promote Structure-Function Changes That Enhance Infection. ACS Infect Dis **6:**250-260.
124. **Brown GD, Willment JA, Whitehead L.** 2018. C-type lectins in immunity and homeostasis. Nature Reviews Immunology **18:**374-389.
125. **Marzi A, Möller P, Hanna SL, Harrer T, Eisemann J, Steinkasserer A, Becker S, Baribaud F, Pöhlmann S.** 2007. Analysis of the interaction of Ebola virus glycoprotein with DC-SIGN (dendritic cell-specific intercellular adhesion molecule 3-grabbing nonintegrin) and its homologue DC-SIGNR. J Infect Dis **196 Suppl 2:**S237-246.
126. **Pipirou Z, Powlesland AS, Steffen I, Pöhlmann S, Taylor ME, Drickamer K.** 2011. Mouse LSECtin as a model for a human Ebola virus receptor. Glycobiology **21:**806-812.
127. **Becker S, Spiess M, Klenk HD.** 1995. The asialoglycoprotein receptor is a potential liver-specific receptor for Marburg virus. J Gen Virol **76 (Pt 2):**393-399.
128. **Takada A, Fujioka K, Tsuiji M, Morikawa A, Higashi N, Ebihara H, Kobasa D, Feldmann H, Irimura T, Kawaoka Y.** 2004. Human macrophage C-type lectin specific for galactose and N-acetylgalactosamine promotes filovirus entry. J Virol **78:**2943-2947.
129. **Ji X, Olinger GG, Aris S, Chen Y, Gewurz H, Spear GT.** 2005. Mannose-binding lectin binds to Ebola and Marburg envelope glycoproteins, resulting in blocking of virus interaction with DC-SIGN and complement-mediated virus neutralization. J Gen Virol **86:**2535-2542.
130. **Brudner M, Karpel M, Lear C, Chen L, Yantosca LM, Scully C, Sarraju A, Sokolovska A, Zariffard MR, Eisen DP, Mungall BA, Kotton DN, Omari A, Huang**

IC, Farzan M, Takahashi K, Stuart L, Stahl GL, Ezekowitz AB, Spear GT, Olinger GG, Schmidt EV, Michelow IC. 2013. Lectin-dependent enhancement of Ebola virus infection via soluble and transmembrane C-type lectin receptors. PLoS One **8:**e60838.
131. **Favier AL, Gout E, Reynard O, Ferraris O, Kleman JP, Volchkov V, Peyrefitte C, Thielens NM.** 2016. Enhancement of Ebola Virus Infection via Ficolin-1 Interaction with the Mucin Domain of GP Glycoprotein. J Virol **90:**5256-5269.
132. **Salvador B, Sexton NR, Carrion R, Nunneley J, Patterson JL, Steffen I, Lu K, Muench MO, Lembo D, Simmons G.** 2013. Filoviruses Utilize Glycosaminoglycans for Their Attachment to Target Cells. Journal of Virology **87:**3295-3304.
133. **O'Hearn A, Wang M, Cheng H, Lear-Rooney CM, Koning K, Rumschlag-Booms E, Varhegyi E, Olinger G, Rong L.** 2015. Role of EXT1 and Glycosaminoglycans in the Early Stage of Filovirus Entry. J Virol **89:**5441-5449.
134. **Fadok VA, Voelker DR, Campbell PA, Cohen JJ, Bratton DL, Henson PM.** 1992. Exposure of phosphatidylserine on the surface of apoptotic lymphocytes triggers specific recognition and removal by macrophages. J Immunol **148:**2207-2216.
135. **Hoffmann PR, deCathelineau AM, Ogden CA, Leverrier Y, Bratton DL, Daleke DL, Ridley AJ, Fadok VA, Henson PM.** 2001. Phosphatidylserine (PS) induces PS receptor-mediated macropinocytosis and promotes clearance of apoptotic cells. J Cell Biol **155:**649-659.
136. **Amara A, Mercer J.** 2015. Viral apoptotic mimicry. Nat Rev Microbiol **13:**461-469.
137. **Mercer J, Helenius A.** 2008. Vaccinia virus uses macropinocytosis and apoptotic mimicry to enter host cells. Science **320:**531-535.
138. **Moller-Tank S, Albritton LM, Rennert PD, Maury W.** 2014. Characterizing Functional Domains for TIM-Mediated Enveloped Virus Entry. Journal of Virology **88:**6702-6713.
139. **Dahlmann F, Biedenkopf N, Babler A, Jahnen-Dechent W, Karsten CB, Gnirss K, Schneider H, Wrensch F, O'Callaghan CA, Bertram S, Herrler G, Becker S, Pohlmann S, Hofmann-Winkler H.** 2015. Analysis of Ebola Virus Entry Into Macrophages. J Infect Dis **212 Suppl 2:**S247-257.
140. **Rhein BA, Brouillette RB, Schaack GA, Chiorini JA, Maury W.** 2016. Characterization of Human and Murine T-Cell Immunoglobulin Mucin Domain 4 (TIM-4) IgV Domain Residues Critical for Ebola Virus Entry. Journal of Virology **90:**6097-6111.
141. **Dragovich MA, Fortoul N, Jagota A, Zhang W, Schutt K, Xu Y, Sanabria M, Moyer DM, Moller-Tank S, Maury W, Zhang XF.** 2019. Biomechanical characterization of TIM protein–mediated Ebola virus–host cell adhesion. Scientific Reports **9**.
142. **Shimojima M, Takada A, Ebihara H, Neumann G, Fujioka K, Irimura T, Jones S, Feldmann H, Kawaoka Y.** 2006. Tyro3 family-mediated cell entry of Ebola and Marburg viruses. J Virol **80:**10109-10116.
143. **Shimojima M, Ikeda Y, Kawaoka Y.** 2007. The mechanism of Axl-mediated Ebola virus infection. J Infect Dis **196 Suppl 2:**S259-263.
144. **McIntire JJ, Umetsu DT, DeKruyff RH.** 2004. TIM-1, a novel allergy and asthma susceptibility gene. Springer Seminars in Immunopathology **25:**335-348.
145. **`Nishi C, Toda S, Segawa K, Nagata S.** 2014. Tim4- and MerTK-Mediated Engulfment of Apoptotic Cells by Mouse Resident Peritoneal Macrophages. Molecular and Cellular Biology **34:**1512-1520.

146. **Lai C, Lemke G.** 1991. An extended family of protein-tyrosine kinase genes differentially expressed in the vertebrate nervous system. Neuron **6:**691-704.
147. **Stitt TN, Conn G, Gore M, Lai C, Bruno J, Radziejewski C, Mattsson K, Fisher J, Gies DR, Jones PF, et al.** 1995. The anticoagulation factor protein S and its relative, Gas6, are ligands for the Tyro 3/Axl family of receptor tyrosine kinases. Cell **80:**661-670.
148. **Sasaki T, Knyazev PG, Clout NJ, Cheburkin Y, Göhring W, Ullrich A, Timpl R, Hohenester E.** 2006. Structural basis for Gas6-Axl signalling. Embo j **25:**80-87.
149. **Lemmon MA, Schlessinger J.** 2010. Cell signaling by receptor tyrosine kinases. Cell **141:**1117-1134.
150. **Bhattacharyya S, Zagórska A, Lew ED, Shrestha B, Rothlin CV, Naughton J, Diamond MS, Lemke G, Young JA.** 2013. Enveloped viruses disable innate immune responses in dendritic cells by direct activation of TAM receptors. Cell Host Microbe **14:**136-147.
151. **Mayor S, Pagano RE.** 2007. Pathways of clathrin-independent endocytosis. Nat Rev Mol Cell Biol **8:**603-612.
152. **Cossart P, Helenius A.** 2014. Endocytosis of viruses and bacteria. Cold Spring Harb Perspect Biol **6**.
153. **Bhattacharyya S, Warfield KL, Ruthel G, Bavari S, Aman MJ, Hope TJ.** 2010. Ebola virus uses clathrin-mediated endocytosis as an entry pathway. Virology **401:**18-28.
154. **Aleksandrowicz P, Marzi A, Biedenkopf N, Beimforde N, Becker S, Hoenen T, Feldmann H, Schnittler HJ.** 2011. Ebola virus enters host cells by macropinocytosis and clathrin-mediated endocytosis. J Infect Dis **204 Suppl 3:**S957-967.
155. **Empig CJ, Goldsmith MA.** 2002. Association of the caveola vesicular system with cellular entry by filoviruses. J Virol **76:**5266-5270.
156. **Davey RA, Shtanko O, Anantpadma M, Sakurai Y, Chandran K, Maury W.** Mechanisms of Filovirus Entry.
157. **Simmons G, Rennekamp AJ, Chai N, Vandenberghe LH, Riley JL, Bates P.** 2003. Folate receptor alpha and caveolae are not required for Ebola virus glycoprotein-mediated viral infection. J Virol **77:**13433-13438.
158. **Ivanov AI.** 2008. Pharmacological inhibition of endocytic pathways: is it specific enough to be useful? Methods Mol Biol **440:**15-33.
159. **Chen D, Jian Y, Liu X, Zhang Y, Liang J, Qi X, Du H, Zou W, Chen L, Chai Y, Ou G, Miao L, Wang Y, Yang C.** 2013. Clathrin and AP2 are required for phagocytic receptor-mediated apoptotic cell clearance in Caenorhabditis elegans. PLoS Genet **9:**e1003517.
160. **Brodsky FM.** 2016. Clathrin and Clathrin-Dependent Endocytosis, p 384-393. *In* Bradshaw RA, Stahl PD (ed), Encyclopedia of Cell Biology doi:https://doi.org/10.1016/B978-0-12-394447-4.20038-2. Academic Press, Waltham.
161. **Stillwell W.** 2013. Chapter 11 - Long-Range Membrane Properties, p 215-237. *In* Stillwell W (ed), An Introduction to Biological Membranes doi:https://doi.org/10.1016/B978-0-444-52153-8.00011-8. Elsevier, San Diego.
162. **Mercer J, Helenius A.** 2009. Virus entry by macropinocytosis. Nature Cell Biology **11:**510-520.
163. **Swanson JA.** 2008. Shaping cups into phagosomes and macropinosomes. Nat Rev Mol Cell Biol **9:**639-649.

164. **Kumari S, Mg S, Mayor S.** 2010. Endocytosis unplugged: multiple ways to enter the cell. Cell Res **20:**256-275.
165. **Ridley AJ, Paterson HF, Johnston CL, Diekmann D, Hall A.** 1992. The small GTP-binding protein rac regulates growth factor-induced membrane ruffling. Cell **70:**401-410.
166. **Garrett WS, Chen LM, Kroschewski R, Ebersold M, Turley S, Trombetta S, Galán JE, Mellman I.** 2000. Developmental control of endocytosis in dendritic cells by Cdc42. Cell **102:**325-334.
167. **Radhakrishna H, Al-Awar O, Khachikian Z, Donaldson JG.** 1999. ARF6 requirement for Rac ruffling suggests a role for membrane trafficking in cortical actin rearrangements. J Cell Sci **112:**855-866.
168. **Svensson HG, West MA, Mollahan P, Prescott AR, Zaru R, Watts C.** 2008. A role for ARF6 in dendritic cell podosome formation and migration. Eur J Immunol **38:**818-828.
169. **Dharmawardhane S, Schürmann A, Sells MA, Chernoff J, Schmid SL, Bokoch GM.** 2000. Regulation of macropinocytosis by p21-activated kinase-1. Mol Biol Cell **11:**3341-3352.
170. **Amyere M, Payrastre B, Krause U, Van Der Smissen P, Veithen A, Courtoy PJ.** 2000. Constitutive macropinocytosis in oncogene-transformed fibroblasts depends on sequential permanent activation of phosphoinositide 3-kinase and phospholipase C. Mol Biol Cell **11:**3453-3467.
171. **Miyata Y, Nishida E, Koyasu S, Yahara I, Sakai H.** 1989. Protein kinase C-dependent and -independent pathways in the growth factor-induced cytoskeletal reorganization. J Biol Chem **264:**15565-15568.
172. **Grimmer S, van Deurs B, Sandvig K.** 2002. Membrane ruffling and macropinocytosis in A431 cells require cholesterol. J Cell Sci **115:**2953-2962.
173. **Hawkins PT, Eguinoa A, Qiu RG, Stokoe D, Cooke FT, Walters R, Wennström S, Claesson-Welsh L, Evans T, Symons M, et al.** 1995. PDGF stimulates an increase in GTP-Rac via activation of phosphoinositide 3-kinase. Curr Biol **5:**393-403.
174. **Araki N, Johnson MT, Swanson JA.** 1996. A role for phosphoinositide 3-kinase in the completion of macropinocytosis and phagocytosis by macrophages. J Cell Biol **135:**1249-1260.
175. **Ard R, Mulatz K, Pomoransky JL, Parks RJ, Trinkle-Mulcahy L, Bell JC, Gee SH.** 2015. Regulation of Macropinocytosis by Diacylglycerol Kinase zeta. PLoS One **10:**e0144942.
176. **Koivusalo M, Welch C, Hayashi H, Scott CC, Kim M, Alexander T, Touret N, Hahn KM, Grinstein S.** 2010. Amiloride inhibits macropinocytosis by lowering submembranous pH and preventing Rac1 and Cdc42 signaling. The Journal of Cell Biology **188:**547-563.
177. **Kim SM, Nguyen TT, Ravi A, Kubiniok P, Finicle BT, Jayashankar V, Malacrida L, Hou J, Robertson J, Gao D, Chernoff J, Digman MA, Potma EO, Tromberg BJ, Thibault P, Edinger AL.** 2018. PTEN Deficiency and AMPK Activation Promote Nutrient Scavenging and Anabolism in Prostate Cancer Cells. Cancer Discov **8:**866-883.
178. **Kwik J, Boyle S, Fooksman D, Margolis L, Sheetz MP, Edidin M.** 2003. Membrane cholesterol, lateral mobility, and the phosphatidylinositol 4,5-bisphosphate-dependent organization of cell actin. Proc Natl Acad Sci U S A **100:**13964-13969.

179. **Kondratowicz AS, Hunt CL, Davey RA, Cherry S, Maury WJ.** 2013. AMP-activated protein kinase is required for the macropinocytic internalization of ebolavirus. J Virol **87:**746-755.
180. **Merino-Trigo A, Kerr MC, Houghton F, Lindberg A, Mitchell C, Teasdale RD, Gleeson PA.** 2004. Sorting nexin 5 is localized to a subdomain of the early endosomes and is recruited to the plasma membrane following EGF stimulation. J Cell Sci **117:**6413-6424.
181. **Shtanko O, Reyes AN, Jackson WT, Davey RA.** 2018. Autophagy-Associated Proteins Control Ebola Virus Internalization Into Host Cells. J Infect Dis **218:**S346-S354.
182. **Huotari J, Helenius A.** 2011. Endosome maturation. The EMBO journal **30:**3481-3500.
183. **Nelson EA, Dyall J, Hoenen T, Barnes AB, Zhou H, Liang JY, Michelotti J, Dewey WH, DeWald LE, Bennett RS, Morris PJ, Guha R, Klumpp-Thomas C, McKnight C, Chen YC, Xu X, Wang A, Hughes E, Martin S, Thomas C, Jahrling PB, Hensley LE, Olinger GG, Jr., White JM.** 2017. The phosphatidylinositol-3-phosphate 5-kinase inhibitor apilimod blocks filoviral entry and infection. PLoS Negl Trop Dis **11:**e0005540.
184. **Saeed MF, Kolokoltsov AA, Freiberg AN, Holbrook MR, Davey RA.** 2008. Phosphoinositide-3 kinase-Akt pathway controls cellular entry of Ebola virus. PLoS Pathog **4:**e1000141.
185. **Er EE, Mendoza MC, Mackey AM, Rameh LE, Blenis J.** 2013. AKT facilitates EGFR trafficking and degradation by phosphorylating and activating PIKfyve. Sci Signal **6:**ra45.
186. **Gaur P, Munjhal A, Lal SK.** 2011. Influenza virus and cell signaling pathways. Med Sci Monit **17:**Ra148-154.
187. **Haqshenas G, Doerig C.** 2019. Targeting of host cell receptor tyrosine kinases by intracellular pathogens. Science Signaling **12:**eaau9894.
188. **Hussein HAM, Walker LR, Abdel-Raouf UM, Desouky SA, Montasser AKM, Akula SM.** 2015. Beyond RGD: virus interactions with integrins. Archives of Virology **160:**2669-2681.
189. **Cheng H, Lear-Rooney CM, Johansen L, Varhegyi E, Chen ZW, Olinger GG, Rong L.** 2015. Inhibition of Ebola and Marburg Virus Entry by G Protein-Coupled Receptor Antagonists. J Virol **89:**9932-9938.
190. **Le Sommer C, Barrows NJ, Bradrick SS, Pearson JL, Garcia-Blanco MA.** 2012. G Protein-Coupled Receptor Kinase 2 Promotes Flaviviridae Entry and Replication. PLOS Neglected Tropical Diseases **6:**e1820.
191. **Yamauchi Y, Helenius A.** 2013. Virus entry at a glance. Journal of Cell Science **126:**1289.
192. **Mercer J, Schelhaas M, Helenius A.** 2010. Virus Entry by Endocytosis. Annual Review of Biochemistry **79:**803-833.
193. **Suomalainen M, Nakano MY, Boucke K, Keller S, Greber UF.** 2001. Adenovirus-activated PKA and p38/MAPK pathways boost microtubule-mediated nuclear targeting of virus. The EMBO journal **20:**1310-1319.
194. **Robinson M, Schor S, Barouch-Bentov R, Einav S.** 2018. Viral journeys on the intracellular highways. Cellular and Molecular Life Sciences **75:**3693-3714.
195. **Wang X, Huong S-M, Chiu ML, Raab-Traub N, Huang E-S.** 2003. Epidermal growth factor receptor is a cellular receptor for human cytomegalovirus. Nature **424:**456-461.

196. **Soroceanu L, Akhavan A, Cobbs CS.** 2008. Platelet-derived growth factor-α receptor activation is required for human cytomegalovirus infection. Nature **455:**391-395.
197. **Wu Y, Prager A, Boos S, Resch M, Brizic I, Mach M, Wildner S, Scrivano L, Adler B.** 2017. Human cytomegalovirus glycoprotein complex gH/gL/gO uses PDGFR-α as a key for entry. PLOS Pathogens **13:**e1006281.
198. **Eierhoff T, Hrincius ER, Rescher U, Ludwig S, Ehrhardt C.** 2010. The epidermal growth factor receptor (EGFR) promotes uptake of influenza A viruses (IAV) into host cells. PLoS Pathog **6:**e1001099.
199. **Adler B, Scrivano L, Ruzcics Z, Rupp B, Sinzger C, Koszinowski U.** 2006. Role of human cytomegalovirus UL131A in cell type-specific virus entry and release. Journal of General Virology **87:**2451-2460.
200. **Straschewski S, Patrone M, Walther P, Gallina A, Mertens T, Frascaroli G.** 2011. Protein pUL128 of Human Cytomegalovirus Is Necessary for Monocyte Infection and Blocking of Migration. Journal of Virology **85:**5150-5158.
201. **Liu J, Jardetzky TS, Chin AL, Johnson DC, Vanarsdall AL.** 2018. The Human Cytomegalovirus Trimer and Pentamer Promote Sequential Steps in Entry into Epithelial and Endothelial Cells at Cell Surfaces and Endosomes. Journal of Virology **92:**e01336-01318.
202. **Wang D, Shenk T.** 2005. Human Cytomegalovirus UL131 Open Reading Frame Is Required for Epithelial Cell Tropism. Journal of Virology **79:**10330-10338.
203. **Mahmud J, Miller MJ, Altman AM, Chan GC.** 2020. Human Cytomegalovirus Glycoprotein-Initiated Signaling Mediates the Aberrant Activation of Akt. Journal of Virology **94:**e00167-00120.
204. **Stegmann C, Rothemund F, Laib Sampaio K, Adler B, Sinzger C.** 2019. The N Terminus of Human Cytomegalovirus Glycoprotein O Is Important for Binding to the Cellular Receptor PDGFRα. Journal of Virology **93:**e00138-00119.
205. **Morizono K, Xie Y, Olafsen T, Lee B, Dasgupta A, Wu Anna M, Chen Irvin SY.** 2011. The Soluble Serum Protein Gas6 Bridges Virion Envelope Phosphatidylserine to the TAM Receptor Tyrosine Kinase Axl to Mediate Viral Entry. Cell Host & Microbe **9:**286-298.
206. **Meertens L, Carnec X, Lecoin MP, Ramdasi R, Guivel-Benhassine F, Lew E, Lemke G, Schwartz O, Amara A.** 2012. The TIM and TAM families of phosphatidylserine receptors mediate dengue virus entry. Cell Host Microbe **12:**544-557.
207. **Richard AS, Shim B-S, Kwon Y-C, Zhang R, Otsuka Y, Schmitt K, Berri F, Diamond MS, Choe H.** 2017. AXL-dependent infection of human fetal endothelial cells distinguishes Zika virus from other pathogenic flaviviruses. Proceedings of the National Academy of Sciences **114:**2024-2029.
208. **Meertens L, Labeau A, Dejarnac O, Cipriani S, Sinigaglia L, Bonnet-Madin L, Le Charpentier T, Hafirassou ML, Zamborlini A, Cao-Lormeau V-M, Coulpier M, Missé D, Jouvenet N, Tabibiazar R, Gressens P, Schwartz O, Amara A.** 2017. Axl Mediates ZIKA Virus Entry in Human Glial Cells and Modulates Innate Immune Responses. Cell Reports **18:**324-333.
209. **Fedeli C, Torriani G, Galan-Navarro C, Moraz M-L, Moreno H, Gerold G, Kunz S.** 2018. Axl Can Serve as Entry Factor for Lassa Virus Depending on the Functional Glycosylation of Dystroglycan. Journal of Virology **92:**e01613-01617.

210. **Drayman N, Glick Y, Ben-nun-Shaul O, Zer H, Zlotnick A, Gerber D, Schueler-Furman O, Oppenheim A.** 2013. Pathogens Use Structural Mimicry of Native Host Ligands as a Mechanism for Host Receptor Engagement. Cell Host & Microbe **14:**63-73.
211. **Diao J, Pantua H, Ngu H, Komuves L, Diehl L, Schaefer G, Kapadia SB.** 2012. Hepatitis C Virus Induces Epidermal Growth Factor Receptor Activation via CD81 Binding for Viral Internalization and Entry. Journal of Virology **86:**10935.
212. **Zona L, Lupberger J, Sidahmed-Adrar N, Thumann C, Harris Helen J, Barnes A, Florentin J, Tawar Rajiv G, Xiao F, Turek M, Durand Sarah C, Duong François HT, Heim Markus H, Cosset F-L, Hirsch I, Samuel D, Brino L, Zeisel Mirjam B, Le Naour F, McKeating Jane A, Baumert Thomas F.** 2013. HRas Signal Transduction Promotes Hepatitis C Virus Cell Entry by Triggering Assembly of the Host Tetraspanin Receptor Complex. Cell Host & Microbe **13:**302-313.
213. **Zheng K, Xiang Y, Wang X, Wang Q, Zhong M, Wang S, Wang X, Fan J, Kitazato K, Wang Y.** 2014. Epidermal Growth Factor Receptor-PI3K Signaling Controls Cofilin Activity To Facilitate Herpes Simplex Virus 1 Entry into Neuronal Cells. mBio **5:**e00958-00913.
214. **Hynes RO.** 2002. Integrins: Bidirectional, Allosteric Signaling Machines. Cell **110:**673-687.
215. **Wickham TJ, Mathias P, Cheresh DA, Nemerow GR.** 1993. Integrins alpha v beta 3 and alpha v beta 5 promote adenovirus internalization but not virus attachment. Cell **73:**309-319.
216. **Summerford C, Bartlett JS, Samulski RJ.** 1999. αVβ5 integrin: a co-receptor for adeno-associated virus type 2 infection. Nature Medicine **5:**78-82.
217. **Nemerow GR.** 2000. Cell Receptors Involved in Adenovirus Entry. Virology **274:**1-4.
218. **Wu Z, Asokan A, Samulski RJ.** 2006. Adeno-associated virus serotypes: vector toolkit for human gene therapy. Mol Ther **14:**316-327.
219. **Triantafilou K, Triantafilou M, Takada Y, Fernandez N.** 2000. Human Parechovirus 1 Utilizes Integrins αvβ3 and αvβ1 as Receptors. Journal of Virology **74:**5856-5862.
220. **Jokinen J, White DJ, Salmela M, Huhtala M, Käpylä J, Sipilä K, Puranen JS, Nissinen L, Kankaanpää P, Marjomäki V, Hyypiä T, Johnson MS, Heino J.** 2010. Molecular mechanism of α2β1 integrin interaction with human echovirus 1. The EMBO Journal **29:**196-208.
221. **Upla P, Marjomäki V, Kankaanpää P, Ivaska J, Hyypiä T, van der Goot FG, Heino J.** 2003. Clustering Induces a Lateral Redistribution of α2β1 Integrin from Membrane Rafts to Caveolae and Subsequent Protein Kinase C-dependent Internalization. Molecular Biology of the Cell **15:**625-636.
222. **Graham KL, Fleming FE, Halasz P, Hewish MJ, Nagesha HS, Holmes IH, Takada Y, Coulson BS.** 2005. Rotaviruses interact with α4β7 and α4β1 integrins by binding the same integrin domains as natural ligands. Journal of General Virology **86:**3397-3408.
223. **Graham KL, Takada Y, Coulson BS.** 2006. Rotavirus spike protein VP5* binds α2β1 integrin on the cell surface and competes with virus for cell binding and infectivity. Journal of General Virology **87:**1275-1283.
224. **Guerrero CA, Méndez E, Zárate S, Isa P, López S, Arias CF.** 2000. Integrin αvβ3 mediates rotavirus cell entry. Proceedings of the National Academy of Sciences **97:**14644-14649.

225. **Gavrilovskaya IN, Shepley M, Shaw R, Ginsberg MH, Mackow ER.** 1998. β3 integrins mediate the cellular entry of hantaviruses that cause respiratory failure. Proceedings of the National Academy of Sciences **95:**7074-7079.
226. **Raymond T, Gorbunova E, Gavrilovskaya IN, Mackow ER.** 2005. Pathogenic hantaviruses bind plexin–semaphorin–integrin domains present at the apex of inactive, bent αvβ3 integrin conformers. Proceedings of the National Academy of Sciences of the United States of America **102:**1163-1168.
227. **Sharma-Walia N, Naranatt PP, Krishnan HH, Zeng L, Chandran B.** 2004. Kaposi's sarcoma-associated herpesvirus/human herpesvirus 8 envelope glycoprotein gB induces the integrin-dependent focal adhesion kinase-Src-phosphatidylinositol 3-kinase-rho GTPase signal pathways and cytoskeletal rearrangements. Journal of virology **78:**4207-4223.
228. **Schornberg KL, Shoemaker CJ, Dube D, Abshire MY, Delos SE, Bouton AH, White JM.** 2009. Integrin controls ebolavirus entry by regulating endosomal cathepsins. Proceedings of the National Academy of Sciences **106:**8003-8008.
229. **Yoder A, Yu D, Dong L, Iyer SR, Xu X, Kelly J, Liu J, Wang W, Vorster PJ, Agulto L, Stephany DA, Cooper JN, Marsh JW, Wu Y.** 2008. HIV envelope-CXCR4 signaling activates cofilin to overcome cortical actin restriction in resting CD4 T cells. Cell **134:**782-792.
230. **Harmon B, Campbell N, Ratner L.** 2010. Role of Abl Kinase and the Wave2 Signaling Complex in HIV-1 Entry at a Post-Hemifusion Step. PLOS Pathogens **6:**e1000956.
231. **Sodhi A, Montaner S, Gutkind JS.** 2004. Viral hijacking of G-protein-coupled-receptor signalling networks. Nature Reviews Molecular Cell Biology **5:**998-1012.
232. **Chi P-I, Liu H-J.** 2013. Molecular Signaling and Cellular Pathways for Virus Entry. ISRN Virology **2013:**306595.
233. **Kumar R, Khandelwal N, Thachamvally R, Tripathi BN, Barua S, Kashyap SK, Maherchandani S, Kumar N.** 2018. Role of MAPK/MNK1 signaling in virus replication. Virus research **253:**48-61.
234. **Farmer C, Morton PE, Snippe M, Santis G, Parsons M.** 2009. Coxsackie adenovirus receptor (CAR) regulates integrin function through activation of p44/42 MAPK. Experimental cell research **315:**2637-2647.
235. **Huang WR, Wang YC, Chi PI, Wang L, Wang CY, Lin CH, Liu HJ.** 2011. Cell entry of avian reovirus follows a caveolin-1-mediated and dynamin-2-dependent endocytic pathway that requires activation of p38 mitogen-activated protein kinase (MAPK) and Src signaling pathways as well as microtubules and small GTPase Rab5 protein. The Journal of biological chemistry **286:**30780-30794.
236. **Greber UF.** 2002. Signalling in viral entry. Cellular and Molecular Life Sciences CMLS **59:**608-626.
237. **Johansen LM, Brannan JM, Delos SE, Shoemaker CJ, Stossel A, Lear C, Hoffstrom BG, DeWald LE, Schornberg KL, Scully C, Lehár J, Hensley LE, White JM, Olinger GG.** 2013. FDA-Approved Selective Estrogen Receptor Modulators Inhibit Ebola Virus Infection. Science Translational Medicine **5:**190ra179.
238. **Kouznetsova J, Sun W, Martinez-Romero C, Tawa G, Shinn P, Chen CZ, Schimmer A, Sanderson P, McKew JC, Zheng W, Garcia-Sastre A.** 2014. Identification of 53 compounds that block Ebola virus-like particle entry via a repurposing screen of approved drugs. Emerg Microbes Infect **3:**e84.

239. **Basu A, Mills DM, Mitchell D, Ndungo E, Williams JD, Herbert AS, Dye JM, Moir DT, Chandran K, Patterson JL, Rong L, Bowlin TL.** 2015. Novel Small Molecule Entry Inhibitors of Ebola Virus. J Infect Dis **212 Suppl 2:**S425-434.
240. **Johansen LM, DeWald LE, Shoemaker CJ, Hoffstrom BG, Lear-Rooney CM, Stossel A, Nelson E, Delos SE, Simmons JA, Grenier JM, Pierce LT, Pajouhesh H, Lehár J, Hensley LE, Glass PJ, White JM, Olinger GG.** 2015. A screen of approved drugs and molecular probes identifies therapeutics with anti–Ebola virus activity. Science Translational Medicine **7:**290ra289.
241. **Anantpadma M, Kouznetsova J, Wang H, Huang R, Kolokoltsov A, Guha R, Lindstrom AR, Shtanko O, Simeonov A, Maloney DJ, Maury W, LaCount DJ, Jadhav A, Davey RA.** 2016. Large-Scale Screening and Identification of Novel Ebola Virus and Marburg Virus Entry Inhibitors. Antimicrob Agents Chemother **60:**4471-4481.
242. **Martin S, Chiramel AI, Schmidt ML, Chen Y-C, Whitt N, Watt A, Dunham EC, Shifflett K, Traeger S, Leske A, Buehler E, Martellaro C, Brandt J, Wendt L, Müller A, Peitsch S, Best SM, Stech J, Finke S, Römer-Oberdörfer A, Groseth A, Feldmann H, Hoenen T.** 2018. A genome-wide siRNA screen identifies a druggable host pathway essential for the Ebola virus life cycle. Genome Medicine **10:**58.
243. **Lee N, Shum D, König A, Kim H, Heo J, Min S, Lee J, Ko Y, Choi I, Lee H, Radu C, Hoenen T, Min J-Y, Windisch MP.** 2018. High-throughput drug screening using the Ebola virus transcription- and replication-competent virus-like particle system. Antiviral Research **158:**226-237.
244. **Flint M, Chatterjee P, Lin DL, McMullan LK, Shrivastava-Ranjan P, Bergeron E, Lo MK, Welch SR, Nichol ST, Tai AW, Spiropoulou CF.** 2019. A genome-wide CRISPR screen identifies N-acetylglucosamine-1-phosphate transferase as a potential antiviral target for Ebola virus. Nat Commun **10**.
245. **Duong-Ly KC, Peterson JR.** 2013. The human kinome and kinase inhibition. Current protocols in pharmacology **Chapter 2:**Unit2.9-Unit2.9.
246. **Cheng H, Koning K, O'Hearn A, Wang M, Rumschlag-Booms E, Varhegyi E, Rong L.** 2015. A parallel genome-wide RNAi screening strategy to identify host proteins important for entry of Marburg virus and H5N1 influenza virus. Virology Journal **12:**194.
247. **Filone CM, Dower K, Cowley GS, Hensley LE, Connor JH.** 2015. Probing the Virus Host Interaction in High Containment: An Approach Using Pooled Short Hairpin RNA. ASSAY and Drug Development Technologies **13:**34-43.
248. **Mizugishi K, Yamashita T, Olivera A, Miller GF, Spiegel S, Proia RL.** 2005. Essential role for sphingosine kinases in neural and vascular development. Molecular and cellular biology **25:**11113-11121.
249. **Bekerman E, Neveu G, Shulla A, Brannan J, Pu S-Y, Wang S, Xiao F, Barouch-Bentov R, Bakken RR, Mateo R, Govero J, Nagamine CM, Diamond MS, De Jonghe S, Herdewijn P, Dye JM, Randall G, Einav S.** 2017. Anticancer kinase inhibitors impair intracellular viral trafficking and exert broad-spectrum antiviral effects. The Journal of clinical investigation **127:**1338-1352.
250. **Mohr EL, McMullan LK, Lo MK, Spengler JR, Bergeron É, Albariño CG, Shrivastava-Ranjan P, Chiang C-F, Nichol ST, Spiropoulou CF, Flint M.** 2015. Inhibitors of cellular kinases with broad-spectrum antiviral activity for hemorrhagic fever viruses. Antiviral Research **120:**40-47.

251. **Kuroda M, Halfmann P, Kawaoka Y.** 2020. HER2-mediated enhancement of Ebola virus entry. PLOS Pathogens **16:**e1008900.
252. **Brinkmann V, Davis MD, Heise CE, Albert R, Cottens S, Hof R, Bruns C, Prieschl E, Baumruker T, Hiestand P, Foster CA, Zollinger M, Lynch KR.** 2002. The immune modulator FTY720 targets sphingosine 1-phosphate receptors. J Biol Chem **277:**21453-21457.
253. **Paugh SW, Payne SG, Barbour SE, Milstien S, Spiegel S.** 2003. The immunosuppressant FTY720 is phosphorylated by sphingosine kinase type 2. FEBS Lett **554:**189-193.
254. **Shen H, Giordano F, Wu Y, Chan J, Zhu C, Milosevic I, Wu X, Yao K, Chen B, Baumgart T, Sieburth D, De Camilli P.** 2014. Coupling between endocytosis and sphingosine kinase 1 recruitment. Nat Cell Biol **16:**652-662.
255. **Lima S, Milstien S, Spiegel S.** 2017. Sphingosine and Sphingosine Kinase 1 Involvement in Endocytic Membrane Trafficking. J Biol Chem **292:**3074-3088.
256. **Young MM, Takahashi Y, Fox TE, Yun JK, Kester M, Wang HG.** 2016. Sphingosine Kinase 1 Cooperates with Autophagy to Maintain Endocytic Membrane Trafficking. Cell Rep **17:**1532-1545.
257. **Edinger TO, Pohl MO, Stertz S.** 2014. Entry of influenza A virus: host factors and antiviral targets. Journal of General Virology **95:**263-277.
258. **Takahashi Y, Coppola D, Matsushita N, Cualing HD, Sun M, Sato Y, Liang C, Jung JU, Cheng JQ, Mulé JJ, Pledger WJ, Wang H-G.** 2007. Bif-1 interacts with Beclin 1 through UVRAG and regulates autophagy and tumorigenesis. Nature cell biology **9:**1142-1151.
259. **Kim Y-M, Jung CH, Seo M, Kim EK, Park J-M, Bae SS, Kim D-H.** 2015. mTORC1 phosphorylates UVRAG to negatively regulate autophagosome and endosome maturation. Molecular cell **57:**207-218.
260. **Martinez MG, Cordo SM, Candurra NA.** 2007. Characterization of Junín arenavirus cell entry. Journal of General Virology **88:**1776-1784.
261. **Schnute ME, McReynolds MD, Kasten T, Yates M, Jerome G, Rains JW, Hall T, Chrencik J, Kraus M, Cronin CN, Saabye M, Highkin MK, Broadus R, Ogawa S, Cukyne K, Zawadzke LE, Peterkin V, Iyanar K, Scholten JA, Wendling J, Fujiwara H, Nemirovskiy O, Wittwer AJ, Nagiec MM.** 2012. Modulation of cellular S1P levels with a novel, potent and specific inhibitor of sphingosine kinase-1. Biochem J **444:**79-88.
262. **Schnute ME, McReynolds MD, Carroll J, Chrencik J, Highkin MK, Iyanar K, Jerome G, Rains JW, Saabye M, Scholten JA, Yates M, Nagiec MM.** 2017. Discovery of a Potent and Selective Sphingosine Kinase 1 Inhibitor through the Molecular Combination of Chemotype-Distinct Screening Hits. J Med Chem **60:**2562-2572.
263. **Paugh SW, Paugh BS, Rahmani M, Kapitonov D, Almenara JA, Kordula T, Milstien S, Adams JK, Zipkin RE, Grant S, Spiegel S.** 2008. A selective sphingosine kinase 1 inhibitor integrates multiple molecular therapeutic targets in human leukemia. Blood **112:**1382-1391.
264. **Abramovici H, Mojtabaie P, Parks RJ, Zhong XP, Koretzky GA, Topham MK, Gee SH.** 2009. Diacylglycerol kinase zeta regulates actin cytoskeleton reorganization through dissociation of Rac1 from RhoGDI. Mol Biol Cell **20:**2049-2059.
265. **Ard R, Mulatz K, Abramovici H, Maillet J-C, Fottinger A, Foley T, Byham M-R, Iqbal TA, Yoneda A, Couchman JR, Parks RJ, Gee SH.** 2012. Diacylglycerol kinase ζ

regulates RhoA activation via a kinase-independent scaffolding mechanism. Molecular Biology of the Cell **23:**4008-4019.
266. **Ard R, Mulatz K, Pomoransky JL, Parks RJ, Trinkle-Mulcahy L, Bell JC, Gee SH.** 2015. Regulation of Macropinocytosis by Diacylglycerol Kinase ζ. PLOS ONE **10:**e0144942.
267. **Topham MK, Prescott SM.** 1999. Mammalian diacylglycerol kinases, a family of lipid kinases with signaling functions. J Biol Chem **274:**11447-11450.
268. **Sakane F, Imai S-i, Kai M, Yasuda S, Kanoh H.** 2007. Diacylglycerol kinases: Why so many of them? Biochimica et Biophysica Acta (BBA) - Molecular and Cell Biology of Lipids **1771:**793-806.
269. **Chitalia VC, Munawar AH.** 2020. A painful lesson from the COVID-19 pandemic: the need for broad-spectrum, host-directed antivirals. Journal of Translational Medicine **18:**390.
270. **Vigant F, Santos NC, Lee B.** 2015. Broad-spectrum antivirals against viral fusion. Nature Reviews Microbiology **13:**426-437.
271. **Mazzon M, Marsh M.** 2019. Targeting viral entry as a strategy for broad-spectrum antivirals F1000Research **8**.
272. **Vaughn DW, Green S, Kalayanarooj S, Innis BL, Nimmannitya S, Suntayakorn S, Endy TP, Raengsakulrach B, Rothman AL, Ennis FA, Nisalak A.** 2000. Dengue viremia titer, antibody response pattern, and virus serotype correlate with disease severity. J Infect Dis **181:**2-9.
273. **Thi EP, Lee AC, Geisbert JB, Ursic-Bedoya R, Agans KN, Robbins M, Deer DJ, Fenton KA, Kondratowicz AS, MacLachlan I, Geisbert TW, Mire CE.** 2016. Rescue of non-human primates from advanced Sudan ebolavirus infection with lipid encapsulated siRNA. Nat Microbiol **1:**16142.
274. **Cross RW, Mire CE, Feldmann H, Geisbert TW.** 2018. Post-exposure treatments for Ebola and Marburg virus infections. Nature Reviews Drug Discovery **17:**413-434.
275. **Herring S, Oda JM, Wagoner J, Kirchmeier D, O'Connor A, Nelson EA, Huang Q, Liang Y, Evans DeWald L, Johansen LM, Glass PJ, Olinger GG, Ianevski A, Aittokallio T, Paine MF, Fink SL, White JM, Polyak SJ.** 2021. Inhibition of Arenaviruses by Combinations of Orally Available Approved Drugs. Antimicrobial Agents and Chemotherapy doi:10.1128/aac.01146-20**:**AAC.01146-01120.
276. **Flego M, Ascione A, Cianfriglia M, Vella S.** 2013. Clinical development of monoclonal antibody-based drugs in HIV and HCV diseases. BMC medicine **11:**4-4.
277. **Santoro A, Cavina R, Latteri F, Zucali PA, Ginanni V, Campagnoli E, Ferrari B, Morenghi E, Pedicini V, Roncalli M, Alloisio M, Ravasi G, Soto Parra HJ.** 2004. Activity of a specific inhibitor, gefitinib (Iressa™, ZD1839), of epidermal growth factor receptor in refractory non-small-cell lung cancer. Annals of Oncology **15:**33-37.
278. **Liu W-j, Du Y, Wen R, Yang M, Xu J.** 2020. Drug resistance to targeted therapeutic strategies in non-small cell lung cancer. Pharmacology & Therapeutics **206:**107438.
279. **Chan G, Nogalski MT, Yurochko AD.** 2009. Activation of EGFR on monocytes is required for human cytomegalovirus entry and mediates cellular motility. Proceedings of the National Academy of Sciences **106:**22369.
280. **Cai W-Q, Zeng L-S, Wang L-F, Wang Y-Y, Cheng J-T, Zhang Y, Han Z-W, Zhou Y, Huang S-L, Wang X-W, Peng X-C, Xiang Y, Ma Z, Cui S-Z, Xin H-W.** 2020. The

Latest Battles Between EGFR Monoclonal Antibodies and Resistant Tumor Cells. Frontiers in Oncology **10**.
281. **Chun J, Hartung HP.** 2010. Mechanism of action of oral fingolimod (FTY720) in multiple sclerosis. Clin Neuropharmacol **33:**91-101.
282. **Brunkhorst R, Vutukuri R, Pfeilschifter W.** 2014. Fingolimod for the treatment of neurological diseases-state of play and future perspectives. Front Cell Neurosci **8:**283.
283. **Barzegar M, Mirmosayyeb O, Nehzat N, Sarrafi R, Khorvash F, Maghzi AH, Shaygannejad V.** 2020. COVID-19 infection in a patient with multiple sclerosis treated with fingolimod. Neurol Neuroimmunol Neuroinflamm **7**.
284. **Gomez-Mayordomo V, Montero-Escribano P, Matías-Guiu JA, González-García N, Porta-Etessam J, Matías-Guiu J.** 2021. Clinical exacerbation of SARS-CoV2 infection after fingolimod withdrawal. Journal of Medical Virology **93:**546-549.
285. **Resop RS, Fromentin R, Newman D, Rigsby H, Dubrovsky L, Bukrinsky M, Chomont N, Bosque A.** 2020. Fingolimod inhibits multiple stages of the HIV-1 life cycle. PLOS Pathogens **16:**e1008679.
286. **Xia C, Seo Y-J, Studstill CJ, Vijayan M, Wolf JJ, Hahm B.** 2018. Transient inhibition of sphingosine kinases confers protection to influenza A virus infected mice. Antiviral research **158:**171-177.
287. **Kurd R, Ben-Chetrit E, Karameh H, Bar-Meir M.** 2020. Compassionate Use of Opaganib For Patients with Severe COVID-19. medRxiv doi:10.1101/2020.06.20.20099010**:**2020.2006.2020.20099010.

Appendix 1: Authorizations and Permissions

Figure reprinted from the Journal of Autoimmunity (Figure 1.2)

Ebola virus disease: An emerging and re-emerging viral threat

Author:
Manuel Rojas,Diana M. Monsalve,Yovana Pacheco,Yeny Acosta-Ampudia,Carolina Ramírez-Santana,Aftab A. Ansari,M. Eric Gershwin,Juan-Manuel Anaya

Publication: Journal of Autoimmunity

Publisher: Elsevier

Date: January 2020

Figure reprinted from PLOS journal (Figure 1.3)

Licenses and Copyright

The following policy applies to all PLOS journals, unless otherwise noted.

Reuse of PLOS Article Content

PLOS applies the Creative Commons Attribution (CC BY) license to articles and other works we publish. If you submit your paper for publication by PLOS, you agree to have the CC BY license applied to your work. Under this Open Access license, you as the author agree that anyone can reuse your article in whole or part for any purpose, for free, even for commercial purposes. Anyone may copy, distribute, or reuse the content as long as the author and original source are properly cited. This facilitates freedom in re-use and also ensures that PLOS content can be mined without barriers for the needs of research.

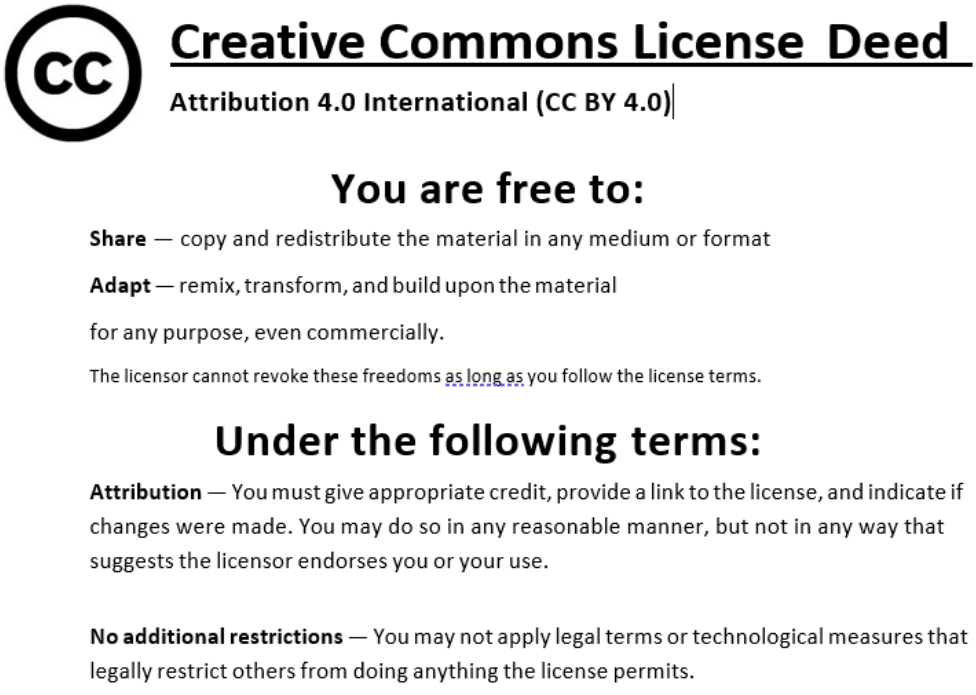

Creative Commons License Deed

Attribution 4.0 International (CC BY 4.0)

You are free to:

Share — copy and redistribute the material in any medium or format

Adapt — remix, transform, and build upon the material

for any purpose, even commercially.

The licensor cannot revoke these freedoms as long as you follow the license terms.

Under the following terms:

Attribution — You must give appropriate credit, provide a link to the license, and indicate if changes were made. You may do so in any reasonable manner, but not in any way that suggests the licensor endorses you or your use.

No additional restrictions — You may not apply legal terms or technological measures that legally restrict others from doing anything the license permits.

Figures created using biorender and exported under an academic subscription.

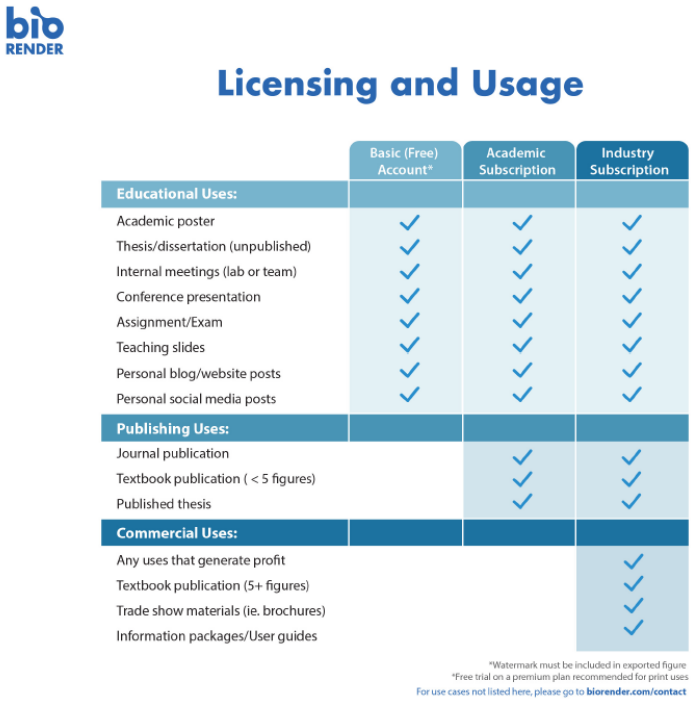

bio RENDER

Licensing and Usage

	Basic (Free) Account*	Academic Subscription	Industry Subscription
Educational Uses:			
Academic poster	✓	✓	✓
Thesis/dissertation (unpublished)	✓	✓	✓
Internal meetings (lab or team)	✓	✓	✓
Conference presentation	✓	✓	✓
Assignment/Exam	✓	✓	✓
Teaching slides	✓	✓	✓
Personal blog/website posts	✓	✓	✓
Personal social media posts	✓	✓	✓
Publishing Uses:			
Journal publication		✓	✓
Textbook publication (< 5 figures)		✓	✓
Published thesis		✓	✓
Commercial Uses:			
Any uses that generate profit			✓
Textbook publication (5+ figures)			✓
Trade show materials (ie. brochures)			✓
Information packages/User guides			✓

*Watermark must be included in exported figure
*Free trial on a premium plan recommended for print uses
For use cases not listed here, please go to **biorender.com/contact**

Appendix 2: Kinase inhibitor screen data

			Relative Transduction %					
	Relative Metabolic Activity (%)		VSV		EBOV		MARV	
Compound	Average of 3 Biological Replicates	StDev	Average of 3 Biological Replicates	StDev	Average of 3 Biological Replicates	StDev	Average of 3 Biological Replicates	StDev
10058-F4	101.38465	4.01687	80.64663	13.73983	82.97597	35.75337	92.82135	12.76816
3-Methyladenine	96.52078	2.76439	79.55451	21.66758	102.09809	26.36324	70.60587	26.51139
6H05	109.25935	7.69951	116.46682	11.61117	97.28841	17.56917	109.84352	15.96114
A66	111.58758	2.76560	122.60194	30.16000	109.22141	42.44553	110.35404	17.67778
A-674563	83.56000	7.18237	17.91867	18.12285	24.90531	20.55261	9.39051	7.05393
A-769662	110.58037	1.98785	136.46148	26.71529	103.99129	43.38762	115.75431	15.30108
AC480 (BMS-599626)	103.01083	10.06641	100.96556	24.45818	118.66853	18.49940	91.26788	29.27130
Acadesine	100.54551	12.75366	86.54645	16.36592	102.66589	19.52073	81.98653	21.32748
AEE788 (NVP-AEE788)	103.87812	10.64516	95.81079	29.08921	74.57837	28.70442	56.08167	16.61434
Afatinib (BIBW2992)	101.10281	8.39993	52.41046	10.18281	24.83941	5.37641	38.45545	10.95866
AG-1024	92.25595	21.74740	55.58932	24.19032	90.53760	38.27227	64.73805	29.91564
AG-1478 (Tyrphostin AG-1478)	106.42508	5.21439	90.06759	22.38899	87.21654	25.55501	70.51560	17.96818
AG-18	112.36551	3.58822	157.26403	20.57895	86.80808	16.02227	128.54619	12.03011
AG-490 (Tyrphostin B42)	103.76839	1.36256	99.13061	14.37101	95.67832	31.38592	75.98468	17.90375
Akti-1/2	96.63250	9.99014	111.69541	4.56893	119.74376	19.48625	110.62360	7.74510
Alisertib (MLN8237)	111.97303	5.18691	122.21038	32.23344	96.84831	9.20813	93.83565	24.45851
AMG319	90.80508	7.78918	85.83909	16.03743	77.39213	47.13290	72.66028	15.81803
AMG-458	97.67651	3.58971	71.86879	17.75351	109.17129	29.61005	67.72617	30.28394
AMG-900	108.74404	7.61201	21.99326	13.89009	21.19579	16.05189	24.56203	4.76139
Amuvatinib (MP-470)	95.19381	22.24319	47.63724	20.65568	71.46251	19.59406	60.75364	22.74236
ANA-12	110.85999	12.61655	137.86295	5.16578	121.15930	29.23226	124.66706	29.79449
Anacardic Acid	97.19709	5.10879	87.20130	18.72461	82.04095	13.80490	82.93779	10.81820
AP26113	124.65205	4.77146	170.53134	9.99672	107.24256	29.93164	128.27610	32.74983
Apatinib	99.21157	11.75811	104.98740	46.62826	168.47751	30.20928	87.16207	29.72814
AR-A014418	91.75836	7.73709	85.41775	2.04389	59.52390	22.49657	90.41142	9.54829
AS-252424	101.32637	6.40220	86.30274	13.31299	109.97292	37.03380	96.77130	12.46273
AS-604850	103.48197	6.40883	89.62839	7.50755	103.07571	31.78342	105.72210	22.52116
Asiatic Acid	90.49965	7.38356	64.84085	7.14578	97.27552	30.72352	93.57253	26.99598
AST-1306	86.41219	6.56830	44.41895	15.83220	73.10437	8.07293	48.97803	7.69626
AT13148	88.57937	10.12629	133.66935	37.72288	119.16441	11.88879	135.35435	11.06516
AT7519	101.62076	15.22026	110.44818	22.44420	84.51556	11.15955	109.05093	7.77235
AT7867	107.11772	11.90155	154.28947	23.50656	157.84639	45.03352	150.23926	20.99252
AT9283	111.79647	7.54570	89.63376	19.50835	77.74071	13.80261	68.90131	25.22231
Aurora A Inhibitor I	91.15657	15.03126	73.24195	28.27378	113.46235	46.40054	68.58055	11.47579
AVL-292	117.99091	13.82125	149.14319	5.93180	112.86350	26.11832	134.12944	47.56190
Axitinib	89.80037	6.96678	78.23652	10.95769	64.75894	16.88909	70.26060	11.92220
AZ 628	98.41727	3.92674	67.85591	23.01534	113.99495	47.66455	74.15318	30.09146
AZ 960	94.90312	7.57305	102.24020	29.82757	108.81772	35.08394	90.68779	14.22141

AZ20	113.29438	6.25644	131.81888	21.80986	100.58926	15.15543	113.44625	32.06198
AZD1080	101.98052	4.63918	88.31061	8.18756	97.09073	22.54845	77.33112	18.73763
AZD1208	113.52508	11.02382	149.61350	17.05527	109.99543	23.28118	125.57835	35.07388
AZD1480	116.36418	9.85667	109.51518	11.14298	105.09815	33.51092	105.48097	28.62829
AZD2014	106.07242	8.03521	102.39764	15.21793	116.35920	25.75443	73.42682	18.15841
AZD2858	105.98900	7.03329	103.88477	7.00198	142.31851	61.72914	99.06901	16.23606
AZD2932	124.32357	4.50865	153.48035	22.49038	87.69448	20.02193	118.77106	20.51212
AZD3463	96.35491	12.07282	81.22852	21.48772	18.86802	14.50832	5.12205	6.37925
AZD4547	114.01118	7.43361	103.25690	19.55367	111.58790	23.66423	89.31139	20.06802
AZD5363	98.53070	2.69622	105.16021	11.29732	91.38537	12.97473	102.80901	6.74288
AZD5438	103.55103	4.04403	104.64304	36.88143	119.10171	49.83700	111.70037	18.65536
AZD6482	106.61643	19.62254	123.31123	24.44165	92.37173	13.55963	122.88642	20.66643
AZD6738	104.98391	2.09585	139.58501	20.31216	100.94358	13.78726	117.82225	17.41767
AZD7762	101.91944	10.76453	107.45692	34.83930	97.57815	2.50772	87.99902	11.97565
AZD8055	94.14577	10.04193	66.01845	26.35537	69.04083	19.33706	65.11802	14.58324
AZD8330	112.79342	15.70764	83.68788	24.88357	83.84659	28.58629	84.49666	17.62609
AZD8931 (Sapitinib)	101.25687	10.05106	74.42395	17.76109	93.51866	26.11492	75.50179	15.82398
AZD9291	92.68077	8.82068	46.70556	3.82365	27.28294	11.42668	14.67786	4.94594
Barasertib (AZD1152-HQPA)	99.71680	7.58280	97.09639	14.19308	93.06585	19.18943	84.89361	19.57771
BAY 11-7082	106.63260	16.20574	113.96214	5.26536	99.77213	21.23222	111.01102	37.02378
Bay 11-7085	90.73235	6.94098	82.75696	13.21321	63.35576	28.53564	92.60869	17.72116
BGT226 (NVP-BGT226)	75.05865	17.82722	-26.70724	3.26619	-26.70627	3.13037	-18.07233	3.47927
BI 2536	55.71165	3.16862	32.49922	30.42398	42.77232	39.37286	9.43523	10.47828
BI-D1870	93.50713	2.53515	116.72912	7.95686	144.24005	30.29085	91.86905	6.26016
Bikinin	91.56471	1.20710	73.28145	6.87419	74.26255	6.64288	80.44438	26.79207
BIO	105.57748	3.45037	93.72411	17.79652	101.64828	24.76033	103.20327	14.56540
BIRB 796 (Doramapimod)	110.96942	15.17329	96.00213	21.96545	148.80659	51.59521	107.32529	16.83291
BIX 02188	112.58376	16.29623	158.32470	67.87362	115.80994	34.54932	127.32131	25.85446
BIX 02189	114.53790	15.45197	140.86737	29.16932	120.90023	23.51692	132.80077	18.52941
BKM120 (NVP-BKM120, Buparlisib)	90.33792	8.66243	63.15416	10.07423	92.15870	31.56680	84.40767	33.75842
BLZ945	95.90753	12.34816	84.20924	13.86890	75.83878	36.14680	75.47325	13.95275
BMS-265246	86.96970	6.52962	28.24725	15.20780	38.71509	2.18378	49.19636	14.36683
BMS-345541	92.90416	5.05849	102.01390	19.85974	73.62795	8.83982	89.08780	15.99398
BMS-536924	99.76785	11.31492	89.04012	10.98731	95.01320	18.79892	85.80032	13.32457
BMS-754807	110.08534	6.65107	155.71435	24.15845	119.22432	12.15283	99.38965	4.05846
BMS-777607	113.50565	12.10785	118.25738	21.70537	102.72868	40.78495	110.06104	20.17718
BMS-794833	110.37430	9.61383	99.76809	24.68007	117.09348	34.06196	95.90650	14.16015
Bosutinib (SKI-606)	102.83646	9.78320	49.22884	3.46524	7.25854	3.30858	16.67048	4.23429
Brivanib (BMS-540215)	116.60242	5.58489	162.52886	23.37548	111.22269	31.67144	121.76976	35.72111
Brivanib Alaninate (BMS-582664)	108.04059	6.05785	127.22737	22.75650	114.38445	7.89875	75.36222	18.31967
BS-181 HCl	94.01881	6.44381	72.73506	17.30437	62.84316	18.18942	59.63494	7.24572
Butein	108.94820	9.52780	188.75040	23.57891	112.70404	12.48083	134.56079	21.46441
BX-795	100.15847	19.74933	97.98005	17.42940	95.51087	14.91443	100.40487	25.40170
BX-912	98.46214	18.03869	93.09793	23.02505	101.52945	26.85016	101.47882	28.45110
BYL719	91.48938	5.80166	67.31004	13.01699	96.78991	23.45756	65.69249	15.77881
Cabozantinib (XL184, BMS-907351)	100.32809	4.01580	97.99281	12.66981	39.32171	2.17567	68.54450	19.49373

Cabozantinib malate (XL184)	108.85691	6.17991	122.86272	8.29328	43.13668	8.14507	79.31788	6.37504
CAL-101 (Idelalisib, GS-1101)	94.09727	4.50632	75.44688	21.75213	109.64338	39.43987	65.03290	9.84135
CCT128930	109.89540	6.22879	129.51244	35.97666	144.18099	45.60161	120.56596	36.09121
CCT129202	94.87910	2.48825	80.91501	11.38546	97.34587	4.92731	75.05938	24.45738
CCT137690	103.19009	3.83332	18.38399	5.84456	29.56117	9.97561	14.67178	4.02001
Cediranib (AZD2171)	93.79145	10.89930	33.22369	20.02926	46.61173	9.58811	18.36711	1.86655
CEP-32496	108.33085	2.21633	144.55000	35.55763	96.63335	12.76103	116.85939	29.44117
CEP-33779	109.99181	10.09804	125.40069	23.69466	140.07391	20.67066	111.00531	17.98409
CGI1746	105.92075	3.68339	125.79304	28.29763	113.47159	39.23760	104.93065	30.32464
CGK 733	101.25072	4.36455	118.22244	10.37942	86.77009	20.26093	95.09908	24.26063
CH5132799	101.07995	0.79903	95.48934	4.78479	95.66402	32.89661	77.56845	9.72807
CHIR-124	90.15032	13.83368	19.94175	7.48855	84.86689	28.52695	16.47216	9.40068
CHIR-98014	105.47111	2.89633	95.65770	13.75869	119.83446	51.03179	106.83735	13.05962
CHIR-99021 (CT99021)	103.86259	9.81685	80.46704	6.95736	103.95680	30.84308	96.00803	23.06950
CHIR-99021 (CT99021) HCl	104.20881	7.97852	80.03643	6.45527	76.12365	37.45743	98.46746	27.70193
Chrysophanic Acid	107.21639	2.61406	81.54022	11.86802	106.17941	33.53057	100.93132	22.64550
CNX-2006	103.53477	5.74846	99.12948	26.67211	141.02160	41.14760	92.32767	15.96023
CNX-774	99.69295	4.77241	78.95920	23.23098	92.05703	13.75745	93.13022	25.35828
CO-1686 (AVL-301)	110.88272	7.44025	146.69736	11.68569	103.35512	13.00912	132.16968	40.86282
Cobimetinib (GDC-0973, RG7420)	102.84134	4.57730	84.84152	8.36304	51.83697	9.77670	59.87090	16.16392
CP-673451	93.63695	6.39641	71.25816	16.83252	88.85915	22.08287	84.25180	23.47455
CP-724714	106.54027	4.51152	125.30924	18.88171	114.79461	10.81734	86.15819	26.38459
Crenolanib (CP-868596)	99.66008	2.81585	85.97545	27.12744	131.94545	31.44018	71.40223	25.53609
Crizotinib (PF-02341066)	115.88782	5.45017	164.74251	21.80568	43.35328	1.03929	87.84314	23.58473
CUDC-101	86.67323	9.90234	122.06074	22.26980	121.21916	43.56364	78.54114	33.78644
CUDC-907	29.84910	5.14504	-36.69660	8.01425	-40.88880	6.80916	-24.72273	8.43832
CX-6258 HCl	117.37484	7.02111	84.16214	54.30169	107.54160	22.24148	42.69843	15.77733
CYC116	92.77696	1.79209	89.29086	17.90594	73.19020	1.44948	70.09364	3.97867
CYT387	96.73450	7.53268	115.81986	50.73225	115.23733	10.97449	123.97502	19.38061
CZC24832	102.06859	7.56730	87.24683	15.71938	61.90418	26.07970	80.74972	18.77843
D 4476	95.19578	11.76175	65.77937	11.93069	65.64213	27.73648	73.64117	5.14311
Dabrafenib (GSK2118436)	109.85403	5.57774	133.41306	15.81470	125.97503	16.47547	120.66306	17.12108
Dacomitinib (PF299804, PF299)	114.50245	10.71226	83.36895	24.85251	32.88173	18.57409	20.54597	1.72313
Danusertib (PHA-739358)	94.94688	4.78979	77.05810	7.03782	81.41052	12.99579	80.60042	22.93139
DASA-58	106.88798	4.04329	138.80671	6.69600	89.55907	15.46729	139.00107	9.11963
Dasatinib	87.70151	12.85748	76.80006	8.59298	93.03101	9.16356	56.86668	13.38299
DCC-2036 (Rebastinib)	120.03203	2.56996	120.76047	32.37404	150.88429	67.76952	115.24158	19.22525
DDR1-IN-1	97.67021	6.45281	87.53602	6.66191	91.14552	11.36943	51.15354	20.49303
Defactinib (VS-6063, PF-04554878)	106.67863	8.00179	136.99109	16.87870	101.93247	2.69348	104.83431	17.85478
Degrasyn (WP1130)	79.62510	4.19194	29.99587	4.74560	48.33996	17.88394	21.77682	10.21260
Dinaciclib (SCH727965)	89.58291	8.24717	38.21264	26.00083	32.29114	8.01431	31.61809	22.61013
Dorsomorphin (Compound C)	96.46281	5.90447	119.45676	44.54796	59.32688	5.28782	6.80907	0.38591

Dovitinib (TKI-258) Dilactic Acid	101.69356	11.00865	56.74218	14.61078	27.78858	8.19649	30.72932	12.16744
Dovitinib (TKI-258, CHIR-258)	90.43224	9.88567	47.79141	18.21966	41.27214	9.62448	33.72123	3.06319
EHop-016	108.55558	4.44872	125.83847	15.38985	12.04188	7.11198	26.11613	6.50177
EHT 1864	96.69434	6.24247	109.79325	18.39822	82.99422	16.34017	90.40344	9.09913
ENMD-2076	94.90997	3.64065	70.59779	21.62370	71.16439	3.97275	41.56057	35.62318
Entrectinib (RXDX-101)	99.12057	7.25650	120.47800	29.69843	97.89618	2.02952	51.10410	20.19335
Enzastaurin (LY317615)	126.76726	9.84258	155.91083	22.68271	182.80263	15.38567	128.83707	16.29358
ERK5-IN-1	89.47049	14.77388	117.34638	9.09762	108.12080	19.49037	16.96017	5.65384
Erlotinib HCl (OSI-744)	107.34518	12.61123	92.45259	14.39286	113.17704	7.24033	82.50635	15.85553
ETP-46464	87.78766	1.41498	59.25604	8.61759	51.33498	8.55036	45.62768	15.32884
Everolimus (RAD001)	109.02813	6.75418	131.39715	25.15026	122.45004	23.24067	89.43107	16.87078
Fasudil (HA-1077) HCl	100.36913	9.85645	97.58280	18.65105	113.86843	31.19143	106.84879	26.83202
FIIN-2	99.78832	2.60677	72.23986	7.70128	85.44585	12.89817	72.41164	17.56700
Filgotinib (GLPG0634)	102.05160	7.45864	126.01434	13.29657	102.37713	16.38382	117.24082	16.38309
Fingolimod (FTY720) HCl	104.53052	8.94932	111.85777	22.93150	53.63452	7.45294	100.07647	32.85069
Flavopiridol (Alvocidib)	86.26855	21.70688	31.45570	31.46419	35.17247	9.80295	47.15757	10.23075
Flavopiridol HCl	101.69884	7.76457	74.05668	53.13761	48.47649	21.95148	50.25222	24.99687
Foretinib (GSK1363089)	101.36396	7.04153	101.93641	60.15489	22.47252	22.14120	12.83141	12.67084
Fostamatinib (R788)	101.17153	4.02366	65.49988	5.21822	86.18832	21.95345	77.53215	23.34301
FRAX597	104.83067	8.95627	96.50956	20.28884	152.21665	11.11622	92.22916	26.14433
G-749	90.39648	12.31783	110.89103	18.34033	13.63596	6.96011	43.15393	14.05723
GDC-0068	106.63971	6.10867	114.15561	3.86388	121.30672	14.65460	93.87089	22.34427
GDC-0349	107.48307	7.05074	143.20944	0.74134	102.54343	19.11192	122.69110	10.70103
GDC-0879	122.23340	10.32746	184.45288	39.15020	159.85151	35.69419	129.95301	37.36031
GDC-0941	92.16981	12.12617	70.64241	11.29364	72.94562	12.94903	58.56429	18.20582
GDC-0980 (RG7422)	108.58980	2.92846	146.28025	36.54995	118.29276	39.63889	96.59928	16.30969
Gefitinib (ZD1839)	109.23652	8.44351	82.59217	12.85741	40.39136	4.67439	64.45986	8.86975
Genistein	98.31601	11.99816	70.03362	11.69801	91.46904	20.53921	89.02635	23.85949
GF109203X	120.95861	10.15299	131.53152	19.32471	118.16347	10.94018	126.81108	30.92308
GNE-0877	98.07058	5.24807	86.66308	1.63111	80.83213	9.36248	82.24133	5.11493
GNE-7915	89.92219	5.82397	75.84981	19.48464	74.63752	7.33677	80.61674	20.11564
GNE-9605	96.34744	6.99113	73.45957	11.68461	84.59822	21.48017	85.83512	8.74776
GNF-2	108.52579	9.94808	115.14812	5.11100	109.74471	30.81616	127.66641	22.54135
GNF-5	96.78114	6.04097	92.24453	16.97490	88.98023	22.23964	97.17954	6.81655
Go 6983	108.14042	8.14432	96.74632	13.60385	93.35021	21.45876	96.90789	32.30818
Golvatinib (E7050)	92.02663	4.00223	71.75008	13.49773	115.16265	31.06186	64.51687	22.03234
GSK1059615	96.36962	12.38136	88.13339	21.67228	94.26073	25.47098	72.24521	14.23814
GSK1838705A	104.67382	8.03363	106.61843	14.70277	101.57527	32.03811	82.02599	15.20980
GSK1904529A	103.04811	5.32696	107.24779	19.85742	139.81531	38.22966	8.58514	5.30326
GSK2126458 (GSK458)	92.02307	3.56972	31.56336	14.47802	27.47569	2.36385	29.51786	9.37298
GSK2334470	117.07207	4.96237	159.54395	31.03051	87.70913	6.88218	127.88449	37.52123
GSK2578215A	109.41801	6.29316	118.45887	4.47302	114.77173	36.77435	120.53283	23.11417
GSK2636771	91.62475	5.72888	69.50602	15.00649	67.39112	3.10230	67.57819	9.36287
GSK429286A	93.92526	6.97045	93.58620	18.70243	86.23600	11.47332	88.64739	20.29528
GSK461364	82.11297	15.46273	13.37110	25.47588	47.07075	15.95565	11.20983	9.71586
GSK621	114.36971	5.93660	172.43854	17.23352	98.71069	25.92725	119.69153	27.89735
GSK650394	113.89320	6.69674	174.29638	11.69800	131.42171	13.69736	154.20849	46.14335

GSK690693	117.53941	6.75501	193.00595	78.05004	136.36597	19.77531	119.55943	14.31167
GW441756	100.78790	15.05570	83.83150	11.61109	94.57968	30.74519	77.66385	29.38534
GW5074	107.01439	10.82842	87.57988	12.22739	95.16912	20.30437	101.40429	56.99321
GZD824	89.01226	5.78313	19.81226	9.19313	5.30240	7.79360	-1.57255	7.08425
H 89 2HCl	116.69877	15.62162	160.08460	36.85991	161.36390	28.32843	119.70754	20.27890
Hesperadin	109.20795	16.35403	36.57030	37.04448	29.32333	11.91234	31.20822	18.19769
HMN-214	99.38765	9.54574	103.22303	12.85070	88.18967	16.44503	99.67639	15.17992
Honokiol	89.48468	7.45585	63.75781	18.60868	91.58987	31.35799	84.84963	34.02088
HS-173	90.63260	2.99315	66.22079	21.24707	60.91898	20.56969	78.95486	24.45303
HTH-01-015	106.63678	2.58913	104.32558	28.78171	111.61222	25.12597	88.92607	14.08434
Ibrutinib (PCI-32765)	109.80459	5.07151	108.20320	18.86757	121.59236	56.82261	103.20123	36.77826
Icotinib	102.99004	15.54490	82.74366	4.00052	71.53864	15.30197	75.89724	29.82656
IKK-16 (IKK Inhibitor VII)	97.93295	13.28621	73.71284	4.59469	25.05534	5.46534	11.88312	1.45056
IM-12	104.33519	9.25306	105.03812	5.08956	98.61640	17.12149	113.24733	10.89042
Imatinib (STI571)	111.39001	1.76695	101.21932	19.45120	154.44625	51.73234	94.96866	22.22225
Imatinib Mesylate (STI571)	110.12112	16.12570	97.67937	6.50005	167.94069	32.90662	88.32846	20.07269
IMD 0354	97.64106	14.01299	-0.61139	15.50817	12.06420	19.49046	6.90920	13.41099
Indirubin	88.47858	8.09709	67.20721	15.87875	86.91908	23.05307	82.85643	30.30963
INK 128 (MLN0128)	90.45417	5.76668	57.96032	8.18809	67.85421	17.33663	54.54085	11.60847
IPA-3	105.73475	5.90371	130.92144	8.45596	105.79215	32.15489	120.63528	28.17471
IPI-145 (INK1197)	101.23084	7.02354	103.34820	24.14065	76.84060	13.16605	94.50839	16.30836
ISRIB (trans-isomer)	98.82866	1.97151	92.17179	12.25977	82.37140	18.38348	91.34605	12.23353
JNJ-38877605	119.36964	10.46298	167.40605	10.49605	126.94342	16.68674	120.25529	25.83529
JNJ-7706621	97.54320	6.14792	77.99180	17.78243	91.92285	12.68103	79.96399	9.79739
JNK Inhibitor IX	91.24506	4.74019	69.79015	61.41415	40.01937	15.51768	38.15045	7.12320
JNK-IN-8	107.94040	7.50888	123.91455	21.36518	115.03150	25.20498	118.29206	46.46638
Ki8751	105.64457	15.32992	106.91694	15.77172	92.90967	17.03185	106.78029	31.34477
KN-62	96.76464	1.63664	94.84284	27.41496	110.68792	39.54335	86.80002	19.22748
KN-93 Phosphate	94.53604	3.78871	81.04777	10.72496	89.29584	13.96740	63.34510	13.80342
K-Ras(G12C) inhibitor 9	108.09167	7.95786	112.71206	10.55463	105.27048	3.37880	64.38639	4.04424
KRN 633	119.29166	18.22582	149.00553	17.50545	136.49829	41.59720	133.69225	24.19288
KU-0063794	91.94362	22.14166	72.29920	6.46412	103.39122	32.49275	74.74767	25.05216
KU-55933 (ATM Kinase Inhibitor)	109.37270	11.68933	122.90090	15.18000	109.47330	14.04120	96.50881	34.36696
KU-60019	98.14020	4.56764	55.56208	10.50912	98.12535	27.77801	70.05294	13.48629
KW-2449	117.64079	11.53383	122.14230	26.25554	131.51270	34.97996	110.15743	21.02810
KX2-391	77.14036	8.50660	1.22823	7.49220	-8.48694	3.50804	-1.40822	2.89555
L-685,458	112.75641	3.72300	127.57883	19.76471	102.49204	27.91015	107.39333	26.36130
Lapatinib	100.08470	10.28108	75.75347	17.08051	83.99145	19.81860	72.08898	12.39281
Lapatinib (GW-572016) Ditosylate	105.21574	11.54010	79.83484	11.74237	68.79476	15.41979	49.28421	15.67109
LDC000067	94.33073	4.26499	97.31858	17.70093	88.79227	18.54119	111.47364	4.49595
LDK378	119.77889	2.57877	181.68119	20.62726	43.68172	24.79244	54.86847	24.66079
LDN-214117	97.11808	3.52561	101.81975	14.81093	143.28124	31.67397	76.63113	6.88744
Lenvatinib (E7080)	115.64940	4.90968	143.94603	30.95595	126.21954	24.13263	97.54688	27.75487
LFM-A13	97.09757	10.96783	106.12808	27.66315	87.45605	5.58182	110.26005	14.34427
Linifanib (ABT-869)	85.99751	9.01900	71.72789	22.05387	73.05339	6.41460	69.92405	12.25627
Losmapimod (GW856553X)	115.44873	2.94716	112.53468	17.23575	92.46930	14.19132	109.02761	29.04337
LY2090314	95.69877	15.60501	235.46530	66.13603	186.68410	70.74620	213.82337	61.76116
LY2228820	102.55256	5.08383	74.87109	20.22855	92.31078	21.01505	71.56209	7.30612

LY2603618	110.72841	0.64685	82.60947	2.67266	105.47865	16.52365	78.10402	5.13773
LY2784544	97.64831	3.78957	64.36741	15.58972	114.90018	40.08749	72.61654	22.48331
LY2835219	96.65016	5.92243	53.08437	20.26015	75.48945	22.89223	43.74650	9.16576
LY294002	109.46512	9.67359	125.97057	10.03101	115.79791	13.86371	89.27129	20.73639
Masitinib (AB1010)	106.32347	5.25963	99.40058	31.41386	150.52083	41.00987	50.04703	11.92661
MEK162 (ARRY-162, ARRY-438162)	116.62029	2.95924	111.54682	14.04299	85.27124	13.29225	102.18048	24.69243
MGCD-265	105.37710	14.50103	92.54871	26.02049	38.20114	16.78013	60.75999	6.18689
Milciclib (PHA-848125)	98.87075	9.33934	97.37909	46.12612	116.69001	33.49237	76.72479	14.32667
MK-2206 2HCl	95.84228	14.41714	83.31582	11.17127	34.94978	8.29927	45.79870	14.33892
MK-2461	113.29089	9.41606	135.82960	21.54756	155.90492	20.63804	103.82652	16.92399
MK-5108 (VX-689)	111.43926	11.77914	134.81743	29.89727	119.79473	18.62082	88.50977	12.98422
MK-8745	103.78970	4.25707	104.64456	26.93192	71.91530	17.68315	100.91445	17.37723
MK-8776 (SCH 900776)	105.02343	9.47931	95.81391	22.80173	116.60192	32.67709	96.38019	25.44557
MLN8054	103.76194	2.74262	132.10509	22.21681	109.46242	6.85638	84.38885	18.93428
Motesanib Diphosphate (AMG-706)	93.52465	10.89390	71.53480	32.25725	85.93823	20.13415	77.04109	22.43772
Mubritinib (TAK 165)	104.23514	7.97807	87.83217	40.95533	67.96684	34.75661	76.30299	7.54621
Nilotinib (AMN-107)	101.43496	10.50795	100.36634	23.42269	162.59159	28.22689	95.92040	16.93611
Nintedanib (BIBF 1120)	103.48366	8.91800	81.85072	16.41144	95.43981	8.26868	84.73472	17.27922
NSC 23766	97.18246	6.31056	109.04800	28.05934	99.24642	29.44461	87.93154	15.50290
NU6027	112.30051	9.13204	145.25416	12.79434	148.38364	11.11200	128.73303	23.85985
NU7441 (KU-57788)	96.75320	0.90431	65.43593	22.02145	78.22856	24.73618	66.94925	18.80083
NVP-ADW742	109.93832	11.43082	146.05950	20.66272	22.76356	3.54532	25.25110	5.11259
NVP-AEW541	106.35624	10.94596	121.54765	13.24844	29.05521	1.32831	46.51620	12.22899
NVP-BHG712	100.28839	14.42717	96.83046	18.46466	146.10365	28.71096	92.89969	23.19470
NVP-BSK805 2HCl	103.21775	5.86494	88.03750	13.95951	45.75461	5.76526	55.42053	10.00421
NVP-BVU972	96.69148	6.70213	72.67305	23.72064	99.86831	39.43141	67.43627	23.65669
ONO-4059	106.00529	14.03053	141.48903	1.51892	114.80585	29.31116	122.35566	16.77358
OSI-027	97.70669	6.14875	69.95748	5.39374	75.71316	22.98911	72.30200	20.05765
OSI-420	93.16974	2.73347	55.45301	8.89369	83.55125	27.48412	66.45398	9.25756
OSI-906 (Linsitinib)	120.85944	6.68363	162.23030	15.95290	136.27764	15.88630	116.11300	24.69215
OSI-930	97.52045	23.74359	83.48385	19.08085	124.67472	60.59744	85.29424	35.64845
OSU-03012 (AR-12)	106.82180	7.05956	103.78992	15.60657	146.75168	53.55288	60.24205	21.41494
p276-00	92.90916	4.54074	85.18354	31.78566	85.10202	11.53971	82.49284	6.56643
Pacritinib	83.10225	8.19731	53.50785	18.34690	4.13833	1.61193	16.45510	18.40635
Palbociclib (PD-0332991) HCl	107.92034	8.31945	88.64685	31.96200	84.95692	15.59065	59.43560	23.57733
Pazopanib	117.52584	3.05028	156.43976	7.13655	124.31175	32.31662	128.25883	40.23119
Pazopanib HCl (GW786034 HCl)	110.66735	10.93164	135.19141	36.07097	130.38344	10.87724	109.77994	10.76108
PD0325901	115.00047	14.20237	83.89642	41.78172	82.38318	15.58882	76.01917	14.90391
PD168393	114.80095	9.73402	107.24987	9.93571	77.55276	21.13343	75.72264	5.09705
PD173074	103.74160	18.45471	89.70676	12.51281	127.29384	33.08704	56.57891	19.79132
PD173955	90.41759	6.84423	98.99938	42.71358	74.72514	13.70217	49.80958	5.37424
PD184352 (CI-1040)	99.22225	7.79748	87.75199	17.49902	99.96110	21.07728	78.97649	19.73718
PD318088	98.89330	10.81891	66.67928	16.03597	78.11398	16.69033	69.94941	20.41404
PD98059	102.44855	2.34602	124.16648	12.80036	99.07985	19.28207	94.12781	7.04259
Pelitinib (EKB-569)	92.72039	11.01216	46.59344	5.05131	40.73955	12.64634	29.31645	11.79119
PF-00562271	110.74590	4.50933	139.05268	52.50178	122.65622	32.34396	103.87037	27.63071
PF-04217903	98.59339	7.90056	78.73835	9.05714	83.34240	6.49377	79.05826	19.16488

PF-04691502	108.04616	4.49750	117.38387	27.26144	108.55921	25.98514	81.96415	30.45361
PF-3758309	93.87012	4.25468	100.50427	4.75209	97.85328	37.48921	109.82075	20.80239
PF-431396	95.49958	10.07616	103.70325	39.34130	75.29006	8.93301	95.96465	9.23997
PF-4708671	100.74440	12.57468	73.10160	17.51036	106.88118	24.53680	80.28041	18.42182
PF-477736	109.14086	13.63030	103.79464	11.85524	102.67342	26.46988	106.05761	33.79550
PF-543	117.34262	5.43916	132.56268	14.74050	60.85707	8.91510	120.51433	32.85912
PF-562271	98.82287	11.59855	82.19756	26.20394	97.52594	24.80758	87.05844	33.86243
PF-573228	99.20270	7.10791	71.71178	14.82291	97.21289	44.87560	71.12303	8.98089
PFK15	109.33007	7.73222	130.04109	14.62326	96.26040	17.97935	118.43519	35.15843
PH-797804	119.11393	10.69616	141.66149	49.45139	107.29765	47.68484	83.12511	12.53143
PHA-665752	116.29317	7.07872	170.79876	27.41866	84.40599	11.34431	83.25365	17.40383
PHA-680632	94.78164	14.42640	101.65282	10.65450	98.56204	27.69732	95.91808	14.05190
PHA-767491	117.57515	9.88763	130.27007	48.76134	139.89390	33.35319	112.65773	21.01192
PHA-793887	113.18490	13.42306	140.50774	36.34750	124.80846	45.93643	128.29848	37.00055
Phenformin HCl	107.01865	2.49537	95.48902	25.07429	104.35110	30.39283	103.59678	35.45276
PHT-427	112.99163	18.58367	137.37761	33.09871	129.13484	33.79307	131.29913	29.63052
PI-103	100.59216	11.46132	96.92616	36.77951	104.21152	11.81788	80.19778	6.39920
Piceatannol	118.67982	3.08853	148.39149	1.66803	97.05141	29.12144	112.54356	29.73876
PIK-293	95.79259	5.91915	75.02855	27.97835	92.02900	15.91381	81.35792	13.14468
PIK-294	96.36302	4.80121	82.88479	43.36428	113.04247	33.36344	87.49426	32.79317
PIK-75	76.98688	7.40677	-16.67670	17.29682	-7.44265	9.70088	1.31487	10.34691
PIK-93	109.70302	10.03590	145.63773	37.65641	122.71385	36.76965	122.18036	15.71408
Pimasertib (AS-703026)	93.71106	11.87913	61.85499	11.79362	77.19199	34.12277	52.55482	15.50784
PLX-4720	110.50965	10.59969	159.97970	21.03466	124.58774	30.35565	111.81290	13.05161
Ponatinib (AP24534)	99.85624	11.68654	60.63576	13.09873	56.31248	16.26369	10.76298	10.83918
PP1	99.12255	2.67192	91.84676	18.35401	67.38166	4.55885	82.02750	18.02689
PP121	99.30882	4.45015	86.36573	15.28174	86.01930	35.06742	90.81266	34.22171
PP2	106.79285	4.73338	112.08108	24.77872	90.65025	25.95146	109.12174	35.17704
PP242	100.47458	9.17768	86.09020	36.80489	95.50517	27.42049	81.09955	27.39679
PQ 401	88.65574	6.79300	87.19481	22.27730	73.25442	28.67450	82.41041	4.92830
PRT062607 (P505-15, BIIB057) HCl	105.06780	13.18915	162.68118	29.29869	133.26962	17.47022	120.98223	21.80604
Purvalanol A	87.94700	5.96076	77.98419	16.55457	76.41924	5.17709	80.21100	19.54803
Quercetin	104.35995	3.01604	72.06839	1.90941	100.58277	29.68348	86.33439	23.32328
Quizartinib (AC220)	109.38446	13.18968	128.99053	38.09363	154.73705	44.11163	55.00027	25.76612
R406	109.23077	14.28229	104.03219	33.37670	112.44424	39.20518	100.43333	8.31047
R406 (free base)	98.96903	8.21586	74.36068	13.08801	75.22842	15.13215	70.48731	13.60855
R428 (BGB324)	90.36670	2.98867	68.05603	11.81973	27.17096	9.72150	3.18250	0.77479
R547	105.76045	10.59869	52.02400	26.83191	40.68085	9.97742	38.86316	19.54472
RAF265 (CHIR-265)	105.26556	9.60181	86.54650	18.92002	75.45171	2.88817	73.12277	10.86053
Rapamycin (Sirolimus)	104.22600	15.90222	75.42897	7.28048	96.65058	12.11394	69.80462	23.34387
Refametinib (RDEA119, Bay 86-9766)	123.44799	15.83037	134.36718	80.00488	98.22228	12.81810	94.58474	18.45282
Regorafenib (BAY 73-4506)	108.41100	1.53957	148.82967	23.86888	135.97935	54.59956	110.52883	27.21281
Rigosertib (ON-01910)	78.75882	16.47207	-11.65610	11.88536	-19.30176	11.95775	-4.65934	0.28812
RKI-1447	93.72627	3.12689	66.94936	5.98127	88.86336	31.72000	87.43240	20.76335
RN486	123.82804	8.06147	173.90724	7.27202	122.16717	15.83987	102.30500	16.12503
Ro3280	95.07800	4.49761	116.75986	29.11004	63.91585	9.20321	84.99708	13.20375
Ro-3306	106.90116	8.12435	157.48986	14.86042	98.04348	9.97077	117.91239	36.37947
Roscovitine (Seliciclib,CYC202)	113.75661	6.53438	151.69797	7.61686	117.36502	22.19350	105.15123	4.31204

Ruxolitinib (INCB018424)	107.62296	17.68970	132.05057	21.46955	114.47865	17.95101	123.01869	29.53467
SAR245409 (XL765)	96.80482	19.45870	76.66974	4.19394	94.92429	36.25752	71.38740	20.29419
Saracatinib (AZD0530)	93.66798	9.40243	77.43649	9.76417	75.60453	2.76304	73.33801	22.83459
SB202190 (FHPI)	102.40383	8.10041	87.02985	34.50517	97.78663	23.26339	64.99606	20.51701
SB203580	105.99184	7.34168	119.76473	14.43139	110.10577	20.96634	100.76009	32.52277
SB216763	120.55025	3.63574	152.14577	20.64377	124.30675	3.80345	125.63420	5.54387
SB239063	107.47323	12.07210	161.73188	27.96078	105.10359	16.94879	112.68905	17.22250
SB415286	101.84686	6.70450	75.93592	13.80394	80.72390	14.26385	83.73925	7.37924
SB590885	108.68035	6.58217	133.10873	37.54472	157.48447	81.20486	91.74951	25.90531
SC-514	102.01057	7.06078	93.37586	11.17095	80.96740	19.39340	81.46390	27.46102
Selumetinib (AZD6244)	98.58152	9.30133	78.80780	12.29800	84.57509	7.57481	78.70795	12.01224
Semaxanib (SU5416)	96.80289	3.22037	99.94077	11.05020	125.12823	10.52261	80.54473	5.90626
SGI-1776 free base	107.89601	10.94300	110.79591	33.05127	16.89033	2.74632	43.41164	11.19581
SGX-523	121.77125	6.49075	182.17216	42.43700	129.31047	14.69306	113.49341	15.07641
Skepinone-L	112.15635	6.12700	83.28325	12.18780	71.50525	7.81132	76.18950	12.09698
SKI II	119.32569	8.99240	169.87646	20.84030	117.90729	12.28360	137.34982	24.56235
SL-327	100.96293	8.84665	104.42964	6.97132	97.32584	8.09660	82.99275	16.97306
SMI-4a	101.74907	10.12905	126.52546	2.05985	111.15763	9.01804	128.79982	9.65652
SNS-032 (BMS-387032)	100.19765	5.09201	106.22958	13.38495	104.94151	33.54236	108.29457	18.97462
SNS-314 Mesylate	105.93007	9.08220	19.79023	29.52466	20.50069	6.01885	15.01622	9.84863
Sorafenib	100.60504	4.41505	91.50457	1.44421	110.72528	52.56669	109.20413	23.68595
Sorafenib Tosylate	106.54770	9.65963	96.38519	8.00190	132.09799	6.25415	76.28292	25.96633
Sotrastaurin	97.66375	1.08649	100.01533	4.28791	112.78507	15.65128	78.28327	27.03704
SP600125	110.37629	17.17251	144.99336	22.84163	116.85239	33.96609	123.96560	37.12841
S-Ruxolitinib (INCB018424)	110.64348	9.64906	130.78571	1.22621	106.54855	21.51086	128.71537	46.52080
SSR128129E	119.56473	12.49123	154.33915	15.82829	108.96380	21.24626	140.73470	25.05797
Staurosporine	62.56204	4.33525	-40.34929	9.25136	-41.78099	14.41031	-20.01673	3.96103
SU11274	106.01963	9.55071	118.51320	32.92683	29.01329	1.77265	75.96883	18.52045
SU6656	103.21504	10.15753	132.65548	4.51476	96.89822	26.42568	125.11435	8.66554
SU9516	89.02124	3.97507	72.91229	31.16321	77.31891	3.39810	80.27550	32.26946
Sunitinib Malate	95.08325	13.18532	85.05195	29.46028	64.79886	8.33686	49.84708	6.39298
TAE226 (NVP-TAE226)	99.58804	9.25813	70.06107	9.06200	86.71723	19.62175	64.30994	5.71190
TAK-285	97.35032	5.81766	98.12125	17.10560	135.81646	28.93466	81.48640	4.49798
TAK-632	107.47072	5.59497	147.81880	12.03652	151.71836	19.50954	134.03040	53.00600
TAK-715	114.54999	3.45556	124.42244	9.26258	96.43364	20.84281	128.86204	22.01057
TAK-733	104.38042	3.41356	71.96758	20.48311	84.36529	27.50145	74.23413	15.37923
TAK-901	112.08723	9.71805	114.93241	33.34618	104.76762	36.35455	103.21754	10.47059
TCS 359	91.20441	4.54281	76.33112	13.19592	76.81675	4.79876	61.77858	18.55412
TDZD-8	104.53108	7.65859	99.12369	19.47210	77.05233	26.87567	102.55214	12.67342
Telatinib	98.26435	3.98898	72.90923	17.04956	104.32689	25.61869	90.10151	24.97562
Temsirolimus (CCI-779, NSC 683864)	98.63765	11.78049	85.85352	16.40243	92.61806	17.67965	83.68626	16.12964
Tepotinib (EMD 1214063)	120.71361	7.81032	170.90963	8.00803	97.44460	24.06531	57.83328	6.58213
TG003	109.95061	3.52188	109.04366	7.44382	88.88365	13.81557	109.28784	15.81748
TG100-115	96.49190	11.13413	58.36138	10.00593	73.86818	15.12504	50.40868	8.45214
TG100713	103.78681	12.53509	87.54190	7.49983	83.92381	25.75708	95.09277	14.35790
TG101209	112.44653	8.66141	150.29255	29.78861	136.53654	41.79599	116.26861	27.20333
TG101348 (SAR302503)	114.61740	7.02121	111.37510	29.67975	137.58192	38.33454	115.82418	23.88753
TGX-221	99.40013	2.55340	89.03364	22.99318	93.15621	33.06846	71.49568	18.37907

Thiazovivin	106.94374	15.89028	129.18486	32.30638	123.32194	52.56982	143.21249	44.52013
TIC10	115.62726	5.40620	139.66002	34.70133	92.77921	15.22883	114.49532	36.18413
Tie2 kinase inhibitor	117.99083	15.15036	141.09345	15.66243	139.42551	27.64250	132.90312	35.80049
Tivantinib (ARQ 197)	107.85108	9.75998	105.81345	37.54350	98.92045	38.01592	92.77668	6.48910
Tivozanib (AV-951)	93.52345	14.82011	65.86341	0.53165	89.69627	33.70602	70.66504	17.59753
Tofacitinib (CP-690550) Citrate	106.84856	7.80993	78.80274	11.94562	80.82139	35.15267	95.12125	21.93442
Tofacitinib (CP-690550,Tasocitinib)	94.70109	3.89650	73.99240	12.20765	93.44989	32.39605	72.74453	26.27121
Torin 2	88.70509	5.12045	41.03169	6.13008	50.68224	6.84841	14.14229	6.91327
TPCA-1	101.63170	8.54103	107.46850	7.39986	109.43275	17.00792	90.05175	5.94972
Trametinib (GSK1120212)	113.45202	4.15022	83.10285	32.93584	66.57154	23.05213	56.36683	13.56151
Triciribine	107.15813	5.49129	88.87875	15.47194	78.36313	33.49178	61.64952	7.86753
TSU-68 (SU6668, Orantinib)	101.01040	12.48179	103.29772	25.17949	86.78368	27.55468	102.54398	18.92820
TWS119	113.09922	14.81479	115.46152	25.33592	100.66076	27.10481	104.88464	20.61496
Tyrphostin 9	97.57282	17.88146	43.45425	13.49495	64.54503	20.37907	29.68018	15.24205
Tyrphostin AG 1296	90.02968	6.65865	78.83867	14.96130	67.63580	24.24273	73.93066	13.05666
Tyrphostin AG 879	95.60691	5.21778	77.80453	11.26960	98.41603	33.34050	59.01957	27.94333
U0126-EtOH	116.05966	7.09489	159.60936	28.11570	128.78077	18.85509	108.39189	17.51781
Ulixertinib (BVD-523, VRT752271)	106.06324	10.63472	150.86903	17.26411	99.62853	24.39897	125.28450	32.00299
URMC-099	91.98749	15.97524	69.56490	13.30031	61.85054	3.13779	12.78653	3.08356
Vandetanib (ZD6474)	108.95186	10.84286	106.64780	36.59484	20.30993	3.95557	40.81988	16.62484
Varlitinib	113.87028	4.04735	109.72204	26.16103	131.70669	50.77031	102.14724	31.58201
Vatalanib (PTK787) 2HCl	113.25606	7.94836	162.06207	42.39819	153.10502	16.14228	106.40339	19.05740
VE-821	107.02411	8.07939	163.35304	23.14113	120.76164	0.50165	127.04977	19.12672
VE-822	86.60904	4.14590	54.13647	28.29258	105.31265	44.76714	33.89899	9.46754
Vemurafenib (PLX4032, RG7204)	102.09495	21.31393	107.02459	17.63501	120.17713	35.83463	96.95846	11.02177
Volasertib (BI 6727)	57.50863	2.94161	1.28398	13.99102	29.69600	33.60875	-6.62928	5.29098
VS-5584 (SB2343)	92.91288	7.94452	81.37714	25.38805	55.58085	2.44843	73.44203	24.94679
VX-680 (Tozasertib, MK-0457)	112.37160	9.26214	116.35648	32.22150	92.88466	11.64604	88.62154	11.92364
VX-702	119.42513	7.18172	142.90498	10.53154	98.31033	23.27314	116.67997	15.70695
VX-745	105.90648	15.24200	113.95940	17.20777	128.55357	45.25137	106.44886	28.43391
WAY-600	106.08801	5.85805	126.66946	26.42600	133.62636	31.08622	59.61094	8.96112
WH-4-023	102.36555	8.03935	114.15339	8.02297	64.67818	7.28186	38.58022	14.15401
WHI-P154	100.06891	12.44340	72.44037	10.87169	65.28620	20.64881	76.72788	5.76018
Wortmannin	106.84400	2.89471	52.88581	8.86952	59.43768	14.68671	57.88978	16.66354
WP1066	98.74417	6.35109	101.33058	14.69674	105.48918	27.37069	60.56512	11.61366
WYE-125132 (WYE-132)	90.27242	3.22011	45.24502	14.46048	49.34637	22.61458	53.22732	11.96458
WYE-354	100.45112	19.11756	94.74966	23.44595	100.61932	29.76809	96.11592	34.56298
WZ3146	85.45954	7.37507	41.54479	21.64841	80.86807	5.46621	32.34397	2.64996
WZ4002	97.05978	6.41464	89.29298	32.95000	91.29023	13.32984	37.38608	27.32413
WZ4003	106.05124	3.86698	101.03132	24.02293	59.32037	5.53774	60.13452	15.38024
WZ8040	102.40648	5.80880	93.01036	25.85900	57.29217	15.24835	29.69420	27.93896
XL019	116.27128	6.63469	159.29142	11.40024	148.24251	30.40710	114.45366	19.59247
XL147	94.38281	4.68146	74.20848	8.00762	74.52947	9.47165	81.97394	21.05937

XMD8-92	84.92130	6.50906	94.99607	9.69914	103.86636	26.55295	110.30880	14.21248
Y-27632 2HCl	122.79486	12.63409	149.60897	47.76275	142.99637	4.02787	121.37756	21.40973
YM201636	95.53611	17.93730	88.28801	15.72565	151.29246	35.04092	73.25092	12.58656
ZCL278	105.30791	3.41510	125.30385	16.09069	81.26828	9.60824	103.38728	30.39654
ZM 306416	101.34762	9.51712	87.21871	5.39493	76.04102	25.23623	100.00109	13.48071
ZM 323881 HCl	99.12451	10.15845	73.20297	15.21265	63.36748	12.75991	81.66305	11.72651
ZM 336372	118.62356	5.62782	166.60000	38.60305	115.67671	38.71551	134.22474	34.84730
ZM 39923 HCl	96.82059	3.85369	107.67133	16.07190	73.69752	10.20674	86.68591	8.26787
ZM 447439	116.87032	8.93593	168.38932	42.96806	136.99594	25.76625	109.72373	19.76397
Zotarolimus(ABT-578)	101.02862	5.49118	125.13529	36.43224	75.60783	16.63621	83.65406	35.78056
ZSTK474	114.01573	8.93137	158.86430	31.62176	148.02067	10.13137	108.40270	13.43648

Appendix 3: Curriculum Vitae

Corina M. Stewart

Academic Background

PhD Candidate in Microbiology and Immunology
University of Ottawa — Sept. 2015 – June 2021 (expected)

Bachelor of Science (with Distinction) in Molecular Biology and Biochemistry
Simon Fraser University — Sept. 2009 – June 2014

Publications

Fu, K., Laroche, G., Mulloy, R. P., Phan, A., **Stewart, C. M.**, Hagan, M., Fink, C., Prévost, J., Beaudoin-Bussières, G., Yockell-Lelievre, J., Stanford, W. L., Giguère, P., Dekaban, G., Finzi, A., Dikeakos, J.D., Kobasa, D., Côté, M. Identification of host proteases required for SARS-CoV-2 Spike-mediated membrane fusion. Manuscript in preparation.

Stewart, C. M., Bo, Y., Fu, K., Hagan, M., Kozak, R. A., Kobinger, G., Kobasa, D., Côté, M. Inhibition of sphingosine kinase 1 impairs endocytic trafficking of Ebola virus to entry-conducive intracellular compartments. Manuscript in preparation.

Rocheleau, L., Laroche, G., Fu, K., **Stewart, C.M.**, Mohamud, A.O., Côté, M., Giguère, P.M., Langlois, M.A., Pelchat, M. Identification of a High-frequency Intra-host SARS-CoV-2 spike Variant with Enhanced Cytopathic and Fusogenic Effect. mBio. 2021.

Stewart, C. M., LeBlond, N. D., Smith, T. K. T., Laroche, G., Giguère, P. M., Fullerton, M. D., Pelchat, M., Kobasa, D., and Côté, M. Ebola virus triggers receptor tyrosine kinase-dependent signaling to promote the delivery of viral particles to entry-conducive intracellular compartments. PLoS Pathog. 2021 Jan 29; 17(1).

Stewart, C. M., Dorion, S. S., Ottenbrite, M. A. F., LeBlond, N. D., Smith, T. K. T., Qiu, S., et al. A Diacylglycerol Kinase Inhibitor, R-59-022, Blocks Filovirus Internalization in Host Cells. Viruses. 2019;11(3).

Qiu, S., Leung, A., Bo, Y., Kozak, R. A., Anand, S. P., **Warkentin, C.**, et al. Ebola virus requires phosphatidylinositol (3,5) bisphosphate production for efficient viral entry. Virology. 2018;513:17-28.

Oral Presentations

American Society for Virology Annual Meeting, Fort Collins, Colorado — June 2020
(meeting cancelled due to COVID-19)

Canadian Society for Virology 2nd Symposium, Halifax, Nova Scotia June 2018
American Society for Virology Annual Meeting, Madison, Wisconsin June 2017
Canadian Society for Molecular Biosciences, Ottawa, Ontario May 2017
American Society for Virology Annual Meeting, Blacksburg, Virginia June 2016
Canadian Society for Virology Symposium, Blacksburg, Virginia June 2016

Awards

Syed Sattar PhD Award, BMI, University of Ottawa 2021
American Society for Virology Travel Award (meeting cancelled due to COVID-19) 2020
NSERC Postgraduate Scholarship – PGSD, University of Ottawa 2018
2016 BMI Poster Award – 1st Place, University of Ottawa 2016
Ontario Graduate Scholarship, University of Ottawa 2016
Canadian Society for Virology Travel Award, CSV Conference, Blacksburg, Virginia 2016
University of Ottawa Admissions Scholarship, University of Ottawa 2015
Molecular Biology and Biochemistry Undergraduate Scholarship, Simon Fraser University 2013
Undergraduate Open Scholarship, Simon Fraser University 2010-2014
Summit Entrance Scholarship, Simon Fraser University 2009

Research Experience

PhD Candidate – M. Côté Lab
University of Ottawa Sept. 2015 – Present

Undergraduate Research Assistant – Plettner Research Group
Simon Fraser University May – Sept. 2013 & 2014

Volunteer and Leadership Experience

VP Wellness
BMI Graduate Student Association May 2019 – August 2020

Science Educator
Let's Talk Science Sept. 2016 –Sept. 2018

Teaching Experience

Teaching Assistant, University of Ottawa
MIC4126 – Virology Winter 2018 & 2019
BCH2333 L – Introduction to Biochemistry Lab Winter 2016

Biology Laboratory Instructor
Kwantlen Polytechnic University Jan. 2015 - May 2015